

**Bifurcations in Discontinuous
Mechanical Systems of Filippov-Type**

Cover: drafts of mechanical devices by Leonardo da Vinci.
From: Codex Madrid I (8937), original title: 'Tratado de Estatica y Mechanica en Italiano', (1493).

CIP-DATA LIBRARY TECHNISCHE UNIVERSITEIT EINDHOVEN

Leine, Remco I.

Bifurcations in discontinuous mechanical systems of Filippov-type/
by Remco Ingmar Leine. -

Eindhoven: Technische Universiteit Eindhoven, 2000.

Proefschrift. - ISBN 90-386-2911-7

NUGI 834

Trefwoorden: niet-lineaire dynamica; bifurcaties; stick-slip trillingen; discontinue systemen /

Subject headings: nonlinear dynamics; bifurcations; stick-slip vibrations; discontinuous systems /

Printed by the Universiteitsdrukkerij TU Eindhoven, The Netherlands

Cover design by Ben Mobach

Typeset by the author with $\text{\LaTeX}2_{\epsilon}$

Copyright © 2000 by R. I. Leine

All rights reserved. No parts of this publication may be reproduced or utilized in any form or by any means, electronic or mechanical, including photocopying, recording or by any information storage and retrieval system, without permission of the copyright holder.

This research was financed by the Dutch Technology Foundation (STW).

Bifurcations in Discontinuous Mechanical Systems of Filippov-Type

PROEFSCHRIFT

ter verkrijging van de graad van doctor
aan de Technische Universiteit Eindhoven,
op gezag van de Rector Magnificus, prof.dr. M. Rem,
voor een commissie aangewezen door het College voor Promoties
in het openbaar te verdedigen op
donderdag 15 juni 2000 om 16.00 uur

door

REMCO INGMAR LEINE

geboren te Bleiswijk

Dit proefschrift is goedgekeurd door de promotoren:

prof.dr.ir. D.H. van Campen
en
prof.dr. H. Nijmeijer

Copromotor:
dr.ir. A. de Kraker

*'L'essentiel est invisible pour les
yeux'*

Antoine de Saint-Exupéry,
Le Petit Prince

Voor Ilse

Contents

Summary	ix
Samenvatting	xiii
1 Introduction	1
1.1 Motivation	1
1.2 Nonlinear Dynamics and Bifurcations	2
1.3 Discontinuous Systems	3
1.4 Literature Survey	5
1.5 Objective and Scope of the Thesis	7
1.6 Outline of the Thesis	7
2 Filippov Theory	9
2.1 The Construction of a Solution	9
2.2 Numerical Approximation	18
2.3 Dry Friction Models and Differential Inclusions	19
2.4 Example: The Stick-slip System	22
3 Fundamental Solution Matrix	27
3.1 Fundamental Solution Matrix for Smooth Systems	27
3.2 Jumping Conditions: A Single Discontinuity	28
3.3 Construction of Saltation Matrices	31
3.4 Example I: The Stick-slip System	34
3.5 Example II: The Discontinuous Support	37
4 Non-smooth Analysis of Filippov Systems	41
4.1 Linear Approximations at the Discontinuity	41
4.2 Generalized Differentials	47
5 Bifurcations of Fixed Points	49
5.1 Smooth Systems	50
5.2 Discontinuous Bifurcation: The Basic Idea	54
5.3 Saddle-node Bifurcation	56
5.4 Transcritical Bifurcation	58
5.5 Pitchfork Bifurcation	61

5.6	Hopf Bifurcation	64
5.7	Hopf–Pitchfork Bifurcation	66
5.8	Discussion and Conclusions	69
6	Bifurcations of Periodic Solutions	73
6.1	Discontinuous Systems	73
6.2	Bifurcations in Smooth Systems	74
6.3	Discontinuous Bifurcation: The Basic Idea	75
6.4	The Poincaré Map	77
6.5	Intersection of Hyper-surfaces of Discontinuity	80
6.6	Fold Bifurcation; Trilinear Spring System	84
6.7	Infinitely Unstable Periodic Solutions	89
6.8	Symmetry-Breaking Bifurcation; Forced Vibration with Dry Friction	92
6.9	Flip Bifurcation; Forced Stick-slip System	95
6.10	Discussion and Conclusions	100
7	Concluding Remarks	103
7.1	Overview and Summary of Contributions	103
7.2	Recommendations	105
A	Application to a Simple Model of Drillstring Dynamics	109
A.1	Motivation	109
A.2	Principles of Oilwell Drilling	110
A.3	Downhole Measurements	112
A.4	Modeling of Stick-slip Whirl Interaction	116
A.5	Fluid Forces	116
A.6	Contact Forces	118
A.7	Whirl Model	119
A.8	Stick-slip Model	125
A.9	Stick-slip Whirl Model	126
A.10	Discussion and Conclusions	131
A.11	Coordinate Systems	132
B	Some Theoretical Aspects of Periodic Solutions	133
B.1	Transformation to an Autonomous System	133
B.2	The Variational Equation	134
C	Parameter Values	135
	Bibliography	137
	Acknowledgments	145
	Curriculum Vitae	147

Summary

Physical phenomena such as dry friction, impact and backlash in mechanical systems or diode elements in electrical circuits are often studied by means of mathematical models with some kind of discontinuity. Filippov systems form a subclass of discontinuous dynamical systems which can be described by a set of first-order ordinary differential equations with a discontinuous right-hand side.

Mechanical systems with dry friction constitute an important example of Filippov systems. The presence of dry friction-induced self-sustained vibrations can be highly detrimental to the performance of mechanical systems. Many other practical problems in engineering are related to vibrations caused or influenced by discontinuous characteristics of physical phenomena. It is therefore desirable to know whether periodic solutions of a system with dry friction (or Filippov systems in general) exist for a certain parameter set and how these periodic solutions change for a varying parameter of the system. Such parameter studies are usually conducted by means of path-following techniques where a branch of fixed points or periodic solutions is followed while varying a parameter. A branch of fixed points or periodic solutions can fold or can split into other branches at critical parameter values. This qualitative change in the structural behaviour of the system is called ‘bifurcation’. Bifurcations in smooth systems are well understood but little is known about bifurcations in discontinuous systems.

The objective of the thesis is to investigate different aspects of bifurcations of fixed points in non-smooth continuous systems and of periodic solutions in Filippov systems. Filippov systems expose non-conventional bifurcations called ‘discontinuous bifurcations’, being different from the conventional bifurcations occurring in smooth systems. In this thesis, Filippov theory, generalized derivatives and Floquet theory are combined, which leads to new insight into bifurcations in discontinuous systems.

First, Filippov’s solution concept for differential equations with discontinuous right-hand side is reviewed. Systems with dry friction require special attention. Differential equations with discontinuous right-hand side are extended to differential inclusions with Filippov’s convex method. Existence of solutions to differential inclusions is guaranteed under additional conditions but no uniqueness of solutions is guaranteed. Non-uniqueness plays an important role in the bifurcation behaviour of Filippov systems.

The local stability of a periodic solution is governed (for the hyperbolic case) by the fundamental solution matrix. The fundamental solution matrix is also essential

for the understanding of bifurcations of periodic solutions. Discontinuities of the vector field in Filippov systems cause jumps in the fundamental solution matrix. The discontinuous behaviour of the fundamental solution matrix is explained and elucidated in mechanical examples.

The jumps in the fundamental solution matrix can be analyzed by the linear approximation method which approximates a discontinuous system by a non-smooth continuous system. The linear approximation method replaces a discontinuity in the vector field by a boundary layer with a vector field that varies linearly between the left and right limit on the edges of the boundary layer. It is found that the jump of the fundamental solution matrix can be expressed as a convex combination of the fundamental solution matrices before and after the jump. The linear approximation method as well as the relation to non-smooth analysis and generalized differentials are discussed in the thesis.

For Filippov systems different definitions for the term bifurcation exist in literature and it is shown that they can be inconsistent with one another. One particular definition, which is applicable to Filippov systems, has been chosen in this thesis as definition for bifurcation.

As a stepping stone to the study of bifurcations of periodic solutions in Filippov systems (being one of the objectives of the thesis), first bifurcations of fixed points in non-smooth continuous systems are studied. The Poincaré map relates the bifurcations of fixed points in non-smooth continuous systems to bifurcations of periodic solutions in Filippov systems.

Bifurcations of fixed points of non-smooth continuous systems are treated and it is shown that discontinuous bifurcations of fixed points occur in non-smooth continuous systems. Explicit expressions are found for the bifurcation points of the simplest types of non-smooth continuous systems. The encountered elementary discontinuous bifurcations are compared with their smooth counterpart.

Some important fundamental questions about bifurcations of fixed points in non-smooth systems are addressed. It is shown that a bifurcation in non-smooth continuous systems can be discontinuous in the sense that an eigenvalue jumps over the imaginary axis under the variation of a parameter. A discontinuous counterpart is found for the saddle-node, transcritical, pitchfork and Hopf bifurcation. Also, a bifurcation is found which cannot directly be interpreted as a discontinuous counterpart of a bifurcation in a smooth system. A conjecture about the existence of discontinuous bifurcations of fixed points is formulated and an attempt to a partial classification of those bifurcations is made.

Finally we have the important ingredients to study bifurcations of periodic solutions in discontinuous systems of Filippov-type. Branches of periodic solutions in Filippov systems expose discontinuous bifurcations. The basic idea is that Floquet multipliers (eigenvalues of the fundamental solution matrix) of periodic solutions in Filippov systems can jump when a parameter of the system is varied. Such a jump can occur if a periodic solution becomes tangential to the tip of a non-smooth hypersurface on which the vector field is discontinuous. If a Floquet multiplier jumps over the unit circle in the complex plane, a discontinuous bifurcation is encountered. We explore how the discontinuous bifurcations arise through jumps of the fundamental solution matrix and show how discontinuous bifurcations are related to conventional

bifurcations in smooth systems.

Several mechanical examples are discussed which show discontinuous fold, flip and symmetry-breaking bifurcations. It is shown that in a stick-slip system a bifurcation exists which connects a branch of stable periodic solutions to a branch of unstable periodic solutions with a Floquet multiplier at infinity. Filippov theory turns out to be essential for the understanding of this type of bifurcation as it is caused by the non-uniqueness of solutions. A combined discontinuous fold–flip bifurcation is investigated and it is explained how it can be described by the tent map. The observations from the preceding examples help to discuss fundamental questions about bifurcations of periodic solutions in discontinuous systems.

Samenvatting

Fysische fenomenen zoals droge wrijving, botsing en speling in mechanische systemen of dioden in elektrische circuits worden vaak bestudeerd door middel van mathematische modellen met een discontinu karakter. Filippov-systemen vormen een deelklasse van discontinue dynamische systemen, die worden beschreven door een stelsel eerste-orde gewone differentiaalvergelijkingen met een discontinu rechterlid.

Mechanische systemen met droge wrijving vormen een belangrijk voorbeeld van Filippov-systemen. Droge wrijving kan zich-zelf-in-stand-houdende trillingen veroorzaken die zeer schadelijk kunnen zijn voor mechanische systemen. Echter ook andere praktische problemen in de ingenieurspraktijk zijn gerelateerd aan trillingen die worden veroorzaakt of beïnvloed door het discontinue karakter van fysische fenomenen. Het is daarom wenselijk te weten of er periodieke oplossingen van een systeem met droge wrijving (of Filippov-systemen in het algemeen) bestaan voor een bepaalde parameter-set en hoe deze periodieke oplossingen veranderen voor een veranderende systeemparameter. Dit soort parameterstudies wordt meestal uitgevoerd door middel van continueringmethoden waarmee een tak van evenwichtspunten of periodieke oplossingen wordt gevolgd voor een veranderende systeemparameter. Een tak van evenwichtspunten of periodieke oplossingen kan omvouwen of vertakken bij een kritische waarde van de systeemparameter. Deze kwalitatieve verandering in het dynamische gedrag van het systeem wordt ‘bifurcatie’ genoemd. Bifurcaties die optreden in gladde systemen zijn goed begrepen maar weinig is bekend over bifurcaties in discontinue dynamische systemen.

Het doel van dit proefschrift is om verschillende aspecten te onderzoeken van bifurcaties van evenwichtspunten in niet-gladde continue systemen en van periodieke oplossingen in Filippov-systemen. In Filippov-systemen komen niet-conventionele bifurcaties voor die we ‘discontinue bifurcaties’ noemen. Deze verschillen van de conventionele bifurcaties die in gladde systemen optreden. In dit proefschrift worden de theorie van Filippov, gegeneraliseerde afgeleiden en de theorie van Floquet gecombineerd, wat leidt tot nieuwe inzichten in bifurcaties in discontinue systemen.

Eerst wordt een overzicht gegeven van Filippov’s oplossingsconcept voor differentiaalvergelijkingen met een discontinu rechterlid. Systemen met droge wrijving vragen om speciale aandacht. Differentiaalvergelijkingen met een discontinu rechterlid worden door middel van de convexe methode van Filippov uitgebreid naar differentiaal-inclusies. De existentie van oplossingen van differentiaal-inclusies is onder bepaalde voorwaarden gegarandeerd maar de uniciteit van oplossingen is niet gegarandeerd.

Niet-uniciteit speelt een belangrijke rol in het bifurcatiegedrag van Filippov-systemen.

De lokale stabiliteit van een periodieke oplossing wordt bepaald (voor het hyperbolische geval) door de fundamentealmatrix. De fundamentealmatrix is ook van belang voor het begrip van bifurcaties van periodieke oplossingen. Discontinuïteiten in het vectorveld van Filippov-systemen veroorzaken sprongen in de fundamentealmatrix. Het discontinue gedrag van de fundamentealmatrix wordt behandeld en verduidelijkt door middel van mechanische voorbeelden.

De sprongen in de fundamentealmatrix kunnen worden onderzocht door middel van de lineaire approximatie-methode, die een discontinue systeem benadert door een niet-glad continue systeem. De lineaire approximatie-methode vervangt een discontinuïteit in het vectorveld door een dunne laag waarin het vectorveld lineair varieert tussen de linker en rechter limiet op de randen van de dunne laag. Het blijkt dat een sprong in de fundamentealmatrix kan worden uitgedrukt als een convexe combinatie van de fundamenteal matrices voor en na de sprong. De lineaire approximatie-methode en de relatie tussen niet-gladde analyse en gegeneraliseerde afgeleiden worden behandeld in het proefschrift.

Verschillende definities voor de term bifurcatie bestaan in de literatuur en deze definities kunnen inconsistent zijn voor Filippov-systemen. In dit proefschrift is gekozen voor een definitie die toepasbaar is op Filippov-systemen.

Als opstap naar de studie van bifurcaties van periodieke oplossingen in Filippov-systemen (hetgeen een doel is van het proefschrift) worden eerst bifurcaties van evenwichtspunten in niet-gladde continue systemen bestudeerd. De Poincaré-afbeelding relateert bifurcaties van evenwichtspunten in niet-gladde continue systemen aan bifurcaties van periodieke oplossingen in Filippov-systemen.

Bifurcaties van evenwichtspunten in niet-gladde continue systemen worden behandeld en aangetoond wordt dat discontinue bifurcaties bestaan in niet-gladde continue systemen. Expliciete uitdrukkingen worden gevonden voor de bifurcatiepunten in de eenvoudigste typen niet-gladde continue systemen. De elementaire discontinue bifurcaties worden vergeleken met hun glatte tegenhanger.

Een aantal belangrijke fundamentele vragen over bifurcaties in niet-gladde continue systemen wordt besproken. Bifurcaties in niet-gladde continue systemen blijken discontinue te kunnen zijn, in de zin dat een eigenwaarde over de imaginaire as springt bij variatie van een systeemparemeter. Een discontinue tegenhanger is gevonden voor de zadel-knoop-, transkritische-, stemvork- en Hopf-bifurcatie. Ook is er een bifurcatie gevonden die niet direct kan worden geclassificeerd als een discontinue tegenhanger van een bifurcatie in een glad systeem. Een vermoeden wordt uitgesproken over de existentie van discontinue bifurcaties van evenwichtspunten en een poging wordt gedaan tot gedeeltelijke classificatie van deze bifurcaties.

Belangrijke ingediënten voor de bestudering van bifurcaties van periodieke oplossingen in discontinue Filippov-systemen zijn nu voorradig. Op takken van periodieke oplossingen in Filippov-systemen doen zich discontinue bifurcaties voor. De achterliggende gedachte is dat er zich sprongen voordoen in de Floquet-multipliatoren (die de eigenwaarden zijn van de fundamentealmatrix) van een periodieke oplossing in een Filippov-systeem onder invloed van een veranderende systeemparemeter. Deze sprongen treden op als de periodieke oplossing een tip raakt van een niet-glad hypervlak dat de discontinuïteit definiëert in het vectorveld. Als een

Floquet-multiplicator over de eenheidscirkel springt in het complexe vlak, dan treedt er een discontinue bifurcatie op. In het proefschrift wordt uitgelegd hoe discontinue bifurcaties ontstaan door sprongen in de fundamentealmatrix, terwijl voorts de relatie tussen discontinue bifurcaties en conventionele bifurcaties in gladde systemen wordt beschouwd.

Een aantal mechanische voorbeelden wordt besproken die discontinue ‘fold’-, ‘flip’- en ‘symmetry-breaking’-bifurcaties illustreren. In een stick-slip-systeem treedt een bifurcatie op die een tak met stabiele periodieke oplossingen verbindt met een tak met instabiele periodieke oplossingen waarvan een Floquet-multiplicator oneindig groot is. De theorie van Filippov blijkt essentieel te zijn voor het begrijpen van dit soort bifurcaties, daar deze wordt veroorzaakt door de niet-uniciteit van de oplossing. Een gecombineerde discontinue fold–flip bifurcatie wordt behandeld en de relatie met de tent-afbeelding wordt besproken. De waargenomen bifurcaties uit de voorbeelden geven een ondersteuning voor een discussie over fundamentele vragen met betrekking tot bifurcaties van periodieke oplossingen in discontinue systemen.

Chapter 1

Introduction

‘If one looks at the different problems of the integral calculus which arise naturally when one wishes to go deep into the different parts of physics, it is impossible not to be struck by the analogies existing. Whether it be electrostatics or electrodynamics, the propagation of heat, optics, elasticity, or hydrodynamics, we are led always to differential equations of the same family.’

HENRI POINCARÉ
American Journal of Physics 12 (1890) 211.

In this introductory chapter we give a motivation for the thesis. After discussing different types of discontinuous systems and their characteristics, we define the objective of the thesis. An outline of the succeeding chapters is given next.

1.1 Motivation

Dry friction is a nonlinearity which is abundant in nature, machines and other processes. Although friction may be a desirable property in brakes and violins, it is generally an impediment. The presence of dry friction can induce self-sustained vibrations like machine tool chattering, squealing noise of rail wheels, torsional vibration in oilwell drillstrings and many other vibrations which are highly detrimental to the performance of mechanical systems. Dry friction is therefore an important topic in scientific and engineering research.

Tribologists conducted many experiments on sliding contact during the last decades and explained the observed frictional phenomena with respect to surface chemistry and physics. The classical Amontons-Coulomb model was validated but also more complex tribological models are now available which take some of the

underlying mechanisms of friction into account. Mechanical engineers and applied mathematicians have been concerned with the dynamical behaviour of systems with friction. Studies on frictional dynamics are almost all based on the classical Amontons-Coulomb model for dry friction. The Amontons-Coulomb model has the advantage to have a limited amount of parameters and to account only for the essential features of dry friction, while more complex friction models are only validated for one type of material combination and are therefore not generally applicable. Furthermore, the Amontons-Coulomb model allows for an efficient numerical integration of the equations of motion of a system subjected to dry friction.

Application of the Amontons-Coulomb model to dynamical models of systems with dry friction results in differential equations of Filippov-type. Filippov systems form a class of discontinuous systems described by differential equations with a discontinuous right-hand side. To the class of Filippov systems do not only belong mechanical systems with Amontons-Coulomb friction but also electrical circuits with diode elements, controlled systems with switching control laws, mechatronical systems with encoders and many other systems, being mechanical or non-mechanical, where a kind of switching is involved.

The undesired friction-induced vibrations can be prevented by changing the design of the system or can be combatted with the aid of control theory. Knowledge on the dynamical behaviour of the system is therefore essential to improve the performance. Profound insight in the dynamical behaviour of dynamical systems can be gained from modern analysis techniques developed in the nonlinear dynamics community. The theoretical knowledge and available methods are however only applicable to smooth dynamical systems. This motivates a theoretical study on the nonlinear dynamics of Filippov systems.

The nonlinear dynamics of mechanical Filippov systems is explored in this thesis. Systems with dry friction constitute an important example of mechanical Filippov systems and are used as key applications of the theory throughout the thesis. Firstly, we try to provide a theoretical basis for practical investigations of systems of this class. Secondly, it may form a starting point for in-depth mathematical investigations. Hence, in the thesis we attempt to establish a bridge between engineering-oriented and mathematics-oriented research in this field.

The next section reviews some basic terminology in the theory on nonlinear dynamics and bifurcations.

1.2 Nonlinear Dynamics and Bifurcations

Mathematical models are frequently used in many disciplines of science to study complex behaviour of systems. Systems that can be modeled by nonlinear differential equations are called *nonlinear dynamical systems*. Examples of such systems occur in economics (economical models of markets), biology (predator-prey models), chemistry (A-B-C reactions), electronics (electrical circuits with nonlinear elements) and mechanics (models of machines or moving bodies in general).

A dynamical system starting from a particular initial state can evolve towards a steady state or to irregular chaotic motion. This steady state may be a stationary

state, called *fixed point* in this thesis but also often referred to as equilibrium. The state of the system may also evolve towards a periodic state, called *periodic solution* in this thesis, or to a quasi-periodic state. Stationary and (quasi-)periodic states can be stable, thereby attracting neighbouring solutions, or be unstable. The knowledge of the steady states of a system for a certain parameter set is important as they partly determine the long term dynamical behaviour of the system.

It is often desirable to know how the fixed points and (quasi-)periodic solutions of a system change when a parameter of the system is changed. Such parameter studies are usually conducted by means of path-following techniques where a branch of fixed points or periodic solutions is followed while varying a parameter. The number and type of fixed points and (quasi-)periodic solutions (being stable or unstable) can change at a certain parameter value. This qualitative change in the structural behaviour of the system is called *bifurcation*, an originally French word introduced by Poincaré [1899].

Bifurcations occur in many physical systems. Examples of bifurcations can be found in morphodynamics (the forming of meanders in rivers), structural mechanics (the buckling of a beam), flutter oscillation of suspension bridges, hunting motion of rail-way bogies and cardiac arrhythmias in malfunctioning hearts.

1.3 Discontinuous Systems

In this thesis bifurcations in discontinuous¹ and non-smooth dynamical systems are studied. A dynamical system can be expressed as a set of first-order ordinary differential equations. Before proceeding we should clarify what we mean with the term '*discontinuous dynamical system*' (see Van der Schaft and Schumacher [1997]).

Physical systems can often operate in different modes, and the transition from one mode to another can sometimes be idealized as an instantaneous, discrete transition. Examples include mechanical systems with dry friction, impact and backlash or electrical circuits with diode elements. Since the time scale of the transition from one mode to another is often much smaller than the scale of the dynamics of the individual modes, it may be very advantageous to model the transitions as being instantaneous. For instance, diode elements are often modeled as being ideal diodes and mathematical models of mechanical systems subjected to dry friction are considered to switch between a slip mode and a (pure) stick mode. The mathematical modeling of physical systems therefore may lead to discontinuous dynamical systems, which switch between different modes, where the dynamics in each mode is associated with a different set of differential equations.

Discontinuous dynamical systems can be divided in three types according to their degree of discontinuity:

1. Non-smooth continuous systems with a discontinuous Jacobian, like systems with purely elastic one-sided supports. Those systems are described by a continuous vector field but the vector field is non-smooth.

¹A function $f(x)$ is *continuous* at $x \in X$ provided that for all $\varepsilon > 0$, there exists $\delta > 0$ so that $y \in B(x; \delta)$ implies $|f(x) - f(y)| \leq \varepsilon$. Roughly speaking, for single-valued functions this means that we can draw the graph of the function without taking the pencil of the paper. A function $f(x)$ is *smooth* if it is continuously differentiable up to any order in x .

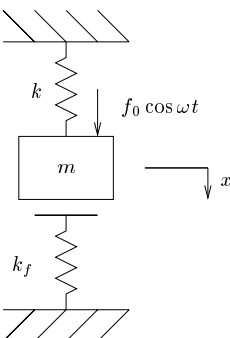
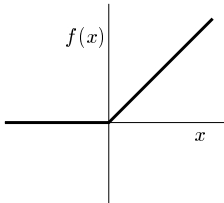
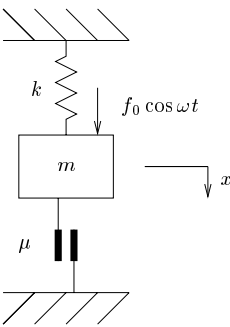
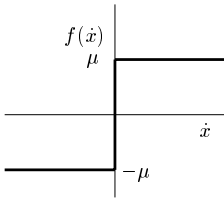
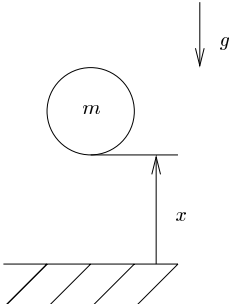
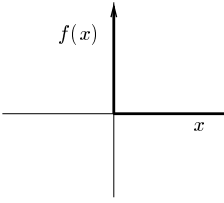
model	description	function
<p>(1) elastic support</p> 	$m\ddot{x} + kx = f_0 \cos \omega t - f(x)$ $f(x) = \begin{cases} 0 & x \leq 0 \\ k_f x & x > 0 \end{cases}$	<p>non-smooth continuous</p> 
<p>(2) dry friction</p> 	$m\ddot{x} + kx = f_0 \cos \omega t - f(\dot{x})$ $f(\dot{x}) \in \begin{cases} -\mu & \dot{x} < 0 \\ [-\mu, \mu] & \dot{x} = 0 \\ \mu & \dot{x} > 0 \end{cases}$	<p>discontinuous of Filippov-type</p> 
<p>(3) impact</p> 	$m\ddot{x} = -g + mf(x)$ $x(t_k) = 0$ $\dot{x}_+(t_k) = -e\dot{x}_-(t_k)$ $f(x) = (\dot{x}_+(t_k) - \dot{x}_-(t_k))\delta_{t_k}$ $x(t) \geq 0, \quad f(x) \geq 0,$ $xf(x) = 0$	<p>impulsive</p> 

Table 1.1: Non-smooth and discontinuous systems.

2. Systems described by differential equations with a discontinuous right-hand side, also called *Filippov systems* (Chapter 2). The vector field of those systems is discontinuous. Examples are systems with visco-elastic supports and dry friction.
3. Systems which expose discontinuities (or jumps) in the state, like impacting systems with velocity reversals (not treated in this thesis).

Table 1.1 shows examples of each type of system together with its characteristic function for the force at the discontinuity. The first example is a mass on a one-sided elastic spring, where the spring force is a non-smooth continuous function of the position. The second example is a mass with a dry friction damper, where the dry friction force is a discontinuous function of velocity. The third example is an impacting ball on a floor, where the contact force exhibits a Dirac pulse at the instant of impact. In all three cases a kind of switching is involved and those systems are therefore often called *switching systems* or *differential equations with switching conditions* [Eich-Soellner and Führer, 1998]. In the field of systems and control theory, the term *hybrid system* is frequently used for systems composed of continuous differential equations and discrete event parts [Brogliato, 1999]. Nowadays, the term *hybrid system* is used for any system which exposes a mixed continuous and discrete nature, even if the system is not controlled [Heemels, 1999]. Discontinuous (or switching/hybrid) systems can be considered as dynamical extensions of Linear Complementarity Problems, which gives another term : *complementarity systems* ([Heemels, 1999] and references therein).

1.4 Literature Survey

Discontinuous systems

The amount of publications on discontinuous systems is vast. Only a review of the literature in the mathematical and mechanical field is given here.

The mathematical literature is mainly concerned with existence and uniqueness of solutions of discontinuous differential equations. The fundamental work of Filippov [Filippov, 1964, 1988; Sastry, 1999] extends a discontinuous differential equation to a differential inclusion (see Chapter 2). More results on differential inclusions can be found in Aubin and Cellina [1984] and Clarke et al. [1998]. Deimling and Szilagyı [1994], Fečkan [1998] and Kunze and Küpper [1997] treat dry friction problems as differential inclusions and address existence of periodic solutions. Aizerman and Gantmakher [1958] derived jumping conditions of fundamental solution matrices (see Chapter 3) and their results were extended to systems with a discontinuous state by Müller [1995]. Contemporary literature in the field of control theory focuses on hybrid systems and complementarity systems, which encompasses also Filippov systems [Heemels, 1999; Van der Schaft and Schumacher, 1997].

Publications in the field of mechanical systems are mainly concerned with dry friction/stick-slip oscillations and impact. An extensive literature review on dry friction models can be found in [Armstrong et al., 1994; Feeny and Guran, 1997; Ibrahim, 1994a,b]. Dynamics of impacting systems (not treated in this thesis) is reviewed exhaustively by Brogliato [1999]. Glocker [1995] and Pfeiffer and Glocker [1996] apply

the theory of Linear Complementarity to multibody systems with impact and friction. Non-existence of solutions of impacting systems is discussed in [Brogliato, 1999; Génot and Brogliato, 1999].

Bifurcations

During the last decades many textbooks about bifurcation theory for smooth systems appeared and bifurcations of periodic solutions in smooth vector fields are well understood [Guckenheimer and Holmes, 1983; Hagedorn, 1988; Kuznetsov, 1995; Seydel, 1994]. However, little understanding exists about bifurcations of periodic solutions in discontinuous vector fields.

Andronov et al. [1987] treat periodic solutions of discontinuous systems. They revealed many aspects of discontinuous systems and addressed periodic solutions with sliding modes (Chapter 2) but did not treat periodic solutions in discontinuous systems with regard to Floquet theory underlying those solutions.

Many publications deal with bifurcations in discontinuous systems of Filippov-type. Published bifurcation diagrams were often constructed from data obtained by brute force techniques and only show stable branches of periodic solutions [Begley and Virgin, 1997, 1998; Blazejczyk-Okolewska and Kapitaniak, 1996; Dankowicz and Nordmark, 2000; Galvanetto et al., 1995; Galvanetto and Knudsen, 1997; Hinrichs, 1997; Hinrichs et al., 1998; Kunze and Küpper, 1997; Oancea and Laursen, 1998; Popp, 1992; Popp and Stelzer, 1990; Popp et al., 1995; Stelzer, 1992; Wiercigroch, 1994, 1996, 1997] (this list is far from complete). Bifurcation diagrams calculated with path-following techniques show bifurcations to unstable periodic solutions but the bifurcations behave as conventional bifurcations in smooth systems [Stelzer and Sestro, 1991; Van de Vrande et al., 1999].

Dankowicz and Nordmark [2000] study bifurcations of stick-slip oscillations but the applied friction model, with internal states which allow for history and rate dependence, yields a non-smooth continuous system. A small number of publications show non-conventional bifurcations in Filippov systems [Elmer, 1997; Yoshitake and Sueoka, 2000]. Yoshitake and Sueoka [2000] also address Floquet theory and remark that the Floquet multipliers ‘jump’ at the bifurcation point.

The work of Feigin [1974, 1978, 1995] and Di Bernardo et al. [1999a,b] studies non-conventional bifurcations in Filippov systems and refers to those bifurcations as ‘C-bifurcations’ (see Chapter 6). Non-conventional bifurcations of non-smooth discrete mappings were also addressed by Nusse and York [1992].

Another type of non-conventional bifurcation is the ‘grazing bifurcation’ which occurs in impacting systems. Bifurcations in impacting systems are studied by [Brogliato, 1999; Ivanov, 1993, 1996; Foale and Bishop, 1994; Meijaard, 1996; Molenaar et al., 1999; Nordmark, 1997; Peterka, 1996].

Numerical methods to calculate periodic solutions in discontinuous systems can be found in [Eich-Soellner and Führer, 1998; Leine et al., 1998; Meijaard, 1997; Reithmeier, 1991].

The body of this thesis has been published in [Leine et al., 1998; Leine and Van Campen, 1999, 2000; Leine et al., 2000].

1.5 Objective and Scope of the Thesis

The theory of bifurcations in smooth dynamical systems is well developed. This is not the case for bifurcations in discontinuous dynamical systems. Many practical problems in engineering are related to vibrations caused or influenced by physical discontinuities. Depending on the way of modeling, a mathematical model of the physical system may fall in one of the three classes of discontinuous dynamical systems mentioned in the Section 1.3. This urges for a description of the bifurcation behaviour of discontinuous dynamical systems. Existence of solutions for systems with a discontinuous state is not guaranteed, which complicates the study of bifurcations of those systems. In this sense Filippov systems are less complex as existence of solutions is guaranteed (under some conditions, see chapter 2). We will therefore confine our study to Filippov systems and non-smooth continuous systems (which can be regarded as a subclass of Filippov systems). Filippov systems embrace systems with dry friction and compliant impact but not systems with impact between rigid bodies. Filippov systems arise also in models of electrical circuits with (ideal) diode elements, controlled systems with encoders and in other scientific fields. In this thesis, however, we will focus on mechanical systems although the results apply to Filippov systems in general. As mentioned before, an important category is the class of systems with dry friction and we will address these types of systems in Sections 2.3, 2.4, 3.4 and 6.7 to 6.9. We will especially pay much attention to periodic solutions of systems with dry friction. Bifurcations of periodic solutions of Filippov systems are closely related to bifurcations of fixed points in non-smooth continuous systems (discontinuous Jacobian). We will therefore also address bifurcations of fixed points in non-smooth continuous systems.

The *objective of the thesis* is to investigate different aspects of bifurcations of

1. fixed points in non-smooth continuous systems
2. periodic solutions in discontinuous systems of Filippov-type

and to study the relation between bifurcations in 1) and 2).

Filippov systems expose non-conventional bifurcations, which we will call *discontinuous bifurcations*. The basic idea is that Floquet multipliers of Filippov systems can jump when a parameter of the system is varied. If a Floquet multiplier jumps over the unit circle in the complex plane a discontinuous bifurcation is encountered. In the thesis it is explained how the discontinuous bifurcations come into being through jumps of the fundamental solution matrix and it is shown how discontinuous bifurcations are related to conventional bifurcations in smooth systems.

1.6 Outline of the Thesis

The thesis contains an introductory part which surveys the theory of Filippov and of Aizerman and Gantmakher. It then proceeds with an investigation of bifurcations in discontinuous dynamical systems which is the actual body of the thesis.

First, the theory of Filippov is briefly discussed in Chapter 2. This theory gives a generalized definition of the solution of differential equations with a discontinuous right-hand side. Numerical methods are also addressed.

The fundamental solution matrix is essential for the understanding of bifurcations of periodic solutions. Discontinuities of the vector field cause jumps in the fundamental solution matrix. The discontinuous behaviour of the fundamental solution matrix is explained in Chapter 3. The underlying theory is due to Aizerman and Gantmakher. Some elucidating examples on jumps in the fundamental solution matrix are given in Section 3.4 and 3.5. After this, the introductory part ends and the actual body of the thesis begins: a treatment of bifurcations in discontinuous and non-smooth systems.

Chapter 4 discusses a linear approximation which approximates a discontinuous system by a stiff continuous system or a non-smooth continuous system by a smooth system. The relation with non-smooth analysis and generalized differentials is discussed.

Chapter 5 deals with bifurcations of fixed points of non-smooth continuous systems. Explicit expressions are found for the bifurcation points of the simplest types of non-smooth continuous systems. The results on bifurcations of fixed points of non-smooth continuous systems are used as a stepping stone to bifurcations of periodic solutions of Filippov systems. The treatise is restricted to one-parameter bifurcations. The simplest discontinuous bifurcations are treated next to their smooth counterparts which enlarges the insight (although the theory for smooth systems is well known). The saddle-node, transcritical, pitchfork and Hopf bifurcations are discussed. A conjecture about the existence of discontinuous bifurcations of fixed points is formulated and an attempt to a partial classification of those bifurcations is made.

How bifurcations of periodic solutions of Filippov systems come into being is explained in Chapter 6. The Poincaré map relates the bifurcations of fixed points in non-smooth continuous systems to bifurcations of periodic solutions in Filippov systems. A comparison is made between continuous bifurcations in smooth systems and discontinuous bifurcations in Filippov systems.

Several mechanical examples are discussed which show discontinuous fold, flip and symmetry-breaking bifurcations (Sections 6.6 to 6.9). It is shown that bifurcations exist which connect a branch with stable periodic solutions to a branch with infinitely unstable periodic solutions (Section 6.7). Filippov theory turns out to be essential for the understanding of infinitely unstable periodic solutions. A combined discontinuous fold–flip bifurcation is addressed in Section 6.9 and it is explained how it can be described by the tent map.

Finally, in Chapter 7 a short overview of the thesis is given and the contributions of the thesis are summarized. Several open problems are recommended for further research and recommendations are given about terminology.

The theory developed in the preceding chapters is applied in Appendix A to a simple model of drillstring dynamics.

Chapter 2

Filippov Theory

‘He who loves practice without theory is like the sailor who boards ship without a rudder and compass and never knows where he may cast.’

LEONARDO DA VINCI (1452–1519)

This chapter discusses a solution concept for differential equations with a discontinuous right-hand side. After discussing an example which illustrates the basic problem, a concise review will be given of Filippov’s convex method which extends a discontinuous differential equation to a differential inclusion. Existence and uniqueness problems will be addressed. A numerical technique is presented for the integration of differential inclusions. Special attention is given to the relation between differential inclusions and friction models. A ‘switch model’ is developed to allow for an efficient solution of dry friction problems.

2.1 The Construction of a Solution

A dynamical system is usually expressed as the following set of ordinary differential equations

$$\dot{\underline{x}}(t) = \underline{f}(t, \underline{x}(t)) \quad \underline{x}(t) \in \mathbb{R}^n \quad (2.1)$$

where \underline{x} is the n -dimensional state vector and $\underline{f}(t, \underline{x}(t))$ is the vector of right-hand sides describing the time derivative of the state vector. A dot (·) denotes differentiation with respect to time t . We will assume that $\underline{f}(t, \underline{x})$ is linearly bounded [Clarke et al., 1998], i.e. there exist positive constants γ and c such that

$$\|\underline{f}(t, \underline{x})\| \leq \gamma \|\underline{x}\| + c \quad \forall (t, \underline{x}). \quad (2.2)$$

If the vector field is smooth, that is \underline{f} is continuously differentiable up to any order both in \underline{x} and t , then a solution $\underline{x}(t)$ of the system (2.1) exists for any given initial

condition and is globally unique. In fact, smoothness of the vector field is not a necessary condition for existence and uniqueness of the solution, as can be concluded from the following theorem by Clarke et al. [1998] (theorem 1.1, page 178):

Theorem 2.1 (Existence and uniqueness of continuous systems)

Suppose that $\tilde{f}(t, \underline{x})$ is continuous, and let $(t_0, \underline{x}_0) \in \mathbb{R} \times \mathbb{R}^n$ be given. Then the following holds:

1. There exists a solution of (2.1) on an open interval $(t_0 - \delta, t_0 + \delta)$, for $\delta > 0$, satisfying $\underline{x}(t_0) = \underline{x}_0$.
2. If in addition we assume that $\tilde{f}(t, \underline{x})$ is linearly bounded, so that (2.2) holds, then there exists a solution of (2.1) on $(-\infty, \infty)$ such that $\underline{x}(t_0) = \underline{x}_0$.
3. Let us now add the hypothesis that $\tilde{f}(t, \underline{x})$ is locally Lipschitz, i.e. there exists a constant $L > 0$ such that

$$\|\tilde{f}(t, \underline{x}) - \tilde{f}(t, \underline{y})\| \leq L\|\underline{x} - \underline{y}\|, \forall \underline{x}, \underline{y} \in \mathbb{R}^n.$$

Then there exists a unique solution of (2.1) on $(-\infty, \infty)$ such that $\underline{x}(t_0) = \underline{x}_0$.

Remark that the continuous systems implied in the above theorem can be allowed to be *non-smooth*.

However, differential equations stemming from physical systems may be discontinuous, i.e. the right-hand side \tilde{f} can be discontinuous in \underline{x} . The theory of Filippov [Filippov, 1964, 1988; Sastry, 1999] gives a generalized¹ definition of the solution of differential equations which incorporates systems with a discontinuous right-hand side. The solution $\underline{x}(t)$ in the sense of Filippov to a differential equation with a discontinuous right-hand side (also called Filippov systems, see Chapter 1) is continuous in time. Systems with a discontinuous solution, i.e. ‘jumps’ in $\underline{x}(t)$ at certain time instances t (occurring for systems with impact between rigid bodies), are not described by the theory of Filippov. Filippov’s theory will be briefly outlined in this chapter.

In order to make things be as clear as possible, we first look at a very simple one-dimensional example (see Kunze and Küpper [1997]). Consider the following differential equation with a discontinuous right-hand side

$$\begin{aligned} \dot{x} = f(x) &= 1 - 2 \operatorname{sgn}(x) \\ &= \begin{cases} 3 & x < 0 \\ 1 & x = 0 \\ -1 & x > 0 \end{cases} \end{aligned} \quad (2.3)$$

¹Note : ‘generalized’ in the sense that the definition holds for a larger class of differential equations.

with $\text{sgn}(0) = 0$. For a given initial condition $x(0) \neq 0$ we can obtain a solution of the IVP (initial value problem)

$$x(t) = \begin{cases} 3t + C_1 & x < 0 \\ -t + C_2 & x > 0 \end{cases} \quad (2.4)$$

with constants C_1 and C_2 being determined by the initial condition. Each solution reaches $x = 0$ in finite time. If the solution arrives at $x = 0$, it can not leave $x = 0$, because $\dot{x} > 0$ for $x < 0$ and $\dot{x} < 0$ for $x > 0$. The solution will therefore stay at $x = 0$, which implies $\dot{x}(t) = 0$. Note that $x(t) = 0$ with $\dot{x}(t) = 0$ is not a solution in the classical sense since $0 \neq 1 - 2 \text{sgn}(0)$. The natural idea to extend the notion of solution is to replace the right-hand side $f(x)$ by a *set-valued* function $F(x)$ such that $F(x) = \{f(x)\}$ if f is continuous in x . If f is discontinuous in x a suitable choice of $F(x)$ is required. The differential equation is then replaced by the differential inclusion ([Filippov, 1964, 1988])

$$\dot{x} \in F(x). \quad (2.5)$$

Define the set-valued² sign function

$$\text{Sgn}(x) = \begin{cases} \{-1\} & x < 0 \\ [-1, 1] & x = 0 \\ \{1\} & x > 0 \end{cases} \quad (2.6)$$

which is set-valued at $x = 0$. With this definition $x(t) = 0$ is a unique global solution of the differential inclusion

$$\dot{x} \in 1 - 2 \text{Sgn}(x) \quad (2.7)$$

with initial condition $x(0) = 0$.

The above example is one-dimensional. We now need to define a differential equation with a discontinuous right-hand side in a more general sense for any dimension n . We restrict ourselves to differential equations with a right-hand side that is discontinuous on a number of hyper-surfaces. We start with a single hyper-surface. The state space \mathbb{R}^n is split into two subspaces \mathcal{V}_- and \mathcal{V}_+ by a hyper-surface Σ such that $\mathbb{R}^n = \mathcal{V}_- \cup \Sigma \cup \mathcal{V}_+$. The hyper-surface Σ is defined by a scalar indicator function $h(\underline{x}(t))$.³ The state $\underline{x}(t)$ is in Σ when

$$h(\underline{x}(t)) = 0. \quad (2.8)$$

The normal \underline{n} perpendicular to the hyper-surface Σ is given by

$$\underline{n} = \underline{n}(\underline{x}(t)) = \text{grad}(h(\underline{x}(t))). \quad (2.9)$$

²With the set $[a, b]$ we mean the interval $\{x \in \mathbb{R} \mid a \leq x \leq b\}$. With $\{a, b\}$ we mean the set comprising the elements a and b .

³The indicator function $h(\underline{x})$ is considered to be autonomous. Non-autonomous systems can give rise to non-autonomous indicator functions. However, non-autonomous time-periodic systems can be transformed into autonomous systems having autonomous indicator functions (see Appendix B.1).

An indicator function h to define a certain hyper-surface Σ is not unique. Different indicator functions can define the same Σ . We assume that the indicator function $h(\underline{x}(t))$ is chosen such that it always holds that

$$\text{grad}(h(\underline{x}(t))) \neq \underline{0}. \quad (2.10)$$

The subspaces \mathcal{V}_- and \mathcal{V}_+ and hyper-surface Σ can be formulated as

$$\begin{aligned} \mathcal{V}_- &= \{\underline{x} \in \mathbb{R}^n \mid h(\underline{x}(t)) < 0\} \\ \Sigma &= \{\underline{x} \in \mathbb{R}^n \mid h(\underline{x}(t)) = 0\} \\ \mathcal{V}_+ &= \{\underline{x} \in \mathbb{R}^n \mid h(\underline{x}(t)) > 0\} \end{aligned} \quad (2.11)$$

The function $\underline{f}(t, \underline{x})$ is assumed to be locally continuous, smooth and linearly bounded for all $\underline{x} \notin \Sigma$. From this assumption it follows that the solution $\underline{x}(t)$ within each subspace \mathcal{V}_- and \mathcal{V}_+ exists and is unique (cf. Theorem 2.1).

The set-valued extension of $\underline{f}(t, \underline{x})$ of (2.1) for $\underline{x} \in \Sigma$ is given by the closed convex hull of all the limits

$$\underline{F}(t, \underline{x}) = \overline{\text{co}}\{\underline{y} \in \mathbb{R}^n \mid \underline{y} = \lim_{\underline{\hat{x}} \rightarrow \underline{x}} \underline{f}(t, \underline{\hat{x}}), \underline{\hat{x}} \in \mathbb{R}^n \setminus \Sigma\} \quad (2.12)$$

where $\overline{\text{co}}(A)$ denotes the smallest closed convex set containing A . All the limits exist because $\underline{f}(t, \underline{x})$ is assumed to be locally continuous, smooth and linearly bounded for all $\underline{x} \notin \Sigma$.

We are now able to consider the following n -dimensional nonlinear system with discontinuous right-hand side

$$\dot{\underline{x}}(t) = \underline{f}(t, \underline{x}(t)) = \begin{cases} \underline{f}_-(t, \underline{x}(t)) & \underline{x} \in \mathcal{V}_- \\ \underline{f}_+(t, \underline{x}(t)) & \underline{x} \in \mathcal{V}_+, \end{cases} \quad (2.13)$$

with the initial condition $\underline{x}(0) = \underline{x}_0$. As mentioned before, the right-hand side $\underline{f}(t, \underline{x})$ is assumed to be discontinuous but such that it is piecewise continuous and smooth on \mathcal{V}_- and \mathcal{V}_+ and discontinuous on Σ . The function $\underline{f}_-(t, \underline{x})$ is therefore assumed to be C^1 on $\mathcal{V}_- \cup \Sigma$ and $\underline{f}_+(t, \underline{x})$ is assumed to be C^1 on $\mathcal{V}_+ \cup \Sigma$. It is not required that $\underline{f}_-(t, \underline{x})$ and $\underline{f}_+(t, \underline{x})$ agree on Σ . The system described by (2.13) does not define $\underline{f}(t, \underline{x}(t))$ if $\underline{x}(t)$ is on Σ . We can overcome this problem with the following set-valued extension $\underline{F}(t, \underline{x})$

$$\dot{\underline{x}}(t) \in \underline{F}(t, \underline{x}(t)) = \begin{cases} \underline{f}_-(t, \underline{x}(t)) & \underline{x} \in \mathcal{V}_- \\ \overline{\text{co}}\{\underline{f}_-(t, \underline{x}(t)), \underline{f}_+(t, \underline{x}(t))\} & \underline{x} \in \Sigma \\ \underline{f}_+(t, \underline{x}(t)) & \underline{x} \in \mathcal{V}_+, \end{cases} \quad (2.14)$$

where the convex set with two right-hand sides \underline{f}_- and \underline{f}_+ can be cast in

$$\overline{\text{co}}\{\underline{f}_-, \underline{f}_+\} = \{(1-q)\underline{f}_- + q\underline{f}_+, \forall q \in [0, 1]\}. \quad (2.15)$$

The parameter q is a parameter which defines the convex combination and has no physical meaning. The extension (or convexification) of a discontinuous system (2.13) into a convex differential inclusion (2.14) is known as *Filippov's convex method*.

It was stated that the set-valued extension \underline{F} of \underline{f} should be *suitable*. If the discontinuous system (2.13) is a mathematical model of a physical system, then we are interested in a solution concept that guarantees existence of solutions. For practical reasons therefore, we demand that the choice for \underline{F} guarantees existence of solutions. Existence can be guaranteed with the following notion of upper semi-continuity of set-valued functions.

Definition 2.1 (Upper Semi-continuity)

A set-valued function $\underline{F}(\underline{x})$ is upper semi-continuous in \underline{x} if for $\underline{y} \rightarrow \underline{x}$

$$\sup_{\underline{a} \in \underline{F}(\underline{y})} \inf_{\underline{b} \in \underline{F}(\underline{x})} \|\underline{a} - \underline{b}\| \rightarrow 0$$

The following theorem is proven in Aubin and Cellina [1984](theorem 3, page 98):

Theorem 2.2 (Existence of solution of a differential inclusion)

Let \underline{F} be a set-valued function. We assume that \underline{F} is upper semi-continuous, closed, convex and bounded for all $\underline{x} \in \mathbb{R}^n$. Then, for each $\underline{x}_0 \in \mathbb{R}^n$ there exists a $\tau > 0$ and an absolutely continuous function $\underline{x}(t)$ defined on $[0, \tau]$, which is a solution of the initial value problem

$$\dot{\underline{x}} \in \underline{F}(t, \underline{x}(t)), \quad \underline{x}(0) = \underline{x}_0.$$

Filippov's convex method together with the above existence theorem defines the *solution in the sense of Filippov* for a discontinuous differential equation.

Definition 2.2 (Solution in the sense of Filippov)

An absolute continuous function $\underline{x}(t) : [0, \tau] \rightarrow \mathbb{R}^n$ is said to be a solution of $\dot{\underline{x}}(t) = \underline{f}(t, \underline{x})$ (2.13) in the sense of Filippov if for almost all⁴ $t \in [0, \tau]$ it holds that

$$\dot{\underline{x}}(t) \in \underline{F}(t, \underline{x}(t)),$$

where $\underline{F}(t, \underline{x}(t))$ is the closed convex hull of all the limits of $\underline{f}(t, \underline{x}(t))$ (2.12).

Remarks: If $\underline{x}(t)$ is in a region where the vector field is continuous, $\underline{x}(t) \in \mathcal{V}$, then of course must hold $\underline{F}(t, \underline{x}(t)) = \{\underline{f}(t, \underline{x}(t))\}$. If the solution $\underline{x}(t)$ slides along a surface of discontinuity, $\underline{x}(t) \in \Sigma$, then $\dot{\underline{x}}(t) \in \underline{F}(t, \underline{x}(t))$. However, $\dot{\underline{x}}(t)$ is not defined at time instances where the solution arrives at a hyper-surface of discontinuity Σ or leaves Σ . The set of t for which $\underline{x}(t)$ arrives or leaves Σ is of measure zero.

It was assumed in (2.2) that $\underline{f}(t, \underline{x})$ is linearly bounded. In addition $\underline{F}(t, \underline{x}(t))$ is assumed to be bounded on values (t, \underline{x}) for which \underline{F} is set-valued. Consequently, $\underline{F}(t, \underline{x}(t))$ is linearly bounded, i.e. there exist positive constants γ and c such that for all $t \in [0, \infty)$ and $\underline{x} \in \mathbb{R}^n$ holds:

$$\|\underline{F}(t, \underline{x})\| \leq \gamma \|\underline{x}\| + c.$$

Solutions $\underline{x}(t)$ to (2.14) therefore exist on $[0, \infty)$ (see [Aubin and Cellina, 1984; Clarke et al., 1998]) but uniqueness is not guaranteed.

⁴for almost all t means except for a set t of measure 0.

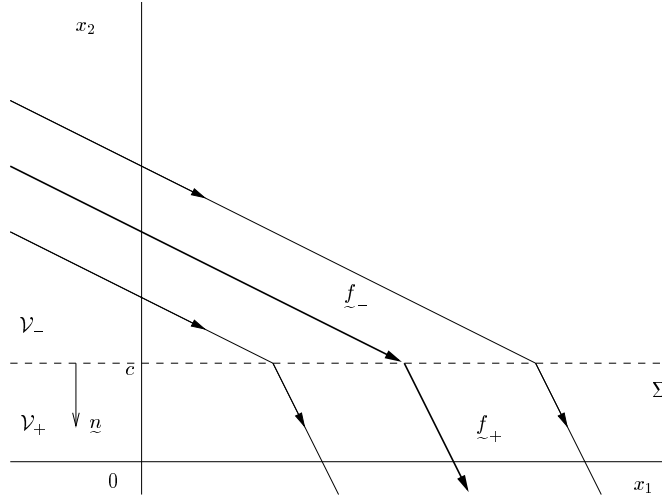


Figure 2.1: Transversal intersection.

A complication of Filippov systems is the possibility of ‘accumulation points’ [Filippov, 1988; Heemels, 1999]. At an accumulation point, an infinite number of mode switches occur in a finite time. We will not address this phenomenon in this thesis and we will assume that no accumulation points occur.

Solutions of differential inclusions do not have to be unique. Obviously, the solution of the IVP where $x_0 \notin \Sigma$ is locally unique, because $\tilde{f}_-(t, \underline{x})$ and $\tilde{f}_+(t, \underline{x})$ are smooth. Uniqueness problems of IVPs for initial conditions on Σ will be illustrated in the following examples which show three basic ways in which the vector field around Σ can behave.

Example 2.1

Consider the discontinuous system

$$\begin{aligned} \dot{x}_1 &= 4 + 2 \operatorname{sgn}(x_2 - c) \\ \dot{x}_2 &= -4 + 2 \operatorname{sgn}(x_2 - c) \end{aligned} \quad (2.16)$$

which can be extended to a set-valued vector field at $\Sigma = \{x_2 = c\}$ by replacing ‘ $\operatorname{sgn}(x)$ ’ with ‘ $\operatorname{Sgn}(x)$ ’ and ‘ $=$ ’ with ‘ \in ’. We take $h = c - x_2$ as indicator function which defines the subspaces \mathcal{V}_- and \mathcal{V}_+ by (2.11). The normal \underline{n} to Σ is given by $\underline{n} = [0, -1]^T$. The phase plane of the system is depicted in Figure 2.1. The vector field is pushing the solution to Σ in the space $\mathcal{V}_- = \{x_2 > c\}$ and pushing from Σ in the space $\mathcal{V}_+ = \{x_2 < c\}$. A solution of (2.16) with an initial condition in \mathcal{V}_- will after some time hit Σ , cross it transversally and proceed in \mathcal{V}_+ . This is called a transversal intersection. Note that the word ‘transversal’ refers to the *solution* which is transversal to Σ and does not refer to the vector field \tilde{f} . Any solution of (2.16) with an initial condition in \mathcal{V}_- , exposing a transversal intersection, therefore exists

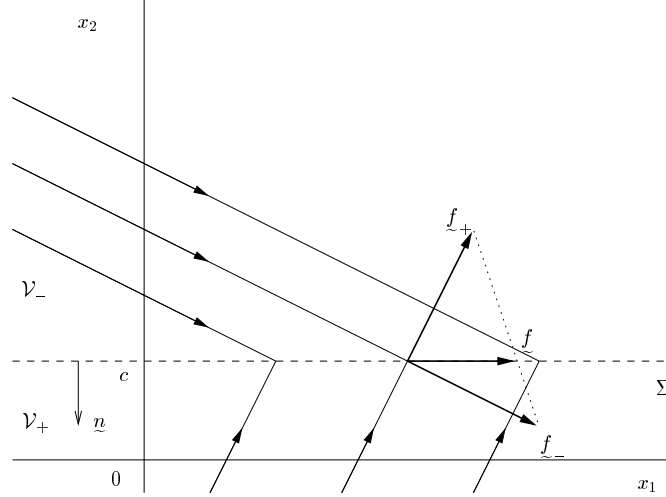


Figure 2.2: Attraction sliding mode.

and is unique. A necessary condition for a transversal intersection at Σ is

$$(\underline{n}^T \underline{f}_-(t, \underline{x}(t))) (\underline{n}^T \underline{f}_+(t, \underline{x}(t))) > 0 \quad \underline{x}(t) \in \Sigma \quad (2.17)$$

where $\underline{n}^T \underline{f}_-$ and $\underline{n}^T \underline{f}_+$ are the projections of \underline{f}_- and \underline{f}_+ on the normal to the hyper-surface Σ .

The vector field could also push the solution to Σ in both \mathcal{V}_- and \mathcal{V}_+ . This will be demonstrated in the following example.

Example 2.2

Consider the system

$$\begin{aligned} \dot{x}_1 &= 4 + 2 \operatorname{sgn}(x_2 - c) \\ \dot{x}_2 &= 2 - 4 \operatorname{sgn}(x_2 - c) \end{aligned} \quad (2.18)$$

with the phase plane depicted in Figure 2.2. The solution will hit Σ but cannot leave it and will therefore move along the plane Σ . This is often called a *sliding mode*. Because the hyper-surface attracts the solution, we call this an *attraction sliding mode*. During the sliding mode the solution will continue along Σ with time derivative \underline{f} given by

$$\underline{f} = \alpha \underline{f}_+ + (1 - \alpha) \underline{f}_- \quad (2.19)$$

with

$$\alpha = \frac{\underline{n}^T \underline{f}_-}{\underline{n}^T (\underline{f}_- - \underline{f}_+)} \quad (2.20)$$

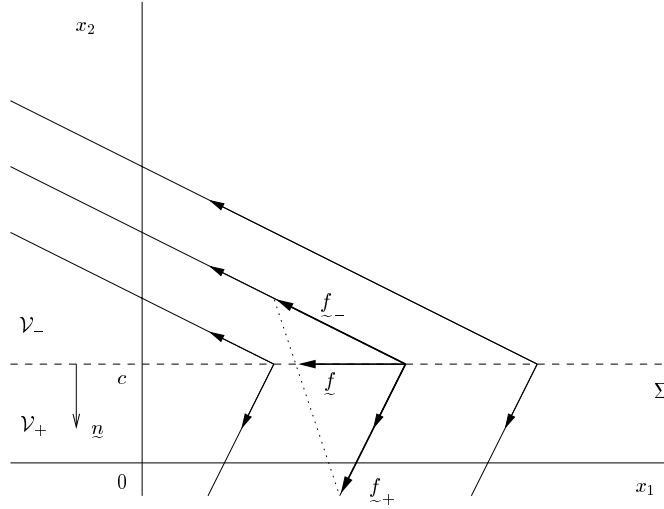


Figure 2.3: Repulsion sliding mode.

The scalar α can be regarded as the value for q in (2.15) that chooses one $\underline{f} \in \underline{F}$ such that it lies along Σ . The solution of (2.18), being an attracting sliding mode, exists and is unique in forward time. An attraction sliding mode at Σ occurs if

$$\underline{n}^T \underline{f}_-(t, \underline{x}(t)) > 0 \quad \text{and} \quad \underline{n}^T \underline{f}_+(t, \underline{x}(t)) < 0 \quad \underline{x}(t) \in \Sigma \quad (2.21)$$

where the inequality signs depend of course on the choice of h (in this case $h(\underline{x}) > 0$ in \mathcal{V}_+ and $h(\underline{x}) < 0$ in \mathcal{V}_-).

The third possible case is depicted in Figure 2.3 which is the vector field of the following example.

Example 2.3

Consider the system

$$\begin{aligned} \dot{x}_1 &= -4 - 2 \operatorname{sgn}(x_2 - c) \\ \dot{x}_2 &= -2 + 4 \operatorname{sgn}(x_2 - c) \end{aligned} \quad (2.22)$$

Note that this vector field is the vector field of (2.18) in reverse time. Here the solutions are diverging from Σ . A solution which starts close to Σ will move away from it. But a solution emanating from Σ can stay on Σ , obeying Filippov's solution, or leave Σ by entering either \mathcal{V}_- or \mathcal{V}_+ . This type of vector field around the hypersurface is addressed as *repulsion sliding mode* as the vector field is repulsing from Σ . The IVP with initial condition on Σ has three possible solutions. The solution still exists but is not unique in forward time.

We also give a one-dimensional example of non-uniqueness.

Example 2.4

Consider the one-dimensional system

$$\dot{x}(t) \in \text{Sgn}(x(t)), \quad x(0) = 0 \quad (2.23)$$

This IVP has three solutions

$$x(t) = \begin{cases} -t & x < 0 \\ 0 & x = 0 \\ t & x > 0 \end{cases} \quad (2.24)$$

A repulsion sliding mode at Σ occurs if

$$\underline{n}^T \underline{f}_-(t, \underline{x}(t)) < 0 \quad \text{and} \quad \underline{n}^T \underline{f}_+(t, \underline{x}(t)) > 0 \quad \underline{x}(t) \in \Sigma. \quad (2.25)$$

In the preceding examples a locally unique solution in forward time was found for the transversal intersection and for the attraction sliding mode, whereas non-uniqueness was shown to exist for the repulsion sliding mode. One can come to the false conclusion that (2.17) is a sufficient condition for local uniqueness in forward time. As is shown by the following counter example this is not the case.

Example 2.5

Consider the one-dimensional differential inclusion

$$\dot{x} \in F(x) = \begin{cases} 2 + \text{sgn}(x) & x \neq 0 \\ [-1, 4] & x = 0 \end{cases}$$

with initial condition $x(0) = 0$. Existence of the solutions is guaranteed because F is upper semi-continuous, non-empty, closed, convex and bounded (Theorem 2.2). Equation (2.17) is also fulfilled. However, the solution is not unique. There are two possible solutions $x(t) = 0$ and $x(t) = 3t$. Non-uniqueness is caused by $0 \in F(0)$ which allows the solution to stay on Σ . Remark that $F(x)$ is not the *smallest* convex set containing $2 + \text{sgn}(x)$. The smallest convex set is $2 + \text{Sgn}(x)$, for which holds $0 \notin F(0)$ and which has a unique solution in forward time.

The set-valued function \underline{F} in the differential inclusion (2.14) is the smallest closed convex set that contains the discontinuous function \underline{f} of (2.13). If \underline{F} obeys condition (2.17) at a point on Σ , then there is no selection from \underline{F} which lies along Σ . We conclude that the solution of the differential inclusion (2.14) with $\underline{x}_0 \in \Sigma$ is locally unique in forward time if

1. the projections of the vector field point to the same side of Σ , i.e.

$$\underline{n}^T \underline{f}_-(0, \underline{x}_0) \underline{n}^T \underline{f}_+(0, \underline{x}_0) > 0,$$

or if

2. the projections point to Σ , i.e.

$$\underline{n}^T \underline{f}_-(0, \underline{x}_0) > 0 \quad \text{and} \quad \underline{n}^T \underline{f}_+(0, \underline{x}_0) < 0$$

Filippov's theory will turn out to be very important to understand periodic solutions where part of the orbit is a sliding mode.

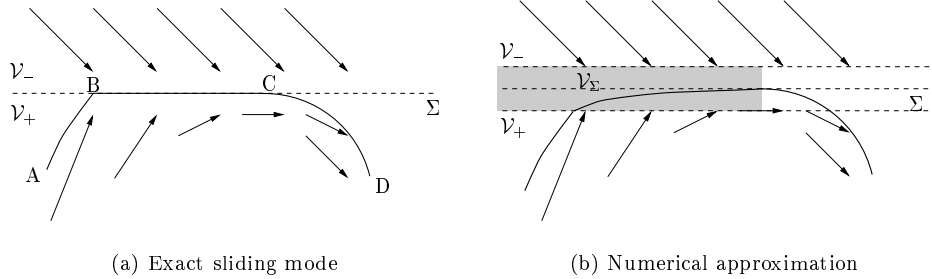


Figure 2.4: Numerical approximation of a sliding mode.

2.2 Numerical Approximation

As explained in the previous section, solutions to differential inclusions can contain sliding modes. The occurrence of a sliding mode poses a difficulty for numerical integration. In this section we present a numerical technique for the integration of differential inclusions with sliding modes.

The vector field of Figure 2.4a pushes the solution which starts in point A to the hyper-surface Σ at point B in finite time. The solution then slides along Σ and leaves Σ when the vector field in the space \mathcal{V}_+ becomes parallel to Σ . The solution will then bend off at point C, i.e. the point at which the vector field is parallel to Σ , and reaches point D. This scenario is the attraction sliding mode. The solution from A to D is unique. If we consider the solution in backward time, that is from D to A, then the vector field reverses and the sliding mode will be of the repulsion type. The reverse solution is clearly not unique. This insight is essential to understand bifurcations of periodic solutions with sliding modes which will be treated in the next chapters.

If we try to integrate such a scenario numerically we are faced with a difficulty: a Runge-Kutta algorithm, for example, will have collocation points in both \mathcal{V}_- and \mathcal{V}_+ between B and C. The integration algorithm will find the correct solution but it will take an enormous amount of integration points.

Instead, we propose to construct a ‘band’ or ‘boundary layer’ around Σ , namely the space \mathcal{V}_Σ , to allow for an efficient numerical approximation. In the space \mathcal{V}_Σ , the vector field is such that the solution is pushed to the middle of the band, i.e. to Σ . The space \mathcal{V}_Σ ends when the vector field in \mathcal{V}_+ or \mathcal{V}_- becomes parallel to Σ . The width of \mathcal{V}_Σ should be taken sufficiently small to yield a good approximation.

As an alternative, the discontinuous vector field is often approximated by a smoothed vector field (see for instance Hinrichs [1997]; Van de Vrande et al. [1999]). For instance $\text{sgn}(x)$ can be approximated by $\frac{2}{\pi} \arctan(\varepsilon x)$. The smooth approximation normally yields a good approximation for large values of ε although difficulties can be expected at repulsion sliding modes. It should be noted that the smooth approximation always has existence and uniqueness of solutions whereas this is not the case for the discontinuous system. However, the main disadvantage of the smoothing method is the fact that it yields stiff differential equations which

are expensive to solve. The method proposed in this section, with a boundary layer which replaces the attraction sliding mode, is far more efficient than the smoothing method, as is pointed out in the Section 2.4 where the two methods are compared.

2.3 Dry Friction Models and Differential Inclusions

Dry friction plays an important role in the dynamic behaviour of mechanical systems, as mentioned in Section 1.1. In this section we discuss three commonly used friction models and relate them to the theory of differential inclusions. We will apply similar friction models to systems which expose stick-slip vibrations in Sections 2.4, 3.4 and 6.7 to 6.9.

In tribology, dry friction is defined as a force that resists relative motion between two contacting surfaces of different bodies. The bodies ‘stick’ to each other when the relative velocity between the contacting surfaces is zero. If the bodies slide over each other with a non-zero velocity, we speak of ‘slip’. In rolling contact of two bodies, ‘stick’ should be regarded as pure rolling without slip. Dry friction is characterized by a different behaviour in the slip and stick phase. The friction force in the stick phase adjusts itself to make equilibrium with external forces on the bodies. The bodies remain sticking as long as equilibrium is ensured. If the friction force in the stick phase exceeds a threshold, called break-away friction force or maximum static friction force, the bodies will begin to slip over each other. The maximum static friction force will be denoted by F_s and the friction force F must be in the interval $-F_s \leq F \leq F_s$ when the bodies stick. In the slip phase, the friction force is a single-valued function of the relative velocity v_{rel} , i.e. $F = F(v_{\text{rel}})$. The friction force during slip is often called the ‘dynamic’ friction force and is more or less constant. Pure viscous friction does not contain a stick phase and can be regarded as dynamic friction. A model for dry friction contains both a description for the stick and slip phase. Many different models are proposed for the mathematical description of dry friction which mostly differ in the way the stick phase is modeled. Three different friction models are depicted in Figure 2.5. The friction models (a), (b) and (c) are ordered to their degree of smoothness. All these models are symmetric although friction models can be non-symmetric. We will study the differences between these friction models when they are applied to the simple mechanical model depicted in Figure 2.6. The model consists of a rigid block with mass m that can slide over a floor with velocity v relative to the floor under the action of an external force F_{ex} . First an important remark has to be made concerning the meaning of friction models (b) and (c) from a mechanical point of view. Friction models (b) and (c) should be understood such that only a transition from stick to slip can take place if $|F_{\text{ex}}|$ exceeds F_s . This mechanical understanding of the friction models can conflict with the mathematical interpretation where the friction models are interpreted as inclusions. This problem will be further explained in the following paragraphs.

Friction model (a) describes the friction force F as a smooth single-valued function of v_{rel} on the whole domain. The equation of motion of the block with friction model (a) therefore reads

$$m\dot{v}(t) = F_{\text{ex}} - F(v(t)). \quad (2.26)$$

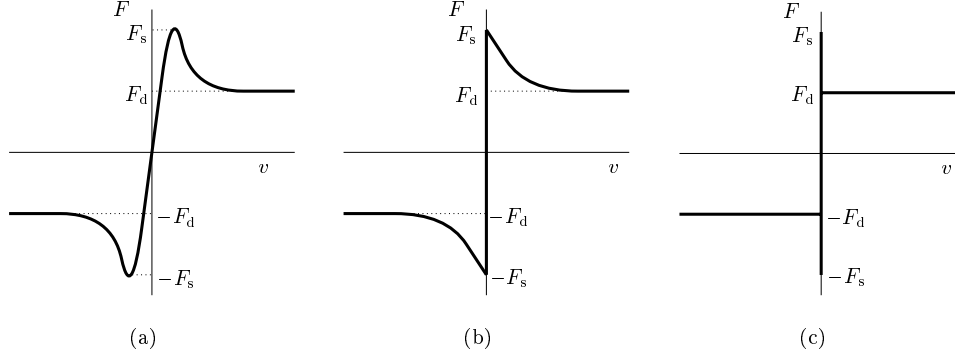


Figure 2.5: Friction models.

A suitable choice for the function F , which has the characteristics of friction model (a), is

$$F(v(t)) = \frac{2}{\pi} \arctan(\varepsilon v(t)) \left[\frac{F_s - F_d}{1 + \delta|v(t)|} + F_d \right], \quad (2.27)$$

where $\varepsilon \gg 1$ and $\delta > 0$. The slope of the function is very steep for small $|v(t)|$. The friction force (2.27) has a maximum which is approximately F_s for large values of ε . This maximum was already introduced as the static friction force. The upward ramp is followed by a downward ramp which brings the friction force to an almost constant value F_d . This model has the advantage that the resulting equation of motion is a smooth ordinary differential equation. All standard integration routines can therefore be directly applied and the solution of the IVP always exists and is unique. The disadvantages are twofold. Firstly, the model cannot describe the stick phase properly. The friction force is zero at zero velocity. The block will therefore always slip over the floor if an external force is present. We could define ‘stick’ for this model as the phase where the friction is on the upward ramp but this notion of ‘stick’ becomes unclear if the friction force does not contain a maximum (for instance if $F_s = F_d$). The second disadvantage is the steep slope of the upward and downward ramps. The equation of motion with friction model (a) will be a very stiff differential equation which is inconvenient from a numerical point of view.

In friction model (b), the upward ramp of friction model (a) is replaced by a set-valued function at $v = 0$. The equation of motion with friction model (b) can be regarded as a differential inclusion, i.e.

$$m\dot{v}(t) \in \begin{cases} F_{\text{ex}} - \frac{F_s - F_d}{1 + \delta|v(t)|} - F_d & v(t) > 0 \\ F_{\text{ex}} + [-F_s, F_s] & v(t) = 0 \\ F_{\text{ex}} + \frac{F_s - F_d}{1 + \delta|v(t)|} + F_d & v(t) < 0 \end{cases} \quad (2.28)$$

where the choice for the friction force in the slip phase is similar to the one in friction model (a). Friction model (b) describes the stick phase correctly as it allows the body to stick to the floor with zero velocity under the action of an external force.

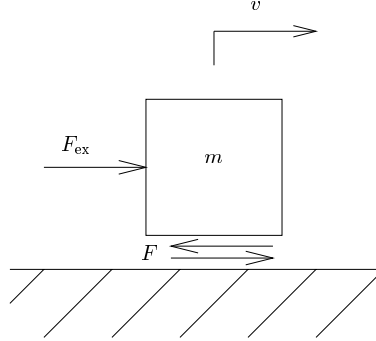


Figure 2.6: Block on a floor.

Remark that friction model (a) is a smoothed version of friction model (b). The solution of the differential inclusion (2.28) exists as F is upper semi-continuous, non-empty, closed, convex and bounded (Theorem 2.2). Moreover, the set $[-F_s, F_s]$ at $v(t) = 0$ is the *smallest* closed convex set that contains the left and right limits, $\lim v \downarrow 0$ and $\lim v \uparrow 0$ of F . If $-F_s \leq F_{\text{ex}} \leq F_s$, then $\dot{v} < 0$ for $v(t) > 0$ and $\dot{v} > 0$ for $v(t) < 0$. Consequently, there exists an attraction sliding mode at $v = 0$ if $-F_s \leq F_{\text{ex}} \leq F_s$. In the same way we can infer that a transversal intersection exists at $v = 0$ if $|F_{\text{ex}}| > F_s$. A repulsion sliding mode is not possible with friction model (b). Uniqueness of the solution of the differential inclusion (2.28) is therefore always ensured. This is due to the fact that the friction force is dissipating energy and because the set-valued part of F is the smallest closed convex set that obeys upper semi-continuity. Provided an efficient integration algorithm is available to solve the IVP for a differential inclusion (see the previous section), then friction model (b) can be more efficient than friction model (a). The slope of the downward ramp, however, can still be steep for large values of δ .

Friction model (c) also folds the downward ramp into the set-valued part at $v = 0$. This friction model is known as the *signum model with static friction point*. If we regard friction model (c) as a differential inclusion, we obtain

$$m\dot{v}(t) \in \begin{cases} F_{\text{ex}} - F_d & v(t) > 0 \\ F_{\text{ex}} + [-F_s, F_s] & v(t) = 0 \\ F_{\text{ex}} + F_d & v(t) < 0 \end{cases} \quad (2.29)$$

where $F_d < F_s$. The solution of the differential inclusion (2.29) exists as F is upper semi-continuous, non-empty, closed, convex and bounded. Remark that the set $[-F_s, F_s]$ at $v(t) = 0$ is *not* the smallest closed convex set that contains the left and right limits, $\lim v \downarrow 0$ and $\lim v \uparrow 0$ of F . The smallest closed convex set would be $[-F_d, F_d]$. This has important consequences for the uniqueness of the solution. There exists an attraction sliding mode at $v = 0$ if $-F_d \leq F_{\text{ex}} \leq F_d$. A transversal intersection exists at $v = 0$ if $|F_{\text{ex}}| > F_s$.

If $F_d < F_{\text{ex}} < F_s$, then $\dot{v} > 0$ for $v(t) \neq 0$ but $\dot{v}(t) = 0 \in F_{\text{ex}} + [-F_s, F_s]$. Consequently, the IVP with $v(0) = 0$ as initial condition has two distinct solutions $v(t) = 0$ and $v(t) = (F_{\text{ex}} - F_d)t$ if $F_d < F_{\text{ex}} < F_s$. A same kind of reasoning can

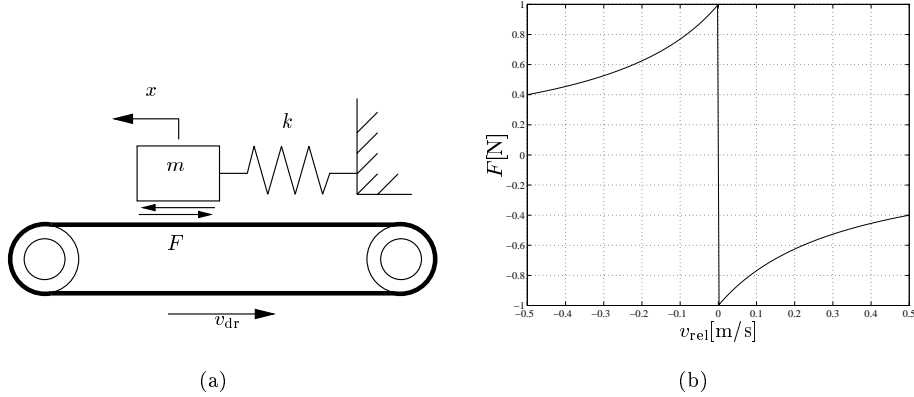


Figure 2.7: 1-DOF model with dry friction.

be held for $-F_d > F_{\text{ex}} > -F_s$. The solution of the differential inclusion (2.29) is therefore not unique if $F_d < |F_{\text{ex}}| < F_s$.

In friction models (a) and (b) the external force $|F_{\text{ex}}|$ has to exceed F_s to force the block to slip starting from stick. We conclude that friction models (a) and (b) are consistent with the mechanical concept of friction. If friction model (c) is regarded as a differential inclusion, then a transition from stick to slip is possible for $|F_{\text{ex}}| < F_s$ which results in non-uniqueness of solutions. The differential inclusion of friction model (c) is clearly inconsistent with the mechanical concept of friction.⁵

Friction models of type (c) are frequently used in literature [Andersson, 1980; Begley and Virgin, 1997; Fečkan, 1998; Hinrichs, 1997; Hinrichs et al., 1998; Ibrahim, 1994a; Karnopp, 1985; Oestreich, 1998; Popp et al., 1995; Van den Steen, 1997]. Care should be taken how friction models of type (c) are to be understood.

2.4 Example: The Stick-slip System

A single-degree-of-freedom model will be used to introduce and evaluate the numerical aspects of the methods described in the preceding sections. The same model treated in Galvanetto et al. [1995] and Van de Vrande et al. [1999] is used to facilitate the comparison of results.

Consider a mass m attached to inertial space by a spring k . The mass is riding on a driving belt, that is moving at constant velocity v_{dr} (Figure 2.7a). Parameter values are given in Appendix C.1. Between mass and belt, dry friction occurs, with a friction force F . The state equation, describing this model, reads as

$$\dot{\tilde{x}} = \tilde{f}(\tilde{x}) = \begin{bmatrix} \dot{x} \\ -\frac{k}{m}x + \frac{F(x, v_{\text{rel}})}{m} \end{bmatrix}, \quad (2.30)$$

⁵A remark related to this problem has been made by Glocker [1995]. In Glocker [1995] an equivalent description of the friction model is given by a so-called 'superpotential'. It is stated that a superpotential does not exist for friction models of type (c).

where $\underline{x} = [x \ \dot{x}]^T$. The relative velocity of the mass m with respect to the belt is denoted by $v_{\text{rel}} = \dot{x} - v_{\text{dr}}$. The friction force $F(x, v_{\text{rel}})$ is in the slip phase a function of the relative velocity v_{rel} and in the stick phase a function of the spring force kx . The friction model reads as

$$F(x, v_{\text{rel}}) = \begin{cases} F(x) = \min(|kx|, F_s) \operatorname{sgn}(kx), & v_{\text{rel}} = 0 \quad \text{stick}, \\ F(v_{\text{rel}}) = -\frac{F_s \operatorname{sgn} v_{\text{rel}}}{1 + \delta|v_{\text{rel}}|}, & v_{\text{rel}} \neq 0 \quad \text{slip}. \end{cases} \quad (2.31)$$

The friction force in the stick phase is limited by the maximum static friction force, i.e. $|F(x)| \leq F_s$. The friction curve is drawn in Figure 2.7b. This friction model is identical to the friction model depicted in Figure 2.5b with $F_d = 0$.

The friction curve is often approximated by a smooth function. One possible approximation for F is [Van de Vrande et al., 1999]

$$\tilde{F}(v_{\text{rel}}) = -\frac{2}{\pi} \frac{F_s \arctan \varepsilon v_{\text{rel}}}{1 + \delta|v_{\text{rel}}|}. \quad (2.32)$$

The smoothed friction model is identical to the friction model depicted in Figure 2.5a with $F_d = 0$. Clearly, increasing the steepness parameter ε improves the approximation, especially for v_{rel} close to 0. The friction curve will almost be the same as in Figure 2.7b for large values of the steepness parameter ($\varepsilon = 10^6$). However, a steep slope in \tilde{F} arises at $v_{\text{rel}} = 0$, given by $-(2/\pi)\varepsilon F_s$. This causes a stiff differential equation, which is numerically costly to integrate.

Another method of integrating the system of equations starts from the Karnopp friction model [Armstrong et al., 1994; Haessig and Friedland, 1991; Karnopp, 1985]. The classical Karnopp model has the advantage of generating ordinary differential equations, but suffers from some numerical instabilities in the stick phase [Sepehri et al., 1996]. In the following a so-called switch model is proposed, which does not possess this disadvantage and which can be considered to be an extended version of the Karnopp model.

The switch model treats the system as three different sets of ordinary differential equations: one for the slip phase, a second for the stick phase and a third for the transition from stick to slip. The state space is therefore divided in a number of subspaces which are depicted in Figure 2.8. Each subspace has its own *smooth* ordinary differential equation. There are two subspaces for the slip phase: \mathcal{S}_+ for positive relative velocity and \mathcal{S}_- for negative relative velocity. Beside the subspaces, a number of solutions are depicted in Figure 2.8, which show how different solutions enter from one subspace into another. The subspace \mathcal{U} defines the stick mode. Additionally, there are two subspaces for the transition from stick to slip: \mathcal{T}_+ and \mathcal{T}_- . At each timestep the state vector is inspected to determine whether the system is in one of the slip modes, in the stick mode or in one of the transition modes. The corresponding time derivative of the state vector is then chosen. The conditions for changing to the stick mode or the slip mode operate as switches between the systems. A region of small velocity is defined as $|v_{\text{rel}}| < \eta$, where $\eta \ll v_{\text{dr}}$. The system is considered to be in one of the slip modes if the relative velocity lies outside this narrow band. Inside this narrow band, the system can be in the stick mode or in a transition mode. The finite region is necessary for digital computation since an

exact value of zero will rarely be computed. If the relative velocity lies within the narrow band and if the static friction force, needed to make equilibrium with the applied forces on the mass, exceeds the break-away friction force F_s , the system is considered to be in transition from stick to slip. The transition modes \mathcal{T}_+ and \mathcal{T}_- are necessary to enforce the solution, coming from the stick mode \mathcal{U} , into the correct slip mode (\mathcal{S}_+ or \mathcal{S}_-). Remark that the stick phase is in fact an attraction sliding mode and the vector field is identical to the one depicted in Figure 2.4a. The switch model uses the same technique as in Figure 2.4b, where a narrow band is constructed around the sliding mode. The switch model can be elucidated in pseudo code:

```

if  $|v_{\text{rel}}| > \eta$  then
     $\dot{\underline{x}} = \underline{f}(\underline{x}) = \begin{bmatrix} \dot{x} \\ -\frac{k}{m}x + \frac{F(v_{\text{rel}})}{m} \end{bmatrix}$     slip,  $\underline{x} \in \mathcal{S}_+ \vee \underline{x} \in \mathcal{S}_-$ 
elseif  $|kx| > F_s$ 
     $\dot{\underline{x}} = \underline{f}(\underline{x}) = \begin{bmatrix} \dot{x} \\ -\frac{k}{m}x + \frac{F_s}{m} \text{sgn } kx \end{bmatrix}$     transition,  $\underline{x} \in \mathcal{T}_+ \vee \underline{x} \in \mathcal{T}_-$ 
else
     $\dot{\underline{x}} = \underline{f}(\underline{x}) = \begin{bmatrix} v_{\text{dr}} \\ -v_{\text{rel}}\sqrt{\frac{k}{m}} \end{bmatrix}$     stick,  $\underline{x} \in \mathcal{U}$ 
end;

```

The thickness parameter of the narrow band η , the Runge-Kutta tolerance TOL and the perturbation parameter ξ for numerical computation of the fundamental solution matrix by sensitivity analysis [Leine et al., 1998] have to be chosen by the user. The parameter η should be chosen *sufficiently small*. With *sufficiently small* is meant that η is small enough to have no qualitative influence on the solution. In practice, η is therefore often chosen much smaller than the amplitude of the velocity, $A(\dot{x})$, or smaller than the velocity of the belt v_{dr} . The perturbations on the initial condition for sensitivity analysis should be small with respect to the size of the subspaces \mathcal{U} , \mathcal{S}_{\pm} and \mathcal{T}_{\pm} . The parameter ξ should therefore be chosen much smaller than the thickness parameter η . The collocation points of the Runge-Kutta integration method during the stick mode should all be situated within the narrow band to avoid numerical instability problems of the classical Karnopp model. This can be achieved by centering the relative velocity in the stick band and taking a Runge-Kutta tolerance TOL much smaller than η but for an accurate computation of the fundamental solution matrix TOL should be much smaller than ξ . Typically, for a periodic solution the parameters are chosen as $TOL \ll \xi \ll \eta \ll \min(A(\dot{x}), v_{\text{dr}})$.

The acceleration of the mass during the stick mode is set to $-v_{\text{rel}}\sqrt{\frac{k}{m}}$ to force the relative velocity to zero, i.e. the solution is pushed to the center of the narrow band. The multiplier $\sqrt{\frac{k}{m}}$ determines how ‘fast’ the solution is pushed to the center. The choice of the multiplier is somewhat arbitrary but the multiplier is large for high frequencies of oscillation, therefore for small stick times, which is a convenient property, and has the correct dimension, $[\text{s}^{-1}]$.

The proposed algorithm maintains the continuity of the state vector and yields a set of ordinary differential equations that do not exhibit numerical instabilities.

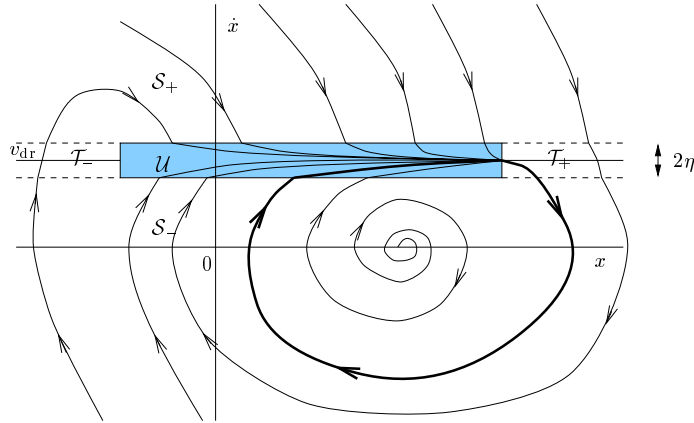


Figure 2.8: Phase spaces of the stick-slip system.

It can be inferred from Figure 2.8 that this system has an unstable equilibrium with a stable periodic solution around it. Other friction models, in which the friction force increases for increasing v_{rel} at higher values of v_{rel} , can have multiple periodic solutions (even for a single degree-of-freedom system). One of the objectives of this thesis is to follow branches of periodic solutions of Filippov systems, like the switch model, and finally arrive at bifurcations. To prove that this model has only one stable periodic solution is beyond the scope of this section. Existence of at least one periodic solution can be proved by using a non-smooth version of the Poincaré-Bendixson theorem [Filippov, 1988; Kunze and Küpper, 1997] and has been observed before [Andersson, 1980; Galvanetto et al., 1995; Kunze and Küpper, 1997; Leine et al., 1998, 2000; Van de Vrande et al., 1999]. Our aim in this section is to present a numerical method that simulates friction induced periodic solutions correctly. We also study if the switch model works efficiently if combined with the shooting method. The shooting method is a numerical method that finds a periodic solution given an initial guess for the state vector and the period time and is used to follow branches of periodic solutions [Fey, 1992; Parker and Chua, 1989; Van de Vorst, 1996]. It suffices here to state that the system has a periodic solution and we will compare how the switch model and the smoothing method perform if combined with the shooting method.

The periodic solution computed with the switch model for the stick-slip system is depicted in Figure 2.9b. The periodic solution was obtained with a shooting method using sensitivity analysis [Leine et al., 1998]. The computation took 110232 floating-point-operations to obtain a shooting accuracy of 10^{-5} with a Runge-Kutta-Fehlberg tolerance of 10^{-8} . Small timesteps are taken only near the transitions between slip and stick phase, resulting in 123 integration points (of the last iteration of the shooting method). In fact, the adaptive timestep control of the integration algorithm determines the switching point with the desired accuracy. The constant η was taken to be 10^{-6} . The initial guess for the state vector was $\underline{x}_0 = [1.1, 0]^T$, whereas for the period time it was $T_0 = 12[s]$.

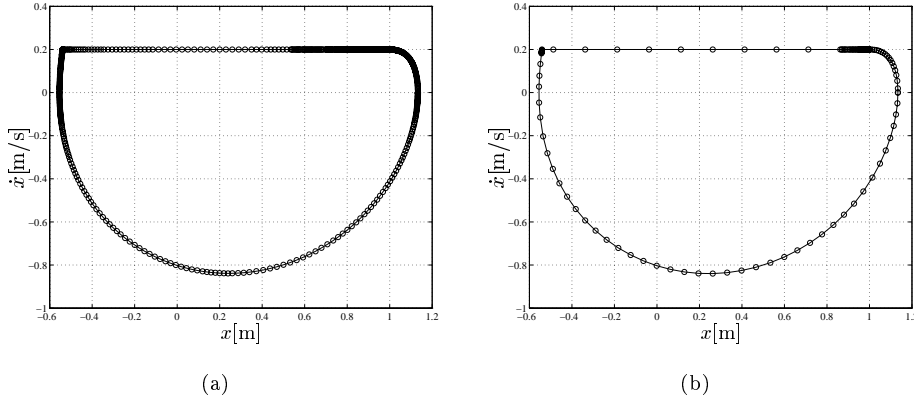


Figure 2.9: Periodic solutions obtained with the smoothing method ($\varepsilon = 10^6$) (a) and with the switch model (b).

In Figure 2.9a the results obtained with the smoothing method are plotted for $\varepsilon = 10^6$. A Backward Differentiation Formula (BDF) proved to be the best integration method for the extremely stiff differential equation. This computation took 3493510 floating-point-operations to obtain the same accuracy as in the previous case starting from the same initial guess. Small timesteps are not only necessary near the transitions but during the whole stick phase, resulting in 1217 integration points. The smoothing method needed 31.7 times more floating point operations and about 10 times more data storage. Consequently, the smoothing method is clearly more expensive than the switch model. The slip phase calculated with the smoothing method contains more integration points than the slip phase of the switch model because of the differences between the BDF and the Runge-Kutta-Fehlberg integration method.

While using the smoothing method, the friction force should be a continuous function of velocity. If an isolated static friction point was added to the discontinuous friction curve, like the friction model depicted in Figure 2.5c, a second steep slope would be added to the smooth approximation yielding an even stiffer differential equation. The switch model can easily be extended with an isolated static friction point. The small timesteps just after stick to slip transition in Figure 2.9b are due to a continuous transition from a static to a dynamic friction force. The addition of an isolated static friction point would limit this region of refinement and speed up the integration process.

The switch model was introduced in this section as an efficient numerical method for integrating a system with dry friction. The importance of the switch model for theoretical considerations will become evident in Sections 3.4. The concept of the switch model with a finite narrow band for the stick phase will turn out to be essential to understand bifurcations occurring in systems with dry friction (Sections 6.7 to 6.9).

Chapter 3

Fundamental Solution Matrix

'In which, if it were to summarize the prodigious revelations of which it speaks, the title would have to be as long as the chapter itself, contrary to the usage'

UMBERTO ECO, *The Name of the Rose*
(7th day, night)

In this chapter the discontinuous behaviour of fundamental solution matrices of discontinuous systems is discussed. The definition of a fundamental solution matrix for smooth systems is reviewed. Jumping conditions of the fundamental solution matrix are then discussed and applied to two examples.

3.1 Fundamental Solution Matrix for Smooth Systems

In this chapter we consider the stability of periodic solutions of the nonlinear dynamical system

$$\dot{\underline{x}}(t) = \underline{f}(t, \underline{x}(t)), \quad \underline{x}(t) \in \mathbb{R}^n. \quad (3.1)$$

We assume that (3.1) has a known periodic solution denoted by $\underline{x}_P(t)$ with minimum period T . A disturbance $\underline{y}(t)$ is superimposed on \underline{x}_P resulting in the solution

$$\underline{x}(t) = \underline{x}_P(t) + \underline{y}(t) \quad (3.2)$$

Substituting (3.2) in (3.1), assuming that $\underline{f}(t, \underline{x})$ is at least twice continuously differentiable, expanding the results in a Taylor series around \underline{x}_P , and retaining only linear terms in the disturbance, we obtain

$$\dot{\underline{y}}(t) = \frac{\partial \underline{f}(t, \underline{x}(t))}{\partial \underline{x}} \underline{y}(t) + O(\|\underline{y}\|^2) \quad (3.3)$$

or

$$\dot{\underline{y}}(t) \cong \underline{J}(t, \underline{x}_P(t))\underline{y}(t) \quad (3.4)$$

where $\underline{J}(t, \underline{x}_P(t))$ is the Jacobian matrix of $\underline{f}(t, \underline{x}_P(t))$.

The n -dimensional linear system (3.4) has n linearly independent solutions $\underline{y}_i(t)$, where $i = 1, 2, \dots, n$. These solutions are usually called a fundamental set of solutions. This fundamental set can be expressed in the form of a square matrix called a *fundamental solution matrix* as

$$\underline{\Phi}(t) = [\underline{y}_1(t) \quad \underline{y}_2(t) \quad \dots \quad \underline{y}_n(t)]. \quad (3.5)$$

The eigenvalues of the fundamental solution matrix $\underline{\Phi}(T)$ are called *Floquet multipliers* [Guckenheimer and Holmes, 1983; Nayfeh and Balachandran, 1995; Nayfeh and Mook, 1979; Parker and Chua, 1989]. Each Floquet multiplier provides a measure of the local orbital divergence or convergence along a particular direction over one period of the periodic solution. The Floquet multipliers determine therefore the stability of the periodic motion. A fundamental solution matrix can be regarded as a set of fundamental solutions of the linearization in the disturbance of the nonlinear system. The concept of a fundamental solution matrix is therefore important in the stability analysis of periodic solutions of nonlinear dynamical systems.

Fundamental solution matrices are furthermore used in shooting methods for finding periodic solutions, in continuation methods to follow branches of periodic solutions, and they are used in the determination of Lyapunov exponents.

For continuous systems the fundamental solution matrix can be obtained in an elegant manner by integrating the so-called variational equation (see [Ascher et al., 1995; Parker and Chua, 1989] and Appendix B.2). Discontinuous systems however, exhibit discontinuities (or 'saltations' / 'jumps') in the time evolution of the fundamental solution matrix.

The jumps in the fundamental solution matrix can be computed analytically by means of the theory of Aizerman and Gantmakher [1958], which will be discussed in Sections 3.2 and 3.3.

The theory of Aizerman and Gantmakher was used by Bockman [1991] and Müller [1995] to calculate Lyapunov exponents of discontinuous systems.

3.2 Jumping Conditions: A Single Discontinuity

In this section we will derive how the fundamental solution matrix $\underline{\Phi}$ jumps if the solution $\underline{x}(t)$ crosses a hyper-surface Σ , on which the vector field is discontinuous. Consider the nonlinear system (2.14) with discontinuous right-hand side as described in Chapter 2

$$\dot{\underline{x}}(t) \in \underline{F}(t, \underline{x}(t)) = \begin{cases} \underline{f}_-(t, \underline{x}(t)) & \underline{x}(t) \in \mathcal{V}_- \\ \underline{co}\{\underline{f}_-(t, \underline{x}(t)), \underline{f}_+(t, \underline{x}(t))\} & \underline{x}(t) \in \Sigma \\ \underline{f}_+(t, \underline{x}(t)) & \underline{x}(t) \in \mathcal{V}_+, \end{cases} \quad (3.6)$$

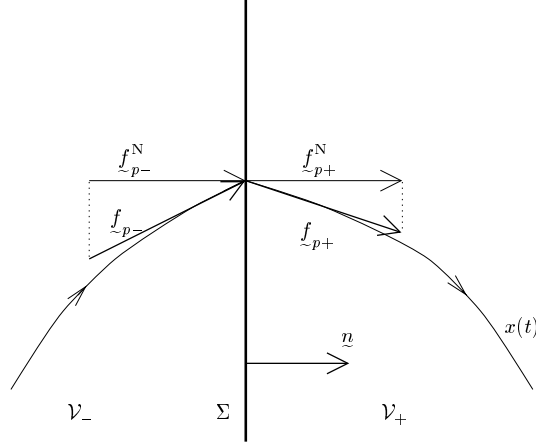


Figure 3.1: Projection of derivatives on the normal.

with the initial condition

$$\underline{x}(t=0) = \underline{x}_0. \quad (3.7)$$

Assume that at a certain point in time, say t_p , the solution $\underline{x}(t)$ will cross Σ . With the definition of the indicator function (2.8) we obtain

$$h(\underline{x}(t_p)) = 0.$$

At this hyper-surface there are two derivatives \underline{f}_{p-} and \underline{f}_{p+} which lie in the direction of the solution as denoted in Figure 3.1. The derivatives have components \underline{f}_{p-}^N and \underline{f}_{p+}^N perpendicular to the hyper-surface with magnitudes $\underline{n}^T \underline{f}_{p-}$ and $\underline{n}^T \underline{f}_{p+}$. We first consider only transversal intersections. Uniqueness of the solution is therefore assured (this is not the case for a repulsion sliding mode problem). In order to assure a transversal intersection, we assume that the projections of the derivatives \underline{f}_{p-} and \underline{f}_{p+} on the normal \underline{n} have the same sign

$$\underline{n}^T \underline{f}_{p-} \underline{n}^T \underline{f}_{p+} > 0. \quad (3.8)$$

Equation (3.8) assures that the solution leaves the hyper-surface and stays on the hyper-surface at one point of time and not on an interval of time (i.e. the solution curve *crosses* the hyper-surface).

An infinitesimal disturbance $\delta \underline{x}_0$ on the initial condition will cause a disturbance $\delta \underline{x}(t)$ on the state $\underline{x}(t)$. The fundamental solution matrix $\underline{\Phi}(t, t_0)$ relates $\delta \underline{x}(t)$ to $\delta \underline{x}_0$,

$$\delta \underline{x}(t) = \underline{\Phi}(t, t_0) \delta \underline{x}_0 + O(\|\underline{x}_0\|^2). \quad (3.9)$$

The dependence of $\underline{\Phi}(t, t_0)$ on \underline{x}_0 has been omitted for brevity. Let the solution start in the subspace \mathcal{V}_- , that is $\underline{x}_0 \in \mathcal{V}_-$. Suppose the solution curve crosses the

hyper-surface Σ at $t = t_p$, i.e. $h(\underline{x}(t_p)) = 0$. The system is continuous on the interval $D = \{t \in \mathbb{R} \mid t_0 \leq t \leq t_p\}$. The fundamental solution matrix will also be continuous on the interior of D . The time evolution of the fundamental solution matrix on the interior of D can be obtained from the initial value problem

$$\dot{\underline{\Phi}}(t, t_0) = \frac{\partial \underline{f}(t, \underline{x}(t))}{\partial \underline{x}} \underline{\Phi}(t, t_0), \quad \underline{\Phi}(t_0, t_0) = \underline{\Phi}_0 = \underline{I}, \quad t_0, t \in D. \quad (3.10)$$

Equation (3.10) is called the *variational equation* (see [Ascher et al., 1995; Parker and Chua, 1989] and Appendix B.2). The Jacobian $\partial \underline{f} / \partial \underline{x}$ is not uniquely defined on the border of D at $t = t_p$ where $\underline{x}(t_p)$ is located on the hyper-surface Σ . This causes a jump (or discontinuity) in the fundamental solution matrix. We will derive an expression for the jump in Section 3.3. For the moment we will assume that we know how the fundamental solution matrix jumps and we assume that we can express the jump with a matrix \underline{S} , which maps the fundamental solution matrix just before the jump, $\underline{\Phi}(t_{p-}, t_0)$, to the fundamental solution matrix just after the jump, $\underline{\Phi}(t_{p+}, t_0)$, as

$$\underline{\Phi}(t_{p+}, t_0) = \underline{S} \underline{\Phi}(t_{p-}, t_0), \quad (3.11)$$

where

$$\underline{\Phi}(t_{p-}, t_0) = \lim_{t \uparrow t_p} \underline{\Phi}(t, t_0). \quad (3.12)$$

On D the fundamental solution matrix can be obtained from integrating the variational equation (3.10) which gives for $\underline{\Phi}(t_{p-}, t_0)$

$$\underline{\Phi}(t_{p-}, t_0) = \int_{t_0}^{t_p} \dot{\underline{\Phi}}(t, t_0) dt + \underline{I}. \quad (3.13)$$

The fundamental solution matrix after the jump can then be obtained by (3.11) where \underline{S} should of course be known. The solution enters the subspace \mathcal{V}_+ (as transversality was assumed) at $t = t_p$, and traverses \mathcal{V}_+ during the interval $G = \{t \in \mathbb{R} \mid t_p \leq t \leq t_q\}$. We can now construct the fundamental solution matrix on G after the jump as

$$\begin{aligned} \underline{\Phi}(t_q, t_0) &= \underline{\Phi}(t_q, t_{p+}) \underline{\Phi}(t_{p+}, t_0) \\ &= \left(\int_{t_p}^{t_q} \dot{\underline{\Phi}}(t, t_0) dt + \underline{I} \right) \underline{\Phi}(t_{p+}, t_0). \end{aligned} \quad (3.14)$$

If the fundamental solution matrix is known on G , then we can express $\underline{\Phi}(t_{p+}, t_0)$ by the right time limit to the jump as

$$\underline{\Phi}(t_{p+}, t_0) = \lim_{t \downarrow t_p} \underline{\Phi}(t, t_0). \quad (3.15)$$

In general $\underline{\Phi}(t_{p-}, t_0) \neq \underline{\Phi}(t_{p+}, t_0)$.

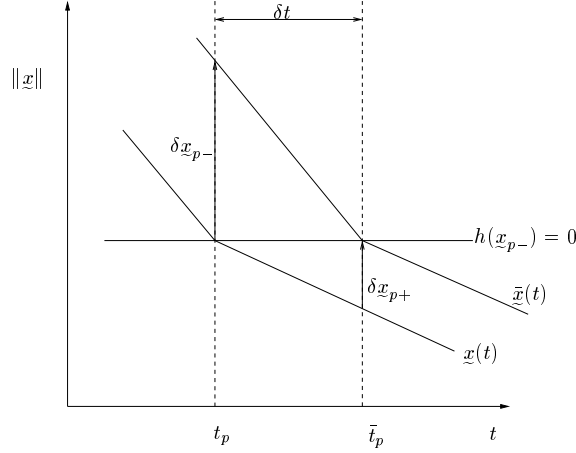


Figure 3.2: Disturbed and undisturbed solution.

We name the matrix \underline{S} the *saltation matrix* (or 'jump' matrix) because it describes the jump by mapping $\underline{\Phi}(t_{p-}, t_0)$ to $\underline{\Phi}(t_{p+}, t_0)$ with (3.11). The saltation matrix can be regarded as a fundamental solution matrix from time t_{p-} to t_{p+}

$$\underline{S} = \underline{\Phi}(t_{p+}, t_{p-}). \quad (3.16)$$

Substitution of (3.11) in (3.14) yields

$$\underline{\Phi}(t_q, t_0) = \underline{\Phi}(t_q, t_{p+}) \underline{S} \underline{\Phi}(t_{p-}, t_0). \quad (3.17)$$

The construction of saltation matrices (or jump conditions) is due to Aizerman and Gantmakher [1958] and is explained in the next section.

3.3 Construction of Saltation Matrices

One question has not been answered up to now: how do we obtain the saltation matrix \underline{S} ? The saltation matrix will be derived by inspecting the nonlinear dynamical system in the neighbourhood of the occurrence of a discontinuity. Consider the disturbed and undisturbed solutions depicted in Figure 3.2. Time is on the horizontal axis of Figure 3.2 and an arbitrary norm of \underline{x} is on the vertical axis. The disturbed solution $\tilde{x}(t)$ is due to an initial disturbance

$$\tilde{x}_0 = x_0 + \delta x_0. \quad (3.18)$$

The disturbed solution stays $\delta t = \bar{t}_p - t_p$ longer (if $\delta t > 0$) or shorter (if $\delta t < 0$) in \mathcal{V}_- before hitting the hyper-surface Σ . The differences between the disturbed and undisturbed solutions at the crossings are denoted by

$$\delta x_{p-} = \tilde{x}(t_p) - x(t_p), \quad (3.19)$$

$$\delta \underline{x}_{p+} = \bar{\underline{x}}(\bar{t}_p) - \underline{x}(\bar{t}_p). \quad (3.20)$$

We can express the undisturbed and disturbed solutions in a first-order Taylor expansion

$$\underline{x}(\bar{t}_p) \approx \underline{x}(t_p) + \underline{f}_{p+} \delta t, \quad (3.21)$$

$$\bar{\underline{x}}(\bar{t}_p) \approx \underline{x}(t_p) + \delta \underline{x}_{p-} + \underline{f}_{p-} \delta t \quad (3.22)$$

with the abbreviations

$$\begin{aligned} \underline{f}_{p+} &= \underline{f}(t_{p+}, \underline{x}(t_{p+})) \\ \underline{f}_{p-} &= \underline{f}(t_{p-}, \underline{x}(t_{p-})) \end{aligned} \quad (3.23)$$

The Equations (3.21) and (3.22) are inserted into (3.20)

$$\begin{aligned} \delta \underline{x}_{p+} &= \bar{\underline{x}}(\bar{t}_p) - \underline{x}(\bar{t}_p) \\ &\approx \underline{x}(t_p) + \delta \underline{x}_{p-} + \underline{f}_{p-} \delta t - (\underline{x}(t_p) + \underline{f}_{p+} \delta t) \\ &\approx \delta \underline{x}_{p-} + \underline{f}_{p-} \delta t - \underline{f}_{p+} \delta t \end{aligned} \quad (3.24)$$

The disturbed solution satisfies the indicator function (2.8). We apply a Taylor series expansion up to the first-order terms [Müller, 1995]:

$$\begin{aligned} 0 &= h(\bar{\underline{x}}(\bar{t}_p)) \\ &\approx h(\underline{x}(t_p) + \delta \underline{x}_{p-} + \underline{f}_{p-} \delta t) \\ &\approx \underbrace{h(\underline{x}(t_p))}_{=0} + \underline{n}^T (\delta \underline{x}_{p-} + \underline{f}_{p-} \delta t) \\ &\approx \underline{n}^T (\delta \underline{x}_{p-} + \underline{f}_{p-} \delta t), \end{aligned} \quad (3.25)$$

where the normal \underline{n} is defined by (2.9).

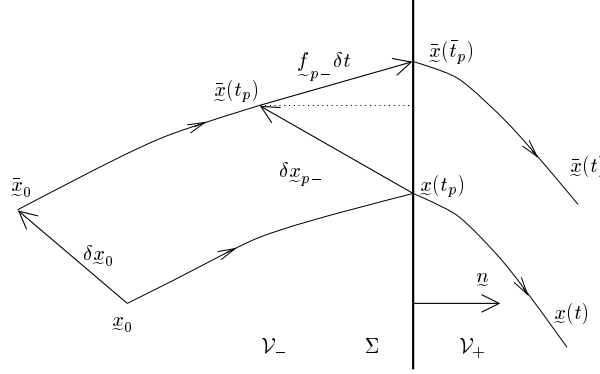
From (3.25) we can express the variation δt in terms of $\delta \underline{x}_{p-}$.

$$\delta t = - \frac{\underline{n}^T \delta \underline{x}_{p-}}{\underline{n}^T \underline{f}_{p-}} \quad (3.26)$$

The dependence between the variation δt and $\delta \underline{x}_{p-}$ can be envisaged from Figure 3.3. Due to the variation $\delta \underline{x}_{p-}$ the disturbed solution after a time t_p does not lie exactly on the (fixed) surface Σ . The disturbed solution has to stay a time δt longer/shorter in \mathcal{V}_- , covering an additional distance $\underline{f}_{p-} \delta t$, to reach Σ . We infer from Figure 3.3 that the vectors $\delta \underline{x}_{p-}$ and $\underline{f}_{p-} \delta t$ are related by

$$\underline{n}^T \underline{f}_{p-} \delta t = -\underline{n}^T \delta \underline{x}_{p-}, \quad (3.27)$$

from which we can derive (3.26).


 Figure 3.3: Construction of δt for autonomous Σ .

Combining (3.24) and (3.26) gives

$$\delta \underline{x}_{p+} = \delta \underline{x}_{p-} + (\underline{f}_{p+} - \underline{f}_{p-}) \frac{\underline{n}^T \delta \underline{x}_{p-}}{\underline{n}^T \underline{f}_{p-}}. \quad (3.28)$$

We have now expressed the variation $\delta \underline{x}_{p+}$ in terms of the variation $\delta \underline{x}_{p-}$. The saltation matrix relates $\delta \underline{x}_{p+}$ to $\delta \underline{x}_{p-}$

$$\delta \underline{x}_{p+} = \underline{S} \delta \underline{x}_{p-}. \quad (3.29)$$

We obtain the saltation matrix $\underline{S} = \underline{\Phi}(t_{p+}, t_{p-})$ from (3.28) and (3.29) as

$$\underline{S} = \underline{I} + \frac{(\underline{f}_{p+} - \underline{f}_{p-}) \underline{n}^T}{\underline{n}^T \underline{f}_{p-}}. \quad (3.30)$$

The inverse of the saltation matrix $\underline{S}^{-1} = \underline{\Phi}(t_{p-}, t_{p+})$ is given by (for non-singular \underline{S})

$$\underline{S}^{-1} = \underline{I} + \frac{(\underline{f}_{p-} - \underline{f}_{p+}) \underline{n}^T}{\underline{n}^T \underline{f}_{p+}}. \quad (3.31)$$

The saltation matrix \underline{S} becomes singular if $\underline{n}^T \underline{f}_{p+} = 0$ which will not happen if the transversality condition (3.8) is fulfilled.

The saltation matrix was derived in this section for an autonomous indicator function $h(\underline{x}(t))$. Non-autonomous systems can give rise to non-autonomous indicator functions. However, non-autonomous time periodic systems can be transformed into autonomous systems having autonomous indicator functions (see Appendix B.1). Alternatively, one can derive the saltation matrix for a non-autonomous indicator function $h(t, \underline{x}(t))$ [Aizerman and Gantmakher, 1958; Filippov, 1988; Müller,

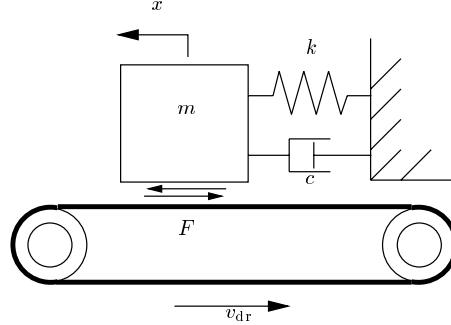


Figure 3.4: 1-DOF model with dry friction.

1995]. The saltation matrix for a non-autonomous indicator function is given by

$$\underline{S} = \underline{I} + \frac{(\underline{f}_{p+} - \underline{f}_{p-})\underline{n}^T}{\underline{n}^T \underline{f}_{p-} + \frac{\partial h}{\partial t}(t_p, \underline{x}(t_p))}. \quad (3.32)$$

3.4 Example I: The Stick-slip System

To demonstrate the above theory we will study a one-dimensional system with dry friction that possesses a stick-slip periodic solution.

Consider a mass m attached to inertial space by a spring k and damper c (Figure 3.4). The mass is riding on a driving belt, that is moving at a constant velocity v_{rel} . A friction force F acts between the mass and belt which is dependent on the relative velocity (see Appendix C.2 for the parameter values).

The state equation of this autonomous system reads as

$$\dot{\underline{x}} = \underline{f}(\underline{x}) = \begin{bmatrix} \dot{x} \\ -\frac{k}{m}x - \frac{c}{m}\dot{x} + \frac{F}{m} \end{bmatrix}, \quad (3.33)$$

where $\underline{x} = [x \quad \dot{x}]^T$ and F is given by a signum model with static friction point

$$F = \begin{cases} F(v_{\text{rel}}) = -F_{\text{slip}} \text{sgn } v_{\text{rel}}, & v_{\text{rel}} \neq 0 \quad \text{slip} \\ F(x, \dot{x}) = \min(|F_{\text{ex}}|, F_{\text{stick}}) \text{sgn}(F_{\text{ex}}), & v_{\text{rel}} = 0 \quad \text{stick} \end{cases} \quad (3.34)$$

with

$$F_{\text{ex}}(x, \dot{x}) = kx + c\dot{x}.$$

The maximum static friction force is denoted by F_{stick} and $v_{\text{rel}} = \dot{x} - v_{\text{dr}}$ is the relative velocity. This friction model is identical to the friction model of type (c) in Figure 2.5. Friction model (3.34) should be understood such that only a transition from stick to slip can take place if $|F_{\text{ex}}|$ exceeds F_{stick} .

This model permits explicit solutions for $c = 0$ due to its simplicity but it is not directly applicable in numerical analysis. Instead, an approximating switch model

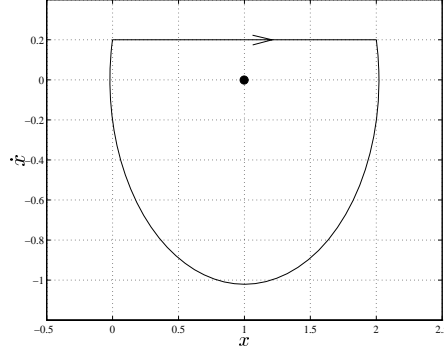


Figure 3.5: Phase portrait.

will be studied, which was discussed in Section 2.4. The state equation for the switch model reads as

$$\dot{\tilde{x}} = \begin{cases} \begin{bmatrix} -\frac{k}{m}x - \frac{c}{m}\dot{x} - \frac{F_{\text{slip}}}{m} \text{sgn } v_{\text{rel}} \\ \dot{x} \end{bmatrix} & |v_{\text{rel}}| > \eta \text{ or } |F_{\text{ex}}| > F_{\text{stick}} \\ \begin{bmatrix} v_{\text{dr}} \\ -v_{\text{rel}}\sqrt{\frac{k}{m}} \end{bmatrix} & |v_{\text{rel}}| < \eta \text{ and } |F_{\text{ex}}| < F_{\text{stick}} \end{cases} \quad (3.35)$$

A region of near-zero velocity is defined as $|v_{\text{rel}}| < \eta$. The space \mathbb{R}^2 is divided in three subspaces \mathcal{V} , \mathcal{W} and \mathcal{D} as indicated in Figure 3.6. The small parameter η is enlarged in Figure 3.6 to make \mathcal{D} visible.

A stable stick-slip periodic solution of this system exists and is depicted in Figure 3.5 together with the equilibrium point $(x, \dot{x}) = (1, 0)$. As this system is autonomous, the hyper-surfaces are not dependent on time. It can be seen that the state traverses \mathcal{V} (the slip phase) and \mathcal{D} (the stick phase). If the state leaves \mathcal{V} and enters \mathcal{D} , the hyper-surface Σ_α is crossed with normal \underline{n}_α where

$$h_\alpha(x, \dot{x}) = \dot{x} - v_{\text{dr}}, \quad (3.36)$$

and

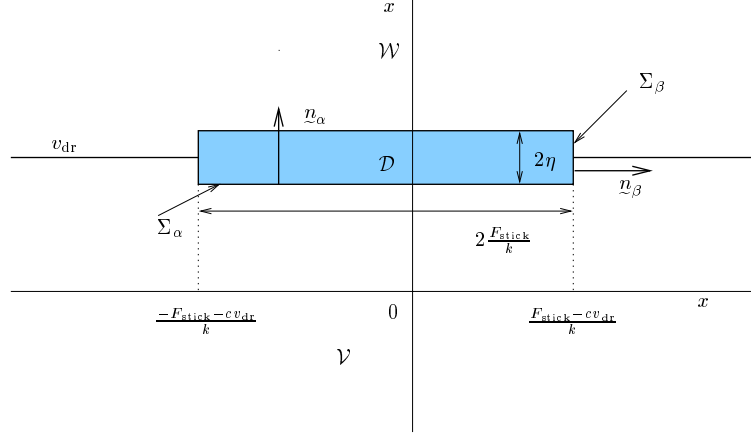
$$\underline{n}_\alpha = \begin{bmatrix} 0 \\ 1 \end{bmatrix}. \quad (3.37)$$

Likewise, if the state leaves \mathcal{D} and enters \mathcal{V} again, the hyper-surface Σ_β is crossed with normal \underline{n}_β where

$$h_\beta(x, \dot{x}) = kx + cv_{\text{dr}} - F_{\text{stick}}, \quad (3.38)$$

and

$$\underline{n}_\beta = \begin{bmatrix} 1 \\ 0 \end{bmatrix}. \quad (3.39)$$

Figure 3.6: Definition of subspaces \mathcal{V} , \mathcal{W} and \mathcal{D} .

Let us assume that the state vector crosses Σ_α at $t = t_\alpha$ and Σ_β at $t = t_\beta$. We can now construct the saltation matrices $\underline{\mathcal{S}}_\alpha$ and $\underline{\mathcal{S}}_\beta$. The right-hand sides of (3.35) at $t = t_\alpha$ for $\lim \eta \downarrow 0$ are

$$\underline{f}_{\alpha-} = \begin{bmatrix} v_{\text{dr}} \\ \ddot{x}_{\alpha-} \end{bmatrix}, \quad \underline{f}_{\alpha+} = \begin{bmatrix} v_{\text{dr}} \\ 0 \end{bmatrix}. \quad (3.40)$$

The saltation matrix $\underline{\mathcal{S}}_\alpha$ yields

$$\underline{\mathcal{S}}_\alpha = \underline{I} + \frac{(\underline{f}_{\alpha+} - \underline{f}_{\alpha-})n_\alpha^\text{T}}{n_\alpha^\text{T}\underline{f}_{\alpha-}} = \begin{bmatrix} 1 & 0 \\ 0 & 0 \end{bmatrix}, \quad (3.41)$$

which is independent of any system parameter.

Conducting the same for $\underline{\mathcal{S}}_\beta$ yields

$$\underline{f}_{\beta-} = \begin{bmatrix} v_{\text{dr}} \\ 0 \end{bmatrix}, \quad \underline{f}_{\beta+} = \begin{bmatrix} v_{\text{dr}} \\ -\frac{\Delta F}{m} \end{bmatrix}, \quad (3.42)$$

with $\Delta F = F_{\text{stick}} - F_{\text{slip}}$. Substitution yields $\underline{\mathcal{S}}_\beta$

$$\underline{\mathcal{S}}_\beta = \underline{I} + \frac{(\underline{f}_{\beta+} - \underline{f}_{\beta-})n_\beta^\text{T}}{n_\beta^\text{T}\underline{f}_{\beta-}} = \begin{bmatrix} 1 & 0 \\ -\frac{\Delta F}{mv_{\text{dr}}} & 1 \end{bmatrix}. \quad (3.43)$$

Note that the saltation matrix $\underline{\mathcal{S}}_\alpha$ is singular causing the fundamental solution matrix to be singular. The physical meaning of this is that the solution of the state vector is uniquely mapped from \underline{x}_0 in \mathcal{V} to $\underline{x}(t)$ in \mathcal{D} but the inverse mapping does not exist. If different vector bundles enter the stick phase, they all pass the same states on the stick phase and leave the stick phase from the same state \underline{x}_β . So, if the solution enters the stick phase, knowledge about its initial state is lost. The fundamental solution matrix for the periodic solution of system (3.35) is plotted in Figure 3.7. Jumps at $t = t_\alpha$ and $t = t_\beta$ in the fundamental solution matrix can be clearly distinguished.

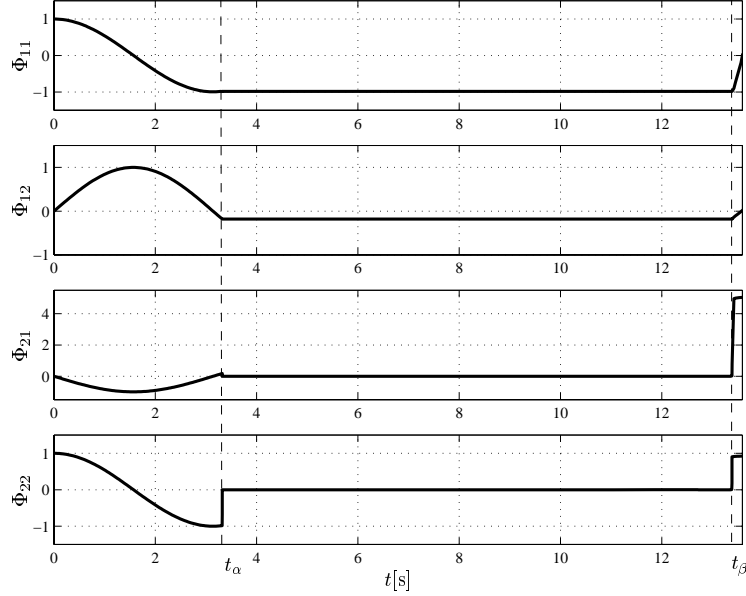


Figure 3.7: Fundamental solution matrix.

3.5 Example II: The Discontinuous Support

As a second example we will consider a mass-spring system with a discontinuous support (Figure 3.8a). The support is massless, has a spring stiffness k_f and damping coefficient c_f , which makes the support a first-order system. The displacement of the mass relative to the equilibrium position is denoted by x and of the support by y . The system has two possible modes: the mass is in contact with the support or the mass is not in contact with the support. Let f_c denote the contact force between mass and support. If the mass is not in contact the following holds:

$$x < y \quad \text{and} \quad f_c = 0,$$

and if the mass is in contact, we have:

$$x = y \quad \text{and} \quad f_c = k_f y + c_f \dot{y} = k_f x + c_f \dot{x} \geq 0.$$

The support, being a first-order system, relaxes to the equilibrium state, $y = 0$, if the mass is not in contact with the support. If we assume that the relaxation time of the support is much smaller than the time between two contact events, we can neglect the free motion of the support. It is therefore assumed that the support is at rest at the moment that contact is made. This assumption reduces the system to one with a second-order equation. The free motion of the mass satisfies the ordinary differential equation

$$m\ddot{x} + kx = f_0 \cos \omega t \quad \text{no contact,} \quad (3.44)$$

whereas the equation of motion of the mass in contact with the support is

$$m\ddot{x} + c_f\dot{x} + (k + k_f)x = f_0 \cos \omega t \quad \text{contact.} \quad (3.45)$$

The mass comes in contact with the support if the displacement becomes zero, i.e. if $x = 0$. The mass loses contact with the support if the contact force becomes zero, i.e. if $f_c = k_f x + c_f \dot{x} = 0$. We introduce the state-vector $\underline{x} = [x \quad \dot{x}]^T$ and define the following two indicator functions:

$$h_\alpha(x, \dot{x}) = x, \quad (3.46)$$

$$h_\beta(x, \dot{x}) = k_f x + c_f \dot{x}. \quad (3.47)$$

The mass is not in contact with the support if $\underline{x} \in \mathcal{V}_-$, with

$$\mathcal{V}_- = \{\underline{x} \in \mathbb{R}^2 \mid h_\alpha(x, \dot{x}) < 0 \vee h_\beta(x, \dot{x}) < 0\}, \quad (\text{no contact})$$

and the mass is in contact with the support if $\underline{x} \in \mathcal{V}_+$, with

$$\mathcal{V}_+ = \{\underline{x} \in \mathbb{R}^2 \mid h_\alpha(x, \dot{x}) > 0 \wedge h_\beta(x, \dot{x}) > 0\} \quad (\text{contact}).$$

The hyper-surface Σ , which divides the state-space \mathbb{R}^2 in the subspaces \mathcal{V}_- and \mathcal{V}_+ , consists of the conjunction of two surfaces Σ_α and Σ_β . The hyper-surface Σ_α is defined by

$$\Sigma_\alpha = \{\underline{x} \in \mathbb{R}^2 \mid h_\alpha(x, \dot{x}) = 0, h_\beta(x, \dot{x}) \geq 0\}, \quad (3.48)$$

and has the normal

$$\underline{n}_\alpha = \begin{bmatrix} 1 \\ 0 \end{bmatrix}. \quad (3.49)$$

The hyper-surface Σ_β is defined by

$$\Sigma_\beta = \{\underline{x} \in \mathbb{R}^2 \mid h_\alpha(x, \dot{x}) \geq 0, h_\beta(x, \dot{x}) = 0\}, \quad (3.50)$$

and has the normal

$$\underline{n}_\beta = \begin{bmatrix} k_f \\ c_f \end{bmatrix}. \quad (3.51)$$

The hyper-surface Σ , consisting of Σ_α and Σ_β , and the subspaces \mathcal{V}_- and \mathcal{V}_+ are depicted in Figure 3.8b. Remark that the hyper-surface Σ is non-smooth at the origin.

The state equation of this non-autonomous discontinuous system reads as

$$\dot{\underline{x}}(t) = \underline{f}(t, \underline{x}(t)) = \begin{cases} \underline{f}_-(t, \underline{x}(t)) & \underline{x} \in \mathcal{V}_- \\ \underline{f}_+(t, \underline{x}(t)) & \underline{x} \in \mathcal{V}_+, \end{cases} \quad (3.52)$$

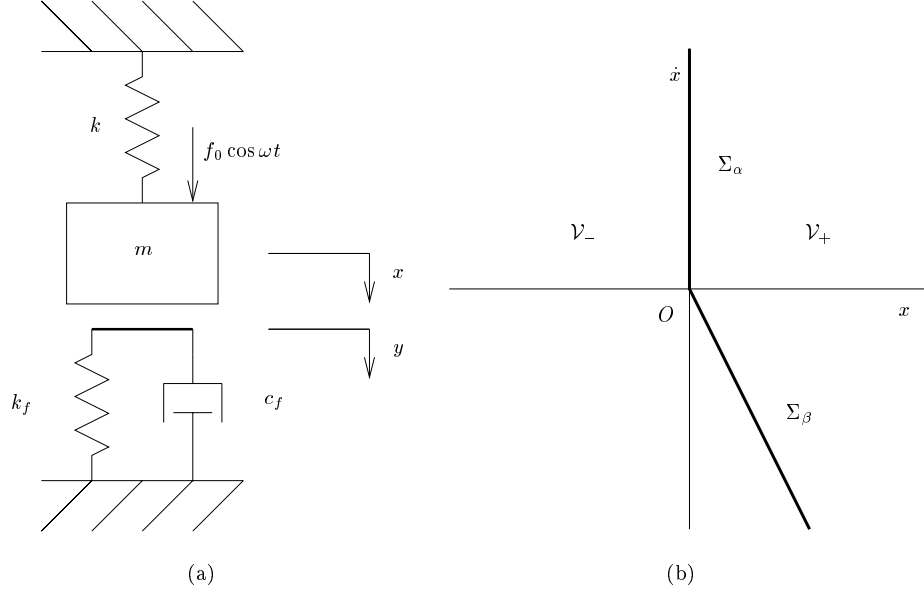


Figure 3.8: Mass with discontinuous support.

with

$$\underline{f}_-(t, \underline{x}) = \begin{bmatrix} \dot{x} \\ -\frac{k}{m}x + \frac{f_0}{m} \cos \omega t \end{bmatrix}, \quad (3.53)$$

and

$$\underline{f}_+(t, \underline{x}) = \begin{bmatrix} \dot{x} \\ -\frac{k+k_f}{m}x - \frac{c_f}{m}\dot{x} + \frac{f_0}{m} \cos \omega t \end{bmatrix}. \quad (3.54)$$

System (3.52), which is discontinuous for $\underline{x} \in \Sigma$, can be extended to a differential inclusion with Filippov's convex method as described in Chapter 2.

We first consider the contact event, which is the transition from the mode without contact to the mode with contact. Let us assume that trajectory $\underline{x}(t)$ crosses Σ , leaving \mathcal{V}_- and entering \mathcal{V}_+ , at $t = t_\alpha$. The trajectory crosses therefore the Σ_α part of Σ at this instance. We can now construct the saltation matrix \underline{S}_α of the contact event. The right-hand sides at the instance t_α are

$$\underline{f}_{\alpha-} = \begin{bmatrix} \dot{x}_\alpha \\ -\frac{k}{m}x_\alpha + \frac{f_0}{m} \cos \omega t_\alpha \end{bmatrix}, \quad (3.55)$$

$$\underline{f}_{\alpha+} = \begin{bmatrix} \dot{x}_\alpha \\ -\frac{k+k_f}{m}x_\alpha - \frac{c_f}{m}\dot{x}_\alpha + \frac{f_0}{m} \cos \omega t_\alpha \end{bmatrix}. \quad (3.56)$$

The saltation matrix \underline{S}_α becomes

$$\begin{aligned}\underline{S}_\alpha &= \underline{I} + \frac{(f_{\alpha+} - f_{\alpha-})n_\alpha^\top}{\tilde{n}_\alpha^\top \tilde{f}_{\alpha-}} \\ &= \underline{I} + \begin{bmatrix} 0 & 0 \\ -\frac{c_f}{m} & 0 \end{bmatrix} = \begin{bmatrix} 1 & 0 \\ -\frac{c_f}{m} & 1 \end{bmatrix}.\end{aligned}\quad (3.57)$$

We now consider the transition from the mode with contact to the mode without contact. Let us assume that the state vector crosses Σ , leaving \mathcal{V}_+ and entering \mathcal{V}_- , at $t = t_\beta$. The state crosses therefore the Σ_β part of Σ at this instance. Consequently, the following holds

$$f_c = k_f x_\beta + c_f \dot{x}_\beta = 0. \quad (3.58)$$

We can now construct the saltation matrix \underline{S}_β . The right-hand sides at the instance t_β are

$$\tilde{f}_{\beta-} = \begin{bmatrix} \dot{x}_\beta \\ -\frac{k+k_f}{m}x_\beta - \frac{c_f}{m}\dot{x}_\beta + \frac{f_0}{m}\cos\omega t_\beta \end{bmatrix}, \quad (3.59)$$

$$\tilde{f}_{\beta+} = \begin{bmatrix} \dot{x}_\beta \\ -\frac{k}{m}x_\beta + \frac{f_0}{m}\cos\omega t_\beta \end{bmatrix}. \quad (3.60)$$

If we substitute (3.58) in (3.59) and (3.60), then the latter equations appear to be identical

$$\tilde{f}_{\beta-} = \tilde{f}_{\beta+}.$$

Consequently, \underline{S}_β is simply the identity matrix.

$$\underline{S}_\beta = \underline{I} \quad (3.61)$$

The results show that the saltation matrices \underline{S}_α and \underline{S}_β are not dependent on the support stiffness k_f . The saltation matrix \underline{S}_α is affected, however, by the ratio $\frac{c_f}{m}$. The physical interpretation must be sought in the discontinuity of the contact force f_c . The spring force before the contact event, kx , is equal to the spring force after the contact event, $(k + k_f)x$, because contact is made when $x = 0$. But the damping force before the contact event, being zero, is not equal to the damping force after the contact event, $c_f \dot{x}$. The contact force f_c will be continuous for the transition from contact to no-contact, which is the reason that \underline{S}_β is equal to the identity matrix.

If the damping coefficient c_f is set to zero, the system reduces to a second-order system with discontinuous stiffness, which is a non-smooth continuous system. In this case, the hyper-surfaces Σ_α and Σ_β do not form an angle and Σ is a smooth hyper-plane. The saltation matrices \underline{S}_α and \underline{S}_β are both equal to the identity matrix in this case. It can be concluded that the jumps in the fundamental solution matrix are not caused by the discontinuous stiffness but by the discontinuous damping term.

Chapter 4

Non-smooth Analysis of Filippov Systems

*‘Every scientific truth goes through three stages.
First, people say it conflicts with the Bible. Next
they say it had been discovered before. Lastly, they
say they always believed it.’*

LOUIS AGASSIZ, (1807-1873)

The method of linear approximation is developed in this chapter and applied to saltation matrices and Jacobian matrices. Linear approximation is compared with the generalized differential of Clarke in Section 4.2. The non-smooth analysis tools developed in this chapter will be used to study bifurcation points of non-smooth continuous systems in Chapter 5 and Filippov systems in Chapter 6.

4.1 Linear Approximations at the Discontinuity

Discontinuities in the vector field f cause jumps in the fundamental solution matrix as was shown in the preceding chapter. The discontinuous differential equation is therefore often approximated by a continuous differential equation. The approximation can be chosen to be smooth, which is called the ‘smoothing method’ (see Section 2.4), but this is not necessary. The approximation should at least yield a continuous differential equation and have a residue which tends to zero for increasing order of approximation.

We employ a special approximation in the sequel for analytical purposes. The jump of the vector field f is approximated by a linear variation of f from f_- to f_+ in a thin space around the hyper-surface of discontinuity. We should keep in mind that a smooth (or continuous) approximation does not necessarily describe all solutions of the discontinuous system. This is for instance the case when the

discontinuous system exposes a repulsion sliding mode which implies non-uniqueness of solutions. The smooth or continuous approximation has uniqueness of solutions and can therefore not describe the behaviour at the repulsion sliding mode.

It will be shown that this linear approximation of the vector field at the hyper-surface of discontinuity also yields a linear variation of the saltation matrix.

The linear approximation at the discontinuity is suitable for analytical purposes, due to its simplicity, and will prove to be an important tool in the bifurcation analysis of discontinuous systems.

In Section 4.2 we will show that the concept of linear approximation is identical to the generalized derivative.

A single hyper-surface

Consider again the discontinuous system 2.13 where the indicator equation h defines the hyper-surface of discontinuity Σ .

$$\dot{\underline{x}}(t) = \underline{f}(t, \underline{x}(t)) = \begin{cases} \underline{f}_-(t, \underline{x}(t)) & \underline{x} \in \mathcal{V}_- \\ \underline{f}_+(t, \underline{x}(t)) & \underline{x} \in \mathcal{V}_+, \end{cases} \quad (4.1)$$

with

$$\begin{aligned} \mathcal{V}_- &= \{\underline{x} \in \mathbb{R}^n \mid h(\underline{x}(t)) < 0\} \\ \Sigma &= \{\underline{x} \in \mathbb{R}^n \mid h(\underline{x}(t)) = 0\} \\ \mathcal{V}_+ &= \{\underline{x} \in \mathbb{R}^n \mid h(\underline{x}(t)) > 0\} \end{aligned} \quad (4.2)$$

In the following we will briefly denote a function $g(t, \underline{x}(t))$ by g .

The hyper-surface Σ , on which \underline{f} is discontinuous, will now be replaced by a thin space $\tilde{\Sigma}$ with thickness ν . If ν approaches zero, then the space $\tilde{\Sigma}$ becomes infinitely thin. The discontinuous vector field \underline{f} is replaced by a continuous vector field $\tilde{\underline{f}}$. The vector field $\tilde{\underline{f}}$ in $\tilde{\Sigma}$ varies linearly from \underline{f}_- to \underline{f}_+ to ensure continuity.

$$\dot{\underline{x}}(t) = \tilde{\underline{f}} = \begin{cases} \underline{f}_- & \underline{x} \in \tilde{\mathcal{V}}_- \\ (\underline{f}_+ - \underline{f}_-)\frac{h}{\nu} + \underline{f}_- & \underline{x} \in \tilde{\Sigma} \\ \underline{f}_+ & \underline{x} \in \tilde{\mathcal{V}}_+, \end{cases} \quad (4.3)$$

with

$$\begin{aligned} \tilde{\mathcal{V}}_- &= \{\underline{x} \in \mathbb{R}^n \mid h(\underline{x}(t)) < 0\} \\ \tilde{\Sigma} &= \{\underline{x} \in \mathbb{R}^n \mid 0 \leq h(\underline{x}(t)) \leq \nu\} \\ \tilde{\mathcal{V}}_+ &= \{\underline{x} \in \mathbb{R}^n \mid h(\underline{x}(t)) > \nu\} \end{aligned} \quad (4.4)$$

Clearly, the vector field $\tilde{\underline{f}}$ is continuous and converges asymptotically to \underline{f} as $\nu \downarrow 0$. The Jacobian of $\tilde{\underline{f}}$ follows from (4.3) and (2.9) to be

$$\tilde{\underline{J}}(t, \underline{x}(t)) = \begin{cases} \underline{J}_- & \underline{x} \in \tilde{\mathcal{V}}_- \\ (\underline{J}_+ - \underline{J}_-)\frac{h}{\nu} + \underline{J}_- & \underline{x} \in \tilde{\Sigma} \\ \underline{J}_+ & \underline{x} \in \tilde{\mathcal{V}}_+, \end{cases} \quad (4.5)$$

and is in fact not properly defined on the borders between $\tilde{\mathcal{V}}_-$, $\tilde{\mathcal{V}}_+$ and $\tilde{\Sigma}$ as \tilde{f} is not necessarily smooth. This will not turn out to be problematic. Remark that system (4.3) is a non-smooth continuous system, which has existence and uniqueness of solutions (Theorem 2.1).

We are interested in bifurcations of periodic solutions of discontinuous systems. The fundamental solution matrix of a discontinuous system can jump as we elaborated in Chapter 3. A periodic solution can be regarded as a fixed point of a Poincaré map $P(\underline{x})$ on a Poincaré section (see Section 6.4). The derivative of the Poincaré map $DP(\underline{x})$ can therefore also jump as it is directly related to the fundamental solution matrix, see (6.7). We assume the Poincaré map itself to be locally continuous at the fixed point. As periodic solutions are fixed points of $P(\underline{x})$, we will also study bifurcations of fixed points of non-smooth systems. Having periodic solutions in mind, we will study only fixed points of continuous vector fields with discontinuous Jacobians. We consider therefore continuous but non-smooth *mappings*:

Bifurcations of fixed points: the vector field is

- a) continuous: $\tilde{f}_-(t, \underline{x}(t)) = \tilde{f}_+(t, \underline{x}(t))$ if $\underline{x}(t) \in \Sigma$
- b) non-smooth: $\tilde{J}_-(t, \underline{x}(t)) \neq \tilde{J}_+(t, \underline{x}(t))$ if $\underline{x}(t) \in \Sigma$

Bifurcations of periodic solutions:

- a) the Poincaré map $P(\underline{x})$ is continuous in \underline{x}
- b) the derivative $DP(\underline{x})$ of the Poincaré map is non-smooth, which yields $\tilde{f}_- \neq \tilde{f}_+$ if $\underline{x}(t) \in \Sigma$

Remarks: The statement that only continuous mappings will be considered is too restrictive. Poincaré mappings are in general discontinuous (for example the Lorenz system, see Guckenheimer and Holmes [1983], page 313). We will mainly consider mappings which are continuous in a sufficiently large neighbourhood around the fixed point of the mapping. In Section 6.7, however, an example will be given where the Poincaré map is discontinuous at the fixed point, which results in infinitely unstable periodic solutions. Note that this is a sliding mode problem for which (3.8) does not hold.

We now study how the saltation matrix changes as the solution $\underline{x}(t)$ is crossing the space $\tilde{\Sigma}$ from $\tilde{\mathcal{V}}_-$ to $\tilde{\mathcal{V}}_+$ (Figure 4.1), that is $\underline{x}(t)$ crosses the hyper-surface $\tilde{\Sigma}$ *transversally* and (2.17) is satisfied. Neighbouring solutions of $\underline{x}(t)$ will also cross $\tilde{\Sigma}$ transversally. Uniqueness of solutions in forward and backward time (Theorem 2.1) assures that the neighbouring solutions do not join with $\underline{x}(t)$. We denote the state at the border of $\tilde{\mathcal{V}}_-$ and $\tilde{\Sigma}$ by \underline{x}_0 at time t_0 . We denote the state at the border of $\tilde{\mathcal{V}}_+$ and $\tilde{\Sigma}$ by \underline{x}_1 at time t_1 . Let the solution starting from \underline{x}_0 travel a distance $\Delta \underline{x}$ in $\tilde{\Sigma}$ during a time Δt . The following holds

$$\begin{aligned} t_0 &\leq t_0 + \Delta t \leq t_1 \\ \Delta \underline{x}(t_0) &= \underline{0} \\ \underline{x}_1 &= \underline{x}_0 + \Delta \underline{x}(t_1) \end{aligned} \tag{4.6}$$

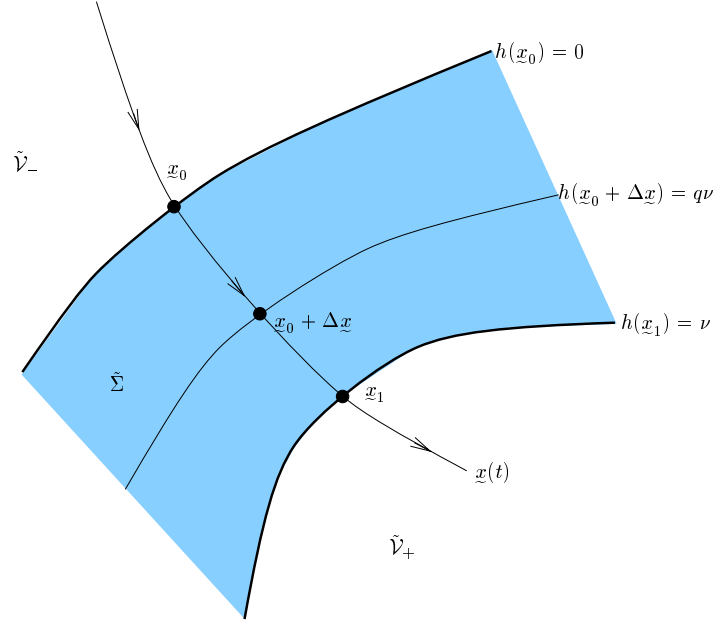


Figure 4.1: Linear approximation over a hyper-surface.

We expand the indicator function $h(\underline{x})$ as a Taylor approximation around \underline{x}_0 ,

$$h(\underline{x}_0 + \Delta \underline{x}) = h(\underline{x}_0) + \frac{\partial h}{\partial \underline{x}^T} \Delta \underline{x} + O(\Delta \underline{x}^2). \quad (4.7)$$

The indicator function should be chosen such that it always holds that

$$\frac{\partial h}{\partial \underline{x}^T} \neq \underline{0}. \quad (4.8)$$

As ν approaches zero, the space $\tilde{\Sigma}$ becomes infinitely thin and $\Delta \underline{x} \downarrow \underline{0}$ and $\Delta t \downarrow 0$. It therefore suffices to take only the linear term into account in the Taylor approximation of (4.7) as $\nu \downarrow 0$. It follows from the definition of $\tilde{\mathcal{V}}_-$ in (4.4) that

$$h(\underline{x}_0) = 0 \quad (4.9)$$

and that

$$h(\underline{x}_1) = \nu. \quad (4.10)$$

We assume that the indicator function in $\tilde{\Sigma}$ has values between 0 and ν

$$\begin{aligned} h(\underline{x}_0) &\leq h(\underline{x}_0 + \Delta \underline{x}) \leq h(\underline{x}_1) \\ 0 &\leq h(\underline{x}_0 + \Delta \underline{x}) \leq \nu. \end{aligned} \quad (4.11)$$

and, additionally, that the indicator function in $\tilde{\Sigma}$ increases monotonically from 0 to ν when t is increased from t_0 to t_1 . This assumption holds when $\tilde{\Sigma}$ is infinitely

thin and when (4.8) holds. Consequently, due to monotonicity and the omission of higher-order terms it is allowed to express the indicator function for $\nu \downarrow 0$ as a linear function of a variable $q(t)$

$$h(\underline{x}_0 + \Delta \underline{x}(t)) = q(t)\nu \quad (4.12)$$

where $0 \leq q(t) \leq 1$ on $t_0 \leq t \leq t_1$. The variable $q(t)$ is a parameterization of the transversal solution $\underline{x}(t)$ in the space $\tilde{\Sigma}$, where $q(t_0) = 0$ corresponds to $\underline{x}(t_0)$ on the border between $\tilde{\mathcal{V}}_-$ and $\tilde{\Sigma}$ and $q(t_1) = 1$ corresponds to $\underline{x}(t_1)$ on the border between $\tilde{\Sigma}$ and $\tilde{\mathcal{V}}_+$. The value of $q(t)$ is found from (4.12) with $\underline{x}(t) = \underline{x}_0 + \Delta \underline{x}(t) \in \tilde{\Sigma}$. Similarly, we express the distance $\Delta \underline{x}(t_0 + \Delta t)$ as a Taylor approximation up to the linear term with $\Delta t \downarrow 0$ for $\nu \downarrow 0$

$$\Delta \underline{x}(t_0 + \Delta t) = \int_{t_0}^{t_0 + \Delta t} \tilde{f} dt = \underline{f}_- \Delta t + O(\Delta t^2) \quad (4.13)$$

Substitution of (4.9) and (4.12) in (4.7) yields

$$q(t_0 + \Delta t)\nu = \underline{n}^T \underline{f}_- \Delta t \quad (4.14)$$

for $\nu \downarrow 0$. We will omit the dependence of q on t in the sequel.

The Jacobian can be approximated for small ν and bounded \tilde{f} by

$$\tilde{\underline{J}}(t_0 + \Delta t, \underline{x}_0 + \Delta \underline{x}(t)) = \frac{1}{\nu} (\underline{f}_+ - \underline{f}_-) \underline{n}^T + O(1) \quad (4.15)$$

which becomes *large* for $\nu \downarrow 0$ and $\underline{f}_+ \neq \underline{f}_-$. We can now construct the saltation matrix $\tilde{\underline{S}} = \underline{\Phi}(t_0 + \Delta t, t_0)$ for $\nu \downarrow 0$ from the previous results

$$\begin{aligned} \tilde{\underline{S}} &= \underline{I} + \int_{t_0}^{t_0 + \Delta t} \tilde{\underline{J}}(t, \underline{x}(t)) \underline{\Phi}(t_0 + \Delta t, t_0) dt \\ &= \underline{I} + (\underline{f}_+ - \underline{f}_-) \frac{\underline{n}^T}{\nu} \Delta t + O(\Delta t) \\ &= \underline{I} + q \frac{(\underline{f}_+ - \underline{f}_-) \underline{n}^T}{\underline{n}^T \underline{f}_-} + O(\Delta t) \end{aligned} \quad (4.16)$$

The saltation matrix $\tilde{\underline{S}}$ converges therefore for $\nu \downarrow 0$ to the set

$$\begin{aligned} \tilde{\underline{S}} &= \left\{ \underline{I} + q \frac{(\underline{f}_+ - \underline{f}_-) \underline{n}^T}{\underline{n}^T \underline{f}_-}, \forall 0 \leq q \leq 1 \right\} \\ &= \left\{ \underline{I} + q(\underline{S} - \underline{I}), \forall 0 \leq q \leq 1 \right\} \end{aligned} \quad (4.17)$$

where \underline{S} is the saltation matrix over Σ given by (3.30). The saltation matrix therefore behaves linearly over $\tilde{\Sigma}$ if $\nu \downarrow 0$. The derivation is given for autonomous h but the same result could have been obtained for non-autonomous h .

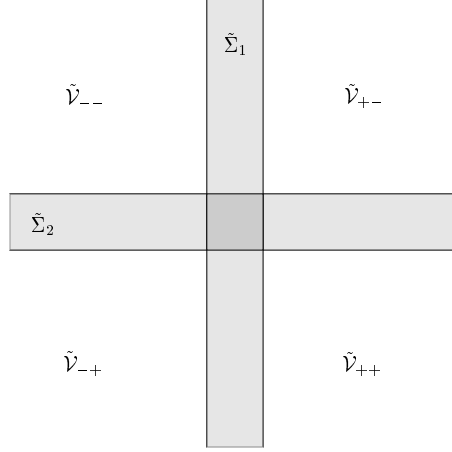


Figure 4.2: Linear approximation with two hyper-surfaces.

For fixed points we have $\underline{f}_{-} = \underline{f}_{+}$ and the Jacobian on $\tilde{\Sigma}$ is therefore given by

$$\tilde{\underline{J}}(t, \underline{x}_0 + \Delta \underline{x}(t)) = (\underline{J}_{+} - \underline{J}_{-})q(t) + \underline{J}_{-} \quad (4.18)$$

The Jacobian of fixed points behaves therefore linearly in $\tilde{\Sigma}$. If $\nu \downarrow 0$, then the space $\tilde{\Sigma}$ reduces to the hyper-surface Σ and the Jacobian on Σ becomes set-valued. The set-valued Jacobian is given by

$$\tilde{\underline{J}}(t, \underline{x}) = \{(\underline{J}_{+} - \underline{J}_{-})q + \underline{J}_{-}, \forall 0 \leq q \leq 1\} \quad (4.19)$$

where $\underline{x} \in \Sigma$. For fixed points of non-smooth continuous systems, the linear approximation with $\nu > 0$ smoothens the continuous non-smooth vector field. For periodic solutions of Filippov systems, the linear approximation with $\nu > 0$ replaces the discontinuous vector field by a continuous vector field.

A double hyper-surface

The fixed point could also be located on the intersection of two hyper-surfaces Σ_1 and Σ_2 . The linear approximation is analogous to the one given in the previous subsection but more elaborate. Each hyper-surface Σ_j has now to be replaced by a corresponding thin space $\tilde{\Sigma}_j$ with parameter q_j (Figure 4.2). The fixed point is located in the double-hatched zone where the hyper-surfaces intersect. The two hyper-surfaces divide the state-space in four spaces \mathcal{V}_{--} , \mathcal{V}_{+-} , \mathcal{V}_{-+} and \mathcal{V}_{++} with Jacobians \underline{J}_{--} , \underline{J}_{+-} , \underline{J}_{-+} and \underline{J}_{++} . The linear approximation of the Jacobian over hyper-surface $\tilde{\Sigma}_1$ at the fixed point is

$$\begin{aligned} \tilde{\underline{J}}_I &= \{q_1(\underline{J}_{++} - \underline{J}_{--}) + \underline{J}_{--}, \forall 0 \leq q_1 \leq 1\} && \text{above } \tilde{\Sigma}_2 \\ \tilde{\underline{J}}_{II} &= \{q_1(\underline{J}_{++} - \underline{J}_{-+}) + \underline{J}_{-+}, \forall 0 \leq q_1 \leq 1\} && \text{below } \tilde{\Sigma}_2 \end{aligned} \quad (4.20)$$

with

$$\underline{J}_{+-} - \underline{J}_{--} = \underline{J}_{++} - \underline{J}_{-+}$$

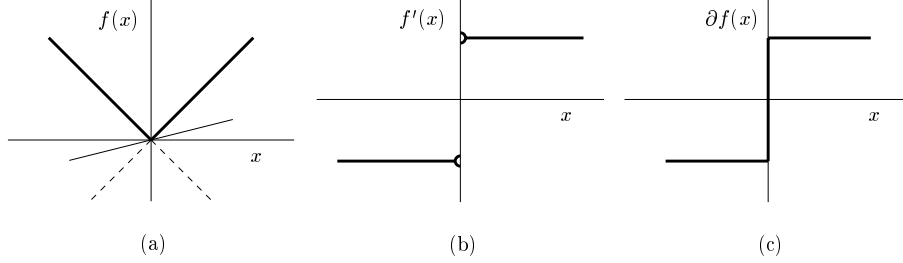


Figure 4.3: Function (a), classical derivative (b) and generalized derivative (c).

because the same hyper-surface is crossed. With a second linear approximation we can set up the Jacobian over the other hyper-surface

$$\begin{aligned} \tilde{J} &= \{q_2(\tilde{J}_{II} - \tilde{J}_I) + \tilde{J}_I, \forall 0 \leq q_2 \leq 1\} \\ &= \{q_2(\underline{J}_{-+} - \underline{J}_{--}) + q_1(\underline{J}_{+-} - \underline{J}_{--}) + \underline{J}_{--}, \forall 0 \leq q_1 \leq 1, \forall 0 \leq q_2 \leq 1\} \end{aligned} \quad (4.21)$$

which is a linear combination in q_1 and q_2 in the double shaded space around the fixed point.

4.2 Generalized Differentials

The concept of *linear approximation* is closely related with the subdifferential of Clarke [Clarke et al., 1998; Tikhomirov, 1989], also called *generalized differential*.

Consider a scalar continuous piecewise differentiable function $f(x)$ with a kink at one value of x , such as $f(x) = |x|$ (Figure 4.3). The derivative $f'(x)$ is defined by the tangent line to the graph of f when the graph is smooth at x . Although the function is not absolutely differentiable at every point x , it possesses a left and right derivative defined as

$$f'_-(x) = \lim_{y \uparrow x} \frac{f(y) - f(x)}{y - x}, \quad f'_+(x) = \lim_{y \downarrow x} \frac{f(y) - f(x)}{y - x}. \quad (4.22)$$

The *generalized derivative* of f at x is declared as *any* value $f'_q(x)$ included between its left and right derivatives. Such an intermediate value can be expressed as a convex combination of the left and right derivatives.

$$f'_q(x) = (1 - q)f'_-(x) + qf'_+(x) \quad , \quad 0 \leq q \leq 1 \quad (4.23)$$

Geometrically, a generalized derivative is the slope of *any* line drawn through the point $(x, f(x))$ and between the left and right tangent lines (drawn by dashed lines in Figure 4.3a). The set of all the generalized derivatives of f at x , more generally the convex hull of the derivative extremes, is called the *generalized differential* of f at x .

$$\begin{aligned} \partial f(x) &= \overline{\text{co}}\{f'_-(x), f'_+(x)\} \\ &= \{f'_q(x) \mid f'_q(x) = (1 - q)f'_-(x) + qf'_+(x), \forall q \mid 0 \leq q \leq 1\} \end{aligned} \quad (4.24)$$

The generalized differential is the set of all the slopes of all the lines included in the cone bounded by the left and right tangent lines and is a closed convex set. Alternatively, it consists in closing the graph of $f'(x)$ at the points where it is discontinuous (Figure 4.3b,c). In non-smooth analysis, the generalized differential is used to define a local extremum of f at x by $0 \in \partial f$, which is the generalized form of $f'(x) = 0$ in smooth analysis [Clarke et al., 1998; Tikhomirov, 1989].

In the previous section the concept of linear approximation was introduced with approximation parameter ν . Considering the limit of ν going to zero, it was shown that the Jacobian behaves on the hyper-surface as (4.18)

$$\tilde{\underline{J}} = \{(1 - q)\underline{J}_- + q\underline{J}_+, \forall 0 \leq q \leq 1\}.$$

and the saltation matrix as (4.17)

$$\tilde{\underline{S}} = \{(1 - q)\underline{I} + q\underline{S}, \forall 0 \leq q \leq 1\},$$

or in terms of the fundamental solution matrix

$$\tilde{\underline{\Phi}} = \{(1 - q)\underline{\Phi}_- + q\underline{\Phi}_+, \forall 0 \leq q \leq 1\}. \quad (4.25)$$

The Jacobian of the linear approximation, $\tilde{\underline{J}}$, can be regarded as the generalized Jacobian in the sense of Clarke, that is, the generalized differential of the vector field \underline{f} with respect to the state \underline{x}

$$\tilde{\underline{J}} = \partial_{\underline{x}} \underline{f}. \quad (4.26)$$

Similarly, the generalized fundamental solution matrix can be defined as the generalized differential of the solution $\underline{x}(t)$ with respect to the initial condition \underline{x}_0 .

$$\tilde{\underline{\Phi}}(t, t_0) = \partial_{\underline{x}_0} \underline{x}(t) \quad (4.27)$$

We conclude that the approximation of the vector field by a linear approximation, as outlined in the previous section, converges for the Jacobian and fundamental solution matrix to their generalized differential forms. We could raise the hypothesis that *any* nonlinear monotone asymptotic approximation converges to the results of the generalized differential (see also Anosov [1959]). The linear approximation was obtained from the Taylor expansion of the indicator function (4.7) by neglecting higher-order terms. The linear approximation came naturally without prior assumptions. Any monotone approximation will therefore converge to the linear approximation which in the limit converges to the generalized differential.

This chapter applied linear approximation and the concept of generalized differentials to fundamental solution matrices. This is a new application of the generalized differential and will be of use to study bifurcation points of non-smooth continuous systems and Filippov systems in the next chapters.

Chapter 5

Bifurcations of Fixed Points

*'In questions of science the authority of a thousand
is not worth the humble reasoning of a single
individual'*

GALILEO GALILEI, (1564-1642)

As stated in the introduction, it is often desirable to know how the fixed points of a system change when a parameter of the system is changed. The number and type of fixed points can change at a certain parameter value. This qualitative change in the structural behaviour of the system is called *bifurcation*.

The theory of bifurcations of fixed points in smooth vector fields is well understood [Guckenheimer and Holmes, 1983; Hagedorn, 1988; Kuznetsov, 1995; Seydel, 1994]. However, little is known about bifurcations of fixed points in non-smooth continuous vector fields. In this chapter, we will study bifurcations of fixed points occurring in *non-smooth continuous systems*. It will be shown that a bifurcation in a non-smooth continuous system can be discontinuous, in the sense that an eigenvalue jumps over the imaginary axis under the variation of a parameter. We will try to compare the bifurcations found in non-smooth systems with bifurcations of smooth systems. Bifurcations of fixed points will be used as a stepping stone to bifurcations of periodic solutions in discontinuous systems of Filippov-type in the next chapter.

Some facts about bifurcations of fixed points in smooth systems will briefly be repeated in Section 5.1. Next, the basic idea of a discontinuous bifurcation is presented in Section 5.2. In Sections 5.3 to 5.7 different bifurcations of fixed points of smooth and non-smooth continuous systems will subsequently be studied. The different bifurcations are compared and conclusions are drawn in the discussion of Section 5.8.

5.1 Smooth Systems

In this chapter, we consider bifurcations of fixed points of autonomous systems which depend on one single parameter μ :

$$\dot{\underline{x}} = \underline{f}(\underline{x}, \mu). \quad (5.1)$$

Let n denote the dimension of the system. The system (5.1) is called *smooth* if it is differentiable up to any order in both \underline{x} and μ . Fixed points of (5.1) are solutions of the algebraic equations

$$\underline{0} = \underline{f}(\underline{x}, \mu). \quad (5.2)$$

In order to illustrate graphically the dependence of a fixed point \underline{x} on μ , we require a scalar measure of the n -vector \underline{x} . We shall use the notation $[\underline{x}]$ for such a measure of \underline{x} . Examples are $[\underline{x}] = x_1$ and $[\underline{x}] = \|\underline{x}\|$. A diagram depicting $[\underline{x}]$ versus μ , where (\underline{x}, μ) solves equation (5.2), will be called a *bifurcation diagram*. An example of a bifurcation diagram is Figure 5.4a. The continuous curves of solutions of (5.2) under variation of μ are called *branches*. The branches of smooth systems are continuous and smooth but can split into one or more other branches. On a regular point of the branch, that is on a point where the branch does not split or turn around, we can define the *slope* of the branch. We will use the following abbreviations

$$\underline{J}(\underline{x}, \mu) = \frac{\partial \underline{f}(\underline{x}, \mu)}{\partial \underline{x}} \quad \text{and} \quad \underline{f}_{,\mu}(\underline{x}, \mu) = \frac{\partial \underline{f}(\underline{x}, \mu)}{\partial \mu}. \quad (5.3)$$

Both derivatives exist for a smooth system. Using the implicit function theorem [Kuznetsov, 1995; Seydel, 1994] it follows that, provided $\underline{J}(\underline{x}, \mu)$ is non-singular, locally (5.2) is equivalent to writing \underline{x} as a function of μ , i.e. $\underline{0} = \underline{f}(\underline{x}(\mu), \mu)$. Then it follows from differentiating (5.2) with respect to μ that

$$\underline{J}(\underline{x}, \mu) \frac{d\underline{x}}{d\mu} + \underline{f}_{,\mu}(\underline{x}, \mu) = \underline{0} \quad (5.4)$$

As $\underline{J}(\underline{x}, \mu)$ is non-singular we can solve for $d\underline{x}/d\mu$. Clearly, a point (\underline{x}, μ) is regular if $\det(\underline{J}(\underline{x}, \mu)) \neq 0$. The slope s of a branch on a regular point can be found from

$$s = \frac{d[\underline{x}]}{d\mu} = \frac{\partial[\underline{x}]}{\partial \underline{x}} \frac{d\underline{x}}{d\mu} = -\frac{d[\underline{x}]}{d\underline{x}} \underline{J}^{-1}(\underline{x}, \mu) \underline{f}_{,\mu}(\underline{x}, \mu) \quad (5.5)$$

The scalar measure $[\underline{x}]$ should of course be such that it is indeed differentiable with respect to \underline{x} at all fixed points on the branch. The choice $[\underline{x}] = \|\underline{x}\|$ can cause problems as it is not everywhere differentiable.

Some definitions from bifurcation theory will be repeated. Seydel [1994] defines a *bifurcation point* in the following way:

Definition 5.1 (Bifurcation point (Seydel [1994]))

A bifurcation point (with respect to μ) is a solution (\underline{x}^*, μ^*) , where the number of fixed points or (quasi-)periodic solutions changes when μ passes μ^* .

The definition is to be understood that also the number of fixed points and (quasi-) periodic solutions at the point under consideration have to be taken into account. Consider for instance the bifurcation diagram depicted in Figure 5.5a. In this case there are two fixed points for $\mu < 0$, one fixed point for $\mu = 0$ (which is the point under consideration) and two fixed points for $\mu > 0$. The point $(x, \mu) = (0, 0)$ is therefore a bifurcation point because the number of fixed points changes at this point for varying μ (the change is: 2-1-2). We conclude that if branches intersect, then their intersection point must be a bifurcation point.

Likewise, the system $\dot{x} = \mu x$ has one fixed point for $\mu < 0$, infinitely many fixed points for $\mu = 0$ (which is the point under consideration) and one fixed point for $\mu > 0$ (the change is: 1- ∞ -1). The point $(x, \mu) = (0, 0)$ is therefore a bifurcation point. Stability is often exchanged at bifurcation points but this is not necessary. Consider for instance the two-dimensional system

$$\begin{aligned}\dot{x}_1 &= \mu x_1 \\ \dot{x}_2 &= x_2\end{aligned}$$

Clearly, there is a bifurcation at $(x, \mu) = (0, 0)$ but stability is not exchanged (the fixed point changes from a saddle to a source). For one-dimensional smooth systems however, a bifurcation is accompanied by an exchange of stability.

Another example is the saddle-node (or turning point) bifurcation depicted in Figure 5.4a: there are zero fixed points for $\mu < 0$, one fixed point for $\mu = 0$ and two fixed points for $\mu > 0$. One could be tempted to think that a bifurcation occurs if the slope of the branch becomes vertical. A counter example is the system

$$\dot{x} = f(x, \mu) = \mu - x^3$$

The Jacobian is $\underline{J}(x, \mu) = -3x^2$ and therefore $\underline{J}(0, 0) = 0$. Furthermore, $f_{,\mu} \neq 0$ so the slope at $(0, 0)$ is vertical. But, if we study the bifurcation diagram in Figure 5.1, then we see that $(0, 0)$ is not a bifurcation point according to Definition 5.1. Such a point is called a hysteresis point (Seydel [1994]). Remark that the hysteresis effect is caused by the fact that

$$\frac{\partial^2 f(0, 0)}{\partial x^2} = 0.$$

A bifurcation diagram can be misleading. Two branches can cross each other in the two-dimensional bifurcation diagram without intersecting in the multi-dimensional space. Such a point is not a bifurcation point. The problem is caused by the projection of the multi-dimensional state-parameter space on the two-dimensional bifurcation diagram and can be circumvented by another choice for $[x]$. We will make the assumption that a crossing of two branches in the bifurcation diagram represents an intersection of the branches in the multi-dimensional space. Note that this is never a problem if $n = 1$.

Many bifurcations in the sense of Definition 5.1 expose a topological change of the phase portrait of the system as its parameter passes the bifurcation point. We will adopt the following definition for topological equivalence taken from Kuznetsov [1995]:

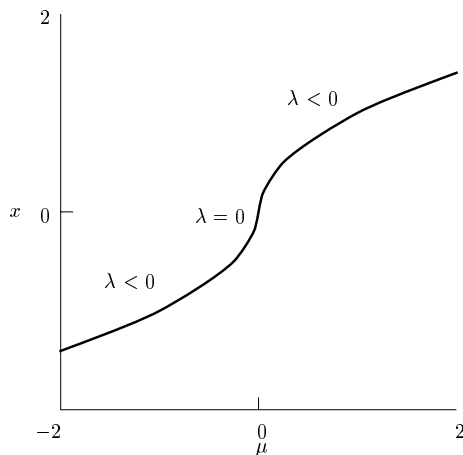


Figure 5.1: Hysteresis point.

Definition 5.2 (Topological equivalence (Kuznetsov [1995]))

A dynamical system $\dot{\underline{x}} = \underline{f}(\underline{x})$, $\underline{x} \in \mathbb{R}^n$, is topologically equivalent in a region $U \subset \mathbb{R}^n$ to a dynamical system $\dot{\underline{y}} = \underline{g}(\underline{y})$, $\underline{y} \in \mathbb{R}^n$, in a region $V \subset \mathbb{R}^n$ if there is a homeomorphism $h : \mathbb{R}^n \rightarrow \mathbb{R}^n$, $h(U) = V$, mapping trajectories of the first system in U onto trajectories of the second system in V , preserving the direction of time.

Remark: A homeomorphism is an invertible map such that both the map and its inverse are continuous.

Kuznetsov [1995] gives a definition of a bifurcation based on topological nonequivalence of the phase portrait (Definition 5.2):

Definition 5.3 (Bifurcation (Kuznetsov [1995]))

The appearance of a topologically nonequivalent phase portrait under variation of parameters is called a bifurcation.

A third definition of a bifurcation is given by Guckenheimer and Holmes [1983].

Definition 5.4 (Bifurcation value (Guckenheimer and Holmes [1983]))

A value μ^* of equation (5.1) for which the solution of (5.1) is not structurally stable is a bifurcation value of μ .

Remark: A fixed point is structurally stable if the Jacobian matrix (or the linearized system around the fixed point) does not have eigenvalues on the imaginary axis.

Definition 5.4 is unsatisfactory. The system $\dot{x} = f(x, \mu) = 0$ is structurally unstable for all values of μ . Definition 5.4 suggests that all values of μ are bifurcation points. No bifurcation exists according to Definitions 5.1 and 5.3. Also a hysteresis point would be a bifurcation point according to Definition 5.4. Definition 5.4 will therefore not be used. It should be noted that, for smooth systems, if a point is a bifurcation point according to Definitions 5.1 and 5.3, then it is also a bifurcation according to Definition 5.4. The implication does not hold in the other direction.

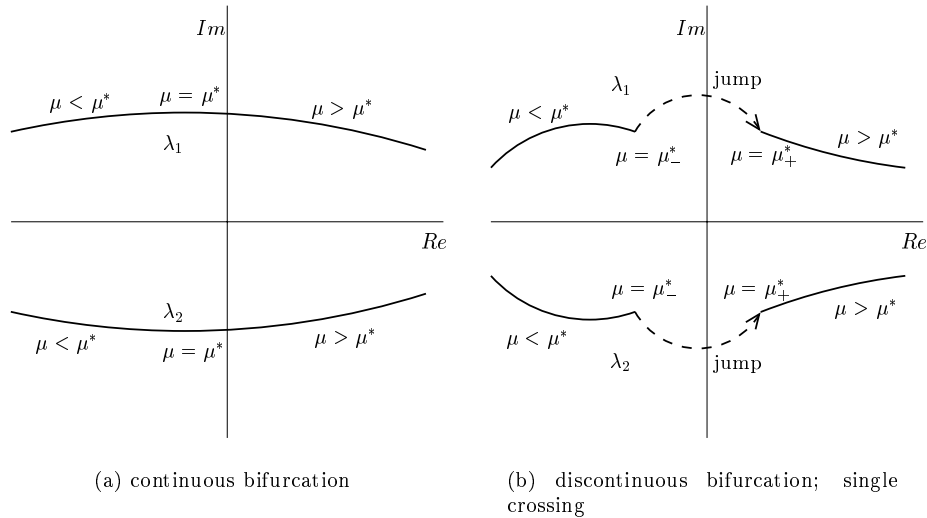


Figure 5.2: Eigenvalue paths at a bifurcation.

The Definitions 5.1 and 5.3 are consistent with each other for all the examples of smooth systems given in this thesis in the sense that a bifurcation appears at a bifurcation point. Although Definitions 5.1, 5.2 and 5.3 were originally defined for smooth continuous systems, we can apply them to non-smooth or discontinuous systems. For periodic solutions of discontinuous systems, Definitions 5.1 and 5.3 can be inconsistent with each other. A bifurcation in the sense of Definition 5.3 is not always a bifurcation in the sense of Definition 5.1. But a bifurcation in the sense of Definition 5.1 is always a bifurcation in the sense of Definition 5.3. With the aim to study non-smooth and discontinuous systems in mind, we will take Definition 5.1 as the definition for bifurcation in this thesis.

Fixed points of smooth systems can expose the following bifurcations: (a) saddle-node bifurcation, (b) transcritical bifurcation, (c) pitchfork bifurcation or (d) Hopf bifurcation. Bifurcations (a)-(c) are static bifurcations, at which only branches of fixed points meet, and (d) is a dynamic bifurcation of a fixed point where a branch of periodic solutions is created at the bifurcation point. The Jacobian matrices of smooth systems are smooth continuous functions of the state vector and parameter. The eigenvalues of the Jacobian matrix will therefore also depend continuously (but not necessarily smooth) on the parameter. A bifurcation of a fixed point of a smooth system occurs when one eigenvalue (or a pair of them) passes the imaginary axis when a parameter is varied. The scenario is depicted in Figure 5.2a where a pair of complex conjugated eigenvalues passes the imaginary axis when a parameter μ is varied and a Hopf bifurcation occurs at some critical value $\mu = \mu^*$. The bifurcations occurring in smooth systems are called *continuous bifurcations* in this thesis because the eigenvalues behave continuously.

5.2 Discontinuous Bifurcation: The Basic Idea

Non-smooth continuous systems possess hyper-surfaces on which the vector field is non-smooth. Let \underline{x} be a fixed point of (5.1) at some value for μ and let Σ be a hyper-surface which divides the state space in the smooth subspaces \mathcal{V}_- and \mathcal{V}_+ . If \underline{x} is not on Σ , then we can find a single-valued Jacobian matrix $\underline{J}(\underline{x}, \mu)$. If \underline{x} is on Σ , then there are two Jacobian matrices $\underline{J}_-(\underline{x}, \mu)$ and $\underline{J}_+(\underline{x}, \mu)$ on either side of Σ associated with the vector field in \mathcal{V}_- and \mathcal{V}_+ . Assume that we vary μ such that the fixed point \underline{x} moves from \mathcal{V}_- to \mathcal{V}_+ via Σ . Let \underline{x}_Σ denote the unique fixed point on Σ for $\mu = \mu_\Sigma$. The Jacobian matrix $\underline{J}(\underline{x}, \mu)$ varies as μ is varied and is discontinuous at $\mu = \mu_\Sigma$ for which $\underline{x} = \underline{x}_\Sigma$. Loosely speaking, we say that $\underline{J}(\underline{x}, \mu)$ ‘jumps’ at $\mu = \mu_\Sigma$ from $\underline{J}_-(\underline{x}_\Sigma, \mu_\Sigma)$ to $\underline{J}_+(\underline{x}_\Sigma, \mu_\Sigma)$. A jump of the Jacobian matrix under the influence of a parameter implies a jump of the eigenvalues. In the previous chapter we elaborated how we can define a ‘generalized Jacobian’ $\tilde{\underline{J}}(\underline{x}, \mu)$ which is set-valued at $(\underline{x}_\Sigma, \mu_\Sigma)$. The generalized Jacobian is the closed convex hull of $\underline{J}_-(\underline{x}, \mu)$ and $\underline{J}_+(\underline{x}, \mu)$ at $(\underline{x}_\Sigma, \mu_\Sigma)$

$$\begin{aligned} \tilde{\underline{J}}(\underline{x}_\Sigma, \mu_\Sigma) &= \overline{\text{co}}\{\underline{J}_-(\underline{x}_\Sigma, \mu_\Sigma), \underline{J}_+(\underline{x}_\Sigma, \mu_\Sigma)\} \\ &= \{(1-q)\underline{J}_-(\underline{x}_\Sigma, \mu_\Sigma) + q\underline{J}_+(\underline{x}_\Sigma, \mu_\Sigma), \forall q \mid 0 \leq q \leq 1\}. \end{aligned} \quad (5.6)$$

In fact, (5.6) defines *how* the Jacobian ‘jumps’ at Σ . To be more precise, (5.6) gives the set of values which the generalized Jacobian can attain on Σ . From the set-valued generalized Jacobian we can obtain the set-valued eigenvalues. We can look upon $\text{eig}(\tilde{\underline{J}}(\underline{x}_\Sigma, \mu_\Sigma))$ together with (5.6) as if it gives a *unique* path of eigenvalues ‘during’ the jump as q is varied from 0 to 1. It is important to realize that for smooth systems the eigenvalues are single-valued functions of the parameter μ and that the eigenvalues are set-valued functions in μ for non-smooth continuous systems. An eigenvalue can pass the imaginary axis while varying μ , leading to a smooth bifurcation, but it can also cross the imaginary axis during its jump along a path defined by the generalized Jacobian. Examples will be given in the next sections where jumps of eigenvalues over the imaginary axis lead to non-classical bifurcations.

We will name a bifurcation associated by a jump of an eigenvalue (or a pair of them) over the imaginary axis a *discontinuous bifurcation*. A typical scenario of a discontinuous bifurcation is depicted in Figure 5.2b where the unique path of a pair of complex conjugated eigenvalues on the jump is indicated by the dashed lines. The path depends on the Jacobian matrices $\underline{J}_-(\underline{x}_\Sigma, \mu_\Sigma)$ and $\underline{J}_+(\underline{x}_\Sigma, \mu_\Sigma)$. Note that *another pair* of these two Jacobian matrices could yield the scenario depicted in Figure 5.3a. The eigenvalues before and after the jump are the same as in Figure 5.2b but the path of the pair of eigenvalues on the jump is different. The possibility of the eigenvalues to become set-valued greatly complicates the bifurcation behaviour as the eigenvalue could also cross the imaginary axis multiple times during its jump. This is depicted in Figure 5.3b where a pair of complex conjugated eigenvalues cross the imaginary axis twice during the jump. One can suggest that for this case there exists a discontinuous bifurcation which is a combination of two classical Hopf bifurcations. Other combinations would also be possible, like Hopf – saddle-node, saddle-node – saddle-node, etc. The discontinuous bifurcation can therefore be a single crossing bifurcation which behaves very much like a conventional smooth bifurcation, or it

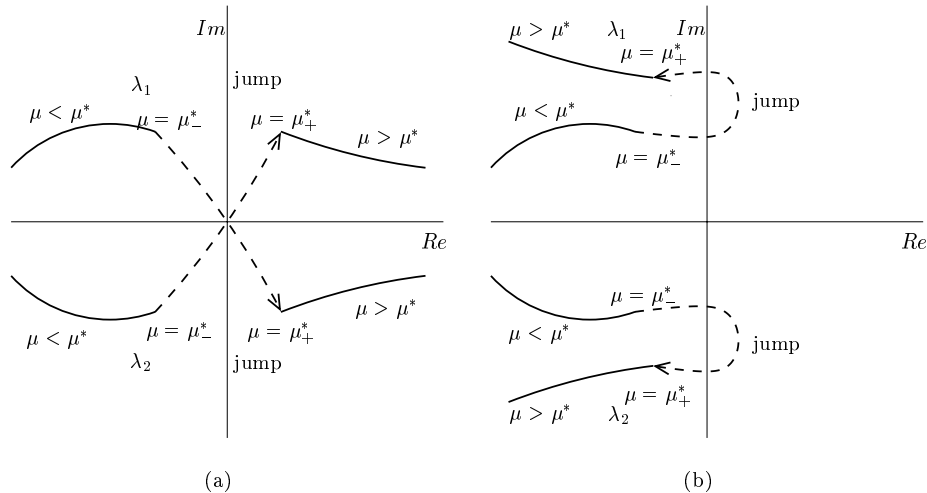


Figure 5.3: Eigenvalue paths at a bifurcation.

can be a multiple-crossing bifurcation being far more complex.

We call the type of bifurcation, at which set-valued eigenvalues cross the imaginary axis, a discontinuous bifurcation because the eigenvalues behave discontinuous at the bifurcation point.

Definition 5.5 (Discontinuous Bifurcation)

A bifurcation point, as defined by Definition 5.1, is called a discontinuous bifurcation point if the eigenvalues at the bifurcation point are set-valued and contain a value on the imaginary axis.

Some important fundamental questions arise at this point:

1. Does a jump of an eigenvalue (or a pair of them) over the imaginary axis under the influence of a parameter *imply* a bifurcation in the sense of Definition 5.1?
2. Can we classify a discontinuous bifurcation by inspecting the point where the path of the set-valued eigenvalue (or a pair of eigenvalues) cross the imaginary axis?
3. Does a continuous bifurcation for a smooth approximating system exist if the non-smooth system exposes a discontinuous bifurcation?
4. Is the discontinuous bifurcation of the non-smooth system related to the continuous bifurcation of a smooth approximating system (assuming that it exists)?
5. Do discontinuous bifurcations exist that do not have a continuous counterpart? In other words: do discontinuous bifurcations exist that behave qualitatively different from any continuous bifurcation?

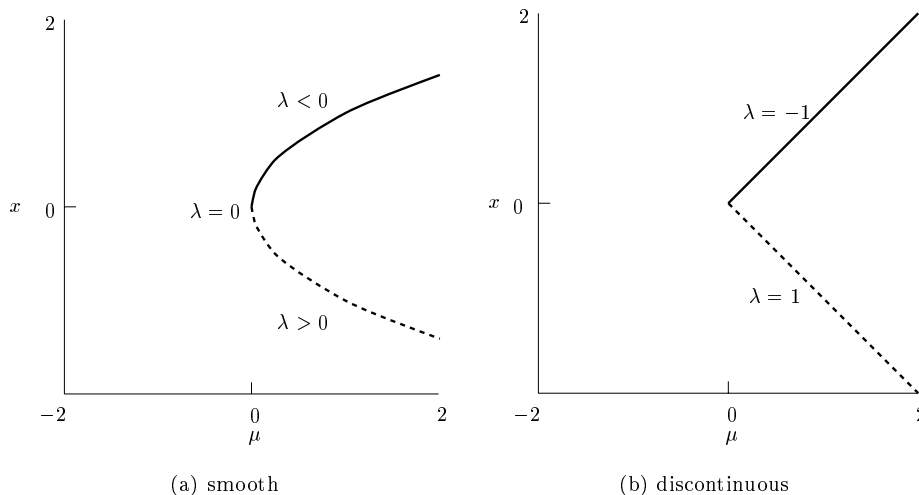


Figure 5.4: Saddle-node bifurcation.

The answers to these questions are not straightforward. Some examples which illustrate the problems around these questions will be studied in the next sections. We will return to these questions in the last section.

A treatise of some discontinuous bifurcations of fixed points will be given in the next sections. For each of the continuous bifurcations (a)-(d) we try to find a similar discontinuous (single crossing) bifurcation occurring in a non-smooth continuous system. The non-smooth system should be as simple as possible and will therefore be chosen as a piecewise-linear continuous function. First the continuous bifurcation is briefly treated, and then its discontinuous counterpart is discussed. The insight in discontinuous bifurcations of fixed points of non-smooth continuous systems is important in its own right but will also be of value for the understanding of bifurcations of periodic solutions of discontinuous systems in the next chapter.

5.3 Saddle-node Bifurcation

The smooth scalar system

$$\dot{x} = f(x, \mu) = \mu - x^2 \quad (5.7)$$

has two fixed points for $\mu > 0$

$$x = \sqrt{\mu}, \quad x = -\sqrt{\mu} .$$

The Jacobian $\underline{J} = -2x$ becomes singular at $x = 0$. There exists a bifurcation at $(x, \mu) = (0, 0)$ in the $x - \mu$ space (Figure 5.4a), which is known as a saddle-node bifurcation point. The upper branch is stable (solid line) and the lower one unstable (dashed line). At a continuous saddle-node bifurcation, $f_{,\mu}$ (cf. (5.3)) does not

belong to the range of the matrix \underline{J} (cf. Theorem 3.1 in Kuznetsov [1995]). Hence the matrix $[\underline{J}|f,\mu]$ has rank n . This can be geometrically interpreted as stating that the *continuation problem* is unique, i.e. we can follow the branch up to the bifurcation and continue uniquely on the other part of the branch. However, the fact that the continuation problem is unique does not necessarily imply that $[\underline{J}|f,\mu]$ has full rank.

We now replace the term x^2 by $|x|$ which yields a non-smooth system:

$$\dot{x} = f(x, \mu) = \mu - |x| \quad (5.8)$$

which has again two fixed points for $\mu > 0$

$$x = \mu, \quad x = -\mu .$$

with the generalized set-valued Jacobian $\tilde{\underline{J}}(x, \mu) = -\text{Sgn } x$ and $f_{,\mu}(x, \mu) = 1$. The linear approximation of the Jacobian $\tilde{\underline{J}}(x, \mu)$ at $(x, \mu) = (0, 0)$ takes the form

$$\tilde{\underline{J}}(0, 0) = \{-2q + 1, \forall 0 \leq q \leq 1\}, \quad (5.9)$$

which becomes singular at $q = \frac{1}{2}$. The bifurcation diagram is depicted in Figure 5.4b and looks similar to the one for the continuous version. Again there is a stable branch and an unstable branch but they now meet at an acute angle. From inspection of the bifurcation diagram we see that a static bifurcation (in the sense of Definition 5.1) exists at $(x, \mu) = (0, 0)$. We also conclude that the single eigenvalue on the bifurcation point is set-valued, i.e. $\lambda = [-1, 1]$. Where for the smooth case the eigenvalue passed the origin, the set-valued eigenvalue of the non-smooth system ‘jumps’ over the imaginary axis through the origin. For this reason, we will call the point $(x, \mu) = (0, 0)$ a *discontinuous* bifurcation point. The matrix $[\tilde{\underline{J}}(0, 0)|f_{,\mu}(0, 0)]$ for $q = \frac{1}{2}$ has rank n similar to the smooth case. However, it seems not justified to conclude from this that the continuation problem (i.e. the possibility to follow the branch after the bifurcation point) is unique because the slope of the branch is not properly defined on the non-smooth bifurcation point.

The jump of the eigenvalue and the acute conjunction of branches are properties of discontinuous bifurcations which we will also encounter for bifurcations of periodic solutions.

It should be noted that, if we select to smoothen the non-smooth system with the following arctangent function

$$\dot{x} \approx \mu - \frac{2}{\pi} \arctan(\varepsilon x)x \approx \mu - \frac{2}{\pi} \varepsilon x^2 + O(x^4),$$

then the resulting bifurcation will be a continuous saddle-node bifurcation for all ε as can be seen from the expansion around the bifurcation point ($x = 0$). Whether *every* smoothing function will reveal a saddle-node bifurcation is not clear. But still, the discontinuous bifurcation in Figure 5.4b resembles the smooth saddle-node bifurcation in Figure 5.4a and we will call it therefore a discontinuous saddle-node bifurcation.

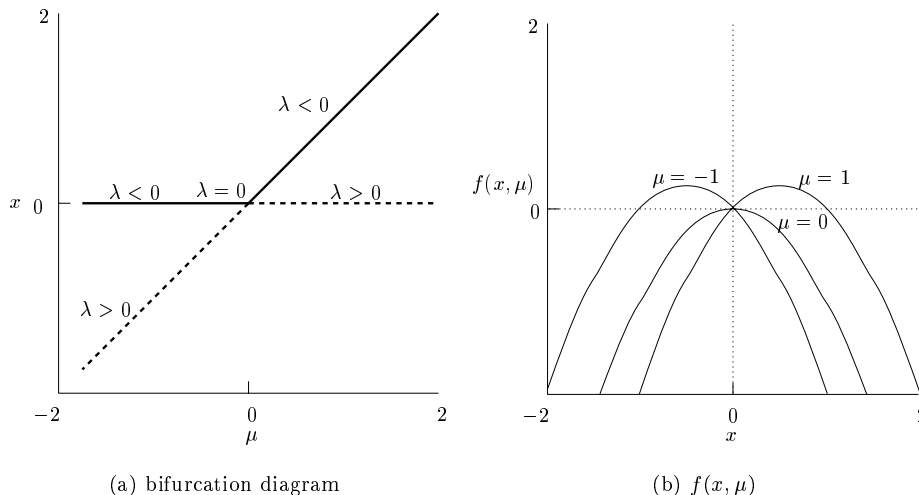


Figure 5.5: Transcritical bifurcation, smooth.

5.4 Transcritical Bifurcation

First, we consider the scalar smooth system

$$\dot{x} = f(x, \mu) = \mu x - x^2. \quad (5.10)$$

There are two fixed points

$$x = 0, \quad x = \mu$$

The Jacobian of (5.10)

$$\underline{J}(x, \mu) = \mu - 2x$$

has the single eigenvalues

$$\begin{aligned} \lambda &= \mu, & \text{at } x = 0 \\ \lambda &= -\mu, & \text{at } x = \mu \end{aligned}$$

The static bifurcation, shown in Figure 5.5a, is a transcritical bifurcation point at which two branches exchange stability. The function $f(x, \mu)$ is depicted in Figure 5.5b for $\mu = -1$, $\mu = 0$ and $\mu = 1$. The function has two distinct zeros for $\mu \neq 0$, where one is always in the origin. At the bifurcation point ($\mu = 0$), the two zeros coincide to one double zero. The two zeros exchange stability when the bifurcation point is passed. At a continuous transcritical bifurcation point, $f_{, \mu}$ does belong to the range of the matrix \underline{J} . The matrix $[\underline{J}|f_{, \mu}]$ has rank $n - 1$ at $(x, \mu) = (0, 0)$. A second branch therefore crosses the bifurcation point, which makes the continuation problem non-unique.

We now study the following non-smooth system:

$$\dot{x} = f(x, \mu) = \left| \frac{1}{2} \mu \right| - \left| x - \frac{1}{2} \mu \right| \quad (5.11)$$

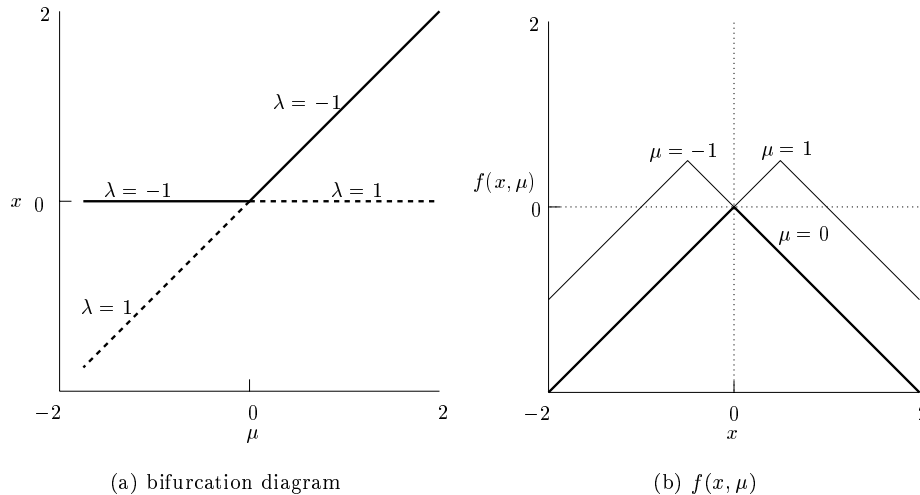


Figure 5.6: Transcritical bifurcation, discontinuous.

This non-smooth system approximates the parabola in Figure 5.5b by a piecewise-linear curve (a tent) as is depicted in Figure 5.6b. The lines are bold where the curves overlap each other. The non-smooth system (5.11) has the same fixed points as the smooth system (5.10)

$$x = 0, \quad x = \mu.$$

From inspection of the bifurcation diagram depicted in Figure 5.6a, we see that a static bifurcation (in the sense of Definition 5.1) exists at $(x, \mu) = (0, 0)$ as the number of fixed points changes (the change is 2–1–2). The bifurcation of the non-smooth system depicted in Figure 5.6a is similar to the transcritical bifurcation in Figure 5.5a. The generalized Jacobian of (5.11) is

$$\tilde{J}(x, \mu) = -\text{Sgn}\left(x - \frac{1}{2}\mu\right)$$

and is set-valued at $(x, \mu) = (0, 0)$. The generalized Jacobian has the eigenvalues

$$\begin{aligned} \lambda &= -1, & \text{at } x = 0 \text{ if } \mu < 0 \\ \lambda &= 1, & \text{at } x = 0 \text{ if } \mu > 0 \\ \lambda &= 1, & \text{at } x = \mu \text{ if } \mu < 0 \\ \lambda &= -1, & \text{at } x = \mu \text{ if } \mu > 0 \\ \lambda &= [-1, 1], & \text{at } (x, \mu) = (0, 0) \end{aligned}$$

Where for the smooth transcritical bifurcation the eigenvalue passed the origin, the set-valued eigenvalue of the non-smooth system ‘jumps’ over the imaginary axis through the origin. For this reason, we will call the point $(x, \mu) = (0, 0)$ a discontinuous bifurcation point (Figure 5.6a). Because the structure of the branches around the discontinuous bifurcation point resembles the structure of the transcritical bifurcation, we will call this bifurcation a discontinuous *transcritical* bifurcation.

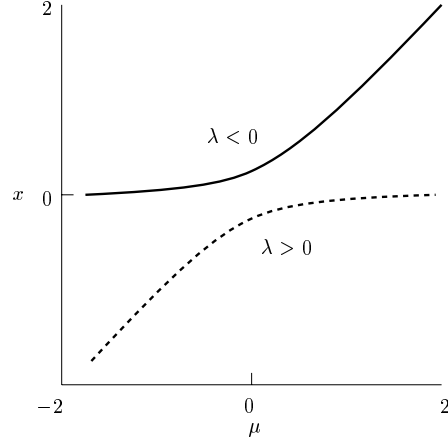


Figure 5.7: Non-symmetric smoothing.

The fixed point $(x, \mu) = (0, 0)$ is located on the intersection of two hyperplanes $\mu = 0$ and $x - \frac{1}{2}\mu = 0$ in the (x, μ) space. Two parameters, q_1 and q_2 , are needed for a linear approximation. The first parameter, q_1 , will be varied to satisfy the condition $\det(\tilde{\mathcal{J}}(0, 0)) = 0$ and the second parameter, q_2 , will be varied to ensure that $[\tilde{\mathcal{J}}(0, 0)|\tilde{f}_{,\mu}(0, 0)]$ has rank $n - 1$.

The linear approximation $\tilde{\mathcal{J}}$ of the Jacobian at $(x, \mu) = (0, 0)$ takes the form

$$\tilde{\mathcal{J}}(0, 0) = \{-2q_1 + 1, \forall 0 \leq q_1 \leq 1\}, \quad (5.12)$$

which becomes singular at $q_1 = \frac{1}{2}$. Furthermore,

$$\tilde{f}_{,\mu}(x, \mu) = \frac{1}{2} \text{Sgn}(\mu) + \frac{1}{2} \text{Sgn}(x - \frac{1}{2}\mu), \quad (5.13)$$

which is set-valued at the bifurcation point. We therefore construct a linear approximation

$$\begin{aligned} \tilde{f}_{,\mu}(0, 0) &= \left\{ \frac{1}{2}(2q_2 - 1) + \frac{1}{2}(2q_1 - 1), \forall 0 \leq q_1 \leq 1, \forall 0 \leq q_2 \leq 1 \right\} \\ &= \{q_2 + q_1 - 1, \forall 0 \leq q_1 \leq 1, \forall 0 \leq q_2 \leq 1\} \end{aligned} \quad (5.14)$$

The matrix $[\tilde{\mathcal{J}}(0, 0)|\tilde{f}_{,\mu}(0, 0)]$ has rank $n - 1$ at $q_1 = \frac{1}{2}, q_2 = \frac{1}{2}$. Because of the non-smoothness of the problem it is not justified to conclude that the continuation problem is non-unique as for the smooth case but a resemblance is present.

If we smoothen the non-smooth system (5.11) with the following particular arc-tangent function

$$\dot{x} \approx \frac{1}{\pi} \arctan\left(\frac{1}{2}\varepsilon\mu\right)\mu - \frac{2}{\pi} \arctan\left(\varepsilon\left(x - \frac{1}{2}\mu\right)\right)\left(x - \frac{1}{2}\mu\right) \approx \frac{2}{\pi}\varepsilon(\mu x - x^2),$$

then the resulting bifurcation will be a continuous transcritical bifurcation for all ε as can be seen from the expansion around the bifurcation point $(x = 0, \mu = 0)$. The

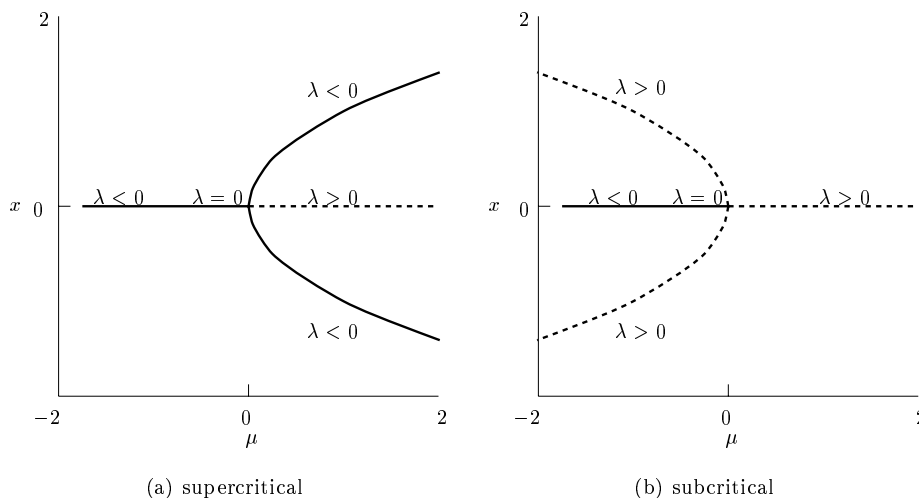


Figure 5.8: Pitchfork bifurcation, smooth.

smoothened system can be transformed to the standard normal form with the time transformation $\tau = \varepsilon t$.

However, not every smoothing function gives a transcritical bifurcation. Consider for instance the following non-symmetric smoothing:

$$\left|\frac{1}{2}\mu\right| \approx \frac{2}{\pi} \arctan\left(\frac{1}{2}\varepsilon\mu\right)\frac{1}{2}\mu + \frac{1}{\varepsilon} \quad (5.15)$$

$$\left|x - \frac{1}{2}\mu\right| \approx \frac{2}{\pi} \arctan(\varepsilon(x - \frac{1}{2}\mu))(x - \frac{1}{2}\mu)$$

which gives

$$\dot{x} \approx \frac{2}{\pi}(\varepsilon(\mu x - x^2) + \frac{1}{\varepsilon}) \quad (5.16)$$

for $|x| \ll 1$ and $\varepsilon \gg 1$. Equation (5.16) has two branches in the bifurcation diagram for varying μ but the branches do not intersect (Figure 5.7). No bifurcation exists for (5.16).

5.5 Pitchfork Bifurcation

We consider the smooth system

$$\dot{x} = f(x, \mu) = \mu x + \alpha x^3, \quad (5.17)$$

where the constant α will be taken as $\alpha = \pm 1$. There is one fixed point for $\frac{\mu}{\alpha} \geq 0$ and are three fixed points for $\frac{\mu}{\alpha} < 0$.

$$\begin{aligned} x = 0 & \quad \text{trivial point} \\ x = \pm\sqrt{-\frac{\mu}{\alpha}} & \quad \text{for } \frac{\mu}{\alpha} < 0 \end{aligned}$$

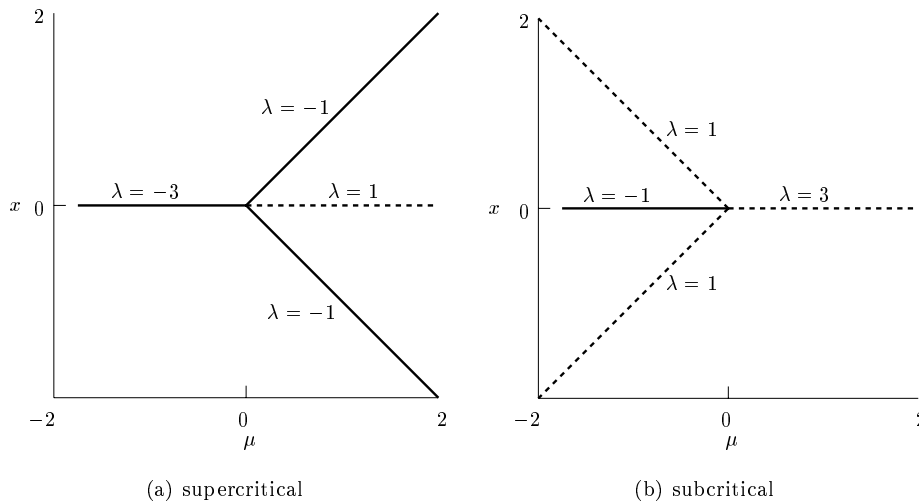


Figure 5.9: Pitchfork bifurcation, discontinuous.

The Jacobian

$$\underline{J} = \mu + 3\alpha x^2$$

has the single eigenvalues

$$\begin{aligned} \lambda &= \mu, & \text{at } x = 0 \\ \lambda &= -2\mu, & \text{at } x = \pm\sqrt{-\frac{\mu}{\alpha}} \text{ for } \frac{\mu}{\alpha} < 0 \end{aligned}$$

For $\alpha = -1$ there is a supercritical pitchfork bifurcation (Figure 5.8a) and for $\alpha = 1$ a subcritical pitchfork bifurcation (Figure 5.8b). At a continuous pitchfork bifurcation point, $f_{,\mu}$ does belong to the range of the matrix \underline{J} (cf. Theorem 3.1 in Kuznetsov [1995]). The matrix $[\underline{J}|f_{,\mu}]$ has rank $n - 1 = 0$ at $(x, \mu) = (0, 0)$, which is consistent with the fact that two branches intersect at the bifurcation point.

We now study the following non-smooth system:

$$\dot{x} = f(x, \mu) = -x + |x + \frac{1}{2}\mu| - |x - \frac{1}{2}\mu| \quad (5.18)$$

There exists one fixed point for $\mu \leq 0$ and three fixed points for $\mu > 0$

$$\begin{aligned} x &= 0 & \text{trivial point} \\ x &= \pm\mu & \text{for } \mu > 0 \end{aligned}$$

From inspection of the bifurcation diagram depicted in Figure 5.9a, we observe that a static bifurcation (in the sense of Definition 5.1) exists at $(x, \mu) = (0, 0)$ as the number of fixed points changes (the change is 1–1–3).

The generalized Jacobian of (5.18)

$$\tilde{\underline{J}}(x, \mu) = -1 + \text{Sgn}(x + \frac{1}{2}\mu) - \text{Sgn}(x - \frac{1}{2}\mu)$$

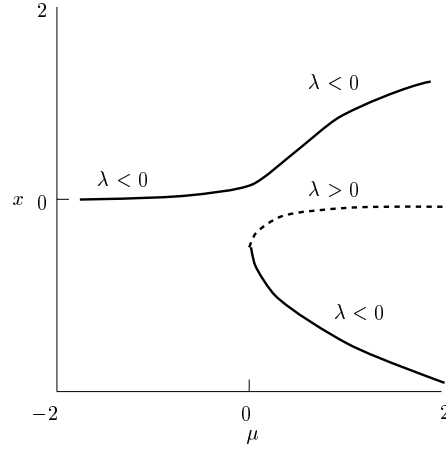


Figure 5.10: Non-symmetric smoothing.

has the single eigenvalues

$$\begin{aligned} \lambda &= -3, & \text{at } x = 0, \mu < 0 \\ \lambda &= 1, & \text{at } x = 0, \mu > 0 \\ \lambda &= -1, & \text{at } x = \pm\mu, \mu > 0 \end{aligned}$$

and is set-valued at $(x, \mu) = (0, 0)$. As there are two hyperplanes where the vector field is discontinuous, we need two parameters for a linear approximation of the Jacobian at $(x, \mu) = (0, 0)$

$$\begin{aligned} \tilde{\mathcal{J}}(0, 0) &= \{-1 + (-2q_1 + 1) - (-2q_2 + 1), \forall 0 \leq q_1 \leq 1, \forall 0 \leq q_2 \leq 1\} \\ &= \{2(q_2 - q_1) - 1, \forall 0 \leq q_1 \leq 1, \forall 0 \leq q_2 \leq 1\}, \end{aligned} \quad (5.19)$$

which becomes singular at $q_2 - q_1 = \frac{1}{2}$. Furthermore,

$$\tilde{f}_{,\mu}(x, \mu) = \frac{1}{2} \text{Sgn}(x + \frac{1}{2}\mu) + \frac{1}{2} \text{Sgn}(x - \frac{1}{2}\mu), \quad (5.20)$$

which is set-valued at the bifurcation point. We therefore construct a linear approximation

$$\begin{aligned} \tilde{f}_{,\mu}(0, 0) &= \{\frac{1}{2}(2q_1 - 1) + \frac{1}{2}(2q_2 - 1), \forall 0 \leq q_1 \leq 1, \forall 0 \leq q_2 \leq 1\} \\ &= \{q_1 + q_2 - 1, \forall 0 \leq q_1 \leq 1, \forall 0 \leq q_2 \leq 1\}. \end{aligned} \quad (5.21)$$

The matrix $\left[\tilde{\mathcal{J}}(0, 0) | \tilde{f}_{,\mu}(0, 0) \right]$ has rank $n - 1$ at $q_1 = \frac{3}{4}, q_2 = \frac{1}{4}$. The continuation problem is clearly non-unique as can be seen from the bifurcation diagram (Figure 5.9a). But to conclude this from the rank of $\left[\tilde{\mathcal{J}}(0, 0) | \tilde{f}_{,\mu}(0, 0) \right]$ seems not justified because of the non-smoothness of the problem.

The bifurcation diagram is shown in Figure 5.9a for the discontinuous supercritical pitchfork bifurcation of system (5.18). We call the bifurcation discontinuous

because the eigenvalue ‘jumps’ over the imaginary axis. The discontinuous bifurcation is classified as a discontinuous *pitchfork* bifurcation because it resembles the continuous pitchfork bifurcation. Similarly, the system

$$\dot{x} = f(x, \mu) = x + |x + \frac{1}{2}\mu| - |x - \frac{1}{2}\mu| \quad (5.22)$$

exhibits a discontinuous subcritical pitchfork bifurcation (Figure 5.9b).

We smoothen the non-smooth system (5.18) with a particular arctangent function and apply a Taylor series expansion around $(x = 0, \mu = 0)$

$$\begin{aligned} \dot{x} &= -x + |x + \frac{1}{2}\mu| - |x - \frac{1}{2}\mu| \\ &\approx -x + \frac{2}{\pi} \arctan(\varepsilon(x + \frac{1}{2}\mu))(x + \frac{1}{2}\mu) - \frac{2}{\pi} \arctan(\varepsilon(x - \frac{1}{2}\mu))(x - \frac{1}{2}\mu) \\ &\approx (-1 + \frac{4}{\pi}\varepsilon\mu)x - \frac{8}{3\pi}\varepsilon^3\mu x^3. \end{aligned}$$

The resulting bifurcation is a continuous pitchfork bifurcation with the bifurcation point at $(x = 0, \mu = \frac{\pi}{4\varepsilon})$. The bifurcation point of the smoothened system therefore approaches the origin as ε is increased.

However, not every smoothing function gives a pitchfork bifurcation. Consider for instance the following non-symmetric smoothing:

$$\begin{aligned} |x + \frac{1}{2}\mu| &\approx \frac{2}{\pi} \arctan(\varepsilon(x + \frac{1}{2}\mu))(x + \frac{1}{2}\mu) + \frac{1}{\varepsilon} \\ |x - \frac{1}{2}\mu| &\approx \frac{2}{\pi} \arctan(\varepsilon(x - \frac{1}{2}\mu))(x - \frac{1}{2}\mu) \end{aligned} \quad (5.23)$$

which gives

$$\dot{x} \approx (-1 + \frac{4}{\pi}\varepsilon\mu)x - \frac{8}{3\pi}\varepsilon^3\mu x^3 + \frac{1}{\varepsilon} \quad (5.24)$$

for $|x| \ll 1$ and $\varepsilon \gg 1$. Equation (5.24) has two branches close to the origin in the bifurcation diagram for varying μ , but the branches do not intersect (Figure 5.10). Only a saddle-node bifurcation exists for (5.24).

5.6 Hopf Bifurcation

At a Hopf bifurcation point the fixed point loses its stability and a periodic solution is born (or vice-versa). First, we consider the smooth planar system

$$\begin{aligned} \dot{x}_1 &= \mu x_1 - \omega x_2 + (\alpha x_1 - \beta x_2)(x_1^2 + x_2^2) \\ \dot{x}_2 &= \omega x_1 + \mu x_2 + (\beta x_1 + \alpha x_2)(x_1^2 + x_2^2) \end{aligned} \quad (5.25)$$

where μ, ω, α and β are constants. We will study the fixed points and periodic solutions of system (5.25) for different values of μ . This system has a fixed point $\underline{x} = [x_1, x_2]^T = [0, 0]^T$ for all values of μ and the Jacobian matrix of the linearized system around the fixed point is

$$\underline{J} = \begin{bmatrix} \mu & -\omega \\ \omega & \mu \end{bmatrix}$$

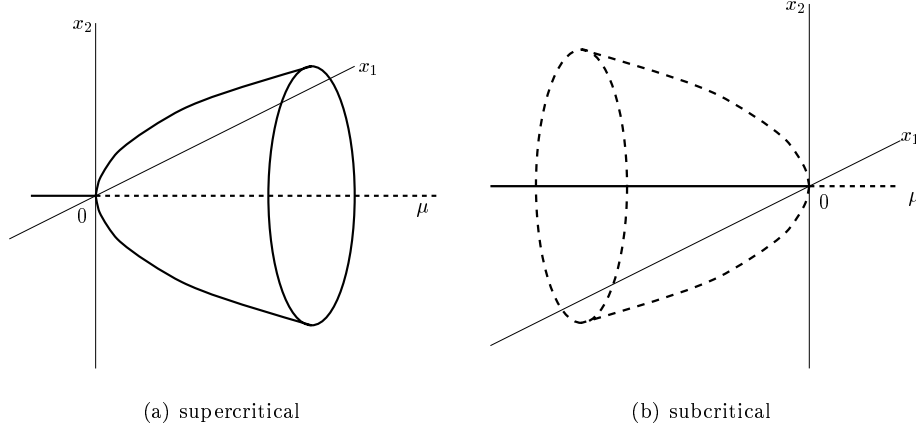


Figure 5.11: Hopf bifurcation, smooth.

with the eigenvalues $\lambda_{1,2} = \mu \pm i\omega$. For $\mu < 0$ the fixed point is asymptotically stable. When μ is increased to $\mu = 0$ the fixed point becomes non-hyperbolic, and for $\mu > 0$ the fixed point becomes unstable. By using the transformation

$$x_1 = r \cos \theta \quad \text{and} \quad x_2 = r \sin \theta \quad (5.26)$$

we transform (5.25) into

$$\dot{r} = \mu r + \alpha r^3 \quad (5.27)$$

$$\dot{\theta} = \omega + \beta r^2 \quad (5.28)$$

The trivial fixed point of (5.27) corresponds to the fixed point of (5.25), and the nontrivial fixed point ($r \neq 0$) of (5.27) corresponds to a periodic solution of (5.25). In the latter case, r is the amplitude and $\dot{\theta}$ is the frequency of the periodic solution that is created by the Hopf bifurcation. The transformation (5.26) therefore transforms the Hopf bifurcation into the pitchfork bifurcation. The bifurcation diagram for the Hopf bifurcation is depicted in Figure 5.11 and the bifurcation diagram for the transformed system (5.27) is identical to Figure 5.8 where x should be replaced by r .

We now study the following non-smooth system

$$\begin{aligned} \dot{x}_1 &= -x_1 - \omega x_2 + \frac{x_1}{\sqrt{x_1^2 + x_2^2}} (|\sqrt{x_1^2 + x_2^2} + \frac{1}{2}\mu| - |\sqrt{x_1^2 + x_2^2} - \frac{1}{2}\mu|) \\ \dot{x}_2 &= \omega x_1 - x_2 + \frac{x_2}{\sqrt{x_1^2 + x_2^2}} (|\sqrt{x_1^2 + x_2^2} + \frac{1}{2}\mu| - |\sqrt{x_1^2 + x_2^2} - \frac{1}{2}\mu|) \end{aligned} \quad (5.29)$$

which is dependent on the parameters μ and ω . We will study the fixed points and periodic solutions of system (5.29) for different values of μ . The non-smooth system (5.29) has the same fixed point as the smooth system with the same stability.

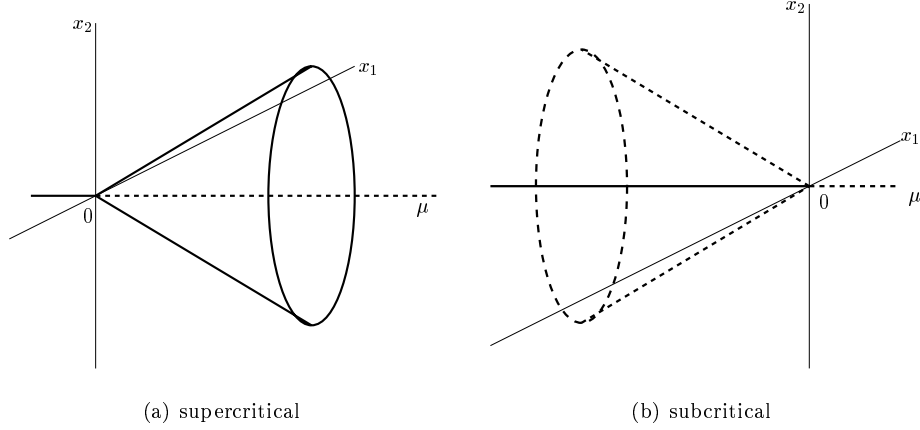


Figure 5.12: Hopf bifurcation, discontinuous.

We transform the system (5.29) with the transformation (5.26) into

$$\dot{r} = -r + |r + \frac{1}{2}\mu| - |r - \frac{1}{2}\mu| \quad (5.30)$$

$$\dot{\theta} = \omega \quad (5.31)$$

The one-dimensional system (5.30) is identical to the non-smooth system (5.18) exposing a discontinuous pitchfork bifurcation. The scenario for the discontinuous Hopf bifurcation is depicted in Figure 5.12 and the scenario for (5.30) is identical to Figure 5.9.

5.7 Hopf–Pitchfork Bifurcation

Consider the non-smooth continuous system

$$\begin{aligned} \dot{x}_1 &= x_2 \\ \dot{x}_2 &= -x_1 + |x_1 + \mu| - |x_1 - \mu| - x_2 - |x_2 + \mu| + |x_2 - \mu| \end{aligned} \quad (5.32)$$

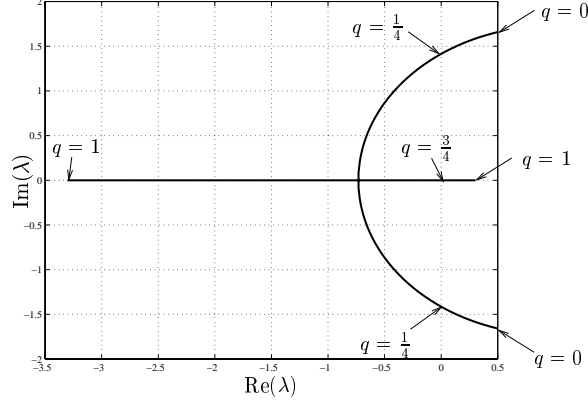
For $\mu > 0$ there are three fixed points

$$\begin{aligned} x_1 &= 0, & x_2 &= 0 \text{ trivial point} \\ x_1 &= \pm 2\mu, & x_2 &= 0 \end{aligned}$$

For $\mu \leq 0$, the only fixed point is the trivial point $x_1 = 0, x_2 = 0$. The Jacobian matrix at the trivial branch jumps at $\mu = 0$ from $\underline{J}(0, 0)_-^{\text{tr}}$ to $\underline{J}(0, 0)_+^{\text{tr}}$.

$$\underline{J}(0, 0)_-^{\text{tr}} = \begin{bmatrix} 0 & 1 \\ -3 & 1 \end{bmatrix}, \quad \mu < 0, \quad \lambda = \frac{1}{2} \pm i\frac{1}{2}\sqrt{11} \quad (5.33)$$

$$\underline{J}(0, 0)_+^{\text{tr}} = \begin{bmatrix} 0 & 1 \\ 1 & -3 \end{bmatrix}, \quad \mu > 0, \quad \lambda = -1\frac{1}{2} \pm \frac{1}{2}\sqrt{13} \approx \{0.30, -3.30\} \quad (5.34)$$


 Figure 5.13: Path of the eigenvalues of $\tilde{\mathcal{J}}(0,0)^{\text{tr}}$.

The trivial fixed point is therefore an unstable focus for $\mu < 0$ and a saddle for $\mu > 0$. The Jacobian matrix on the non-trivial branches is

$$\mathcal{J}(\pm 2\mu, 0)^{\text{non}} = \begin{bmatrix} 0 & 1 \\ -1 & -3 \end{bmatrix}, \quad \mu > 0, \quad (5.35)$$

$$\lambda = -1 \frac{1}{2} \pm \frac{1}{2} \sqrt{5} \approx \{-0.38, -2.62\}$$

Fixed points on the non-trivial branches are therefore stable nodes. The jump of the Jacobian on the trivial branch can be expressed as

$$\tilde{\mathcal{J}}(0,0)^{\text{tr}} = \{(\mathcal{J}(0,0)_+^{\text{tr}} - \mathcal{J}(0,0)_-^{\text{tr}})q + \mathcal{J}(0,0)^{\text{tr}}, \forall 0 \leq q \leq 1\}. \quad (5.36)$$

The eigenvalues of the convex combination $\tilde{\mathcal{J}}(0,0)^{\text{tr}}$ are plotted for $0 \leq q \leq 1$ in Figure 5.13. We observe that the eigenvalues of the convex combination cross the imaginary axis twice. At $q = \frac{1}{4}$ a pair of complex conjugated eigenvalues passes the imaginary axis and at $q = \frac{3}{4}$ a single eigenvalue passes the origin.

With the transformation

$$y_1 = \frac{x_1}{\mu}, \quad y_2 = \frac{x_2}{\mu} \quad (5.37)$$

we can transform system (5.32) for $\mu < 0$ to

$$\begin{aligned} \dot{y}_1 &= y_2 \\ \dot{y}_2 &= -y_1 - |y_1 + 1| + |y_1 - 1| - y_2 + |y_2 + 1| - |y_2 - 1| \end{aligned} \quad (5.38)$$

and for $\mu > 0$ to

$$\begin{aligned} \dot{y}_1 &= y_2 \\ \dot{y}_2 &= -y_1 + |y_1 + 1| - |y_1 - 1| - y_2 - |y_2 + 1| + |y_2 - 1| \end{aligned} \quad (5.39)$$

The transformed systems are independent of μ for $\mu \neq 0$. Fixed points and periodic solutions of (5.38) and (5.39) are after a back-transformation with 5.37 also fixed

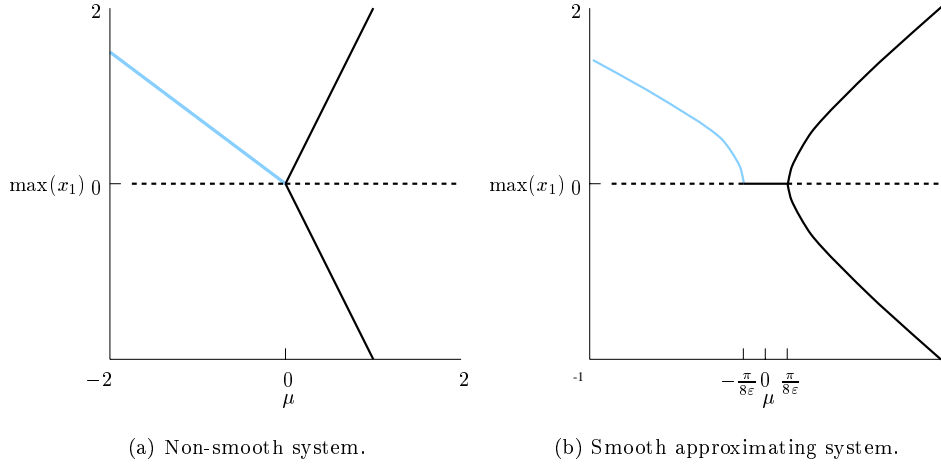


Figure 5.14: Bifurcation diagrams.

points and periodic solutions of system (5.32). The location of the fixed points of system (5.32) scale therefore with μ . But also all periodic solutions of system (5.32) scale with μ . This means that the shape of a periodic solution of (5.32) does not change for varying μ , but the size of the periodic solution scales with μ . The period time is independent of μ . The bifurcation diagram of system (5.32) is depicted in Figure 5.14a. Branches of fixed points are indicated by black lines and periodic branches by grey lines. Stable branches are indicated by solid lines and unstable branches by dashed lines. Explicit expressions were found for the fixed points and the periodic solution was found numerically. The point $(x_1, x_2, \mu) = (0, 0, 0)$ is a bifurcation point where two branches of fixed points bifurcate from the trivial branch and also one periodic solution. This bifurcation behaviour is consistent with the path of the eigenvalues ‘during’ the jump (Figure 5.13). The two crossings with the imaginary axis would suggest a combination of a Hopf and a static bifurcation. This is indeed the case, because a periodic branch and other branches of fixed points are created at the bifurcation point. The magnitude $\max(x_1)$ varies linearly in μ for all branches as was expected from the transformation. The period time of the periodic solution is $T = 4.03$ s and is independent of μ . The stable periodic solution in the transformed coordinates (5.37) is depicted in Figure 5.15 together with the unstable fixed point (denoted by ‘+’) and the lines $y_1 = \pm 1$, $y_2 = \pm 1$ on which the vector field is non-smooth.

We now study the smooth approximating system

$$\begin{aligned}
 \dot{x}_1 &= x_2 \\
 \dot{x}_2 &= -x_1 + \frac{2}{\pi} \arctan(\varepsilon(x_1 + \mu))(x_1 + \mu) - \frac{2}{\pi} \arctan(\varepsilon(x_1 - \mu))(x_1 - \mu) \\
 &\quad - x_2 - \frac{2}{\pi} \arctan(\varepsilon(x_2 + \mu))(x_2 + \mu) + \frac{2}{\pi} \arctan(\varepsilon(x_2 - \mu))(x_2 - \mu)
 \end{aligned} \tag{5.40}$$

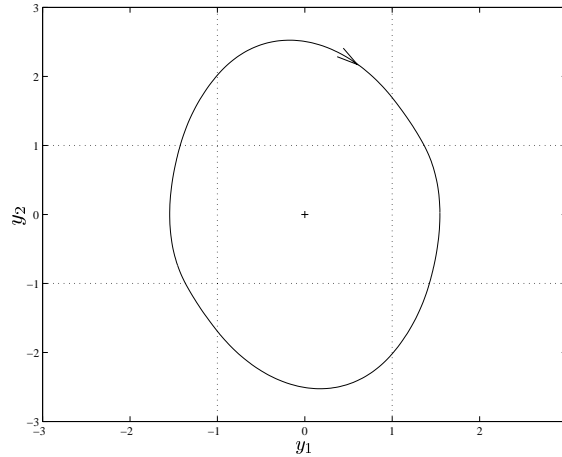


Figure 5.15: Periodic solution.

The system can be expanded in a Taylor series around $x_1 = x_2 = 0$

$$\begin{aligned} \dot{x}_1 &= x_2 \\ \dot{x}_2 &\approx \left(-1 + \frac{8}{\pi}\varepsilon\mu\right)x_1 - \frac{64}{3\pi}\varepsilon^3\mu x_1^3 + \left(-1 - \frac{8}{\pi}\varepsilon\mu\right)x_2 + \frac{64}{3\pi}\varepsilon^3\mu x_2^3 \end{aligned} \quad (5.41)$$

The smooth approximating system (5.40) also has the trivial branch of fixed points $(x_1, x_2) = (0, 0)$. The location of the eigenvalues on the trivial branch are computed numerically (with $\varepsilon = 10$) for varying μ . The eigenvalues are plotted in the complex plane in Figure 5.16 for some values of μ (indicated by *) together with the eigenvalue-path of the convex combination (Figure 5.13), which is indicated by a solid line. The eigenvalues of the smooth approximating system seem to be almost located on the eigenvalue-path of the convex combination of the non-smooth system. The trivial branch of the approximating system also undergoes a Hopf bifurcation and a pitchfork bifurcation but at different values of μ . The bifurcation diagram of the smooth approximating system is sketched in Figure 5.14b. The Hopf bifurcation is approximately located at $\mu = -\frac{\pi}{8\varepsilon}$ and the pitchfork bifurcation approximately at $\mu = \frac{\pi}{8\varepsilon}$. The two bifurcations approach each other for increasing ε .

5.8 Discussion and Conclusions

All classical bifurcations of fixed points of smooth systems were discussed in this chapter and a parallel was shown with non-smooth systems. For each of the classical continuous bifurcations a discontinuous bifurcation was found.

In Section 5.2 some fundamental questions about discontinuous bifurcations were raised. With the preceding examples in mind, we will try to answer these questions one by one.

1. *Does a jump of an eigenvalue (or a pair of them) over the imaginary axis under the influence of a parameter imply a bifurcation in the sense of Definition 5.1?* In all examples the conclusion that a bifurcation exists was taken

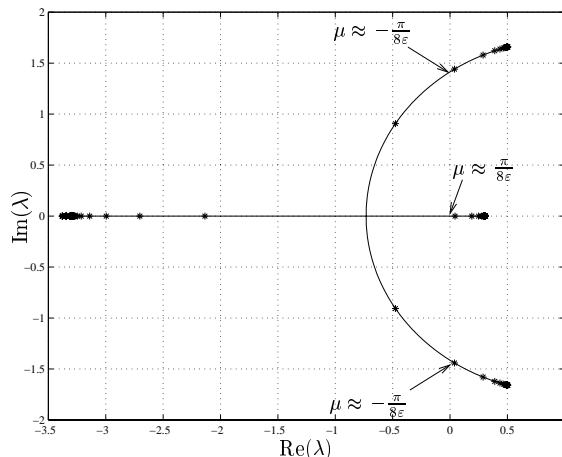


Figure 5.16: Path of the eigenvalues of the approximating system.

from *inspection* of the bifurcation diagram. If there is a change in the number of fixed points for a certain parameter value, then there is a bifurcation at this parameter value according to Definition 5.1. We also observed that a ‘jump’ exists of the eigenvalue over the imaginary axis. Although it is intuitively appealing to state that at a bifurcation an eigenvalue (or a pair of them) *must* ‘jump’ or pass the imaginary axis, we do not have mathematical proof for this.

2. *Can we classify a discontinuous bifurcation by inspecting the point where the path of the set-valued eigenvalue (or a pair of eigenvalues) crosses the imaginary axis?* The discontinuous bifurcations of the preceding examples were classified by comparing their nature with a certain type of continuous bifurcation. If at a discontinuous bifurcation the change of fixed points is the same as for a certain type of continuous bifurcation, then the discontinuous bifurcation can be regarded as the discontinuous counterpart of that type of continuous bifurcation. We observed that all discontinuous static bifurcations expose a jump of an eigenvalue through the origin, like for the continuous static bifurcations. For the discontinuous Hopf bifurcation, a pair of eigenvalues jumps through the imaginary axis, consistent with the continuous Hopf bifurcation. The example in Section 5.7 exposes a discontinuous bifurcation point at which a branch of periodic solutions as well as a branch of fixed points bifurcate. The set-valued eigenvalues cross the imaginary axis twice, suggesting a Hopf and a static bifurcation. Although we cannot classify this discontinuous multiple-crossing bifurcation as a discontinuous counterpart of a continuous bifurcation, we can still look upon the discontinuous bifurcation as a combination of two continuous bifurcations and classify it as such. Whether we can classify the discontinuous bifurcation by inspecting the crossing of the eigenvalue with the imaginary axis is not proven although it seems intuitively correct.
3. *Does a continuous bifurcation exist if the non-smooth system, exposing a dis-*

continuous bifurcation, is approximated by a smooth system? In Section 5.4 a counterexample was given by taking a non-symmetric smoothing function. The smoothed version of the non-smooth system did not expose a bifurcation. It should be remarked that if the smoothing parameter is increased, all branches converge to the branches of the non-smooth system but the branches may not necessarily intersect (implying a bifurcation).

4. *Is the discontinuous bifurcation of the non-smooth system related to the continuous bifurcation of the smoothed system (assuming that it exists)?* In Section 5.5 a non-smooth system exposed a discontinuous pitchfork bifurcation. A non-symmetric smoothing of the non-smooth system exposed a saddle-node bifurcation. We conclude that the bifurcation occurring in the smoothed system is not always related to the discontinuous bifurcation of the original non-smooth system.
5. *Do discontinuous bifurcations exist that do not have a continuous counterpart? In other words: do discontinuous bifurcations exist that behave qualitatively different from any continuous bifurcation?* Section 5.7 showed a discontinuous bifurcation which can be looked upon as the combination of two continuous bifurcations. This bifurcation can therefore not be classified as simply the counterpart of a continuous bifurcation. However, the discontinuous bifurcation still behaves in the same way as the two continuous bifurcations. The qualitative behaviour of the bifurcation is (in this particular case) simply the combination of the behaviour of a Hopf and a pitchfork bifurcation. In Chapter 6 we will encounter a combined flip-fold bifurcation of a periodic solution that behaves like a flip and fold bifurcation but also shows behaviour not covered by a flip or fold bifurcation separately. We are therefore not confident that the behaviour of a multiple-crossing bifurcation of a fixed point is always simply the combination of behaviour of continuous bifurcations.

From the preceding discussion we raise two conjectures.

Conjecture 5.1

A necessary condition for the existence of a discontinuous bifurcation of a fixed point of a non-smooth continuous system is a 'jump' of an eigenvalue (or a pair of them) over the imaginary axis, i.e. the path of the set-valued eigenvalue(s) passes the imaginary axis.

A discontinuous bifurcation point would according to Conjecture 5.1 be structurally unstable in the sense that the set-valued eigenvalue contains a value on the imaginary axis.

Conjecture 5.2

A discontinuous bifurcation of a fixed point of a non-smooth continuous system may be classified by inspecting the point(s) where the path of the set-valued eigenvalue (or a pair of eigenvalues) crosses the imaginary axis.

Remarks: Conjecture 5.2 suggests that we can classify a discontinuous bifurcation *if* it exists. The conjecture does not give a condition for a bifurcation. The conjecture also suggests that we can classify a double-crossing bifurcation as the combination of two continuous bifurcations, like for the Hopf-pitchfork bifurcation, because it exposes the behaviour of both continuous bifurcations. However, the bifurcation can still show features not covered by the two continuous bifurcation separately.

We should be sceptical concerning Conjectures 5.1 and 5.2. One can argue that it might be possible that a double-crossing bifurcation is the combination of two bifurcations that cancel each other out. A smooth approximation of a non-smooth system could show two saddle-node bifurcations (turning the branch in opposite directions) which collide in the limiting case. The bifurcation diagram would then look in the limiting case like a hysteresis point (Figure 5.1). The non-smooth system, showing a double intersection of a set-valued eigenvalue with the origin, might then have no bifurcation at all and would be a non-smooth counterpart of a hysteresis point. Conjecture 5.1 suggests therefore a *necessary* condition for a discontinuous bifurcation and not a sufficient condition. If indeed a discontinuous bifurcation exists, then Conjecture 5.2 suggests that we can classify the discontinuous bifurcation by inspecting the crossing point(s) of the set-valued eigenvalues with the imaginary axis.

These conjectures are raised from observations and agree with one's intuition as they are generalizations of theorems for continuous bifurcations in smooth systems. The conjectures will be assumed to hold in the remainder of this thesis keeping in mind that there exists no mathematical proof that they are correct.

Periodic solutions can be looked upon as fixed points on a Poincaré map. The generalization of eigenvalues for fixed points are Floquet multipliers for periodic solutions. If the above conjectures are correct, then we can expect a discontinuous bifurcation of a periodic solution if a Floquet multiplier (or a pair of them) jumps over the unit circle. The type of discontinuous bifurcation of a periodic solution could then be inferred from the crossing point of the path of the Floquet multiplier(s) with the unit circle. We will discuss bifurcations of periodic solutions in the next chapter. The results on discontinuous bifurcations of periodic solutions will be compared with Conjectures 5.1 and 5.2.

Chapter 6

Bifurcations of Periodic Solutions

'If a man will begin with certainties, he shall end with doubts; but if he will be content to begin with doubts, he shall end in certainties.'

FRANCIS BACON, (1561-1626)

In this chapter we will study bifurcations of periodic solution in discontinuous systems. Section 6.3 explains how a discontinuous bifurcation of a periodic solution can be created when a periodic solution touches a non-smooth hyper-surface. The relation with discontinuous bifurcations of fixed points in non-smooth continuous systems is treated. Fundamental questions about discontinuous bifurcations of periodic solutions are raised. Sections 6.6 to 6.9 treat a number of numerical examples which show discontinuous bifurcations. Section 6.10 draws conclusions from the numerical examples and tries to give answers to the questions of Section 6.3.

6.1 Discontinuous Systems

In this chapter we will study periodic solutions of nonlinear systems with a discontinuous right-hand side, as defined in Chapter 2, under influence of a single parameter. The right-hand side is discontinuous on one or more hyper-surfaces and is assumed to be linearly bounded. An example of such a system is

$$\dot{\underline{x}}(t) = \underline{f}(t, \underline{x}(t), \mu) = \begin{cases} \underline{f}_-(t, \underline{x}(t), \mu) & \underline{x} \in \mathcal{V}_- \\ \underline{f}_+(t, \underline{x}(t), \mu) & \underline{x} \in \mathcal{V}_+, \end{cases} \quad (6.1)$$

with

$$\begin{aligned}\mathcal{V}_- &= \{\underline{x} \in \mathbb{R}^n \mid h(\underline{x}(t), \mu) < 0\} \\ \Sigma &= \{\underline{x} \in \mathbb{R}^n \mid h(\underline{x}(t), \mu) = 0\} \\ \mathcal{V}_+ &= \{\underline{x} \in \mathbb{R}^n \mid h(\underline{x}(t), \mu) > 0\}.\end{aligned}\tag{6.2}$$

The system depends on a single parameter μ . Also, the indicator function h is in general dependent on μ , which implies dependence on μ for the hyper-surface Σ and the spaces \mathcal{V}_- and \mathcal{V}_+ . Discontinuous systems of this type can be extended to differential inclusions by means of the method proposed by Filippov (Chapter 2). The resulting differential inclusion has a set-valued map $\underline{F}(t, \underline{x}, \mu)$ which is upper semi-continuous, convex, closed, non-empty and linearly bounded. Existence of the solution to the IVP is therefore guaranteed. Uniqueness, however, is not guaranteed.

6.2 Bifurcations in Smooth Systems

In the preceding chapter, bifurcations of fixed points were discussed. Jacobian matrices of non-smooth continuous systems can behave discontinuously when a system parameter is varied: they jump. The jump of the Jacobian matrix causes a jump of the eigenvalues. If an eigenvalue jumps over the imaginary axis under influence of a parameter, we presumed that a discontinuous bifurcation can occur (see Conjecture 5.1).

Before introducing the basic idea of discontinuous bifurcations of periodic solutions, we shortly address bifurcations of such solutions in smooth systems. A periodic solution can be regarded as a fixed point of a Poincaré map P on a Poincaré section. The results on bifurcations of fixed points are therefore useful for the investigation of bifurcations of periodic solutions. The stability of a periodic solution is determined by its Floquet multipliers λ_i ($i = 1, \dots, n$), which are the eigenvalues of the fundamental solution matrix $\underline{\Phi}(T + t_0, t_0)$. The Floquet multipliers are the generalization of the eigenvalues at a fixed point. Because solutions of autonomous systems can be shifted in time, one of the Floquet multipliers equals unity for such systems. The periodic solution is stable if all Floquet multipliers (not associated with the phase in the autonomous case) lie within the unit circle. If one or more Floquet multipliers lie outside the unit circle, then the periodic solution is unstable. The periodic solution varies (as well as its Floquet multipliers) as a parameter of the system is varied. The periodic solution changes from stable to unstable (or vice versa) when the largest Floquet multiplier passes through the unit circle.

Like for fixed points, different definitions for a bifurcation of a periodic solution exist. We will take Definition 5.1 as definition for a bifurcation of periodic solutions. According to Definition 5.1, a point is a bifurcation point of a periodic solution if the number of periodic solutions changes for a varying system parameter. One can also give a definition of a bifurcation of a periodic solution based on topological equivalence of the phase portrait, like Definition 5.3. We will discuss in Section 6.10 the difference between these definitions when they are applied to periodic solutions of Filippov systems.

A bifurcation of a periodic solution of a smooth system occurs if a Floquet multiplier (or a pair of them) passes through the unit circle under variation of a

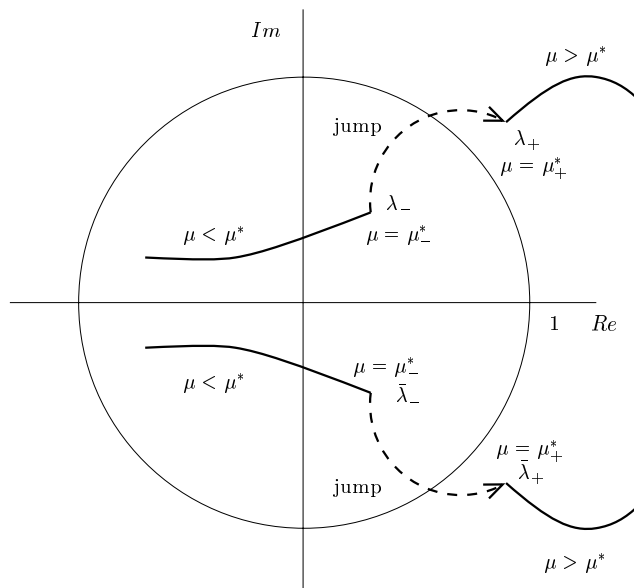


Figure 6.1: Discontinuous bifurcation; single crossing.

system parameter.

6.3 Discontinuous Bifurcation: The Basic Idea

Examples of non-smooth continuous systems in Chapter 5 showed discontinuous bifurcations of fixed points when an eigenvalue jumps over the imaginary axis. Conjecture 5.1 presumed that such a jump over the imaginary axis is a necessary condition for a discontinuous bifurcation. Moreover, we presumed that the crossing of the path of the jump (obtained from a convex combination of two Jacobians) with the imaginary axis determines the type of bifurcation (Conjecture 5.2).

In Chapter 3 we concluded that fundamental solution matrices of the discontinuous systems, $\underline{\Phi}(t, t_0)$, expose jumps at time instances t where a hyper-surface of discontinuity is crossed. Periodic solutions change under influence of a parameter. The crossing of a periodic solution with a hyper-surface can vanish if a parameter is varied. The fundamental solution matrix after the period time $\underline{\Phi}(T + t_0, t_0)$ of a periodic solution can therefore also exhibit a jump if a system parameter is varied. The jump of the fundamental solution matrix implies a jump of one or more Floquet multipliers.

In a similar way as for bifurcations of fixed points, we can expect a discontinuous bifurcation of a periodic solution when a Floquet multiplier jumps over the unit circle under influence of a parameter. The basic idea is depicted in Figure 6.1. The Floquet multipliers jump at a critical value of the parameter $\mu = \mu^*$ from λ_- and $\bar{\lambda}_-$ to λ_+ and $\bar{\lambda}_+$. The path of the jump is obtained from a convex combination of the fundamental solution matrices before and after the jump. The path of the

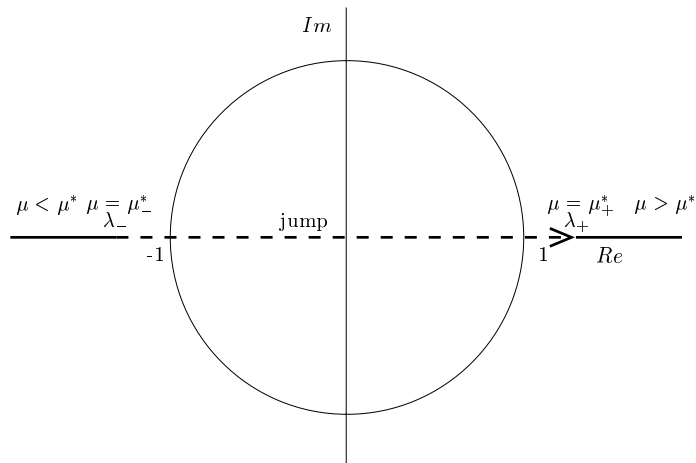


Figure 6.2: Discontinuous bifurcation; double crossing.

Floquet multipliers crosses the unit circle. We presume that this causes a discontinuous bifurcation of a periodic solution (in this case a discontinuous Neimark-Sacker bifurcation). Remark that also other jumps are possible as was explained in the preceding chapter about fixed points (see Figures 5.2 and 5.3).

The numerical examples in the Sections 6.6 to 6.8 show discontinuous counterparts of various types of smooth bifurcations of periodic solutions, all characterized by a single jump over the unit circle at the point where the smooth bifurcation has a Floquet multiplier which passes through the unit circle. Like for discontinuous bifurcations of fixed points also multiple crossings are possible. In Figure 6.2 a jump of a real valued Floquet multiplier is shown which jumps from a value smaller than -1 to a value greater than $+1$ thereby crossing the unit circle twice. It crosses the unit circle at the points -1 , involving a flip bifurcation, and at the point $+1$, involving a fold bifurcation. The discontinuous bifurcation is therefore a combination of a fold and a flip bifurcation. We will discuss an example of this type of combined fold–flip bifurcation in Section 6.9. Similar alternatives for the path of the jump are possible as in Figures 5.2b and 5.3a.

The idea of a discontinuous bifurcation of a periodic solution, at which a Floquet multiplier jumps through the unit circle, is similar to the ‘C-bifurcations’ in the work of Feigin [1974, 1978, 1995] and Di Bernardo et al. [1999a,b]. Feigin classifies C-bifurcations on the number of real-valued eigenvalues of the Poincaré map (see Section 6.4) that are smaller than -1 or larger than $+1$, but does not take complex eigenvalues into account. The classification embraces only the discontinuous fold and flip bifurcation, the combined fold–flip bifurcation and the smooth transition (which is not a bifurcation in the sense of Definition 5.1) [Di Bernardo et al., 1999b]. The possibility of a discontinuous symmetry-breaking bifurcation or other discontinuous bifurcations were not mentioned. Non-classical bifurcations of non-smooth discrete mappings were also addressed by Nusse and York [1992]. Discontinuous

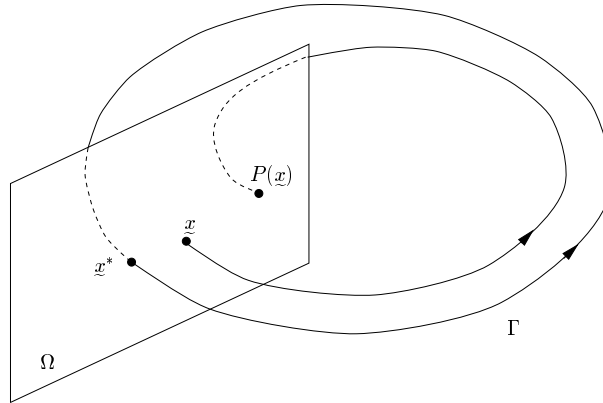


Figure 6.3: Poincaré map for an autonomous system.

bifurcations are based on jumps in the Floquet multipliers which are essentially the same as the derivatives of the Poincaré map. The ‘C-bifurcations’ are therefore also discontinuous bifurcations (except for the smooth transition). In this thesis it is explained how the discontinuous bifurcations come into being through jumps of the fundamental solution matrix. It is shown that the fundamental solution matrix can jump if a periodic solution touches a non-smooth hyper-surface of discontinuity. The jumps are described by saltation matrices which can be expressed explicitly. Furthermore, the path of the Floquet multipliers during the jump is calculated by means of linear approximation. The path of the eigenvalues of the Poincaré map at a C-bifurcation remains on the real axis, whereas the Floquet multipliers at a discontinuous bifurcation can be complex conjugated.

6.4 The Poincaré Map

We can elucidate the relation between continuous bifurcations and discontinuous bifurcations even more by studying the Poincaré map [Parker and Chua, 1989]. Consider an n -th order autonomous system

$$\dot{\underline{x}}(t) = \underline{f}(\underline{x}(t)) \quad (6.3)$$

with a periodic solution Γ shown in Figure 6.3. Let \underline{x}^* be a point on the periodic solution and let Ω be an $(n-1)$ -dimensional hyper-surface transversal to Γ at \underline{x}^* . We will call the hyper-surface Ω the *Poincaré section*. The trajectory emanating from \underline{x}^* will hit Ω at \underline{x}^* in a positive direction in T seconds, where T is the period time of the periodic solution. Trajectories starting on Ω in a sufficiently small neighbourhood of \underline{x}^* will, in approximately T seconds, intersect in a positive direction in the vicinity of \underline{x}^* . Therefore, $\underline{x}(t)$ and Ω define a mapping P of some neighbourhood $U \subset \Omega$ of \underline{x}^* onto another neighbourhood $V \subset \Omega$ of \underline{x}^* . The map $P : U \rightarrow V$ is defined as

$$\underline{x}_{i+1} = P(\underline{x}_i) \quad (6.4)$$

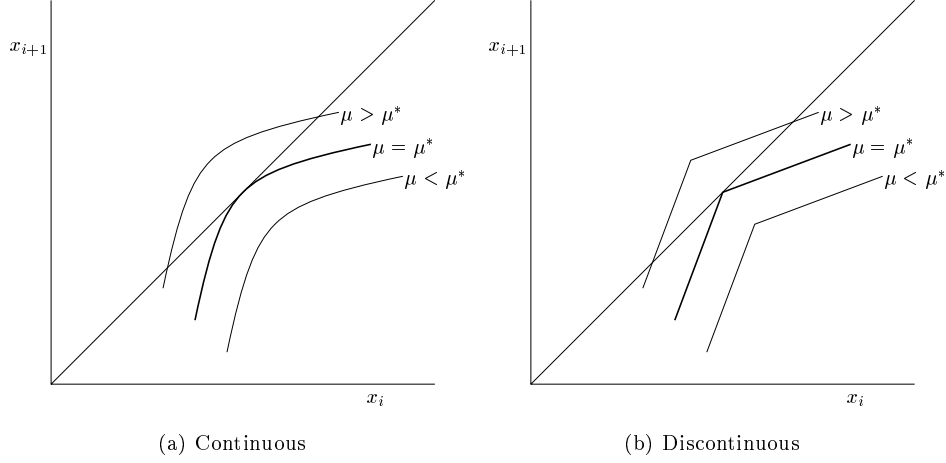


Figure 6.4: Poincaré map at a fold bifurcation.

where $\underline{x}_{i+1} = \underline{x}(t_{i+1}) \in \Omega$ is the first intersection point of the trajectory $\underline{x}(t)$ that starts from $\underline{x}(t_i) = \underline{x}_i \in \Omega$. The map P is called the *Poincaré map* or *first return map* of the autonomous system. The map can be applied to itself $\underline{x}_{i+2} = P(P(\underline{x}_i))$. The time-continuous system (6.3) has been transformed to a discrete map P .

For a point \underline{x}^* on a periodic solution holds of course

$$\underline{x}^* = P(\underline{x}^*). \quad (6.5)$$

A periodic solution Γ is therefore a fixed point of

$$H(\underline{x}) = P(\underline{x}) - \underline{x}. \quad (6.6)$$

The derivative DP of the map P is related to the fundamental solution matrix $\underline{\Phi}$ [Parker and Chua, 1989]

$$DP(\underline{x}_i) = \left[I - \frac{1}{\underline{n}_\Omega^T \underline{f}(t, \underline{x}_{i+1})} \underline{f}(t, \underline{x}_{i+1}) \underline{n}_\Omega^T \right] \underline{\Phi}(t_{i+1}, t_i), \quad (6.7)$$

where $\underline{\Phi}(t_{i+1}, t_i)$ is the fundamental solution matrix along the trajectory $\underline{x}(t)$ of system 6.3 and \underline{n}_Ω is the normal to Ω at \underline{x}_{i+1} . The stability of a periodic solution can be inferred from the eigenvalues of the Poincaré map but also from the Floquet multipliers. The eigenvalues of $DP(\underline{x}^*)$ are $\{0, m_1, \dots, m_{n-1}\}$. One eigenvalue is zero because the eigenvectors of DP lie in the tangent plane to Ω and are therefore linearly dependent. The fundamental solution matrix $\underline{\Phi}_T$ of the periodic solution Γ has eigenvalues $\{1, m_1, \dots, m_{n-1}\}$, which are also called Floquet multipliers. One Floquet multiplier equals unity because the periodic solution of an autonomous system can be shifted in time. The remaining Floquet multipliers are identical to the eigenvalues of the Poincaré map.

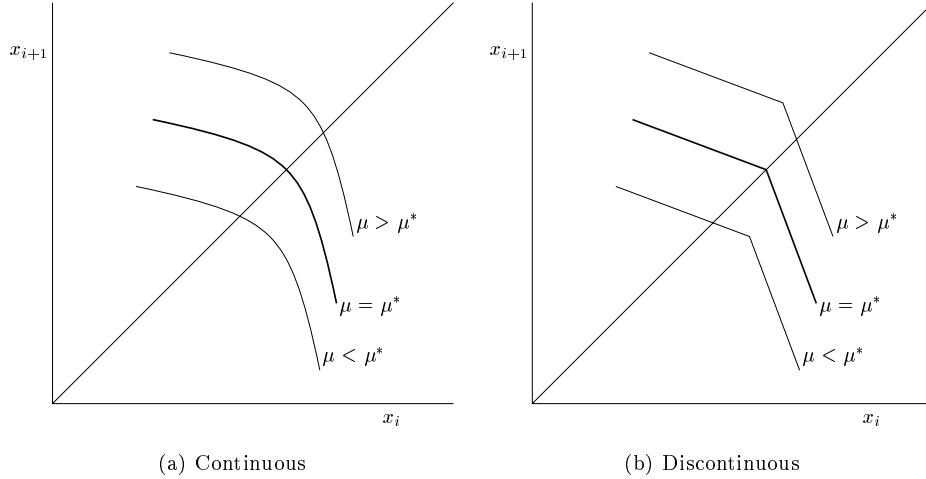


Figure 6.5: Poincaré map at a flip bifurcation.

The Poincaré map can also be defined for non-autonomous time-periodic systems. Consider the system

$$\dot{\underline{x}}(t) = \underline{f}(t, \underline{x}(t)) \quad (6.8)$$

with $\underline{f}(t, \underline{z}) = \underline{f}(t + T, \underline{z})$. For non-autonomous time-periodic systems the period time \tilde{T} is a priori known. We define an n -dimensional hyper-surface $\Theta \in S^1 \times \mathbb{R}^n$ as

$$\Theta = \{(t, \underline{x}) \in S^1 \times \mathbb{R}^n \mid t = kT, k = 0, 1, 2, \dots\} \quad (6.9)$$

Every T seconds, the trajectory $\underline{x}(t)$ of system (6.8) intersects Θ . We can therefore define a mapping $P_N : \Theta \rightarrow \Theta$ which maps the state $\underline{x}(t_0)$ to the state $\underline{x}(t_0 + T)$ as

$$\underline{x}(t_0 + T) = P_N(\underline{x}(t_0)). \quad (6.10)$$

The map P_N is called the Poincaré map for a non-autonomous system or T -advance map. The derivative DP_N of P_N is identical to the fundamental solution matrix $\underline{\Phi}_T$.

The Poincaré map at a fold bifurcation is depicted in Figure 6.4. The map has no intersection points with the diagonal $x_{i+1} = x_i$ for $\mu < \mu^*$. The map is tangent to the diagonal for $\mu = \mu^*$. For $\mu > \mu^*$ the map has two intersection points, which correspond to periodic solutions of the dynamical system. Two periodic solutions are therefore created/destroyed at $\mu = \mu^*$, which is consequently a fold bifurcation. The map at a continuous fold bifurcation, stemming from a smooth system, is smooth and is tangent to the diagonal $x_{i+1} = x_i$, i.e. the slope is $+1$. The map at a discontinuous fold bifurcation, stemming from a discontinuous system, is non-smooth and touches the diagonal with its tip. One limb of the non-smooth map has a slope smaller

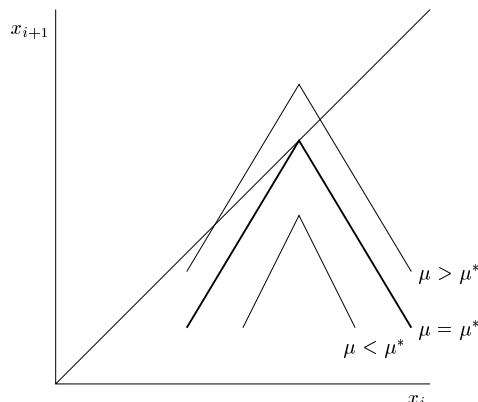


Figure 6.6: Tent map.

than $+1$ and the other limb has a slope larger than $+1$. The derivative of the map therefore jumps from a value smaller than $+1$ to a value larger than $+1$. The Floquet multiplier is directly related to the derivative of the map.

The Poincaré map at a flip bifurcation is depicted in Figure 6.5. The map at a continuous flip bifurcation, stemming from a smooth system, crosses the diagonal with a slope -1 . The map at a discontinuous flip bifurcation, stemming from a discontinuous system, is non-smooth and crosses the diagonal with its tip. One limb of the non-smooth map has a slope smaller than -1 and the other has a slope larger than -1 . The derivative of the map therefore jumps from a value smaller than -1 to a value larger than -1 .

The map at a discontinuous fold bifurcation and the one at a discontinuous flip bifurcation were explained above, but the example of Figure 6.2 shows a discontinuous bifurcation which is a combination of a flip and a fold as the Floquet multiplier jumps from $\lambda < -1$ to $\lambda > +1$. As the slope of the Poincaré map is directly related to the Floquet multiplier, the map should be non-smooth having two limbs where one has a slope larger than $+1$ and the other has a slope smaller than -1 . This map is depicted in Figure 6.6 and appears to be the tent map. This type of bifurcation, with an underlying tent map, will be encountered in Section 6.9.

6.5 Intersection of Hyper-surfaces of Discontinuity

In Chapter 3 we elaborated how fundamental solution matrices of discontinuous systems can jump as the solution crosses a hyper-surface of discontinuity. Jumps of the Jacobian of fixed points are presumed to lead to discontinuous bifurcations when an eigenvalue (or a pair of them) crosses the imaginary axis, as was outlined in the preceding chapter. The question arises: can jumps in the fundamental solution matrix cause discontinuous bifurcations of periodic solutions?

We consider the following scenario (Figure 6.7). The hyper-surface Σ defines a discontinuity and divides the state-space in the two subspaces \mathcal{V}_+ and \mathcal{V}_- . The vector field is discontinuous on Σ , i.e. $\underline{f}_- \neq \underline{f}_+$, but Σ itself is smooth. Assume that

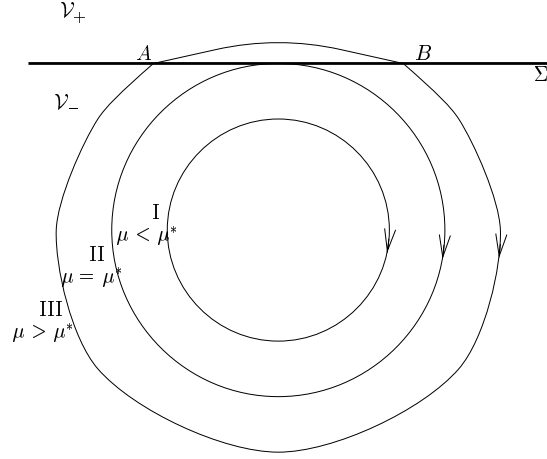


Figure 6.7: Double intersection of a smooth hyper-surface.

a system has one periodic solution that changes under influence of a parameter μ . For a value $\mu < \mu^*$ the periodic solution is denoted by periodic solution I. Periodic solution I does not cross Σ . If we increase the parameter μ to $\mu = \mu^*$, then the periodic solution changes to periodic solution II. Periodic solution II is tangent at one point to Σ . If we increase μ even more to $\mu > \mu^*$, then the periodic solution becomes periodic solution III which crosses Σ twice at points A and B. Let us assume that periodic solution I comes infinitely close to Σ (without crossing it) and that periodic solution III stays an infinitely small time in \mathcal{V}_+ but crosses Σ twice. The periodic solutions I and III are therefore (almost) identical, but the fundamental solution matrix of periodic solution III will jump twice with saltation matrices \underline{S}_A and \underline{S}_B . The crossings occur at $t_A = t_B = t_\Sigma$ as periodic solution III stays an infinitely small time in \mathcal{V}_+ . We can now express the fundamental solution matrix $\underline{\Phi}_{III}$ into $\underline{\Phi}_I$

$$\underline{\Phi}_{III}(T + t_0, t_0) = \underline{\Phi}_I(T + t_0, t_\Sigma + t_0) \underline{S}_B \underline{S}_A \underline{\Phi}_I(t_\Sigma + t_0, t_0) \quad (6.11)$$

However, from (3.30) and (3.31) we conclude that $\underline{S}_B = \underline{S}_A^{-1}$, for non-singular \underline{S}_A and \underline{S}_B . The fundamental solution matrix of periodic solution III is therefore identical to the one of periodic solution I, $\underline{\Phi}_{III}(T + t_0, t_0) = \underline{\Phi}_I(T + t_0, t_0)$. This scenario, in which a single smooth hyper-surface is crossed twice, can consequently not lead to a bifurcation of a periodic solution if \underline{S}_A is non-singular. The singular case arises in sliding mode problems (for instance in Section 6.7).

The preceding scenario did not lead to a bifurcation because the saltation matrix over a smooth hyper-surface is equal to the inverse of the saltation matrix in opposite direction over the same hyper-surface at that point. We will study a second scenario which is depicted in Figure 6.8. The hyper-surface Σ is now non-smooth and consists of two parts Σ_A and Σ_B . The periodic solution III enters \mathcal{V}_+ by crossing Σ_A at point A and leaves \mathcal{V}_+ by crossing Σ_B at point B. The saltation matrix \underline{S}_A is (in general) not equal to \underline{S}_B^{-1} . Consequently, the fundamental solution matrix of periodic

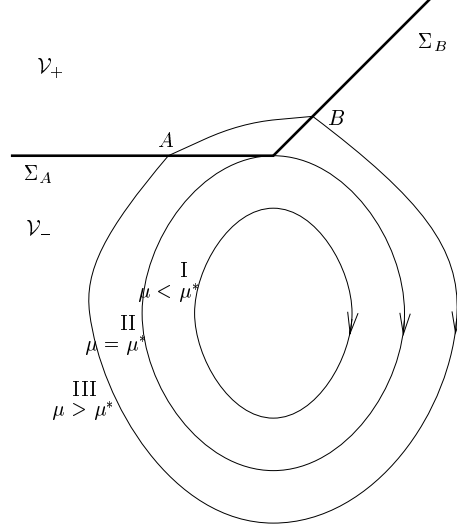


Figure 6.8: Double intersection of a non-smooth hyper-surface.

solution III is not identical to the one of periodic solution I. Therefore, at $\mu = \mu^*$, the fundamental solution matrix over the period time $\underline{\Phi}_{II}(T+t_0, t_0)$ will jump from $\underline{\Phi}_I(T+t_0, t_0)$ to $\underline{\Phi}_{III}(T+t_0, t_0)$. The theory of linear approximation (developed for fixed points) is now applicable, as a periodic solution is a fixed point of a Poincaré map. We combine the two saltation matrices $\underline{\mathcal{S}}_{BA} = \underline{\mathcal{S}}_B \underline{\mathcal{S}}_A$. From Section 4.1 we know that the theory of linear approximation also applies to the saltation matrix. Therefore, the combined saltation matrix can also be approximated linearly

$$\tilde{\underline{\mathcal{S}}}_{BA} = \underline{I} + q(\underline{\mathcal{S}}_{BA} - \underline{I}) \quad 0 \leq q \leq 1. \quad (6.12)$$

We introduce the *generalized fundamental solution matrix* $\tilde{\underline{\Phi}}$ at $\mu = \mu^*$ which is the closed convex hull of $\underline{\Phi}_I$ and $\underline{\Phi}_{III}$

$$\begin{aligned} \tilde{\underline{\Phi}} &= \overline{\text{co}}\{\underline{\Phi}_I(T+t_0, t_0), \underline{\Phi}_{III}(T+t_0, t_0)\} \\ &= \{q(\underline{\Phi}_{III}(T+t_0, t_0) - \underline{\Phi}_I(T+t_0, t_0)) + \underline{\Phi}_I(T+t_0, t_0), \forall 0 \leq q \leq 1\}. \end{aligned} \quad (6.13)$$

The generalized fundamental solution matrix (6.13) is the set-valued fundamental solution matrix of periodic solution II. In fact, (6.13) defines *how* the fundamental solution matrix of the periodic solution ‘jumps’ from $\underline{\Phi}_I$ to $\underline{\Phi}_{III}$ if μ is increased from $\mu < \mu^*$ to $\mu > \mu^*$. From the set-valued generalized fundamental solution matrix we can obtain the set-valued Floquet multipliers. We can look upon $\text{eig}(\tilde{\underline{\Phi}})$ together with (6.13) as if it gives a path of Floquet multipliers ‘during’ the jump as q is varied from 0 to 1.

Other scenarios as the ones depicted in Figure 6.7 and 6.8 are of course also possible. A third scenario is depicted in Figure 6.9. The tip of the non-smooth hyper-surface is again touched by a periodic solution. The third scenario can therefore also lead to a discontinuous bifurcation of a periodic solution.

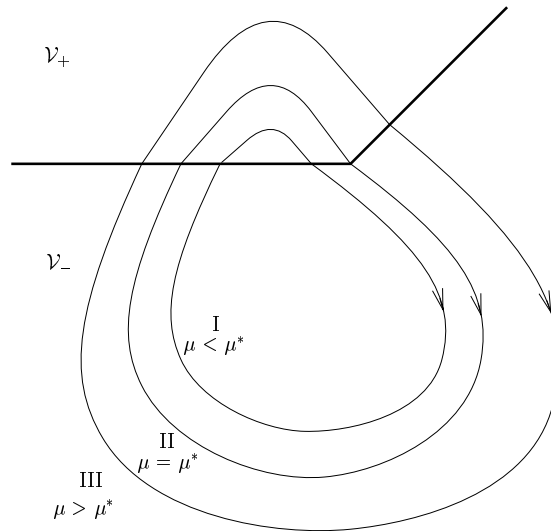


Figure 6.9: Third scenario.

A Floquet multiplier can jump from inside the unit circle to outside the unit circle under influence of a parameter μ . Similar to a discontinuous bifurcation of a fixed point we presume that such a jump of a Floquet multiplier causes a discontinuous bifurcation of a periodic solution. Where the Floquet multiplier crosses the unit circle during its jump is determined by $\tilde{\Phi}$. The jumping Floquet multiplier can also jump from outside the unit circle to another point outside the unit circle in the complex plane. Similar to our treatment of fixed points, we presume that the existence of a bifurcation depends on the path of the Floquet multiplier during its jump. It could have jumped from one point to the other without passing through the unit circle (which would imply no bifurcation) or it could have passed through the unit circle twice. We presume that the latter case causes a discontinuous bifurcation which is the combination of two bifurcations. If the generalized Jacobian determines the existence and type of discontinuous bifurcation of fixed points (i.e. if Conjectures 5.1 and 5.2 hold), then the generalized fundamental solution matrix determines the existence and type of bifurcation of periodic solutions.

The discontinuous vector field can also be approximated in a smooth way, with a ‘stiffness’ depending on the accuracy of approximation. We concluded in the previous chapter that the discontinuous bifurcation of a fixed point may vanish if the vector field is approximated by a smooth vector field. This problem probably also exists for bifurcations of periodic solutions. Floquet multipliers of smooth systems do not jump but move ‘fast’ when the solution is passing through a ‘stiff’ part of the vector field. A smooth approximation which preserves the existence of the bifurcation will yield a continuous path of the Floquet multipliers through the unit circle. A smooth approximation which does not preserve the existence of the bifurcation will yield two unconnected branches that come close to each other. To each branch belongs a continuous path of Floquet multipliers which does not necessarily cross the unit

circle.

The above reflections can be summarized by the following fundamental questions:

1. Do discontinuous bifurcations (in the sense of Definition 5.1) exist of periodic solutions of Filippov systems?
2. Does a discontinuous bifurcation exist caused by the scenario depicted in Figure 6.8?
3. Does a jump of a Floquet multiplier over the unit circle under the influence of a parameter lead to a bifurcation of a periodic solution?
4. Can we classify the bifurcation by inspecting the point where the path of the set-valued Floquet multiplier(s) crosses the unit circle?
5. Do discontinuous bifurcations of periodic solutions exist that do not have a continuous counterpart? In other words: do discontinuous bifurcations exist that behave qualitatively different from any continuous bifurcation?
6. Can Definitions 5.1 and 5.3 be inconsistent when they are applied to periodic solutions of Filippov systems?

These questions are related to each other and are also related to the questions raised in Section 5.2. Some numerical examples in the following sections show discontinuous bifurcations of periodic solutions which illustrate these questions. We will return to the questions in the last section. The bifurcation diagrams in Sections 6.6 to 6.9 have been made with a path-following technique based on the shooting method implemented in MATLAB [Fey, 1992; Parker and Chua, 1989; Van de Vorst, 1996]. The fundamental solution matrix after the period time $\underline{\Phi}_T$, used in the shooting method, was obtained with a sensitivity analysis [Leine et al., 1998].

6.6 Fold Bifurcation; Trilinear Spring System

In this section we will treat a system that exposes a discontinuous fold bifurcation. The forced oscillation of a damped mass on a spring with cubic term leads to the Duffing equation [Hagedorn, 1988; Guckenheimer and Holmes, 1983; Nayfeh and Balachandran, 1995; Nayfeh and Mook, 1979]. The Duffing equation is the classical example where the harmonic resonance peak is bended and two fold bifurcations (also called turning point bifurcations) are born. In our example, we will consider a similar mass-spring-damper system, where the cubic spring is replaced by a trilinear spring. Additionally, trilinear damping is added to the model. The trilinear damping will turn out to be essential for the existence of a *discontinuous* fold bifurcation.

The model is very similar to the model of Natsiavas [Natsiavas, 1989; Natsiavas and Gonzalez, 1992] but the transitions from contact with the support to no contact are different from those in the model of Natsiavas. The model of Natsiavas switches as the position of the mass passes the contact distance (in both transition directions). In our model, contact is made when the position of the mass passes the contact distance (for growing $|x|$), and contact is lost when the contact force becomes zero. It is remarked that our modification of the Natsiavas model is not introduced to

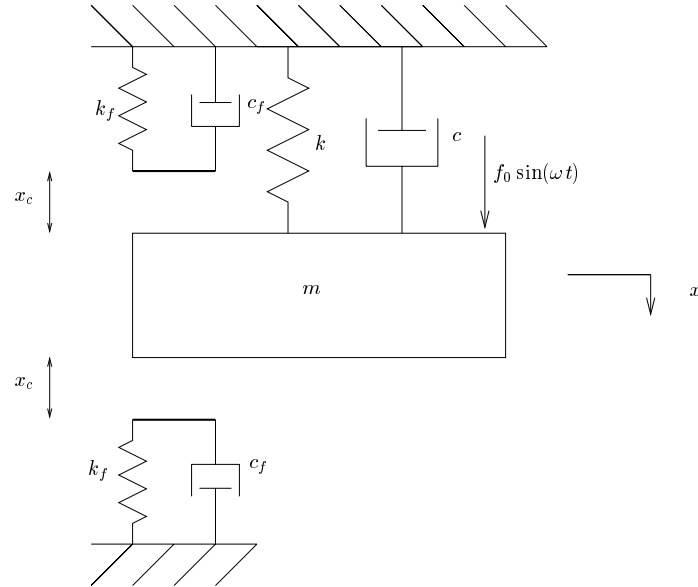


Figure 6.10: Trilinear system.

obtain an improved physical representation but in order to illustrate the theory developed in this thesis.

We consider the system depicted in Figure 6.10. The model is similar to the discontinuous support of Example II in Subsection 3.5 but now has two supports on equal contact distances x_c . The supports are first-order systems which relax to their original state if there is no contact with the mass. If we assume that the relaxation time of the supports is much smaller than the time interval between two contact events, we can neglect the free motion of the supports. It is therefore assumed that the supports are at rest at the moment that contact is made. This is not an essential assumption but simplifies our treatment as the system reduces to a second-order equation.

The second-order differential equation of this system is

$$m\ddot{x} + C(\dot{x}) + K(x) = f_0 \sin(\omega t) \quad (6.14)$$

where

$$K(x) = \begin{cases} kx & [x, \dot{x}]^T \in \mathcal{V}_- \\ kx + k_f(x - x_c) & [x, \dot{x}]^T \in \mathcal{V}_{+1} \\ kx + k_f(x + x_c) & [x, \dot{x}]^T \in \mathcal{V}_{+2} \end{cases} \quad (6.15)$$

is the trilinear restoring force and

$$C(\dot{x}) = \begin{cases} c\dot{x} & [x, \dot{x}]^T \in \mathcal{V}_- \\ (c + c_f)\dot{x} & [x, \dot{x}]^T \in \mathcal{V}_{+1} \cup \mathcal{V}_{+2} \end{cases} \quad (6.16)$$

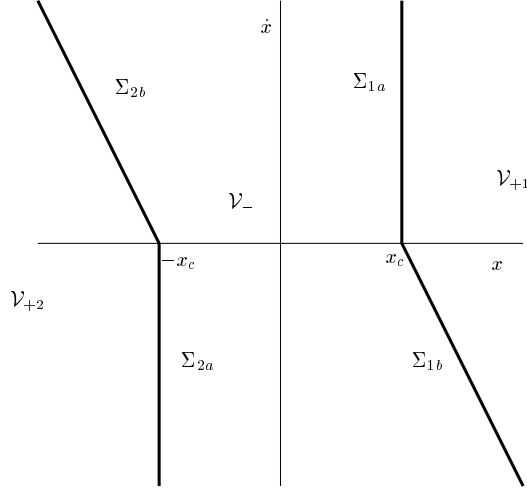


Figure 6.11: Subspaces of the trilinear system.

is the trilinear damping force. The state-space is divided into three subspaces \mathcal{V}_- , \mathcal{V}_{+1} and \mathcal{V}_{+2} (Figure 6.11).

If the mass is in contact with the lower support, then the state is in space \mathcal{V}_{+1}

$$\mathcal{V}_{+1} = \{[x, \dot{x}]^T \in \mathbb{R}^2 \mid x > x_c, k_f(x - x_c) + c_f \dot{x} \geq 0\},$$

whereas if the mass is in contact with the upper support, then the state is in space \mathcal{V}_{+2}

$$\mathcal{V}_{+2} = \{[x, \dot{x}]^T \in \mathbb{R}^2 \mid x < -x_c, k_f(x + x_c) + c_f \dot{x} \leq 0\}.$$

If the mass is not in contact with one of the supports, then the state is in space \mathcal{V}_- defined by

$$\mathcal{V}_- = \{[x, \dot{x}]^T \in \mathbb{R}^2 \mid [x, \dot{x}]^T \notin (\mathcal{V}_{+1} \cup \mathcal{V}_{+2})\}$$

We define the indicator functions $h_{1a}(x, \dot{x})$ and $h_{1b}(x, \dot{x})$ as

$$h_{1a} = x - x_c, \quad h_{1b} = k_f(x - x_c) + c_f \dot{x} \quad (6.17)$$

The hyper-surface Σ_1 between \mathcal{V}_- and \mathcal{V}_{+1} consists of two parts Σ_{1a} and Σ_{1b} . The part Σ_{1a} defines the transition from \mathcal{V}_- to \mathcal{V}_{+1} because contact is made when x becomes larger than x_c

$$\Sigma_{1a} = \{[x, \dot{x}]^T \in \mathbb{R}^2 \mid h_{1a}(x, \dot{x}) = 0, h_{1b}(x, \dot{x}) \geq 0\}. \quad (6.18)$$

The part Σ_{1b} is defined by the indicator equation which defines the transition from \mathcal{V}_{+1} back to \mathcal{V}_- as contact is lost when the support-force becomes zero (the support can only push, not pull on the mass)

$$\Sigma_{1b} = \{[x, \dot{x}]^T \in \mathbb{R}^2 \mid h_{1a}(x, \dot{x}) \geq 0, h_{1b}(x, \dot{x}) = 0\}. \quad (6.19)$$

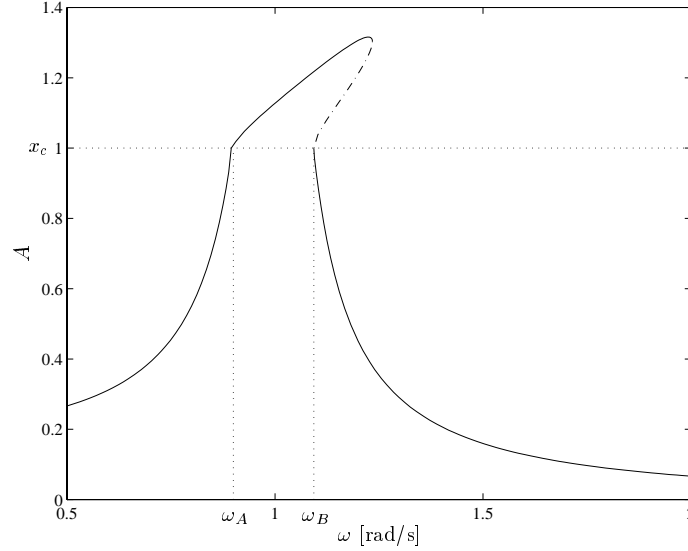


Figure 6.12: Response diagram of trilinear spring system.

Similarly, the hyper-surface Σ_2 between \mathcal{V}_- and \mathcal{V}_{+2} consists of two parts Σ_{2a} and Σ_{2b} defined by the indicator equations

$$h_{2a}(x, \dot{x}) = x + x_c \quad h_{2b}(x, \dot{x}) = k_f(x + x_c) + c_f \dot{x} \quad (6.20)$$

Like we have done in Subsection 3.5 we can construct the saltation matrices. The saltation matrices are of course similar to those of Subsection 3.5

$$\underline{S}_{1a} = \begin{bmatrix} 1 & 0 \\ -\frac{c_f}{m} & 1 \end{bmatrix}, \quad \underline{S}_{1b} = \underline{I} \quad (6.21)$$

$$\underline{S}_{2a} = \begin{bmatrix} 1 & 0 \\ -\frac{c_f}{m} & 1 \end{bmatrix}, \quad \underline{S}_{2b} = \underline{I} \quad (6.22)$$

The hyper-surfaces Σ_1 and Σ_2 are non-smooth. The saltation matrices are not each others inverse, $\underline{S}_{1a} \neq \underline{S}_{1b}^{-1}$ and $\underline{S}_{2a} \neq \underline{S}_{2b}^{-1}$. According to Section 6.3 we now have all the ingredients for the existence of a discontinuous bifurcation.

The response diagram of the trilinear system is shown in Figure 6.12 for varying forcing frequencies with the amplitude A of x on the vertical axis. Stable branches are indicated by solid lines and unstable branches by dashed-dotted lines. The parameter values are given in Appendix C.3.

There is no contact with the support for amplitudes smaller than x_c and the response curve is just the linear harmonic peak. For amplitudes above x_c there will be contact with the support, which will cause a hardening behaviour of the response curve. The resonance peak of the response curve bends to the right like the Duffing system with a hardening spring. The amplitude becomes equal to x_c twice at

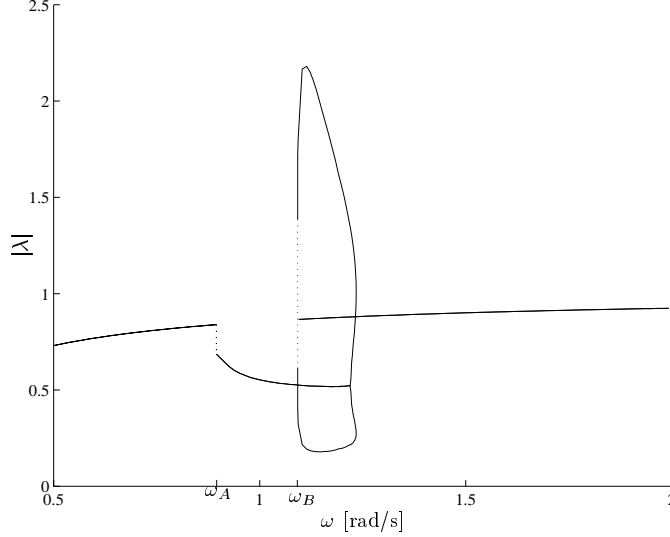


Figure 6.13: Floquet multipliers.

$\omega = \omega_A$ and $\omega = \omega_B$, on both sides of the peak, and corners of the response curve can be seen at these points. The orbit touches the corners of Σ_1 and Σ_2 for $A = x_c$, like solution II in Figure 6.8. The Floquet multipliers can therefore jump at those points. The magnitude of the Floquet multipliers is shown in Figure 6.13. The two Floquet multipliers are complex conjugate for $A < x_c$ (and therefore have the same magnitude). The pair of Floquet multipliers jump at $\omega = \omega_A$ but do not jump through the unit circle. From the numerical calculations depicted in Figure 6.12 it follows that no bifurcation exist (in the sense of Definition 5.1) at $\omega = \omega_A$. However, at $\omega = \omega_B$ the complex pair jumps to two distinct real multipliers, one with a magnitude bigger than one. One of those Floquet multipliers therefore jumps through the unit circle. A bifurcation is observed in Figure 6.12 at $\omega = \omega_B$ (one periodic solution exists for $\omega < \omega_B$ and three periodic solutions co-exist for $\omega > \omega_B$). We presume that this bifurcation is caused by the jump of the Floquet multiplier through the unit circle. The path of the Floquet multipliers on the jump is obtained by the generalized fundamental solution matrix (6.13). One Floquet multiplier crosses +1. The observed bifurcation resembles a continuous fold bifurcation of a smooth system. The bifurcation at $\omega = \omega_B$ at which the Floquet multiplier jumps through +1 is therefore called a *discontinuous fold bifurcation*.

Damping of the support is essential for the existence of this discontinuous fold bifurcation. For $c_f = 0$, all saltation matrices would be equal to the identity matrix and the corner between Σ_{1a} and Σ_{1b} would disappear (and also between Σ_{2a} and Σ_{2b}); therefore no discontinuous bifurcation could take place and the fold bifurcation would be continuous (see also Example 3.5). The model of Natsiavas [Natsiavas, 1989; Natsiavas and Gonzalez, 1992] did not contain a *discontinuous* fold bifurcation because the transitions were modeled such that $\underline{S}_{1a} = \underline{S}_{1b}^{-1}$ and $\underline{S}_{2a} = \underline{S}_{2b}^{-1}$.

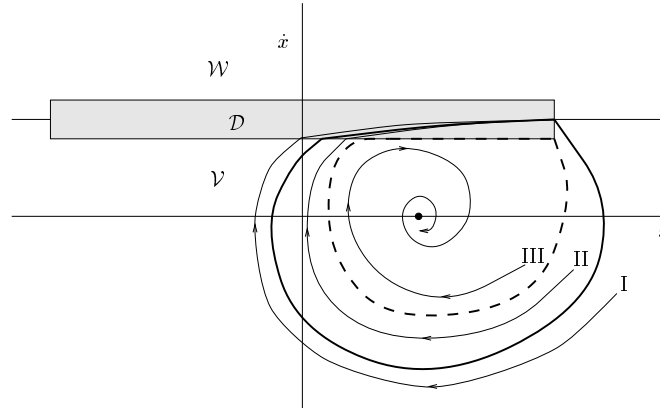


Figure 6.14: Phase plane of the stick-slip system.

6.7 Infinitely Unstable Periodic Solutions

In the preceding section we studied the discontinuous fold bifurcation, where a Floquet multiplier jumped over the unit circle, through $+1$, to a finite value. In this section we will study a discontinuous fold bifurcation where the Floquet multiplier jumps to infinity (crossing $+1$). This results in periodic solutions with a Floquet multiplier at infinity, which we will call *infinitely unstable periodic solutions*.

We consider again the stick-slip system of Section 3.4 depicted in Figure 3.4, but now for positive damping $c > 0$. The equilibrium solution of system (3.33) is given by

$$\mathbf{x}_{eq} = \begin{bmatrix} \frac{F_{slip}}{k} \\ 0 \end{bmatrix} \quad (6.23)$$

and is stable for positive damping ($c > 0$).

The model also exhibits stable periodic stick-slip oscillations. In Section 3.4 it was shown that the saltation matrix for the transition from slip to stick is given by (Equation (3.41))

$$\underline{\mathbf{S}}_{\alpha} = \begin{bmatrix} 1 & 0 \\ 0 & 0 \end{bmatrix},$$

which is singular. The fundamental solution matrix will therefore also be singular. The periodic solution has two Floquet multipliers, of which one is always equal to one as the system is autonomous. The singularity of the fundamental solution matrix implies that the remaining Floquet multiplier has to be equal to zero, independent of any system parameter. The Floquet multipliers of the stable periodic solution of this system are therefore $\lambda_1^{\text{stable}} = 1$ and $\lambda_2^{\text{stable}} = 0$.

The stable periodic solution is sketched in the phase plane in Figure 6.14 (bold line). The equilibrium position is also stable and indicated by a dot. The space \mathcal{D} is enlarged in Figure 6.14 to make it visible but is infinitely thin in theory and is

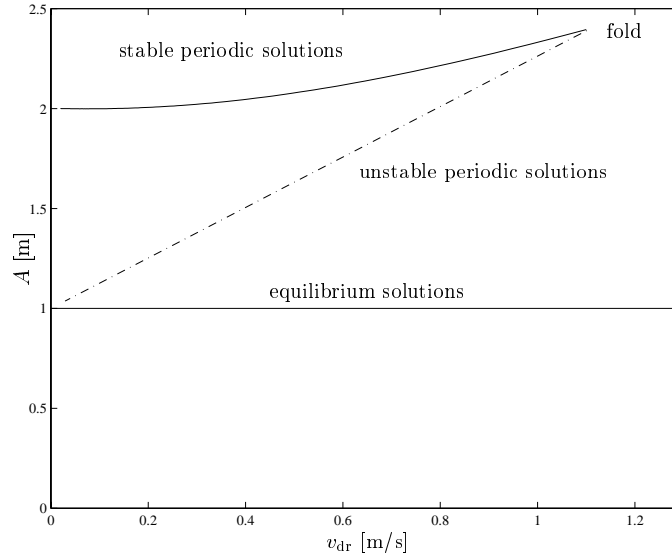


Figure 6.15: Bifurcation diagram of the stick-slip system.

taken very thin in numerical calculations. We assume that the thickness of \mathcal{D} in the numerical calculations is small enough to approximate the qualitative behaviour of the theoretical infinitely thin space \mathcal{D} to a sufficient extent.

A solution outside the stable periodic solution, like solution I in Figure 6.14, will spiral inwards to the stable periodic solution and reach the stick-phase \mathcal{D} . The stick-phase will bring the solution exactly on the stable periodic solution as it is infinitely small. Every point in \mathcal{D} is therefore part of the basin of attraction of the stable periodic solution.

Solution II starts inside the stable periodic solution, spirals around the equilibrium position and hits \mathcal{D} whereupon it is on the stable periodic solution. But a solution inside the stable periodic solution might also spiral around the equilibrium position and not reach the stick phase \mathcal{D} (solution III). It will then be attracted to the equilibrium position.

A solution inside the stable periodic solution can therefore spiral outwards to the stable periodic solution, like solution II, or inwards to the equilibrium position (solution III). Consequently, there must exist a boundary of attraction between the two attracting limit sets. This boundary is the unstable periodic solution sketched by a dashed line in Figure 6.14. The boundary of attraction is partly along the border between \mathcal{D} and \mathcal{V} because solutions in \mathcal{D} will attract to the stable periodic solution and just outside \mathcal{D} to the equilibrium position. The unstable periodic solution is therefore defined by the solution in \mathcal{V} which hits the border of \mathcal{D} tangentially and by a part along the border of \mathcal{D} and \mathcal{V} . The part of the unstable periodic solution along the border of \mathcal{D} is therefore a sliding mode along a discontinuity as discussed in Chapter 2. The solution on either side of the sliding mode is repulsing from it. It is therefore a repulsion sliding mode. The solution starting from a point on a repulsion

sliding mode is not unique as was discussed in Chapter 2. Non-uniqueness causes one Floquet multiplier to be at infinity because a solution may drift away from the periodic solution without any initial disturbance from the periodic solution. The unstable periodic solution is therefore infinitely unstable. As the periodic solution is infinitely unstable, it is not possible to calculate it in forward time. However, calculation of the periodic solution in backward time is possible. The vector field in backward time is identical to the one in forward time but opposite in direction. The repulsion sliding mode in forward time will turn into an attraction sliding mode in backward time. The solution starting from a point on the unstable periodic solution will move counter-clockwise in the phase-plane in backward time and hit the border of \mathcal{D} . It will slide along the border of \mathcal{D} until the vector field in \mathcal{V} becomes parallel to \mathcal{D} , and will then bend off in \mathcal{V} . Any solution starting from a point close to that starting point will hit \mathcal{D} and leave \mathcal{D} at exactly the same point. Information about where the solution came from is therefore lost through the attracting sliding mode. In other words: the saltation matrix of the transition from \mathcal{V} to \mathcal{D} during backward time is singular. The fundamental solution matrix will therefore be singular in backward time because it contains an attracting sliding mode. The Floquet multipliers of the unstable periodic solution in backward time are therefore 1 and 0. The Floquet multipliers in forward time must be their reciprocal values. The second Floquet multiplier is therefore infinity, $\lambda_1^{\text{unstable}} = 1$ and $\lambda_2^{\text{unstable}} = \infty$, which of course must hold for an infinitely unstable periodic solution.

The bifurcation diagram of the system is shown in Figure 6.15 with the velocity of the belt v_{dr} as parameter and the amplitude A of x on the vertical axis. The equilibrium branch and the stable and unstable periodic branches are depicted. The unstable branch is of course located between the stable periodic branch and the equilibrium branch as can be inferred from Figure 6.14. The stable and unstable periodic branches are connected through a fold bifurcation point. The second Floquet multiplier jumps from $\lambda = 0$ to $\lambda = \infty$ at the bifurcation point, and therefore through $+1$ on the unit circle. We will call this bifurcation therefore a discontinuous fold bifurcation. The fold bifurcation occurs when v_{dr} is such that a solution which leaves the stick phase \mathcal{D} , transverses \mathcal{V} , and hits \mathcal{D} tangentially (like the unstable periodic solution). The stable and unstable periodic solutions coincide at this point. Note that there exists again a corner of hyper-surfaces at this point as in Figure 6.8. The saltation matrices are not each others inverse, $\underline{S}_\alpha \underline{S}_\beta \neq \underline{I}$, which is essential for the existence of a discontinuous bifurcation. Moreover \underline{S}_α is singular.

Three Poincaré maps are depicted in Figure 6.16 for different values of v_{dr} ; before, at and after the bifurcation point. The Poincaré section is chosen as $\Omega = \{\underline{x} \in \mathbb{R}^2 \mid x \geq F_{\text{slip}}/k, \dot{x} = 0\}$. The three intersection points of the Poincaré map with the diagonal in Figure 6.16a indicate the equilibrium position at $x = 1$ and the unstable and stable periodic solutions. The slope of the Poincaré map at the intersection points of the periodic solutions is equal to the second Floquet multiplier, which is consistent with $\lambda_2^{\text{stable}} = 0$ and $\lambda_2^{\text{unstable}} = \infty$. The Poincaré map of Figure 6.16b touches the diagonal with its tip similar to the Poincaré map of the discontinuous fold bifurcation in Figure 6.4. The stable and unstable periodic solutions disappeared in Figure 6.16c as is shown in Figure 6.15.

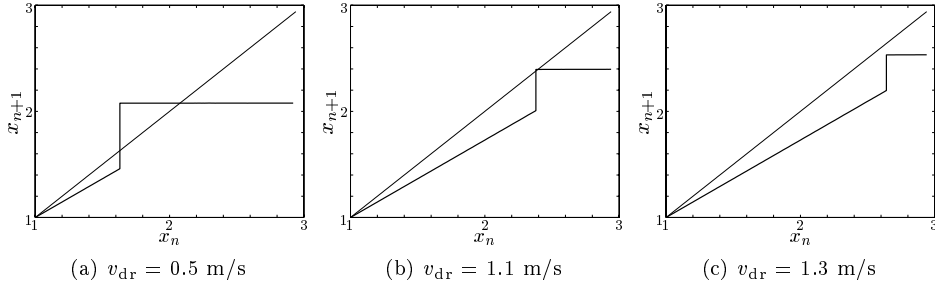


Figure 6.16: Poincaré maps of the stick-slip system.

A similar model was studied in Van de Vrande et al. [1999] with a very accurately smoothed friction curve. The stable branch was followed for increasing v_{dr} but the fold bifurcation could not be rounded to proceed on the unstable branch. As the unstable branch is infinitely unstable for the discontinuous model, it is extremely unstable for the smoothed approximating model. The branch can therefore not be followed numerically in forward time if the friction model is approximated accurately.

The stable branch in Figure 6.15 was followed in forward time up to the bifurcation point. The path-following algorithm was stopped and restarted in backward time to follow the unstable branch.

This section showed that infinitely unstable periodic solutions come into being through repulsion sliding modes. Filippov theory turns out to be essential for the understanding of infinitely unstable periodic solutions. Infinitely unstable periodic solutions and their branches can be found through backward integration. Smoothing of a discontinuous model is not sufficient to obtain a complete bifurcation diagram of a discontinuous system as infinitely unstable branches cannot be found.

6.8 Symmetry-Breaking Bifurcation; Forced Vibration with Dry Friction

The second type of bifurcation of a periodic solution which will be studied is the *symmetry-breaking bifurcation*. Suppose a non-autonomous time-periodic system has the following symmetry property (also called *inversion symmetry*)

$$\tilde{f}(t, \underline{x}) = -\tilde{f}\left(t + \frac{1}{2}T, -\underline{x}\right), \quad (6.24)$$

where T is the period. If $\underline{x}_1(t) = \underline{x}(t)$ is a periodic solution of the system, then also $\underline{x}_2(t) = -\underline{x}(t + \frac{1}{2}T)$ must be a periodic solution. The periodic solution is called *symmetric* if $\underline{x}_1(t) = \underline{x}_2(t)$ and *asymmetric* if $\underline{x}_1(t) \neq \underline{x}_2(t)$. When a Floquet multiplier passes through the unit circle at $+1$, the associated bifurcation depends on the nature of the periodic solution prior to the bifurcation. Suppose that the periodic solution prior to the bifurcation is a symmetric periodic solution. Then, if

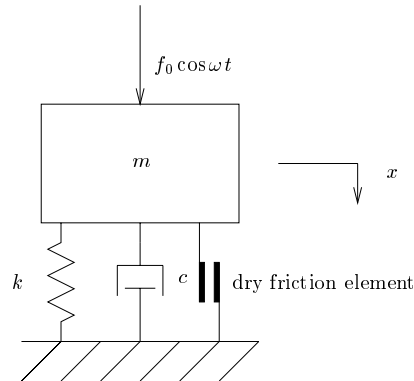


Figure 6.17: Forced vibration with dry friction.

the bifurcation breaks the symmetry of the periodic solution, it is called a symmetry-breaking bifurcation [Nayfeh and Balachandran, 1995].

We will show in this section that the continuous symmetry-breaking bifurcation has a discontinuous counterpart. Consider the forced vibration of the system depicted in Figure 6.17. The mass is supported by a spring, damper and dry friction element. The parameter values are given in Appendix C.4. The equation of motion reads as

$$m\ddot{x} + c\dot{x} + kx = f_{\text{fric}}(\dot{x}, x) + f_0 \cos \omega t \quad (6.25)$$

with the friction model

$$f_{\text{fric}}(\dot{x}, x) = \begin{cases} -F_{\text{slip}} \operatorname{sgn}(\dot{x}), & \dot{x} \neq 0 \quad \text{slip} \\ \min(|F_{\text{ex}}|, F_{\text{stick}}) \operatorname{sgn}(F_{\text{ex}}), & \dot{x} = 0 \quad \text{stick} \end{cases} \quad (6.26)$$

where

$$F_{\text{ex}} = kx - f_0 \cos \omega t.$$

This friction model is identical to type (c) in Figure 2.5. The system (6.25) has been analyzed numerically with the switch-model as in Sections 2.4 and 3.4 and in [Leine et al., 1998; Leine and Van Campen, 2000; Leine et al., 2000]. It can be verified that the system (6.25) has the symmetry property (6.24).

The bifurcation diagram of this system is depicted in Figure 6.18 and shows two branches with periodic solutions. Branch I is unstable between the points A and B. Branch II bifurcates from branch I at point A and B. For large amplitudes, the influence of the dry friction element will be much less than the linear elements. Near the resonance frequency, $\omega_{\text{res}} = \sqrt{k/m} = 1$ [rad/s], branch I will therefore be close to the harmonic resonance peak of a linear one-degree-of-freedom system. We first consider periodic solutions on branch I at the right side of point B. The velocity of the mass \dot{x} becomes zero at two instances of time during one oscillation (as do linear harmonic oscillations). The mass does not come to a stop during an interval of time. In other words: the oscillation contains no *stick event* in which the periodic solution passes the stick phase. The number of stick events on a part of a branch is

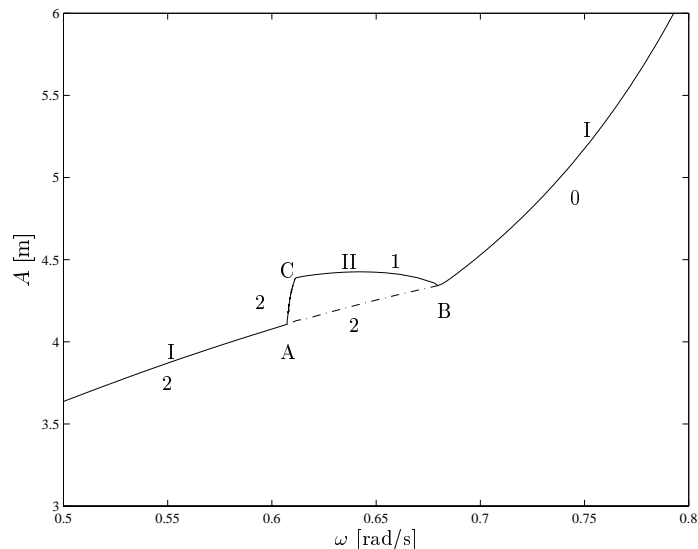


Figure 6.18: Bifurcation diagram of forced vibration with dry friction.

indicated by numbers (0,1,2) in Figure 6.18. The Floquet multipliers on this part of branch I are complex (Figure 6.19). The system therefore behaves ‘almost linearly’. All the periodic solutions on branch I are symmetric.

If this part of branch I with ‘almost linear’ symmetric periodic solutions is followed to frequencies below ω_{res} , then bifurcation point B is met. At bifurcation point B, the symmetric branch I becomes unstable and a second branch II with asymmetric periodic solutions is created. In fact, on the bifurcated asymmetric branch two distinct periodic solutions $x_1(t) \neq x_2(t)$ exist, which have the same amplitude. The periodic solutions on branch I left of point B contain two stick events per cycle. The periodic solutions on branch II between the points B and C contain one stick event, and they contain two stick events between the points A and C. The existence of a stick event during the oscillation causes one Floquet multiplier to be equal to zero. Points B and C are points where stick events are created/destroyed, which cause the Floquet multipliers to be set-valued (they jump). A set-valued Floquet multiplier at B passes +1. The bifurcation at point B resembles a continuous symmetry-breaking bifurcation and is therefore called a *discontinuous symmetry-breaking bifurcation*. We presume that a discontinuous symmetry-breaking bifurcation is always associated with a jump of a Floquet multiplier through +1.

Branch II encounters a jump of the Floquet multipliers at point C but the set-valued Floquet multipliers remain within the unit circle. We observe that point C is not a bifurcation point but the path of branch II is non-smooth at C due to the jump of the Floquet multipliers.

The asymmetric branch meets the symmetric branch again at point A. The Floquet multipliers pass +1 without a jump and point A is therefore a continuous symmetry-breaking bifurcation. No new stick events are created at point A because

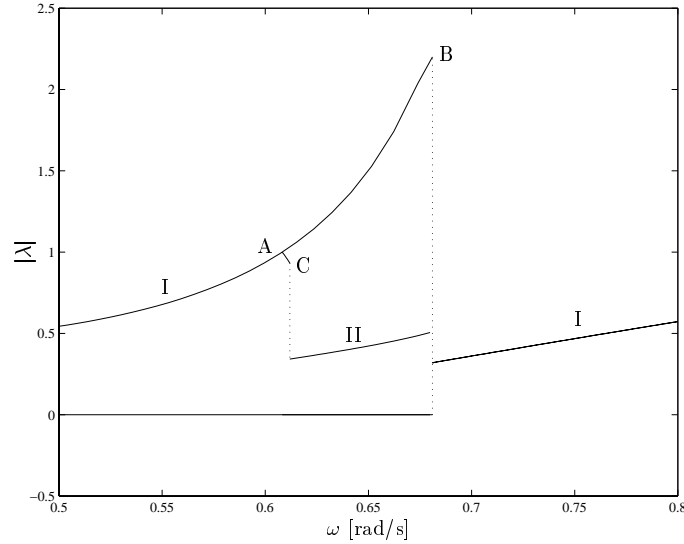


Figure 6.19: Floquet multipliers.

all branches have two stick events per cycle. Remark that the branch I behaves smooth at bifurcation A and non-smooth at bifurcation B.

6.9 Flip Bifurcation; Forced Stick-slip System

Another type of bifurcation of a periodic solution is the *flip bifurcation* which is characterized by a Floquet multiplier which is passing through the unit circle at -1 . A new type of discontinuous bifurcation will be studied in this section which occurs in a forced stick-slip system taken from Yoshitake and Sueoka [2000]. The discontinuous bifurcation is a combination of a continuous fold and flip bifurcation. The system is identical to the stick-slip system of Section 3.4 (Figure 3.4) without linear damping and a different friction model. Additionally, the mass is forced periodically. The parameter values are given in Appendix C.5. The equation of motion reads as

$$m\ddot{x} + kx = f_{\text{fric}}(v_{\text{rel}}, x) + f_0 \cos \omega t \quad (6.27)$$

with $v_{\text{rel}} = \dot{x} - v_{\text{dr}}$. The friction model reads as

$$f_{\text{fric}}(v_{\text{rel}}, x) = \begin{cases} -\alpha_0 \operatorname{sgn}(v_{\text{rel}}) + \alpha_1 v_{\text{rel}} - \alpha_3 v_{\text{rel}}^3, & v_{\text{rel}} \neq 0 \quad \text{slip} \\ \min(|F_{\text{ex}}|, \alpha_0) \operatorname{sgn}(F_{\text{ex}}), & v_{\text{rel}} = 0 \quad \text{stick} \end{cases} \quad (6.28)$$

where

$$F_{\text{ex}} = kx - f_0 \cos \omega t.$$

This friction model is identical to type (b) in Figure 2.5. This model has been analyzed numerically with the switch-model as in Sections 2.4 and 3.4 and in [Leine

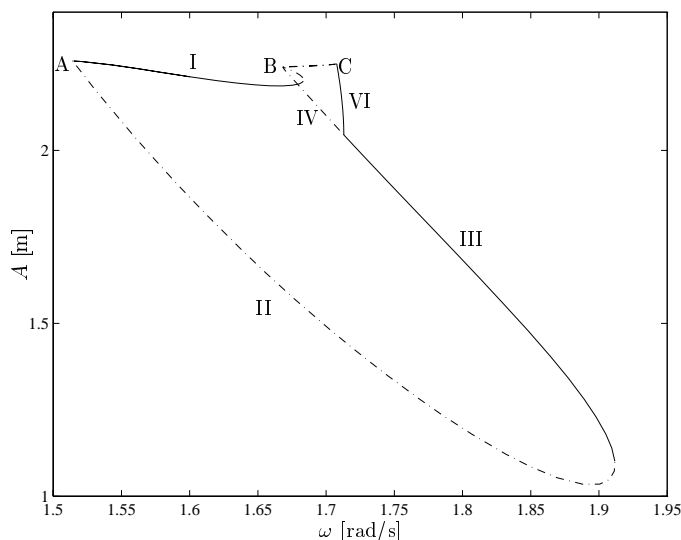


Figure 6.20: Bifurcation diagram of the forced stick-slip system.

et al., 1998; Leine and Van Campen, 2000; Leine et al., 2000], which resulted in Figures 6.20 to 6.23.

The resonance curve of this model has been published by Yoshitake and Sueoka [2000] for $0.2 \leq \omega \leq 4$. The $1/2$ -subharmonic closed resonance curve is of special interest and depicted in Figure 6.20 and a part is enlarged in Figure 6.21. The real part of the largest Floquet multiplier (in magnitude) is depicted in Figure 6.22. All Floquet multipliers are real except on a part of branch III. Stable branches of periodic solutions are denoted by solid lines and unstable branches by dashed-dotted lines. Jumps of the Floquet multiplier (set-valued Floquet multipliers) are denoted by dotted lines.

The $1/2$ -subharmonic closed resonance curve possesses several discontinuous and continuous bifurcations. Branches I-V are period-2 solutions, branches VI and VII are period-4, and branch VIII is period-8. A discontinuous fold bifurcation at point A connects the stable branch I to the unstable branch II and its largest Floquet multiplier jumps through $+1$ (similar to the discontinuous fold bifurcation in Section 6.6). The stable branch I folds smoothly into branch V and stability is exchanged. At point B, the unstable branch V is folded into the unstable branch IV *without exchanging stability*. The set-valued Floquet multiplier at point B crosses the unit circle twice as it jumps from $\lambda > 1$ on branch V to $\lambda < -1$ on branch IV, thereby crossing the points $+1$ and -1 on the unit circle (Figure 6.2). In Section 6.3 we presumed that such a ‘multiple-crossing’ jump of a Floquet multiplier causes a bifurcation which is a combination of a fold and a flip bifurcation. The fold action of the bifurcation is clear as the branch is folded. A conventional continuous flip bifurcation causes a period-doubled branch to bifurcate from the main branch. Branches IV and V are period-2 and branch VII emanates indeed from point B and is period-4.

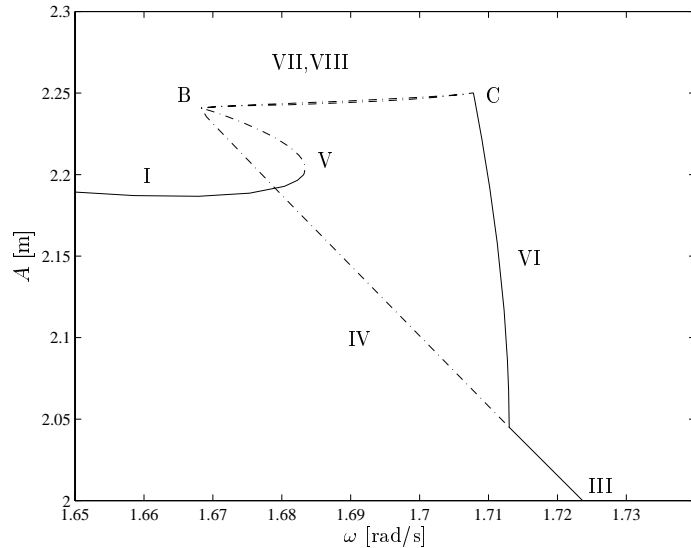


Figure 6.21: Bifurcation diagram of the forced stick-slip system.

The bifurcation at point B therefore also shows a flip action. But branch VIII also bifurcates from B and is period-8. This is not in conformity with the bifurcation theory for smooth systems.

A better understanding of the phenomenon can be obtained by looking at the Poincaré map depicted in Figure 6.23. Remark that the map is indeed similar to the *tent map* of Figure 6.6. In fact, the ‘full’ Poincaré map is a mapping from \mathbb{R}^2 to \mathbb{R}^2 which cannot easily be visualized. Instead, a section of this map is depicted with the displacement $x_n = x(nT)$, where $T = 2\pi/\omega$, on the abscissa and the displacement after two periods x_{n+2} on the ordinate (because we study period-2 oscillations). The velocity \dot{x}_n is iterated with a Newton-Raphson method to be equal to \dot{x}_{n+2} . Fixed points of this reduced map are periodic solutions with period-2 (or period-1) as holds $x(nT) = x((n+2)T)$ and $\dot{x}(nT) = \dot{x}((n+2)T)$. The map is calculated for $\omega = 1.67587$ [rad/s] which is just to the right of the bifurcation point B. It can be seen that there are three fixed points which corresponds to the periodic solutions at the branches I, IV and V. The map exposes a peak between the fixed points IV and V. Although this is a section of a higher-dimensional map, the ‘full’ map will also be similar to the tent map.

The *tent map* has been studied thoroughly in literature [Glendinning, 1994; Martelli, 1992; Rasband, 1990]. The tent map is the non-smooth piece-wise linear version of the logistic map (both non-invertible). The logistic map is smooth and leads to a cascade of period-doublings which is a well known route to chaos. The distance between two succeeding period-doublings is finite for the logistic map. For the tent map however, infinitely many period-doublings occur at the same bifurcation value which leads directly to chaos.

The results on the tent map could explain the behaviour at the bifurcation

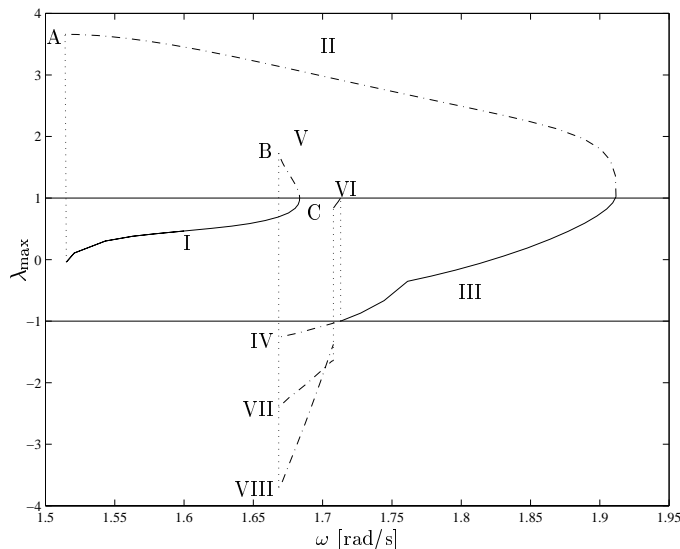
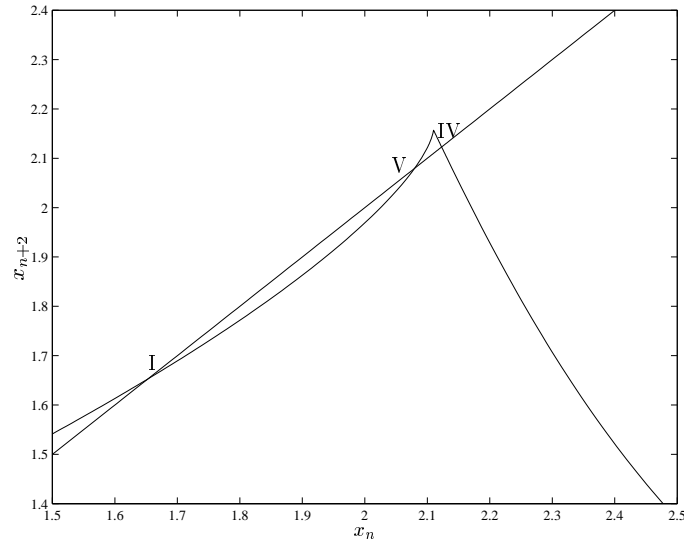


Figure 6.22: Floquet multiplier.

point B. The similarity between the tent map and the Poincaré map suggests that there are infinitely many period-doublings. This would result in an infinite number of other unstable branches starting from point B (period-8, 16, 32...). A period-8 branch (VIII) starting from point B was indeed found beside the ‘expected’ period-4 branch (VII). The infinitely many other branches become more unstable as their period-doubling number increases and the branches become closely located to each other which makes it difficult to find them numerically. These facts agree with the analytical results on the tent map.

How do we classify the discontinuous bifurcation at point B? The discontinuous bifurcation is not a direct counterpart of a continuous bifurcation. In the sequel we will call this bifurcation a discontinuous fold–flip bifurcation because it resembles both bifurcations. The name is not completely satisfactory because branch VIII and the possibly infinitely many branches that are created at the discontinuous bifurcation point are resembled neither by a continuous fold nor by a continuous flip bifurcation.

The branches VII and VIII connect bifurcation point B with bifurcation point C. The Floquet multiplier at point C jumps from inside the unit circle to outside the unit circle through -1 . We call bifurcation point C a discontinuous flip bifurcation because it resembles a continuous flip bifurcation. One question has not been answered: where do those infinitely many branches starting from point B lead to? We can suggest that the infinitely many other unstable branches will probably lead to bifurcation point C. But the Floquet multiplier at C does not seem to pass both $+1$ and -1 , but only -1 . The Poincaré map at point C will look like Figure 6.5b and will not be similar to the tent map. It is therefore not clear whether the infinitely many other unstable branches will be connected to bifurcation point C.

Figure 6.23: Poincaré map ($\omega = 1.67587$ [rad/s]).

As follows from the tent map, the system will behave chaotically for ω -values just to the right of point B.

Yoshitake and Sueoka [2000] studied the model carefully and showed that the underlying Poincaré map is similar to the tent map but did not find the branches VII and VIII (or higher period-doublings). Discontinuous fold and flip bifurcations, where the Floquet multipliers jump at the bifurcation point, were found by Yoshitake and Sueoka. However, they did not show how the Floquet multipliers jump which can be explained from saltation matrices and generalized fundamental solution matrices as elaborated in this thesis. They classified the region between B and C as chaotic and mentioned the similarity with the bifurcations found by Nusse and York [1992]. Nusse and York studied discrete dynamical systems with a tent map and denoted the discontinuous bifurcations they found by ‘border-collision bifurcations’. Their numerical calculations only showed stable solutions. They did not give a method to classify discontinuous bifurcations but conclude their paper with the remark that this is still an open question. In this thesis it is presumed that the discontinuous bifurcations can at least be partly classified by investigating the generalized Jacobian, the generalized fundamental solution matrix or the generalized derivative of the Poincaré map (Section 4.1).

A discontinuous fold-flip bifurcation was discussed in this section and it was shown that it is related to the one-dimensional tent map. It is suggested that infinitely many branches meet at the same bifurcation point and these branches are all period-doublings of the branch under bifurcation.

6.10 Discussion and Conclusions

In Section 6.3 some fundamental questions about discontinuous bifurcations of periodic solutions were raised. With the preceding examples in mind, we will try to answer these questions one by one.

1. *Do discontinuous bifurcations (in the sense of Definition 5.1) exist of periodic solutions of Filippov systems?* The conclusion that a point on a branch is a (continuous or discontinuous) bifurcation point (in the sense of Definition 5.1) was in the preceding examples always drawn from observation of the bifurcation diagram. We call a bifurcation point a discontinuous bifurcation point if it exposes a jump of the Floquet multipliers over the unit circle. Sections 6.6 to 6.9 show a number of discontinuous systems exposing bifurcations of periodic solutions in the sense of Definition 5.1. Some of the bifurcations are accompanied by a Floquet multiplier which passes continuously through the unit circle. The branch of periodic solutions at such bifurcation points remains smooth. We classify those bifurcations as continuous bifurcations. Other bifurcation points are accompanied by a Floquet multiplier which crosses the unit circle discontinuously. The branch on such bifurcation points is continuous but non-smooth. We classify those bifurcations as discontinuous bifurcations of periodic solutions because of the discontinuous behaviour of the Floquet multipliers.
2. *Does a discontinuous bifurcation exist caused by the scenario depicted in Figure 6.8?* Figure 6.12 shows a bifurcation diagram in which there are two points where a periodic solution touches the tip of a non-smooth hyper-surface as depicted in Figure 6.8. The point at $\omega = \omega_A$ is not a bifurcation point and is accompanied by a jump of the Floquet multipliers within the unit circle. The point at $\omega = \omega_B$ is a fold bifurcation point and is accompanied by a jump of the Floquet multipliers through unit circle at +1. We presume that a periodic solution which touches the tip of a non-smooth hyper-surface can only undergo a discontinuous bifurcation if the Floquet multiplier(s) jump through the unit circle. Remark that the stable periodic solution depicted in Figure 6.14 undergoes a discontinuous fold bifurcation depicted in Figure 6.15 if the periodic solution touches the lower-right corner of the stick region \mathcal{D} (Figure 6.14). The discontinuous bifurcation is accompanied by a jump through the unit circle of the second Floquet multiplier.
3. *Does a jump of a Floquet multiplier through the unit circle under the influence of a parameter lead to a bifurcation of a periodic solution?* All the examples show that a discontinuous bifurcation is always accompanied by a jump of Floquet multiplier(s) through the unit circle. Points at which the Floquet multipliers jumped but remained within the unit circle never occurred to be a bifurcation point. We do not have evidence that a jump of a Floquet multiplier should always be accompanied by a bifurcation. We presume that a jump of a Floquet multiplier through the unit circle is a necessary condition for a bifurcation of a periodic solution (in the sense of Definition 5.1).

4. *Can we classify the bifurcation by inspecting the point(s) where the path of the set-valued Floquet multiplier(s) crosses the unit circle?* Sections 6.6 and 6.7 show bifurcations which behave qualitatively like fold bifurcations. They are called discontinuous fold bifurcations because they resemble a conventional fold bifurcation and because of the discontinuous behaviour of the Floquet multipliers. The classification of those bifurcations as fold bifurcations seems consistent with the fact that they are accompanied by a jump of a Floquet multiplier through $+1$. Bifurcation point B in Figure 6.18 is classified as a discontinuous symmetry-breaking bifurcation because it resembles the conventional symmetry-breaking bifurcation. The classification as symmetry-breaking bifurcation seems consistent with the fact that the bifurcation is accompanied by a jump of a Floquet multiplier through $+1$. Along the same reasoning, bifurcation points A and C in Figure 6.20 can be classified as discontinuous fold and flip bifurcations. Bifurcation point B, however, exposes a jump through the unit circle at -1 and $+1$. The discontinuous bifurcation is not a direct counterpart of a continuous bifurcation. We will classify this bifurcation as a discontinuous fold–flip bifurcation because it resembles both bifurcations. The classification is not completely satisfactory because branch VIII and the possibly infinitely many branches that are created at the discontinuous bifurcation point resemble neither a continuous fold nor a continuous flip bifurcation. We conclude that a classification, based on the points where the set-valued Floquet multiplier crosses the unit circle, is only *partly* possible.
5. *Do discontinuous bifurcations of periodic solutions exist that do not have a continuous counterpart? In other words: do discontinuous bifurcations exist that behave qualitatively different from any continuous bifurcation?* Clearly, bifurcation point B in Figure 6.20 is a bifurcation point that does not have a direct continuous counterpart. This bifurcation behaves qualitatively different from any continuous bifurcation.
6. *Can Definitions 5.1 and 5.3 be inconsistent when they are applied to periodic solutions of Filippov systems?* Definition 5.1 is based on a change of the number of fixed points and periodic solutions at a critical value of a parameter of the system. Definition 5.3 is based on a topological change of the phase portrait under variation of a parameter. These two definitions can be inconsistent. If we compare a periodic solution I which is not along an attraction sliding mode with a periodic solution II which is partly along an attraction sliding mode, then we can map every trajectory in the phase plane of periodic solution I to a trajectory in the phase plane of periodic solution II. However, the inverse map (mapping trajectories from II to I) does not exist. Consequently, there is no homeomorphism between the two phase planes. A periodic solution with an attraction sliding mode is therefore topologically different from a periodic solution without a sliding mode. Consider point C in Figure 6.18. The point is not a bifurcation point according to Definition 5.1. The number of stick intervals change at this point from 2 to 1. Each stick interval is an attraction sliding mode. Consequently, point C is a bifurcation according to Definition 5.3. Di Bernardo et al. [1999a] introduce the term ‘sliding bifurcation’ for a change

of a periodic solution with a sliding mode to a periodic solution without a sliding mode under influence of a parameter. The term ‘multi-sliding bifurcation’ is introduced for a change in the number of sliding modes. Point C in Figure 6.18 would according to this definition be a multi-sliding bifurcation. Although not explicitly stated in Di Bernardo et al. [1999a], it seems that a ‘sliding bifurcation’ is a bifurcation in the sense of Definition 5.3.

The different definitions for a bifurcation can lead to confusion when they are applied to discontinuous systems. This urges for a consensus about what is to be understood by ‘bifurcation’. Definition 5.1 seems to be a good candidate as it is very clear from the bifurcation diagram whether or not a point on a branch is a bifurcation point or not.

In the previous chapter we formulated Conjectures 5.1 and 5.2 about existence and classification of bifurcations of fixed points of non-smooth continuous systems. From the preceding discussion we formulate similar conjectures for bifurcations of periodic solutions of discontinuous systems of Filippov-type.

Conjecture 6.1

A necessary condition for the existence of a discontinuous bifurcation in the sense of Definition 5.1 of a periodic solution of a discontinuous system is a ‘jump’ of a Floquet multiplier (or a pair of them) through the unit circle, i.e. the path of the set-valued Floquet multiplier(s) passes through the unit circle.

Conjecture 6.2

A discontinuous bifurcation of a periodic solution of a discontinuous system can be (partly) classified by inspecting the point(s) where the path of the set-valued Floquet multipliers (or a pair of them) passes through the unit circle.

Conjecture 6.2 presumes that we can classify bifurcation point B in Figure 6.20 as a fold–flip bifurcation but we should keep in mind that the bifurcation point shows behaviour not covered by a conventional fold or flip bifurcation separately.

Remark that Conjectures 6.1 and 6.2 are related with Conjectures 5.1 and 5.2 through the Poincaré map. We close this chapter by stating that the results on periodic solutions of discontinuous systems seem to be consistent with the results on fixed points of non-smooth continuous systems.

Chapter 7

Concluding Remarks

*‘We are to admit no more causes of natural things
than such as are both true and sufficient to explain
their appearances’*

ISAAC NEWTON,
Principia (1687), Book III, Rule I.

This chapter gives an overview of the thesis indicating the contributions. The thesis is closed with recommendations for further research.

7.1 Overview and Summary of Contributions

In this section a short overview is given of the thesis, whereas the contributions are stated.

In Chapter 2 the theory of Filippov was reviewed, giving a solution concept for differential equations with a discontinuous right-hand side. Existence and uniqueness problems were addressed. A numerical technique was presented for the integration of differential inclusions. Special attention was given to the relation between differential inclusions and friction models. A ‘switch model’ was developed [Leine et al., 1998, 2000], being an extended version of the Karnopp model, to allow for an efficient solution of dry friction problems. The switch model has been used throughout the thesis for problems involving dry friction.

Jumps in the time evolution of the fundamental solution matrix were discussed in Chapter 3. The theory of saltation matrices describing the jumps is due to Aizerman and Gantmakher [1958]. Saltation matrices were applied to systems with dry friction and discontinuous supports in the examples of Sections 3.4 and 3.5.

In Chapter 4, dealing with non-smooth analysis, the concept of linear approximation at the discontinuity was presented. It was shown in Section 4.2 that the concept of linear approximation is closely related to the generalized derivative of

Clarke [Clarke et al., 1998]. The idea to apply the generalized derivative to the fundamental solution matrix is new.

Bifurcations of fixed points of non-smooth continuous systems were discussed in Chapter 5; these are called ‘discontinuous bifurcations’ in this thesis. Some results on bifurcations in smooth systems were reviewed and different definitions for bifurcations were discussed. In Section 5.2 the basic idea was presented as to how a discontinuous bifurcation of a fixed point originates. Also the new possibility of multiple-crossing bifurcations was explained. A number of examples (Sections 5.3 to 5.7) were developed to show different aspects of discontinuous bifurcations. A discontinuous counterpart for each continuous bifurcation was found. Also a multiple-crossing bifurcation was shown to exist (Section 5.7). The linear approximation of the Jacobian, as developed in Chapter 4, was applied to each of the investigated non-smooth systems. The usefulness of linear approximation became especially clear in Section 5.7. At the end of Chapter 5 a conjecture about the existence of discontinuous bifurcations of fixed points was formulated and an attempt to a partial classification of those bifurcations was made.

Chapter 6 was devoted to bifurcations of periodic solutions in discontinuous systems. The Poincaré map relates the concept of discontinuous bifurcations of fixed points to discontinuous bifurcations of periodic solutions. It was shown that discontinuous bifurcations of periodic solutions can occur if a periodic solution touches a non-smooth hyper-surface for a critical parameter value. This was illustrated by an example in Section 6.6 which showed a discontinuous fold bifurcation. This example extends the trilinear model of Natsiavas [Natsiavas, 1989; Natsiavas and Gonzalez, 1992] to a Filippov system.

An example of a stick-slip system (Section 6.7) showed that a Floquet multiplier can also jump to infinity. We call a periodic solution with a Floquet multiplier at infinity an infinitely unstable periodic solution. A discontinuous fold bifurcation connected in this example a stable branch to a branch with infinitely unstable periodic solutions. The infinitely unstable periodic solution can be understood by Filippov theory. Bifurcation to infinitely unstable periodic solutions led to complete failure of the classical smoothing method to investigate discontinuous systems. This example was developed after a discussion with B.L. van de Vrande who encountered numerical problems during path-following of a similar model with a very accurately smoothed friction curve [Van de Vrande et al., 1999].

In Section 6.8 the differences were illustrated between Definitions 5.1 and 5.3 for bifurcation of periodic solutions. The example in that section showed a discontinuous counterpart of a symmetry-breaking bifurcation. It is noticed that this example is original.

Recently, Yoshitake and Sueoka [2000] discovered a novel type of bifurcation of a periodic solution, characterized by a jump of a Floquet multiplier through the unit circle (which is called ‘discontinuous bifurcation’ in this thesis). Yoshitake and Sueoka also concluded that a jump of a Floquet multiplier from $\lambda < -1$ to $\lambda > 1$ can cause the Poincaré map to be similar to the tent map which leads to chaos. The example treated in Section 6.9 is due to Yoshitake and Sueoka. However, they did not find two branches emanating from a discontinuous flip bifurcation (the branches VII and VIII in Figure 6.21). Neither did they explain why the Floquet multipliers

jump and how we can calculate this jump by means of saltation matrices. The numerical results found by Yoshitake and Sueoka were reproduced, thereby applying the findings of Chapters 2 to 5 to this problem. By linear approximation of the fundamental solution matrix it could be shown that the jump from $\lambda < -1$ to $\lambda > 1$ is indeed through $\lambda = -1$ and $\lambda = +1$. The possibility of infinitely many branches was suggested.

In this thesis the following main contributions to the field of discontinuous systems of Filippov-type were made.

- It was explained how linear approximation and the generalized fundamental solution matrix determine the path of the jump of the eigenvalues. Filippov theory, generalized derivatives and Floquet theory were combined to understand bifurcations in discontinuous systems.
- Discontinuous bifurcations of periodic solutions were shown to occur when a periodic solution touches a non-smooth hyper-surface for a critical parameter value. Saltation matrices are therefore important for the understanding of discontinuous bifurcations.
- Some low-dimensional examples were studied, giving insight into discontinuous bifurcations. Discontinuous counterparts were found of conventional fold, symmetry-breaking and flip bifurcations. A discontinuous bifurcation without a direct continuous counterpart was also found. The discontinuous bifurcation found by Yoshitake and Sueoka [2000], exposing a jump of a Floquet multiplier from $\lambda < -1$ to $\lambda > 1$, was identified as a combined fold–flip bifurcation. The existence of a multiple-crossing bifurcation was demonstrated.
- The switch model was developed, being an extended version of the Karnopp model, for the description of systems with dry friction. The switch model proved not only to be valuable as a numerical tool but also for the theoretical understanding of periodic solutions in systems with dry friction.
- Infinitely unstable periodic solutions were shown to exist and explained by Filippov theory and the switch model. A path of infinitely unstable periodic solutions was followed with path-following techniques in reverse time. A discontinuous fold bifurcation was found at which a Floquet multiplier jumps from zero to infinity, crossing the unit circle through $+1$.

7.2 Recommendations

Many problems are still open for further research. This section gives recommendations and starting points for further research.

Terminology and Definitions

Different definitions exist for the term ‘bifurcation’ (Section 5.1). The different definitions for a bifurcation can lead to confusion when they are applied to discontinuous systems. This urges for a consensus about what is to be understood by

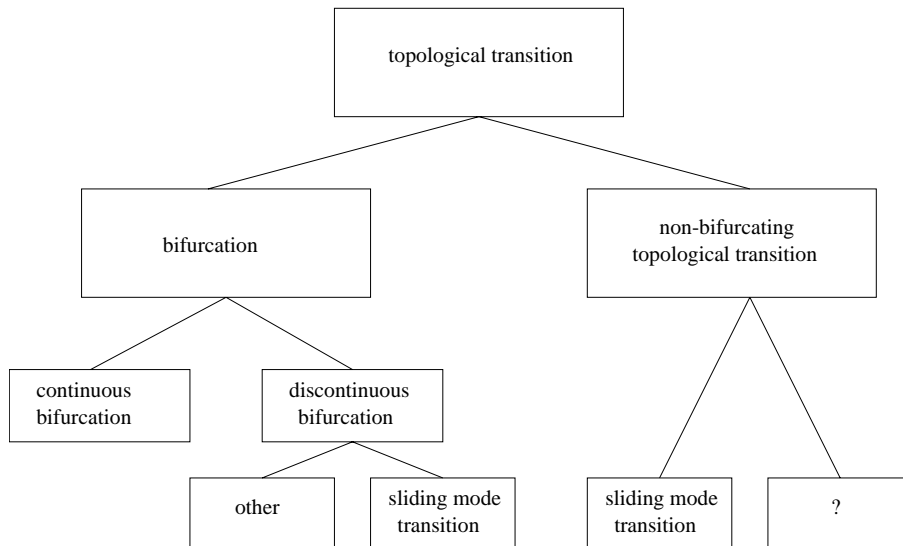


Figure 7.1: Topological transitions of periodic solutions.

‘bifurcation’. Definition 5.3, based on the topological (non-)equivalence of the phase portrait, defines also ‘sliding bifurcations’ [Di Bernardo et al., 1999a] as bifurcation. The word ‘bifurcation’ suggests that a branch bifurcates from another branch. A ‘sliding bifurcation’, however, does not imply branching behaviour or a turning point of the branch. The application of Definition 5.3 to discontinuous systems, as well as the term ‘sliding bifurcation’ seem therefore awkward. Definition 5.1, based on the number of fixed points and (quasi-)periodic solutions, seems to be a good candidate as it is very clear from the bifurcation diagram whether or not a point on a branch is a bifurcation point or not. The number of fixed points or (quasi-)periodic solutions changes at a bifurcation point (according to Definition 5.1), which can be inferred from the bifurcation diagram. This definition implies therefore branching behaviour or a turning point of the branch. In the context of non-smooth and discontinuous dynamical systems, Definition 5.1 as definition for bifurcation therefore seems preferably over other definitions.

A distinction needs to be made between a topological change of the phase portrait and a bifurcation. This may require some new terminology. We recommend to call a topological change of the phase portrait, a *topological transition* (instead of ‘bifurcation’). A *bifurcation* should be defined by Definition 5.1. Every bifurcation is a topological transition but not every topological transition is a bifurcation. Topological changes of a periodic solution with sliding mode to a periodic solution without sliding mode can be named *topological sliding mode transitions* (instead of ‘sliding bifurcations’). A topological sliding mode transition can be a bifurcation or a non-bifurcating topological transition. The topological structure is depicted in Figure 7.1. It is unknown whether there exist non-bifurcating topological transitions that are not sliding mode transitions.

Topics for Further Research

The lack of a theory for discontinuous bifurcations or more general of discontinuous differential equations, which embraces the theory for smooth systems, is felt as a shortcoming in current research. Conjectures 5.1 and 6.1 were formulated about existence of discontinuous bifurcations and an attempt to a partial classification of those bifurcations is made in Conjectures 5.2 and 6.2. Further research is needed in order to reject or prove the conjectures.

Bifurcations of fixed points of non-smooth continuous systems were studied. Discontinuous bifurcations were found to be located on hyper-surfaces at which the vector field is non-smooth. The stability of a fixed point on a hyper-surface was not investigated. Further research could study branches of fixed points that are located on a hyper-surface and bifurcation of those branches.

In the thesis bifurcations of fixed points in non-smooth continuous systems and bifurcations of periodic solutions in discontinuous systems were studied. Bifurcations of fixed points in discontinuous systems of Filippov-type, however, were not studied. In fact, this problem is even more complicated. Some results on stability of fixed points in discontinuous systems exist [Anosov, 1959; Brogliato, 1999; Heemels, 1999; Roxin, 1965]. Brogliato [1999] also gives results on stability of fixed points in impacting systems. Although extremely complicated, further research could study bifurcations of fixed points in Filippov and impacting systems.

Two combined bifurcations were treated in this thesis: a discontinuous Hopf-pitchfork bifurcation and a discontinuous fold-flip bifurcation. It should be investigated whether other examples of combined bifurcations exist that show phenomena not exposed by the two bifurcations separately. It is interesting to know whether a combination exists of more than two conventional bifurcations.

The possibility of accumulation points in the solution of a Filippov system was briefly mentioned in Chapter 2. This phenomenon of Filippov systems was not further addressed in this thesis and it was assumed that no accumulation points occur. It would be interesting to investigate whether periodic solutions in Filippov systems can contain accumulation points. The occurrence of infinitely many mode switches in the periodic solution causes infinitely many jumps of the fundamental solution matrix which complicates the determination of the fundamental solution matrix after the period time. The appearance or disappearance of accumulation points in periodic solutions under variation of a parameter might create a bifurcation.

Many aspects of discontinuous bifurcations of periodic solutions in Filippov systems are shown in the thesis. Much work still has to be done on the numerical aspects of continuation of branches of periodic solutions in discontinuous systems. Standard numerical path-following methods are developed for smooth systems. Application of these methods to Filippov systems leads to numerical difficulties especially at discontinuous bifurcation points.

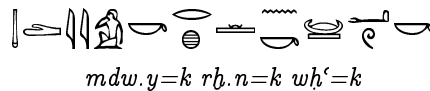
The Zhuravlev-Ivanov transformation [Brogliato, 1999; Ivanov, 1993] is a non-smooth transformation that transforms a system with a single frictionless impact (like system (3) of Table 1.1) to a Filippov system. Periodic solutions of simple impacting problems can therefore be transformed to periodic solutions of Filippov systems which are described in this thesis. The results in this thesis on discontinuous bifurcations of Filippov systems can therefore be used as a stepping stone to bifur-

cations in impacting systems. Further research should study how the discontinuous bifurcations of Filippov systems are related to bifurcations in impacting systems.

From the previous chapters it seems that we are still very distant from a unified theory of bifurcations in discontinuous systems. Many examples are discussed in this thesis, which expose a variety of discontinuous bifurcations. The examples show that on the one hand discontinuous bifurcations occur which can be considered to be counterparts of conventional bifurcations. On the other hand, discontinuous bifurcations exist which behave qualitatively different from conventional bifurcations. All encountered discontinuous bifurcations show a common characteristic (jump of an eigenvalue/Floquet multiplier (or pairs of these) over the imaginary axis/through the unit circle). This has led to the formulation of conjectures about existence and classification of discontinuous bifurcations. It would be of interest to investigate whether or not these conjectures can constitute (part of) a basis for a (possible) unified theory of bifurcations in discontinuous systems of Filippov-type.

Appendix A

Application to a Simple Model of Drillstring Dynamics ¹



May you speak, after you have found out how to solve something.

THE MAXIMS OF PTAH-HOTEP, The Prisse papyrus.

The theory developed in the preceding chapters will be applied in this appendix to a simple model of drillstring dynamics.

A.1 Motivation

Deep wells for the exploration and production of oil and gas are drilled with a rock-cutting tool driven from the surface by a slender structure of pipes, called the drillstring (Figure A.1). Drillstring vibrations are an important cause of premature failure of drillstring components and drilling inefficiency. Stick-slip vibration causes violent torsional vibration of the drillstring and whirl leads to lateral vibrations with large amplitudes. Extensive research on this subject has been conducted for the last four decades, both theoretically [Jansen, 1993; Van den Steen, 1997; Van der Heijden, 1994] and experimentally (for instance [Pavone and Desplans, 1994]). Most of the experimental investigations were only based on field measurements recorded at the surface. Stick-slip vibrations can indeed be detected from the surface, at least in a straight well, but detailed information about the mechanism downhole can not be obtained. Downhole measurements, briefly presented in this appendix, reveal stick-slip vibration coexisting with whirl vibration. Uncertainty exists on the

¹The experimental data in this appendix were analyzed in cooperation with ir. J. Manie.

downhole mechanism which determines whether stick-slip or whirl will be prevalent. This appendix presents a low-dimensional dynamical model, describing stick-slip and whirl in its most elementary form. The system is analyzed with the methods presented in the preceding chapters. This appendix does not aim to present a model which fully explains the observed phenomena in the measurements. The objective of this appendix is to illustrate the theory presented in the preceding chapters and to show that discontinuous bifurcations can arise in simple models of mechanical systems. This appendix is meant as an illustration and we will discuss in Section A.10 the possible merits of this appendix to the insight into drillstring vibration.

The principles of oilwell drilling are first briefly explained in Section A.2. Downhole measurements, which reveal stick-slip motion and whirl in a drillstring, are presented in Section A.3. A simple mathematical model for the investigation of stick-slip and whirl is constructed and analyzed in Sections A.4 to A.9. The theoretical and numerical results will be compared with the measurements in Section A.10.

A.2 Principles of Oilwell Drilling

Oil and gas wells are predominantly drilled using rotary drilling. The basic elements of a rotary drilling system are shown in Figure A.1. A rotary drilling system creates a borehole by means of a rock-cutting tool, called a bit. The oldest type of rotary bit is the roller-cone bit which essentially comprises three metal rollers covered with hard steel teeth that crush the rock. An alternative type of bit is the PDC (Polycrystalline Diamond Compact) bit consisting of a steel body with inserts made of artificial diamond and tungsten carbide. The energy to drive the bit is generated at the surface by a motor with a mechanical transmission box. Via the transmission the motor drives the rotary table: a large disc that acts as kinetic energy storage. The medium to transport the energy from the surface to the bit is formed by a drillstring, mainly consisting of drill pipes: slender tubes, about 9 m (30 ft.) long, coupled with threaded connections, having a typical outside diameter of 127 mm (5") and a wall thickness of 9 mm. However, smaller (e.g. 3.5") and larger (6.5") drill pipe diameters are also used.

The lowest part of the drillstring, the Bottom-Hole-Assembly (BHA), consists of thick-walled tubulars, called drill collars. Dependent on the diameter of the hole, these drill collars usually have an inner diameter of 2.5-3" (64-76 mm) and an outer diameter of 4.75"-9.5" (120-240 mm). The BHA can be several hundreds of meters long, and often contains dedicated downhole tools. The drill collars in the BHA are kept in position by a number of stabilizers, which are short sections with nearly the same diameter of the bit.

The drilling process requires a compressive force on the bit of some 10^4 - 10^6 N. This dynamic force is commonly denoted as Weight On Bit (WOB), although force-on-bit would be a more appropriate name. The entire drillstring is suspended by a hoisting system, consisting of a travelling block with hook, drilling line and winch. The drillstring rests with the bit on the bottom of the hole and is pulled at the hook by a force called the hookload. The hookload ensures that the drill pipe is kept in tension to avoid buckling. The graph at the left of Figure A.1 shows the axial force as a function of the position along the borehole. While the drill pipes run in tension,

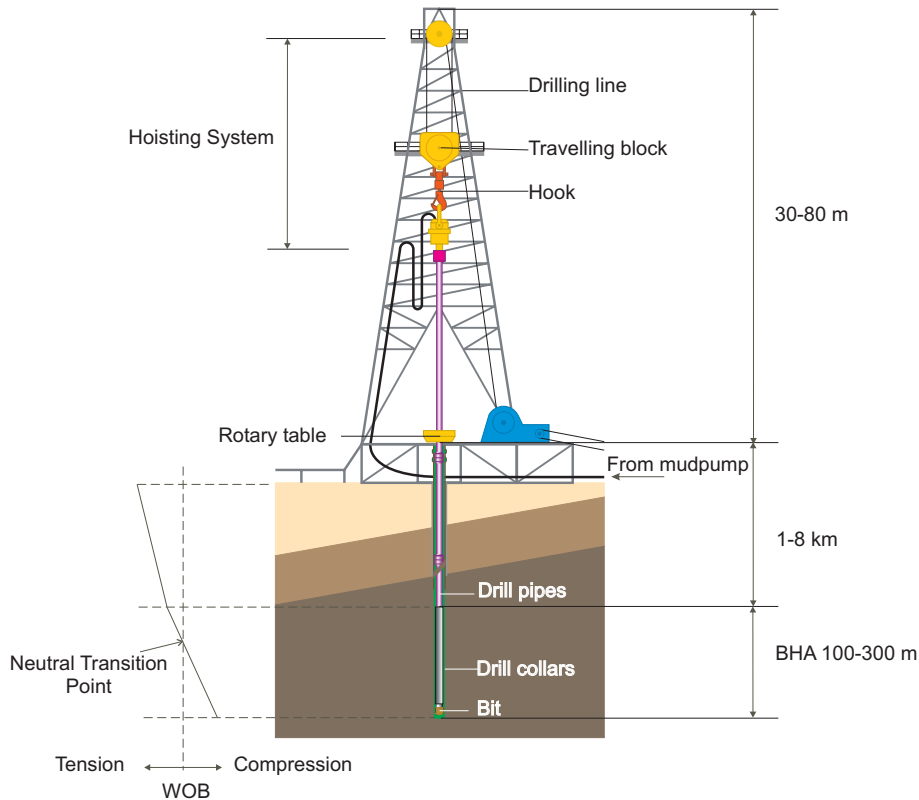


Figure A.1: Drilling Rig.

the BHA is partly loaded in compression. Buckling of the BHA is prevented by the large wall thickness of the drill collars and the placement of stabilizers.

Torque is transmitted from the rotary table to the drillstring. The torque required to drive the bit is referred to as the Torque On Bit (TOB).

A fluid called mud is pumped down through the hollow drillstring, through nozzles in the bit and returns to the surface through the annulus between the drillstring and the borehole wall. The mud compensates the pressure in the rock, lubricates and removes the rock cuttings from the hole.

The drilling process is steered by the hookload, the rotary table speed at the surface (the angular velocity of the top end of the drillstring) and the flow rate of the mud. The downward speed of the drillstring gives an accurate measure of the rate of penetration (ROP). The standpipe pressure (the pressure in the flowline at the top of the drillstring) indicates the total pressure drop in the drillstring and annulus. The ROP and standpipe pressure indicate the progress and state of the drilling process which are interpreted by drilling engineers to adjust the steering parameters.

The drillstring undergoes various types of vibration during drilling [Van den

Steen, 1997]

- Axial (longitudinal) vibrations, due to bouncing of the drilling bit on the rock during rotation (called ‘bitbounce’).
- Bending (lateral) vibrations, often caused by pipe eccentricity, leading to centripetal forces during rotation, named as drillstring whirl:
 - **forward whirl**: the rotation of a deflected drill collar section around the borehole axis in the same direction as it rotates around its axis.
 - **backward whirl**: a rolling motion of the drill collar or the stabilizer over the borehole wall in opposite direction as it rotates around its axis.
- Torsional (rotational) vibrations, caused by non-linear interaction between the bit and the rock or the drillstring with the borehole wall, named as
 - **stick-slip vibration**: the torsional vibration of the drillstring characterized by alternating stops (during which the BHA sticks to the borehole) and intervals of large angular velocity of the BHA.
- Hydraulic vibrations in the circulation system, stemming from pump pulsations.

These vibrations are to some degree coupled: e.g. the interaction between TOB and WOB will link the axial vibrations to the torsional vibrations.

A.3 Downhole Measurements

In the late 1980s the Institut Français du Pétrole designed the Trafor system, a research tool to measure downhole and surface data to improve knowledge about drillstring dynamics. The Trafor system consists of a downhole measurement device, called the Télévigile, and a surface measurement device known as the Survigile. The signals of the Télévigile and Survigile are gathered by a computer and synchronized. The great merit of the Trafor system is the ability to measure both downhole and surface data at real-time. Pavone and Desplans [1994] give a description of the Trafor system. The Télévigile is equipped with sensors that measure Weight On Bit, downhole torque, downhole accelerations in three orthogonal directions and downhole bending moments in two directions. Three magnetic field sensors, known as magnetometers, measure a projection of the earth magnetic field in three orthogonal directions co-rotating with the Télévigile.

The measurements reported in this section were recorded at the research rig Ullrigg in Rogaland, Norway between 1990 and 1993, being a joint project of A/S Norske Shell and Elf Aquitaine. The well is nearly vertical and about 1080 m deep. Various tests with different WOB and angular velocity of the rotary table were conducted. A few tests are used for this appendix, all conducted with the same drillstring setup. The drillstring consisted of 5” drill pipe, 8” drill collars and a 12 1/4” roller-cone bit.

Figure A.2 shows a time history of the downhole angular velocity, calculated from the magnetometer signals. The angular velocity at the surface ω , WOB and

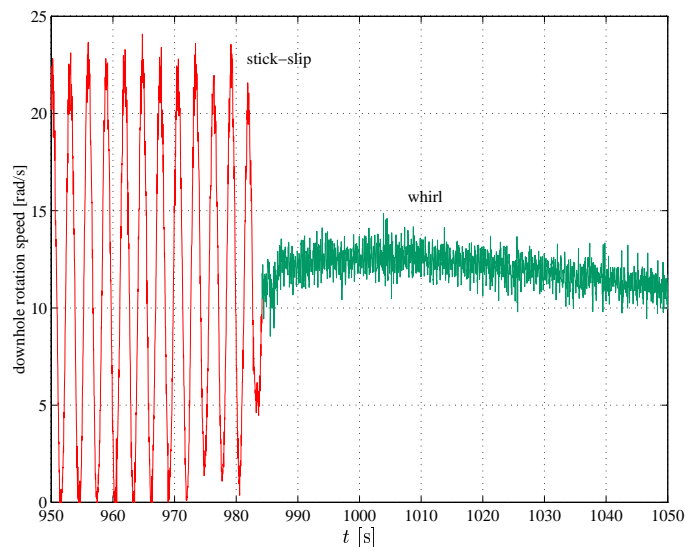


Figure A.2: Measured downhole angular velocity versus time.

other parameters were almost kept constant during the experiment. The drillstring clearly performs stick-slip motion for $t < 985$ s. At $t = 985$ s the stick-slip motion suddenly disappears and backward whirl is prevalent for $t > 985$ s. The stick-slip motion is caused by the dry friction between the BHA and the rock. The friction is due to the drilling bit, which cuts the rock, but also due to the stabilizers, which have contact with the borehole wall. The friction curve of the part of the BHA beneath the Télévigile, relating the torque to the downhole angular velocity, could be reconstructed from the measurements (Figure A.3). The torque on the Télévigile consists of the friction torque of the bit, the torque created by contact (if present) of the drill collar beneath the Télévigile with the borehole wall and by the viscous torque of the drilling mud. During the stick-slip motion the part of the friction curve is traversed with the negative slope. The negative slope of the friction curve causes steady rotation of the drillstring to be unstable, which induces the stick-slip motion. At the transition to whirl, a switch is made to another part of the friction curve with a higher value of friction and a slightly positive slope. The drillstring is not deflected in lateral direction during stick-slip motion. Consequently, the torque on the Télévigile is during stick-slip motion mainly due to the friction torque on the bit. The whirl motion has been identified as being backward whirl caused by rolling of a drill collar section over the borehole wall (with a small amount of slip). The drillstring must consequently be deflected during whirl motion. The torque on the Télévigile will be higher during whirl motion due to the additional torque created by the contact between drill collar and borehole wall and increased drag forces of the mud on the whirling drill collar. This additional torque increases with increasing angular velocity. This would account for the higher torque and slightly positive slope of the friction curve during whirl motion. The slightly positive slope causes

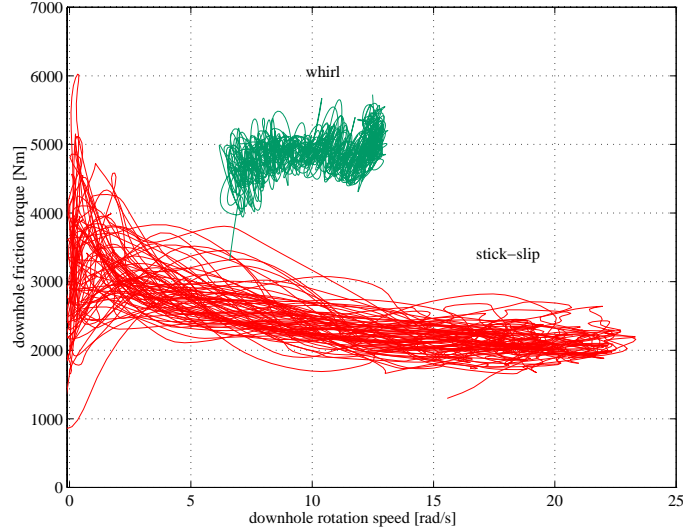


Figure A.3: Measured downhole friction curve.

the constant rotation to be stable which prevents stick-slip motion as is observed in Figure A.2.

Figure A.4 shows the mean bending moment measured by the strain gauges in the *Télévigile* versus the prescribed angular velocity at the surface ω . During this experiment, the value of ω was varied with a sweep-up followed by a sweep-down. The mean bending moment is to some extent a measure for the radial displacement of the drillstring. The system was first in stick-slip motion with a low value of the mean bending moment (consistent with an undeflected drillstring) at low ω . As ω is increased the mean bending moment increases slightly but at $\omega = 11.5$ [rad/s] the motion switches from stick-slip to whirl and the mean bending moment jumps to a higher value, indicating a large radial deflection of the drillstring. The sweep-up test reaches its maximum at $\omega = 12.5$ [rad/s] after which ω is decreased. The drillstring remains in whirl motion down to $\omega = 2$ [rad/s]. The bending moment during whirl motion is not constant for varying ω . The part with positive slope for $2 < \omega < 7$ [rad/s] is consistent with an increasing radial deflection for increasing ω . At $\omega = 7$ [rad/s] the *Télévigile* probably touches the borehole wall and for increasing values of ω , a larger part of the drillstring will become in contact with the borehole wall which decreases the bending moment. We conclude from Figure A.4 that stick-slip and whirl can coexist for an interval of rotary table speed ω . Combined stick-slip whirl motion, however, in which the drillstring performs stick-slip motion with a large radial deflection, is not observed.

The mechanism downhole, which causes the transition from stick-slip to whirl and vice-versa, is not satisfactorily understood. The transition from stick-slip to whirl is presumably caused by an interaction between bending and torsion which destabilizes the concentric position of the drillstring for high values of ω . Possible ways of interaction can be caused by

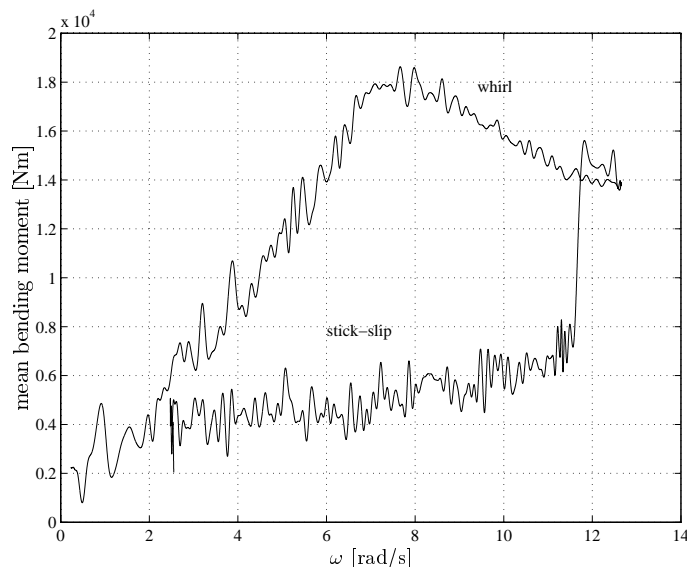


Figure A.4: Measured downhole bending moment versus surface angular velocity.

- Drillstring eccentricity. This causes the drillstring to whirl violently only in the neighbourhood of the bending critical eigenfrequency. The drillstring would not whirl for very high values of ω , contrary to what has been observed from the measurements.
- Gyroscopic effects. They are negligible because the clearance between drillstring and borehole is much smaller than the length of the drillstring.
- Anisotropic bending stiffness of the drillstring. This causes the drillstring to whirl in a small interval of ω which is inconsistent with the measurements.
- Fluid mud forces. They destabilize the concentric position of the drillstring for ω -values higher than a critical value consistent with measurements.

Insight into the mechanism downhole and the possible interaction between bending and torsion can be obtained by studying a simplified model of the drillstring. In the next sections we will study whether fluid forces of the drilling mud can explain the observed phenomena. A low-dimensional model will be analyzed with both torsional and lateral degrees of freedom in a fluid. This small model will be discontinuous of Filippov-type and shows a complicated dynamical behaviour. Bifurcations in Filippov systems were investigated in the preceding chapters but we did not arrive at a unified theory and many questions are still left open. Still, the results of the preceding chapters will be of use to partly explain the complicated dynamical behaviour of the model.

A.4 Modeling of Stick-slip Whirl Interaction

A simple model for the whirling motion of a drill collar section has been developed by Jansen [1993] and has been further analyzed by Van der Heijden [1994]. A simple model to describe the torsional stick-slip motion of a drillstring was presented in Jansen [1993] and extensively analyzed by Van den Steen [1997].

In the following sections we will develop a model which can describe whirl and stick-slip motion in their most elementary form, under influence of fluid forces. The model consists of a submodel for the whirling motion, called the *Whirl Model*, and a submodel for the stick-slip motion, called the *Stick-slip Model*. The full model will be named the *Stick-slip Whirl Model*. Elementary whirling can be described by at least 2 lateral degrees of freedom and stick-slip motion by one torsional degree of freedom. The Stick-slip Whirl Model has therefore 3 degrees of freedom. The Stick-slip Whirl Model is a simplification of a drillstring confined in a borehole wall with mud.

The interaction between torsional vibration and whirl of a rotor was already studied by Lee [1993] and Tondl [1965] but a dry friction torque on the rotor and fluid forces were not considered.

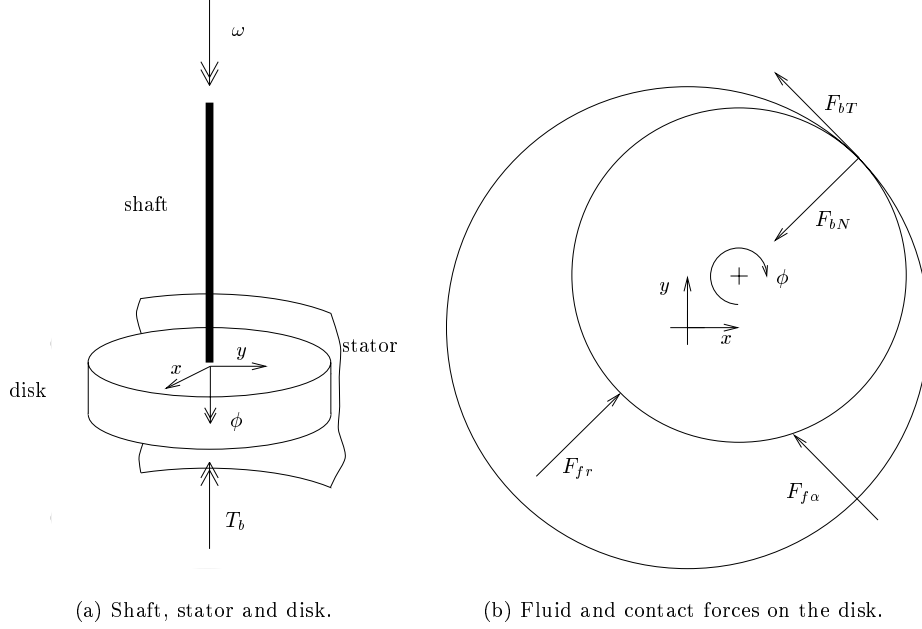
We consider a rigid disk (which models the BHA) at the end of a massless flexible shaft (the drill pipe) as is depicted in Figure A.5a. The shaft and disk are confined in a stator (the borehole) filled with fluid (drilling mud). The upper end of the shaft is driven with constant rotation speed ω (constant speed of the rotary table). The shaft is subjected to bending and torsion with bending stiffness k and torsion stiffness k_φ . The disk with mass m and inertia J is attached to the lower end of the shaft. The displacement of the geometric center of the disk is denoted by x and y in the stationary coordinate system or by the polar coordinates r and α (see Section A.11). The disk is twisted with an angle φ with respect to the upper end of the shaft and with an angle ϕ with respect to the fixed world

$$\phi = \omega t + \varphi. \tag{A.1}$$

On the disk or *rotor* acts a friction torque T_f (the Torque On Bit). The lateral motion of the disk is constrained by the *stator*. The rotor has a radius R and the stator a radius R_b . Contact is made when the radial (lateral) displacement of the rotor r equals R_c , where $R_c = R_b - R$ is the clearance.

A.5 Fluid Forces

The fluid forces on the drillstring are extremely complicated as the fluid motion is non-stationary and possibly turbulent. However, analytical results are available for a constantly rotating rotor in a stator for small clearance and small lateral displacement ($R_c \ll R$ and $r \ll R$) [Fritz, 1970; Muszynska, 1986]. As a first approximation we will use these analytical results for non-stationary motion of a rotor which is confined in a large stator for arbitrary lateral displacements. The



(a) Shaft, stator and disk.

(b) Fluid and contact forces on the disk.

Figure A.5: Stick-slip Whirl Model.

fluid force equations given in [Fritz, 1970; Muszynska, 1986] are

$$\begin{aligned}
 - \begin{bmatrix} F_{fx} \\ F_{fy} \end{bmatrix} &= \begin{bmatrix} m_f & 0 \\ 0 & m_f \end{bmatrix} \begin{bmatrix} \ddot{x} \\ \ddot{y} \end{bmatrix} + \\
 &\begin{bmatrix} D & \omega m_f \\ -\omega m_f & D \end{bmatrix} \begin{bmatrix} \dot{x} \\ \dot{y} \end{bmatrix} + \begin{bmatrix} \psi_2(r) & 0 \\ 0 & \psi_2(r) \end{bmatrix} \begin{bmatrix} \dot{x} \\ \dot{y} \end{bmatrix} + \\
 &\begin{bmatrix} -\frac{\omega^2}{4} m_f & \frac{\omega}{2} D \\ -\frac{\omega}{2} D & -\frac{\omega^2}{4} m_f \end{bmatrix} \begin{bmatrix} x \\ y \end{bmatrix} + \begin{bmatrix} \psi_1(r) & \frac{\omega}{2} \psi_2(r) \\ -\frac{\omega}{2} \psi_2(r) & \psi_1(r) \end{bmatrix} \begin{bmatrix} x \\ y \end{bmatrix},
 \end{aligned} \tag{A.2}$$

where m_f is the added fluid mass and D the fluid friction coefficient.

The fluid forces, depicted in Figure A.5b, can be transformed to polar coordinates

$$\begin{aligned}
 F_{fr} &= -m_f(\ddot{r} - \dot{\alpha}^2 r - \frac{\omega^2}{4} r + \omega \dot{\alpha} r) - (D + \psi_2(r))\dot{r} - \psi_1(r)r \\
 F_{f\alpha} &= -m_f(\ddot{\alpha} r + 2\dot{r}\dot{\alpha} - \omega \dot{r}) - (\dot{\alpha} - \frac{\omega}{2})(D + \psi_2(r))r.
 \end{aligned} \tag{A.3}$$

The nonlinear functions ψ_1 and ψ_2 depend on the radial displacement r . It is assumed (following Muszynska [1986]) that these functions are analytic (with $\psi_1(0) = \psi_2(0) = 0$). As a first approximation, only the following symmetric terms will be taken into account:

$$\psi_1(r) = B_1 r^2, \quad \psi_2(r) = B_2 r^2, \tag{A.4}$$

where B_1 and B_2 are constants.

A.6 Contact Forces

The stator wall will induce normal and tangential forces (Figure A.5b) on the rotor if the radial displacement becomes larger than the clearance, $r > R_c$. The normal contact force can be modeled (in its most simple form) to stem from a linear spring with spring stiffness k_b ,

$$F_{bN} = \begin{cases} k_b(r - R_c) & r > R_c \\ 0 & r \leq R_c. \end{cases} \quad (\text{A.5})$$

The normal contact force induces a tangential contact force due to dry friction between the rotor and the wall. We assume a constant friction coefficient μ_b . If the relative velocity between the rotor and the stator wall is nonzero, then the tangential contact force is

$$F_{bT} = -\mu_b \text{sign}(v_{\text{rel}}) F_{bN} \quad , \quad v_{\text{rel}} \neq 0, \quad (\text{A.6})$$

with the relative velocity being given by $v_{\text{rel}} = \dot{\alpha}r + \omega R$ (for constant rotation of the rotor). During pure rolling ($v_{\text{rel}} = 0$) the tangential contact force must be between

$$-\mu_b F_{bN} \leq F_{bT} \leq \mu_b F_{bN}. \quad (\text{A.7})$$

The contact forces can be expressed in stationary coordinates as

$$F_{bx} = (-F_{bTy} - F_{bNx})/r, \quad F_{by} = (F_{bTx} - F_{bNy})/r. \quad (\text{A.8})$$

The friction due to rotor-stator contact can be treated numerically by making use of the *switch model* (see Section 2.4 and Leine et al. [1998]).

Torques on the disk

We assume that a dry friction torque T_f is acting on the rotor, which only depends on the angular velocity $\dot{\phi}$,

$$T_f = -\text{sgn} \dot{\phi} \frac{T_0}{1 + \delta|\dot{\phi}|}. \quad (\text{A.9})$$

Contact between the rotor and stator induces the contact forces F_{bN} and F_{bT} . The tangential contact force induces a torque on the rotor,

$$T_b = F_{bT}R. \quad (\text{A.10})$$

The fluid forces F_{fr} and $F_{f\alpha}$ (A.3) are derived for stationary motion of the rotor $\dot{\phi} = \omega$. We will assume that they also hold for non-stationary motion, $\dot{\phi} \neq \omega$, and we replace ω by $\dot{\phi}$ in (A.3),

$$\begin{aligned} F_{fr} &= -m_f(\ddot{r} - \dot{\alpha}^2 r - \frac{\dot{\phi}^2}{4}r + \dot{\phi}\dot{\alpha}r) - (D + \psi_2(r))\dot{r} - \psi_1(r)r \\ F_{f\alpha} &= -m_f(\ddot{\alpha}r + 2\dot{r}\dot{\alpha} - \dot{\phi}\dot{r}) - (\dot{\alpha} - \frac{\dot{\phi}}{2})(D + \psi_2(r))r. \end{aligned} \quad (\text{A.11})$$

The fluid forces F_{fr} and $F_{f\alpha}$ act on the rotor but their working lines are through the origin. The force $F_{f\alpha}$ has therefore an arm $-r$ and gives the torque

$$T_d = -F_{f\alpha}r. \quad (\text{A.12})$$

A.7 Whirl Model

In this section we study only the Whirl Model. We assume the rotor to rotate constantly (no torsional vibration). This allows us to find analytical results for the pure whirling motion, which are equilibria of the Whirl Model in polar coordinates and periodic harmonic solutions in stationary coordinates. Polar coordinates are therefore more convenient for the Whirl Model. The equilibria of the Whirl Model are also equilibria of the total Stick-slip Whirl Model but the eigenvalues of the Stick-slip Model may change the stability.

Equations of Motion

The equations of motion for a whirling rotor with fluid and contact forces in stationary coordinates are

$$\begin{aligned} m\ddot{x} + c\dot{x} + kx &= F_{fx} + F_{bx} \\ m\ddot{y} + c\dot{y} + ky &= F_{fy} + F_{by}, \end{aligned} \quad (\text{A.13})$$

where m is the rotor mass, k the lateral bending stiffness and c the lateral bending damping constant. In polar coordinates these equations become

$$\begin{aligned} m(\ddot{r} - \dot{\alpha}^2 r) + c\dot{r} + kr &= F_{fr} - F_{bN} \\ m(\ddot{\alpha}r + 2\dot{r}\dot{\alpha}) + c\dot{\alpha}r &= F_{f\alpha} + F_{bT}. \end{aligned} \quad (\text{A.14})$$

Substitution of the fluid forces (A.3) gives

$$\begin{aligned} m_a(\ddot{r} - \dot{\alpha}^2 r) + (c + D + B_2 r^2)\dot{r} + (k - \frac{\omega^2}{4}m_f + m_f\omega\dot{\alpha} + B_1 r^2)r &= -F_{bN} \\ m_a(\ddot{\alpha}r + 2\dot{r}\dot{\alpha}) + (c + D + B_2 r^2)\dot{\alpha}r &= m_f\omega\dot{r} + (D + B_2 r^2)\frac{\omega}{2}r + F_{bT}, \end{aligned} \quad (\text{A.15})$$

with $m_a = m + m_f$. This fourth-order system can be transformed into a third-order system with the whirl velocity $\Omega = \dot{\alpha}$,

$$\begin{aligned} m_a(\ddot{r} - \Omega^2 r) + (c + D + B_2 r^2)\dot{r} + (k - \frac{\omega^2}{4}m_f + m_f\omega\Omega + B_1 r^2)r &= -F_{bN} \\ m_a(\dot{\Omega}r + 2\dot{r}\Omega) + (c + D + B_2 r^2)\Omega r &= m_f\omega\dot{r} + (D + B_2 r^2)\frac{\omega}{2}r + F_{bT}. \end{aligned} \quad (\text{A.16})$$

Equilibrium without contact

The equilibrium without contact (r_e, Ω_e) of (A.16) has to obey $\dot{r} = \ddot{r} = \dot{\Omega} = 0$ and $r < R_c$. The whirl velocity can be derived from the second equation of (A.16),

$$\Omega_e = \frac{D + B_2 r_e^2}{c + D + B_2 r_e^2} \frac{\omega}{2}. \quad (\text{A.17})$$

Consequently, the rotor is whirling forward in the equilibrium without contact. The first equation of A.16 gives

$$(k - \frac{\omega^2}{4}m_f + m_f\omega\Omega_e - m_a\Omega_e^2 + B_1 r_e^2)r_e = 0. \quad (\text{A.18})$$

Solving the latter equation gives two equilibrium branches of the system without contact. The first branch is the trivial solution

$$r_e = 0, \quad (\text{A.19})$$

and the second branch can be derived from

$$k - \frac{\omega^2}{4}m_f + m_f\omega\Omega_e - m_a\Omega_e^2 + B_1r_e^2 = 0. \quad (\text{A.20})$$

The trivial branch becomes unstable when it meets the second branch. We denote the frequency at which the trivial branch becomes unstable by ω_c . Substitution of (A.17) and (A.19) into (A.20) gives ω_c

$$\omega_c^2 = 4k \frac{(c+D)^2}{c^2m_f + D^2m}. \quad (\text{A.21})$$

Two limiting cases are of special interest: a) $c > 0$ and $D = B_2 = 0$, b) $c = 0$ and $D > 0, B_2 > 0$.

Case a) implies that we consider the system to rotate in a frictionless fluid. The rotor will not whirl due to the absence of fluid friction,

$$\Omega_{e,a} = 0. \quad (\text{A.22})$$

The quasi-static motion of rotor gives

$$c\dot{r}_{e,a} = \left(\frac{\omega^2}{4}m_f - k\right)r_{e,a} - B_1r_{e,a}^3. \quad (\text{A.23})$$

The two stationary solutions (for $r_{e,a} \geq 0$) are

$$r_{e,a} = 0, \quad r_{e,a} = \sqrt{\frac{\frac{\omega^2}{4}m_f - k}{B_1}} \quad (\text{A.24})$$

We conclude that case a) gives a supercritical pitchfork bifurcation ($B_1 > 0$) at

$$\omega_{c,a} = 2\sqrt{\frac{k}{m_f}} \quad (\text{A.25})$$

Case b) implies that we consider the system to have no structural damping but only fluid damping. The rotor will whirl with half the rotation speed ($\frac{1}{2}\omega$ -whirl),

$$\Omega_{e,b} = \frac{1}{2}\omega. \quad (\text{A.26})$$

The quasi-static motion of rotor gives (with $m_a = m + m_f$)

$$(D + B_2r_{e,b}^2)\dot{r}_{e,b} = \left(\frac{\omega^2}{4}m - k\right)r_{e,b} - B_1r_{e,b}^3. \quad (\text{A.27})$$

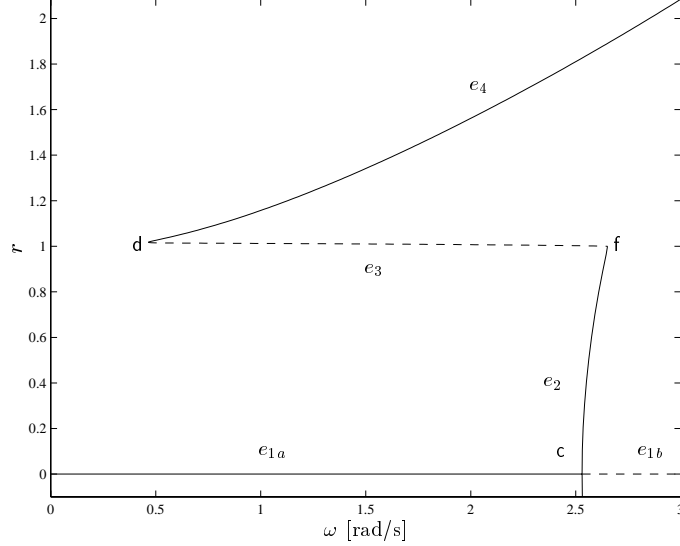


Figure A.6: Whirl Model, equilibrium branches.

The two stationary solutions (for $r_{e,b} \geq 0$) are

$$r_{e,b} = 0, \quad r_{e,b} = \sqrt{\frac{\frac{\omega^2}{4}m - k}{B_1}}. \quad (\text{A.28})$$

We conclude that case b) also gives a supercritical pitchfork bifurcation at twice the natural frequency,

$$\omega_{c,b} = 2\sqrt{\frac{k}{m}}. \quad (\text{A.29})$$

For $\frac{m_f}{m} < 1$ it can be shown that $\omega_{c,b} < \omega_c < \omega_{c,a}$. The pitchfork bifurcation is shown in Figure A.6 for the parameter values given in Appendix C.6. The trivial branch e_{1a} is stable and meets the bifurcation (denoted by c) after which it is unstable and continues as e_{1b} . From the bifurcation point starts a branch of stable forward whirl solutions e_2 .

Equilibrium with pure rolling

The rotor rolls over the stator wall without slipping under three conditions:

1. the relative velocity is zero, $v_{\text{rel}} = \Omega r + \omega R = 0$,
2. positive normal contact force, $F_{bN} > 0$,
3. the tangential contact force does not exceed the maximal friction force, $-\mu_b F_{bN} \leq F_{bT} \leq \mu_b F_{bN}$.

The pure rolling equilibrium ($r = r_p, \Omega = \Omega_p$) has to obey $\dot{r} = \ddot{r} = \dot{\Omega} = 0$.

The whirl velocity can be derived from condition 1,

$$\Omega_p = -\frac{R}{r_p}\omega. \quad (\text{A.30})$$

Consequently, the rotor rolls backward over the stator wall. The equilibrium conditions give

$$\begin{aligned} -m_a\Omega_p^2 r_p + \left(k - \frac{\omega^2}{4}m_f + m_f\omega\Omega_p + B_1 r_p^2\right)r_p &= -F_{bN} \\ &= -k_b(r_p - R_c) \end{aligned} \quad (\text{A.31})$$

and

$$(c + D + B_2 r_p^2)\Omega_p r_p = (D + B_2 r_p^2)\frac{\omega}{2}r_p + F_{bT}. \quad (\text{A.32})$$

Substitution of Ω_p in (A.31) gives a third-order polynomial in r_p . If we neglect the nonlinear fluid term B_1 , (A.31) reduces to a second-order polynomial

$$(k + k_b - \frac{\omega^2}{4}m_f)r_p^2 - (k_b R_c + m_f\omega^2 R)r_p - m_a\omega^2 R^2 = 0. \quad (\text{A.33})$$

Solving for r_p gives two roots of which only one fulfills condition 1,

$$r_p = \frac{k_b R_c + m_f\omega^2 R + \sqrt{(k_b R_c + m_f\omega^2 R)^2 + 4m_a\omega^2 R^2(k + k_b - \frac{\omega^2}{4}m_f)}}{2(k_b R_c + m_f\omega^2 R)}. \quad (\text{A.34})$$

The limit of k_b to infinity gives of course $\lim_{k_b \rightarrow \infty} r_p = R_c$.

If we assume directly an infinitely stiff wall of the stator without neglecting B_1 , then we can solve for the contact forces,

$$F_{bN} = m_a\omega^2 \frac{R^2}{R_c} - \left(k - \frac{\omega^2}{4}m_f + B_1 R_c^2\right)R_c + \omega^2 R m_f, \quad (\text{A.35})$$

$$F_{bT} = -(c + D + B_2 R_c^2)\omega R - (D + B_2 R_c^2)\frac{\omega}{2}R_c. \quad (\text{A.36})$$

Equation (A.35) should fulfill condition 2,

$$\omega^2 > \omega_b^2 = \frac{(k + B_1 R_c^2)R_c}{m_a \frac{R^2}{R_c} + m_f \frac{1}{4}R_c + m_f R}. \quad (\text{A.37})$$

If B_1 is not too large, then $\omega_b < \omega_{c,b}$.

However, pure rolling near $\omega = \omega_b$ is not possible because (A.36) has to fulfill condition 3. We define that condition 3 is violated at $\omega = \omega_d$. Substitution of (A.35) and (A.36) into $-\mu_b F_{bN} = F_{bT}$ gives a second-order polynomial in ω_d ,

$$-\mu_b \left(m_a \frac{R^2}{R_c} + m_f \left(\frac{R_c}{4} + R \right) \right) \omega_d^2 + \left(cR + (D + B_2 R_c^2) \left(R + \frac{R_c}{2} \right) \right) \omega_d + \mu_b R_c (k + B_1 R_c^2) = 0. \quad (\text{A.38})$$

If the fluid damping (D, B_2) and structural damping (c) are small compared to the dry friction caused by μ_b , then we can make the following approximation

$$\omega_d^2 \approx \omega_b^2 + \frac{cR + (D + B_2 R_c^2) \left(R + \frac{R_c}{2} \right)}{\mu_b \left(m_a \frac{R^2}{R_c} + m_f \left(\frac{R_c}{4} + R \right) \right)} \omega_b. \quad (\text{A.39})$$

Fluid damping and structural damping cause that $\omega_d > \omega_b$.

The pure rolling branch for the parameter values of Appendix C.6 is depicted in Figure A.6 as branch e_4 . The point at which the branch stops ($\omega = \omega_d$) is denoted by d . The value R_c is taken as unity. A larger value for the borehole stiffness k_b will cause the pure rolling branch to come closer to $r = R_c$.

Branch e_2 , with stable *forward* whirling solutions without contact, is connected to branch e_4 , with stable *backward* whirling pure rolling solutions, by the unstable branch e_3 . Branch e_3 consists of equilibria with slipping contact.

Equilibrium with slipping contact

The relative velocity v_{rel} between rotor and stator is positive for forward whirling solutions without contact (branch e_2), whereas it is zero for pure rolling solutions (branch e_4). The relative velocity during slipping contact (branch e_3) should be in between. There are two conditions for slipping:

1. the relative velocity is positive, $v_{\text{rel}} = \Omega r + \omega R > 0$,
2. positive normal contact force, $F_{bN} > 0$.

The slipping equilibrium ($r = r_s, \Omega = \Omega_s$) has to obey $\dot{r} = \ddot{r} = \dot{\Omega} = 0$. The equilibrium conditions give

$$-m_a \Omega_s^2 r_s + \left(k - \frac{\omega^2}{4} m_f + m_f \omega \Omega_s + B_1 r_s^2 \right) r_s = -F_{bN}, \quad (\text{A.40})$$

$$(c + D + B_2 r_s^2) \Omega_s r_s = (D + B_2 r_s^2) \frac{\omega}{2} r_s - \mu_b F_{bN}, \quad (\text{A.41})$$

where $F_{bN} = k_b (r_s - R_c)$. This system of equations can be solved to give r_s , which will not be done in this section. The insight can be gained from other considerations. The limit of k_b to infinity gives of course

$$\lim_{k_b \rightarrow \infty} r_s = R_c$$

The branch of slipping equilibrium begins at the point where the equilibrium without contact touches the stator wall $r_e = R_c$ (denoted by f in Figure A.6) and the branch ends at the point where the pure rolling branch begins (point d). Consequently, the slipping branch connects the stable no-contact branch to the stable pure rolling branch. Of much interest is to know *how* the slipping branch is located between the two end-points, which is closely related to its stability. We therefore try to find an expression for $\frac{\partial r}{\partial \omega}$ at the point where the slipping branch and the no-contact branch e_2 connect. To simplify the results we will assume $B_2 = 0$. At the connection point to the no-contact branch we have at $r_s = r_e = R_c$. The following equations hold at this point

$$\Omega_s = \Omega_e = \frac{D}{c+D} \frac{\omega}{2}, \quad (\text{A.42})$$

$$\left(k - \frac{\omega^2}{4} m_f + m_f \omega \Omega_e - m_a \Omega_e^2 + B_1 R_c^2\right) R_c = 0. \quad (\text{A.43})$$

We now differentiate (A.40) with respect to ω . This gives

$$\begin{aligned} & -2m_a \Omega_s \frac{\partial \Omega_s}{\partial \omega} r_s - m_a \Omega_s^2 \frac{\partial r_s}{\partial \omega} + \left(k - \frac{\omega^2}{4} m_f + m_f \omega \Omega_s + B_1 r_s^2\right) \frac{\partial r_s}{\partial \omega} + \\ & \left(-\frac{\omega}{2} m_f + m_f \Omega_s + m_f \omega \frac{\partial \Omega_s}{\partial \omega} + 2B_1 r_s \frac{\partial r_s}{\partial \omega}\right) r_s = -k_b \frac{\partial r_s}{\partial \omega} \end{aligned} \quad (\text{A.44})$$

and when we substitute (A.42) and (A.43),

$$-m_a \frac{D}{c+D} \omega \frac{\partial \Omega_s}{\partial \omega} R_c + \left(-\frac{1}{2} + \frac{1}{2} \frac{D}{c+D} + \frac{\partial \Omega_s}{\partial \omega}\right) m_f \omega R_c = -(2B_1 R_c^2 + k_b) \frac{\partial r_s}{\partial \omega}. \quad (\text{A.45})$$

Differentiating (A.41) gives

$$\frac{\partial \Omega_s}{\partial \omega} r_s + \Omega_s \frac{\partial r_s}{\partial \omega} = \frac{1}{2} \frac{D}{c+D} \left(r_s + \omega \frac{\partial r_s}{\partial \omega}\right) - \frac{\mu_b k_b}{c+D} \frac{\partial r_s}{\partial \omega}$$

or

$$\frac{\partial \Omega_s}{\partial \omega} = \frac{1}{2} \frac{D}{c+D} - \frac{\mu_b k_b}{c+D} \frac{1}{R_c} \frac{\partial r_s}{\partial \omega}. \quad (\text{A.46})$$

After substitution of (A.46) in (A.45) we arrive at an expression for $\frac{\partial r_s}{\partial \omega}$,

$$k_b \left(1 + 2 \frac{B_1}{k_b} R_c^2 - \frac{\mu_b \omega}{(c+D)^2} (m_f c - mD)\right) \frac{\partial r_s}{\partial \omega} = \frac{1}{2} \frac{\omega R_c}{(c+D)^2} (D^2 m + c^2 m_f). \quad (\text{A.47})$$

The limit of k_b to infinity gives of course $\lim_{k_b \rightarrow \infty} \frac{\partial r_s}{\partial \omega} = 0$. Two limiting cases are of special interest:

Case a) $c > 0$, $D = 0$ and $k_b \gg B_1 R_c^2$
 After substitution in (A.47) we obtain

$$k_b \left(1 - \frac{\mu_b \omega m_f}{c}\right) \frac{\partial r_s}{\partial \omega} = \frac{1}{2} \omega R_c m_f. \quad (\text{A.48})$$

Consequently, when

$$\begin{aligned} \frac{\mu_b \omega m_f}{c} > 1 &\implies \frac{\partial r}{\partial \omega} < 0, \\ \frac{\mu_b \omega m_f}{c} < 1 &\implies \frac{\partial r}{\partial \omega} > 0. \end{aligned}$$

Case b) $c = 0$, $D > 0$ and $k_b \gg B_1 R_c^2$
 After substitution in (A.47) we obtain

$$k_b \left(1 + \frac{\mu_b \omega m}{D}\right) \frac{\partial r_s}{\partial \omega} = \frac{1}{2} \omega R_c m. \quad (\text{A.49})$$

Consequently, it must hold that $\frac{\partial r}{\partial \omega} > 0$.

The parameter values of the structural damping and fluid damping are $c = 0.3 \text{ N/(ms)}$ and $D = 0.1 \text{ N/(ms)}$. The numerical example is similar to case a) with $\frac{\mu_b \omega m_f}{c} > 1$. The derivative $\frac{\partial r}{\partial \omega}$ at point f is therefore negative which causes the branch e_3 to be unstable and to connect point d with point f directly. If the parameter values would be different, such that $\frac{\mu_b \omega m_f}{c} < 1$, then branch e_3 would start at point f with a positive slope as a stable branch. It will at some point turn around and continue as an unstable branch in the direction of point d.

Bifurcation points d and f are discontinuous saddle-node bifurcations of the equilibrium branch e_2 - e_3 - e_4 . An eigenvalue jumps over the imaginary axis through the origin at those bifurcation points. At bifurcation point d, being the transition from contact to no-contact, this is caused by the non-smoothness of the normal contact force (A.5). At bifurcation point f, being the transition from slip to stick, this is caused by the non-smoothness of the tangential contact force (A.6). Remark the angle between the branches at a discontinuous bifurcation point.

A.8 Stick-slip Model

In this section we study only the Stick-slip Model. We assume the rotor to rotate concentricly in the stator (no lateral vibration, $r = 0$). As there is no radial displacement, the torques due to fluid forces and contact forces vanish ($T_d = 0$, $T_b = 0$). The equation of motion for pure torsional motion is

$$J \ddot{\varphi} = -k_\varphi \varphi + T_f. \quad (\text{A.50})$$

The Stick-slip Model has an unstable equilibrium branch ($\varphi = T_f(\omega)/k$, $\dot{\varphi} = 0$), which corresponds to the trivial equilibrium branch ($r = 0$, $\varphi = T_f(\omega)/k$) of the full Stick-slip Whirl Model. The trivial equilibrium branch was denoted in the Whirl Model as branch e_1 .

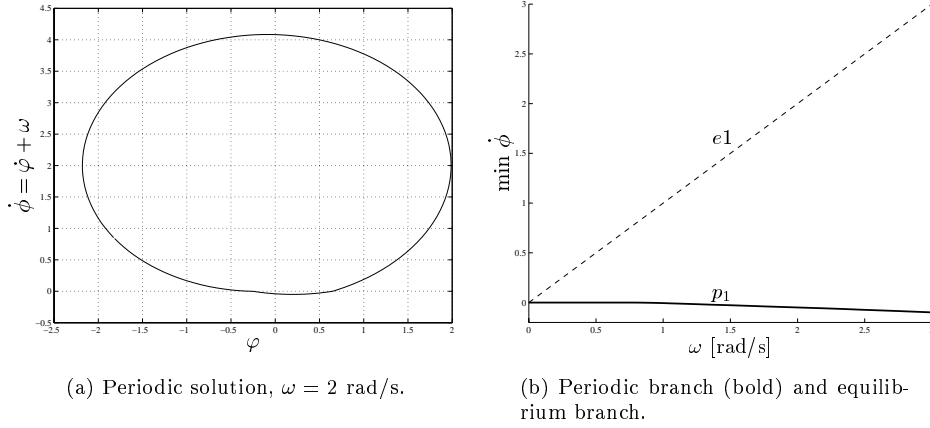


Figure A.7: Stick-slip Model.

Periodic Stick-slip Vibrations

The periodic solutions of the Stick-slip Model are also periodic solutions of the Stick-slip Whirl Model. The periodic stick-slip vibration is depicted in Figure A.7a. The twist φ is on the horizontal axis and the angular velocity $\dot{\phi} = \dot{\varphi} + \omega$ on the vertical axis. The limit cycle is traversed clock-wise. The slip part of the motion takes place at $\dot{\phi} > 0$. When the velocity is decreasing during the slip part, it arrives at $\dot{\phi} = 0$ and continues with backward rotation ($\dot{\phi} < 0$). This backward slip motion is followed by the stick part $\dot{\phi} = 0$, which completes the limit cycle.

The branch of periodic stick-slip solutions (p_1) is numerically determined for varying values of ω and depicted in Figure A.7b. The minimal value of $\dot{\phi}$ is set on the vertical axis. For the trivial equilibrium branch holds $\min \dot{\phi} = \omega$ and this branch is unstable as the friction torque T_f decreases with increasing angular velocity $\dot{\phi}$. The periodic stick-slip branch has a minimal value of $\dot{\phi}$, being smaller or equal than zero depending on the backward slip part. As can be seen from Figure A.7b, backward rotation becomes more pronounced at higher values of ω .

A.9 Stick-slip Whirl Model

The Stick-slip Model and the Whirl Model will be combined in this section which gives the Stick-slip Whirl Model.

Equations of Motion

Combining the lateral and the torsional model and taking into account the non-stationary fluid forces, fluid torque and contact torque (Section A.6) gives the fol-

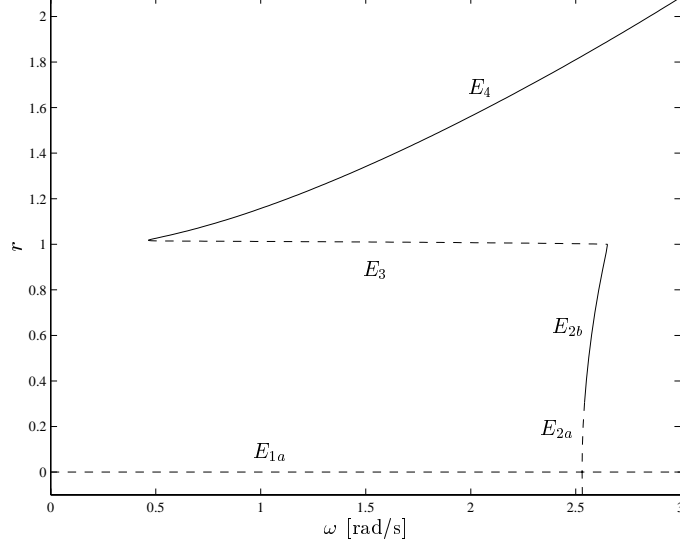


Figure A.8: Stick-slip Whirl Model, equilibrium branches.

lowing set of equations of motion

$$\begin{aligned}
 m_a(\ddot{r} - \Omega^2 r) + (c + D + B_2 r^2)\dot{r} + (k - \frac{\dot{\phi}^2}{4} m_f + m_f \dot{\phi} \Omega + B_1 r^2)r &= -F_{bN} \\
 m_a(\dot{\Omega} r + 2\dot{r}\Omega) + (c + D + B_2 r^2)\Omega r &= m_f \dot{\phi} \dot{r} + (D + B_2 r^2)\frac{\dot{\phi}}{2} r + F_{bT} \\
 J\ddot{\phi} &= -k_\phi \phi + T_f + T_b + T_d.
 \end{aligned} \tag{A.51}$$

Equilibrium Branches

Equilibrium positions of submodels are in general not equilibrium positions of the total model. The torsional and lateral degrees of freedom of the Stick-slip Whirl Model however, are to some extent uncoupled. From (A.51) it follows that for an equilibrium position must hold that $\dot{r} = 0$, $\dot{\Omega} = 0$ and $\dot{\phi} = 0$. The angular velocity of the rotor is therefore constant, $\dot{\phi} = \omega$, which means that the Whirl Model is not influenced by the Stick-slip Model. The equilibrium branches e_1 to e_4 of the Whirl Model are also equilibrium branches of the Stick-slip Whirl Model, denoted by E_1 to E_4 (Figure A.8). The twist angle φ_{eq} in an equilibrium position can be found from substitution of an equilibrium position of the Whirl Model r_{eq} and Ω_{eq} in

$$k_\phi \varphi_{\text{eq}} = T_f(\omega) + T_b(\Omega_{\text{eq}}, \omega, r_{\text{eq}}) + T_d(\Omega_{\text{eq}}, \omega, r_{\text{eq}}). \tag{A.52}$$

Some stable branches may become unstable due to an added eigenvalue of the Stick-slip Model. The trivial branch E_1 of the Stick-slip Whirl Model is totally unstable whereas it was partly stable for the Whirl Model. The branch E_2 contains a Hopf bifurcation which splits the branch in a stable and an unstable part.

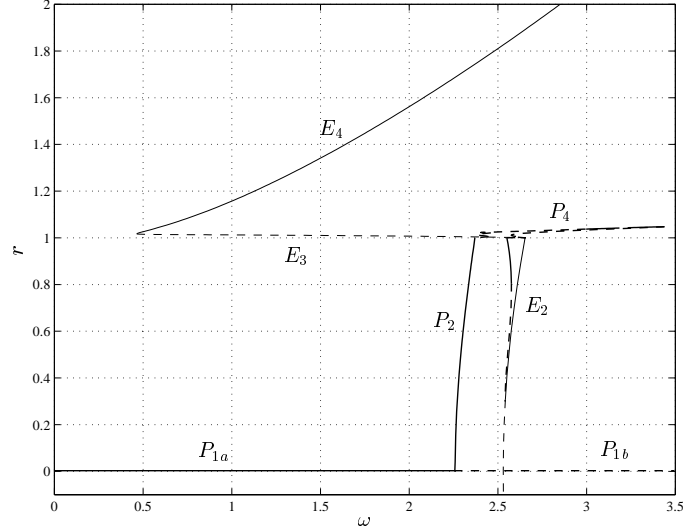


Figure A.9: Stick-slip Whirl Model, periodic branches (bold).

Periodic Branches

The periodic branches of the Stick-slip Whirl Model are depicted in Figure A.9 and partly enlarged in Figures A.10, A.11 and A.12.

As for equilibrium positions, periodic solutions of submodels are in general not periodic solutions of the total model. The torsional and lateral degrees of freedom of the Stick-slip Whirl Model are however uncoupled for $r = 0$ (because T_d and T_b vanish). The Whirl Model has an equilibrium position $r = 0$. Branch p_1 of the Stick-slip Model (Section A.8) therefore also exists for the Stick-slip Whirl Model as branch P_1 with $r = 0$. Whereas branch p_1 is stable, branch P_1 is partly stable due to the added eigenvalues of the Whirl Model.

Branch P_1 consist of pure stick-slip vibrations with $x = 0$ and $y = 0$. The radial deflection is therefore $r = \sqrt{x^2 + y^2} = 0$ but the angular position $\alpha = \arctan(\frac{y}{x})$ is not defined. Branch P_1 can therefore only be described in the stationary coordinate system (x, y, φ) and not in the polar coordinate system (r, α, φ) , which was used for the Whirl Model.

Branch P_1 , described in the stationary coordinate system, contains a Neimark-Sacker (or secondary Hopf) bifurcation after which the branch is unstable.

The equilibrium branches E_2 to E_4 (which are pure whirl solutions) and the pure stick-slip branch P_1 both have a bifurcation point in the Stick-slip Whirl Model which was not existing in Stick-slip or Whirl Model. The equilibrium branches E_2 to E_4 contain equilibria in polar coordinates but are periodic solutions in stationary coordinates with period times $T = \frac{2\pi}{\omega}$. From the Hopf bifurcation on E_2 emanates a branch P_6 (Figure A.10), which is periodic in polar coordinates and quasi-periodic in stationary coordinates. Branch P_6 is connected through branches P_5 , P_4 and P_3 with branch P_2 (Figure A.11). Branch P_2 , which contains periodic solutions in

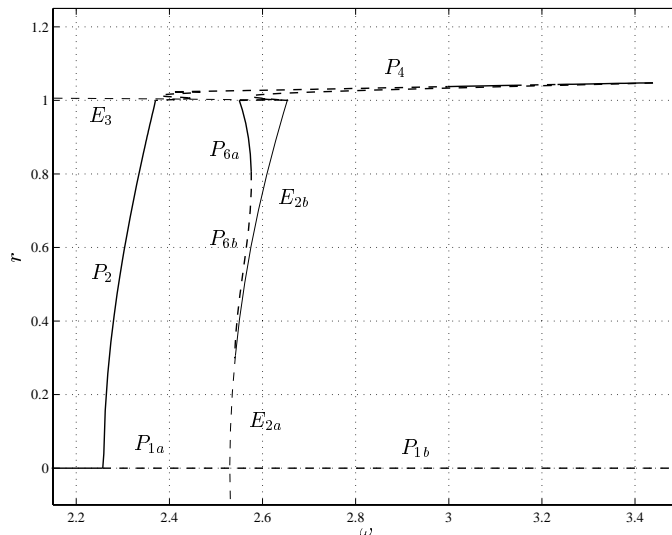


Figure A.10: Stick-slip Whirl Model, zoom of Figure A.9.

polar coordinates and quasi-periodic solutions in stationary coordinates, ends at the Neimark-Sacker bifurcation on P_1 . The Neimark-Sacker bifurcation therefore gives rise to quasi-periodic solutions which is consistent with the theory.

Branches P_2 to P_6 connect the solutions found from the Whirl Model with the solutions found from the Stick-slip Model. Branches P_2 and P_3 are periodic solutions (in polar coordinates) that perform both stick-slip and whirl motion. The periodic solutions on branches P_3 , P_4 and P_5 contains contact events between the rotor and the stator wall.

Branch P_4 is divided in stable and unstable parts P_{4a} to P_{4d} . Branch P_{4a} is connected to P_{4b} by a Neimark-Sacker bifurcation. Branches P_{4b} , P_{4c} and P_{4d} are connected to each other by two flip bifurcations. The branches with period-doubled periodic solutions and quasi-periodic solutions, which start at these bifurcations, have not been calculated.

A number of discontinuous bifurcations exist on the branches P_2 to P_6 . Branch P_2 is connected to P_3 (Figure A.12) by a discontinuous flip bifurcation (the period-doubled branch has not been calculated). The bifurcation occurs when the periodic solution touches the stator, $r = R_c$. The discontinuity of the contact forces causes the discontinuous bifurcation. Similarly, branch P_5 is connected to branch P_6 (Figure A.12) by a discontinuous fold bifurcation at $r = R_c$. Branch P_3 (with stick events) is connected to branch P_4 (without stick events) by a discontinuous fold bifurcation. This bifurcation is due to the discontinuity in the dry friction force.

A remarkable bifurcation occurs on the equilibrium branch connecting branch E_{2b} with E_3 at $r = R_c$ (Figure A.12). This bifurcation point was already encountered in the Whirl Model as a discontinuous saddle-node bifurcation at which the branch turns around (bifurcation point f in Figure A.6). In addition, two periodic branches,

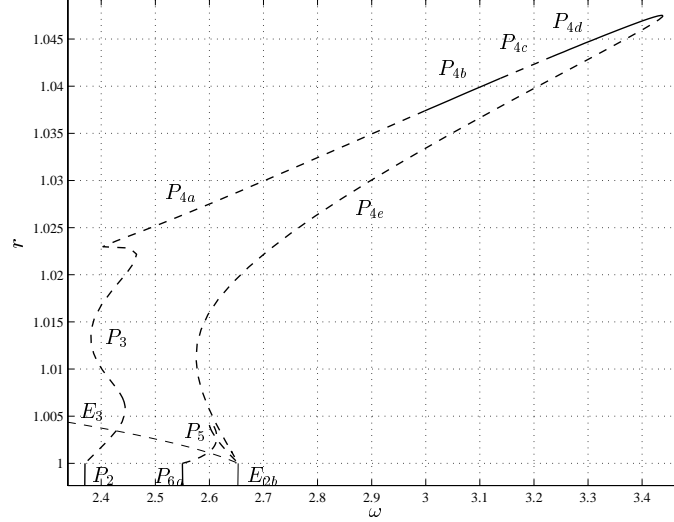


Figure A.11: Stick-slip Whirl Model, zoom of Figure A.10.

P_4 and P_5 , are connected to the bifurcation point in the Stick-slip Whirl Model. This bifurcation point is therefore a combined bifurcation of a saddle-node bifurcation and two Hopf bifurcations.

The bifurcation diagrams certainly do not show all periodic branches that exist. Period-doubled branches were not calculated but also other branches may be missing in the bifurcation diagrams.

A note has to be made concerning the chosen numerical values of the parameters in the Stick-slip Whirl Model. Stiffness and mass/inertia parameters are chosen such that the torsional eigenfrequency of the rotor is close to the first torsional eigenfrequency of the drillstring. Similarly, the lateral eigenfrequency of the rotor is close to the lateral eigenfrequency of the lowest drill collar section. Damping and friction constants are more or less arbitrarily chosen. The equilibrium and periodic branches in the bifurcation diagrams depend of course on the chosen constants. However, the periodic whirl branches, P_2 to P_6 , seem to be close to the equilibrium branch E_2 . The equilibrium branches form a structure to which the periodic branches are attached. A lot about the dynamics of this particular system can already be said once the location of the equilibrium branches are known. The value ω_c , expressed in (A.25) and (A.29), gives the location of branch E_2 . The ratio $\frac{\mu_b \omega m_f}{c}$ determines whether branch E_3 proceeds to the right of bifurcation point f or folds to the left (Figure A.6). The value ω_d (A.39) gives the starting point of branch E_4 . Consequently, ω_c , ω_d and $\frac{\mu_b \omega m_f}{c}$ determine the main structure of the bifurcation diagram.

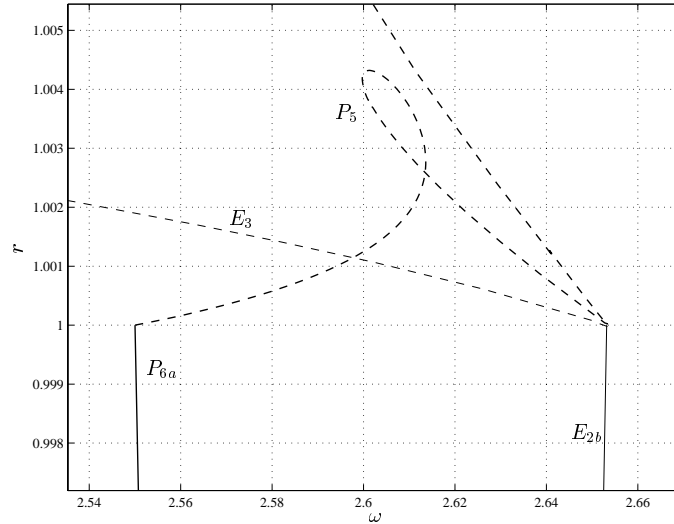


Figure A.12: Stick-slip Whirl Model, zoom of Figure A.11.

A.10 Discussion and Conclusions

In the previous sections a simple model was constructed, based on the assumption that the fluid forces are the cause of the phenomena observed in the measurements. The Stick-slip Whirl Model was analyzed with path-following techniques and bifurcation theory of the preceding chapters. What can we conclude from the Stick-slip Whirl Model with respect to the measurements?

The Stick-slip Whirl Model exhibits both stick-slip motion and whirl motion (which is not possible in the models of Jansen [1993]). Stick-slip motion is prevalent at low angular velocities and backward whirl (during which the rotor rolls backward over the stator) is prevalent for high angular velocities consistent with the measurements. Stick-slip and whirl motion coexist for an interval of ω both in the model and in the measurements. Combined stick-slip whirl motion was not observed in the measurements but was found in the Stick-slip Whirl Model (branches P_2 and P_3). However, this combined motion occurs only in a very small interval of ω in the model. The model is therefore consistent with the measurements in the sense that stick-slip motion occurs *or* whirl motion (both possible for the same value of ω), but a combination is rare or not existing.

The measurements show a hysteresis effect for a sweep-up sweep-down test (Figure A.4). The drillstring starts in stick-slip motion at low angular velocity of the rotary table. When the rotary table speed is increased with small steps, the motion remains in the stick-slip mode but at 11.5 [rad/s] the drillstring suddenly stops to operate in the stick-slip mode and starts to whirl backward. The drillstring remains whirling for increasing rotary table speed also after the rotary table speed is diminished in small steps during the sweep-down test. The mean-bending moment (and whirl radius?) drop between 7 and 2 [rad/s] and stick-slip recommences.

A similar hysteresis effect can be seen for the Stick-slip Whirl Model. At low values of ω the rotor is in stick-slip motion. When ω is increased quasi-statically, branch P_{1a} is followed (Figure A.9) and the rotor will remain in the stick-slip mode. Branch P_1 becomes unstable for increasing ω due to the destabilizing fluid forces and the motion of the rotor will rapidly change via branches P_2 and P_3 to an oscillatory whirl motion on branch P_4 . When ω is increased even more the motion will jump to regular backward whirling motion without slip on branch E_4 . If ω is subsequently quasi-statically decreased, the rotor will remain to operate on branch E_4 until the discontinuous saddle-node bifurcation between E_3 and E_4 is met. The motion will then jump to the stick-slip mode and the hysteresis loop is complete.

The phenomena as described by the Stick-slip Whirl Model resemble to some extent the phenomena observed in the measurements. The transition from stick-slip motion to whirl motion is similar, but the transition from whirl to stick-slip motion seems to be more gradual in the measurements than can be explained from the model.

One could argue whether the observed phenomena in the measurements are really due to fluid forces and not to other possible ways of interaction between torsional and lateral motion. Although the results on the Stick-slip Model look similar, they do not prove that indeed fluid forces are the cause for onset of whirl in drillstrings. This appendix illustrates how the techniques and theory of the preceding chapters can be used to analyze low-dimensional models with discontinuities, in this case the Stick-slip Whirl Model. In the same way, other low-dimensional models can be constructed which study for instance the influence of mass unbalance on the dynamic behaviour of a rotor with lateral and torsional degrees of freedom. The results of the different models can be compared with the experiments which can help to gain insight into the complex dynamic behaviour of the drillstring. Knowledge about bifurcations in discontinuous systems is therefore relevant to dynamic problems in industrial applications.

A.11 Coordinate Systems

$$\begin{aligned} x &= r \cos \alpha \\ y &= r \sin \alpha \end{aligned} \tag{A.53}$$

$$r = \sqrt{x^2 + y^2} \quad \alpha = \arctan\left(\frac{y}{x}\right) \tag{A.54}$$

$$\dot{\alpha} = \frac{\dot{y}x - \dot{x}y}{r^2} \quad \dot{r} = \frac{x\dot{x} + y\dot{y}}{r} \tag{A.55}$$

$$\ddot{r} = \frac{\dot{x}^2 + \dot{y}^2 + \ddot{x}x + \ddot{y}y - \dot{r}^2}{r} \tag{A.56}$$

Appendix B

Some Theoretical Aspects of Periodic Solutions

B.1 Transformation to an Autonomous System

The theory and methods in the body of this thesis were derived for autonomous systems. Some examples however, contain a time-periodic forcing which makes the system non-autonomous. A class of non-autonomous time-periodic systems can be transformed to autonomous time-periodic systems as described in this appendix (see also Doedel et al. [1998]).

Consider an n th-order, non-autonomous, nonlinear dynamical system represented by the differential equation

$$\dot{\underline{x}}(t) = \underline{f}(t, \underline{x}(t)), \quad (\text{B.1})$$

where $\dot{\underline{x}} \equiv d\underline{x}/dt$, \underline{x} is a column with the n state variables of the system, t is time and \underline{f} is a column of nonlinear functions of time t and the components of \underline{x} . Since \underline{f} does depend on t , the system is called non-autonomous, as opposed to autonomous systems, where \underline{f} is not a function of t .

System (B.1) is time-periodic with period time T if

$$\underline{f}(t + T, \underline{x}) = \underline{f}(t, \underline{x}) \quad (\text{B.2})$$

and if T is the minimal number such that (B.2) holds. Assume that the time-periodic system (B.1) can be written as

$$\dot{\underline{x}}(t) = \underline{f}^*(\sin(\beta t), \cos(\beta t), \underline{x}(t)), \quad (\text{B.3})$$

where $\beta = \frac{2\pi}{T}$.

To the time-periodic system (B.1) we add a nonlinear oscillator with $\sin(\beta t)$ and $\cos(\beta t)$ as its solution components. An example of such an oscillator is

$$\begin{aligned} \dot{v} &= v + \beta w - v(v^2 + w^2) \\ \dot{w} &= -\beta v + w - w(v^2 + w^2) \end{aligned} \quad (\text{B.4})$$

with $v(0) = 0$ and $w(0) = 1$. The oscillator (B.4) has the asymptotically stable solution $v(t) = \sin(\beta t)$ and $w(t) = \cos(\beta t)$. We couple this oscillator to the system (B.3) and obtain

$$\begin{aligned}\dot{\underline{x}} &= \underline{f}^*(v, w, \underline{x}) \\ \dot{v} &= v + \beta w - v(v^2 + w^2) \\ \dot{w} &= -\beta v + w - w(v^2 + w^2)\end{aligned}\quad (\text{B.5})$$

This set of differential equations is autonomous and periodic solutions of system (B.3) are also periodic solutions of (B.5) with period T .

B.2 The Variational Equation

An n th-order, smooth nonlinear system is represented by the differential equation with initial condition¹

$$\dot{\underline{x}}(t) = \underline{f}(t, \underline{x}(t)), \quad \underline{x}(t_0) = \underline{x}_0. \quad (\text{B.6})$$

The solution to this equation is written as $\underline{\phi}_t(t_0, \underline{x}_0)$, so

$$\dot{\underline{\phi}}_t(t_0, \underline{x}_0) = \underline{f}(t, \underline{\phi}_t(t_0, \underline{x}_0)), \quad \underline{\phi}_t(t_0, \underline{x}_0) = \underline{x}_0. \quad (\text{B.7})$$

Differentiating (B.7) with respect to \underline{x}_0 gives

$$\frac{\partial \dot{\underline{\phi}}_t(t_0, \underline{x}_0)}{\partial \underline{x}_0} = \frac{\partial \underline{f}(t, \underline{\phi}_t(t_0, \underline{x}_0))}{\partial \underline{x}} \frac{\partial \underline{\phi}_t(t_0, \underline{x}_0)}{\partial \underline{x}_0}, \quad \frac{\partial \underline{\phi}_t(t_0, \underline{x}_0)}{\partial \underline{x}_0} = \underline{I}. \quad (\text{B.8})$$

Defining $\underline{\Phi}_t(t_0, \underline{x}_0) \equiv \partial \underline{\phi}_t(t_0, \underline{x}_0) / \partial \underline{x}_0$, Equation (B.8) becomes

$$\dot{\underline{\Phi}}_t(t_0, \underline{x}_0) = \frac{\partial \underline{f}(t, \underline{\phi}_t(t_0, \underline{x}_0))}{\partial \underline{x}} \underline{\Phi}_t(t_0, \underline{x}_0), \quad \underline{\Phi}_{t_0}(t_0, \underline{x}_0) = \underline{I}, \quad (\text{B.9})$$

which is the *variational equation* for a periodic solution of (B.6). The fundamental solution matrix after a period time T is called the monodromy matrix $\underline{\Phi}_T$.

¹The derivation, presented in this appendix, is taken from Parker and Chua [1989].

Appendix C

Parameter Values

C.1 Switch Model

Section 2.4:

$$k = 1 \text{ N/m}$$

$$m = 1 \text{ kg}$$

$$v_{\text{dr}} = 0.2 \text{ m/s}$$

$$F_s = 1 \text{ N}$$

$$\delta = 3 \text{ [s/m]}$$

$$\eta = 10^{-6} \text{ m/s}$$

$$TOL = 10^{-8}$$

C.2 Stick-slip System

$$k = 1 \text{ N/m}$$

$$c = 0 \text{ Ns/m in Section 3.4}$$

$$c = 0.1 \text{ Ns/m in Section 6.7}$$

$$m = 1 \text{ kg}$$

$$v_{\text{dr}} = 0.2 \text{ m/s in Section 3.4}$$

$$F_{\text{slip}} = 1 \text{ N}$$

$$F_{\text{stick}} = 2 \text{ N}$$

$$\eta = 10^{-4} \text{ m/s}$$

$$TOL = 10^{-8}$$

C.3 Trilinear System

$$m = 1 \text{ kg}$$

$$c = 0.05 \text{ N/(ms)}$$

$$k = 1 \text{ N/m}$$

$$x_c = 1 \text{ m}$$

$$\begin{aligned}
 k_f &= 4 \text{ N/m} \\
 c_f &= 0.5 \text{ N/(ms)} \\
 f_0 &= 0.2 \text{ N}
 \end{aligned}$$

C.4 Forced Vibration with Dry Friction

$$\begin{aligned}
 m &= 1 \text{ kg} \\
 c &= 0.01 \text{ N/(ms)} \\
 k &= 1 \text{ N/m} \\
 f_0 &= 2.5 \text{ N} \\
 F_{\text{slip}} &= 1 \text{ N} \\
 F_{\text{stick}} &= 2 \text{ N}
 \end{aligned}$$

C.5 Forced Stick-slip System

$$\begin{aligned}
 m &= 1 \text{ kg} \\
 c &= 0 \text{ N/(ms)} \\
 k &= 1 \text{ N/m} \\
 v_{\text{dr}} &= 1 \text{ m/s} \\
 \alpha_0 &= 1.5 \text{ N} \\
 \alpha_1 &= 1.5 \text{ Ns/m} \\
 \alpha_3 &= 0.45 \text{ Ns}^3/\text{m}^3 \\
 f_0 &= 0.1 \text{ N}
 \end{aligned}$$

C.6 Stick-slip Whirl Model

$$\begin{array}{lll}
 m = 1 \text{ kg} & c = 0.3 \text{ N/(ms)} & k = 1 \text{ N/m} \\
 m_f = 1 \text{ kg} & D = 0.1 \text{ N/(ms)} & R = 2 \text{ m} \\
 R_b = 3 \text{ m} & R_c = R_b - R = 1 \text{ m} & k_b = 50 \text{ N/m} \\
 c_b = 30 \text{ N/(ms)} & \mu_b = 0.5 & B_1 = 0.1 \text{ N/m}^3 \\
 B_2 = 0 \text{ N/(m}^3 \text{ s)} & J = 1 \text{ kg m}^2 & k_\varphi = 1 \text{ Nm} \\
 T_0 = 0.2 \text{ Nm} & \delta = 0.3 &
 \end{array}$$

Bibliography

- Aizerman, M. A. and Gantmakher, F. R. (1958). 'On the Stability of Periodic Motions', *Journal of Applied Mathematics and Mechanics* (translated from Russian), pp. 1065-1078.
- Andersson, I. (1980). *Stick-slip motion in one-dimensional continuous systems and systems with several degrees-of-freedom*, Ph.D. Thesis, Chalmers University of Technology, Göteborg, Sweden.
- Andronov, A. A., Vitt, A. A. and Khaikin, S. E. (1987). *Theory of Oscillators*, Dover Publications, New York, Reprint. Originally published Pergamon Press, Oxford (1966), translated from Russian.
- Anosov, D. V. (1959). 'Stability of the equilibrium positions in relay systems', *Automation and Remote Control* **20**, pp. 130-143.
- Armstrong-Hélouvry, B., Dupont, P., and Canudas De Wit, C. (1994). 'A survey of models, analysis tools and compensation methods for the control of machines with friction', *Automatica* **30**(7), pp. 1083-1138.
- Aubin, J. P. and Cellina, A. (1984). *Differential Inclusions*. Springer-Verlag, Berlin.
- Ascher, U. M., Mattheij, R. M. M. and Russell, R. D. (1995). *Numerical Solution of Boundary Value Problems for Ordinary Differential Equations*. Society for Industrial and Applied Mathematics, Philadelphia.
- Begley, C. J. and Virgin L. N. (1997). 'A detailed study of the low-frequency periodic behavior of a dry friction oscillator', *Journal of Dynamic Systems, Measurement, and Control*, **119**, pp. 491-497.
- Begley, C. J. and Virgin L. N. (1998). 'Impact response under the influence of friction', *Journal of Sound and Vibration*, **211**(5), pp. 801-818.
- Blazejczyk-Okolewska, B. and Kapitaniak, T. (1996). 'Dynamics of Impact Oscillator with Dry Friction', *Chaos, Solitons & Fractals*, **7**(9), pp. 1455-1459.
- Bockman, S. F. (1991). 'Lyapunov Exponents for Systems Described by Differential Equations with Discontinuous Right-Hand Sides', *Proceedings of the American Control Conference*, pp. 1673-1678.

- Brogliato, B. (1999). *Nonsmooth Mechanics*, Springer, London.
- Brockley, C. A., and Ko, P. L. (1970). 'Quasi-harmonic friction-induced vibration', *ASME Journal of Lubrication Technology*, **92**, pp. 550-556.
- Clarke, F. H., Ledyev, Yu. S., Stern, R. J. and Wolenski, P. R. (1998). *Nonsmooth Analysis and Control Theory*, Graduate Texts in Mathematics 178, Springer, New-York.
- Di Bernardo, M., Johansson, K., and Vasca F. (1999a). 'Sliding Orbits and Their Bifurcations in Relay Feedback Systems', *Proceedings of the 38th Conference on Design & Control, Phoenix, December 1999*, CD-ROM publication, pp. 708-713.
- Di Bernardo, M., Feigin, M. I., Hogan, S. J. and Homer, M. E. (1999b). 'Local analysis of C-bifurcations in n -dimensional piecewise-smooth dynamical systems', *Chaos, Solitons & Fractals*, **10**(11), pp. 1881-1908.
- Dankowicz, H. and Nordmark, A. B. (2000). 'On the origin and bifurcations of stick-slip oscillations', *Physica D*, **136**(3-4), pp. 280-302.
- Deimling, K. and Szilagyi, P. (1994). 'Periodic solutions of dry friction problems', *ZAMP*, **45**, pp. 53-60.
- Doedel, E. J., Champneys, A. R., Fairgrieve, T. F., Kuznetsov, Y. A., Sandstede, B. and Wang, X (1998). *AUTO97: Continuation and Bifurcation Software for Ordinary Differential Equations*, User Manual, <ftp://ftp.cs.concordia.ca/pub/doedel/auto>.
- Elmer, F-J. (1997). 'Nonlinear dynamics of dry friction', *Journal of Physica A: Mat. Gen.*, **30**(17), pp. 6057-6063.
- Eich-Soellner, E. and Führer, C. (1998). *Numerical Methods in Multibody Dynamics*, Teubner, Stuttgart.
- Fečkan, M. (1998). 'Bifurcations of Periodic and Chaotic Solutions in Discontinuous Systems', *Archivum Mathematicum*, **34**, pp. 73-82.
- Feeny, B. and Guran, A. (1997). 'Friction as a nonlinearity in dynamics: a hystorical review', in *Nonlinear Dynamics, The Richard Rand 50th Anniversary Volume* by A. Guran (eds.), World Scientific, London, pp. 168-202.
- Feigin, M. I. (1974). 'On the generation of sets of subharmonic modes in a piecewise-continuous system', *PMM*, **38**(5), pp. 810-818.
- Feigin, M. I. (1978). 'On the structure of C-bifurcation boundaries of piecewise-continuous systems', *PMM*, **42**(5), pp. 820-829.
- Feigin, M. I. (1995). 'The increasingly complex structure of the bifurcation tree of a piecewise-smooth system', *Journal of Applied Mathematics and Mechanics*, **59**(6), pp. 853-863.

- Fey, R. H. B. (1992). *Steady-state behaviour of reduced dynamic systems with local nonlinearities*. Ph.D. thesis, Eindhoven University of Technology, The Netherlands.
- Filippov, A. F. (1964). 'Differential equations with discontinuous right-hand side', *American Mathematical Society Translations*, Series 2, **42**, pp. 199-231.
- Filippov, A. F. (1988). *Differential equations with discontinuous right-hand sides*, Mathematics and Its Applications, Kluwer Academic, Dordrecht.
- Foale, S. and Bishop, R. (1994). 'Bifurcations in Impacting Oscillations', *Nonlinear Dynamics*, **6**, pp. 285-299.
- Fritz, R. J. (1970). 'The Effects of an Annular Fluid on the Vibrations of a Long Rotor, Part 1—Theory', *Journal of Basic Engineering*, pp. 923-929.
- Galvanetto, U., Bishop, S. R. and Briseghella, L. (1995). 'Mechanical stick-slip vibrations', *International Journal of Bifurcation and Chaos*, **5**(3), pp. 637-651.
- Galvanetto, U., and Knudsen, C. (1997). 'Event Maps in a Stick-slip System', *Nonlinear Dynamics*, **13**(2), pp. 99-115.
- Génot, F. and Brogliato, B. (1999). 'New Results on Painlevé paradoxes', *European Journal of Mechanics A/Solids*, **18**, pp. 653-677.
- Glocker, Ch. (1995). *Dynamik von Starrkörpersystemen mit Reibung und Stößen*, Fortschr.-Ber. VDI Reihe 18, Nr. 182, VDI Verlag, Düsseldorf.
- Glendinning, P. (1994). *Stability, instability and chaos: an introduction to the theory of nonlinear differential equations*, Cambridge Texts in Applied Mathematics, Cambridge University Press, Cambridge.
- Guckenheimer, J. and Holmes, P. (1983). *Nonlinear Oscillations, Dynamical Systems, and Bifurcations of Vector Fields*, Applied Mathematical Sciences 42, Springer-Verlag, New York.
- Haessig, Jr. D. A., and Friedland, B. (1991). 'On the modeling and simulation of friction', *ASME Journal of Dynamic Systems, Measurement and Control*, **113**, pp. 354-362.
- Hagedorn, P. (1988). *Non-Linear Oscillations*, Oxford Engineering Science Series 10, Clarendon Press, Oxford.
- Heemels, W. M. H. (1999). *Linear complementarity systems: a study in hybrid dynamics*. Ph.D. thesis, Eindhoven University of Technology, The Netherlands.
- Hinrichs, N. (1997). *Reibungsschwingungen mit Selbst- und Fremderregung: Experiment, Modellierung und Berechnung*, Fortschr.-Ber. VDI Reihe 11, Nr. 240, VDI Verlag, Düsseldorf.
- Hinrichs, N., Oestreich, M. and Popp, K. (1998). 'On the modelling of friction oscillators', *Journal of Sound and Vibration*, **216**(3), pp. 435-459.

- Jansen, J. D. (1993). *Nonlinear Dynamics of Oilwell Drillstrings*, Ph.D. Thesis, Delft University Press, The Netherlands.
- Ibrahim, R. A. (1994a). 'Friction-induced vibration, chatter, squeal and, chaos; Part I: Mechanics of contact and friction', *ASME Applied Mechanics Reviews*, **47**(7), pp. 209-226.
- Ibrahim, R. A. (1994b). 'Friction-induced vibration, chatter, squeal and, chaos; Part II: Dynamics and modeling', *ASME Applied Mechanics Reviews*, **47**(7), pp. 227-253.
- Ivanov, A. P. (1993). 'Analytical methods in the theory of vibro-impact systems', *Journal of Applied Mathematics and Mechanics*, **57**, 2, pp. 221-236.
- Ivanov, A. P. (1996). 'Bifurcations in Impact Systems', *Chaos, Solitons & Fractals*, **7**, 10, pp. 1615-1634.
- Karnopp, D. (1985). 'Computer simulation of stick-slip friction in mechanical dynamic systems', *ASME Journal of Dynamic Systems, Measurement and Control*, **107**, pp. 100-103.
- Kato, S., Sato, N., and Matsubayashi, T. (1972). 'Some considerations on characteristics of static friction of machine tool slideway', *Journal of Lubrication Technology*, **94**, pp. 234-247.
- Kleczka, W., and Kreuzer, E. (1994). 'On approximations of non-smooth functions in bifurcation analysis', in *Nonlinearity and Chaos in Engineering Dynamics*, J. M. T. Thompson and S. R. Bishop (eds.), Wiley, Chichester, pp. 115-123,
- Kunze, M. and Küpper, T. (1997). 'Qualitative bifurcation analysis of a non-smooth friction oscillator model', *ZAMP*, **48**(1), pp. 87-101.
- Kuznetsov, Y. A. (1995). *Elements of Applied Bifurcation Theory*, Applied Mathematical Sciences 112, Springer-Verlag, New York.
- Lee, Chong-Won 1993. *Vibration analysis of rotors*, Kluwer Academic Publishing, Dordrecht, The Netherlands.
- Leine, R. I., Van Campen, D. H., De Kraker, A. and Van den Steen, L. (1998). 'Stick-Slip Vibrations Induced by Alternate Friction Models', *Nonlinear Dynamics*, **16**(1), pp. 41-54.
- Leine, R. I. and Van Campen, D. H. (1999). 'Fold Bifurcations in Discontinuous Systems', *Proceedings of DETC'99 ASME Design Engineering Technical Conferences*, September 12-15, Las Vegas, CD-ROM, DETC99/VIB-8034.
- Leine, R. I. and Van Campen, D. H. (2000). 'Discontinuous Bifurcations of Periodic Solutions', accepted for publication in *Mathematical Modelling of Nonlinear Systems*.

- Leine, R. I., Van Campen, D. H. and Van de Vrande, B. L. (2000). 'Bifurcations in Nonlinear Discontinuous Systems', accepted for publication in *Nonlinear Dynamics*.
- Martelli, M. (1992). *Discrete dynamical systems and chaos*, Pitman Monographs and Surveys in Pure and Applied Mathematics 62, Longman Scientific & Technical, Harlow.
- Meijaard, J. P. (1996). 'A mechanism for the onset of chaos in mechanical systems with motion-limiting stops', *Chaos, Solitons & Fractals*, **7**(10), pp. 1649-1658.
- Meijaard, J. P. (1997). 'Efficient numerical integration of the equations of motion of non-smooth mechanical systems', *Zeitschrift für Angewandte Mathematik und Mechanik*, **77**(6), pp. 419-427.
- Molenaar, J., de Weger, J. G. and Van de Water, W. (1999). 'Near-grazing behaviour of the harmonic oscillator', *Proceedings of DETC'99 ASME Design Engineering Technical Conferences*, September 12-15, Las Vegas, CD-ROM, DETC99/VIB-8036.
- Müller, P. C. (1995). 'Calculation of Lyapunov Exponents for Dynamic Systems with Discontinuities', *Chaos, Solitons & Fractals*, **5**(9), pp. 1671-1681.
- Muszynska, A. (1986). 'Whirl and whip-rotor/bearing stability problems', *Journal of Sound and Vibration*, **110**(3), pp. 443-462.
- Natsiavas, S. (1989). 'Periodic Response and Stability of Oscillators with Symmetric Trilinear Restoring Force', *Journal of Sound and Vibration*, **134**(2), pp. 315-331.
- Natsiavas, S. and Gonzalez, H. (1992). 'Vibration of harmonically excited oscillators with asymmetric constraints', *ASME Journal of Applied Mechanics*, **59**, pp. 284-290.
- Nayfeh, A. H. and Balachandran, B. (1995). *Applied Nonlinear Dynamics; Analytical, Computational, and Experimental Methods*, Wiley-International, Chichester.
- Nayfeh, A. H. and Mook, D. T. (1979). *Nonlinear Oscillations*, Wiley-International, Chichester.
- Nordmark, A. B. (1997). 'Universal limit mapping in grazing bifurcations' *Physical review E*, **55**(1), pp. 266-270.
- Nusse, H. E. and York, J. A. (1992). 'Border-collision bifurcations including "period two to period three" for piecewise smooth systems', *Physica D*, **57**, pp. 39-57.
- Oancea, V. G. and Laursen, T. A. (1998). 'Investigations of low frequency stick-slip motion: experiments and numerical modelling', *Journal of Sound and Vibration*, **213**(4), pp. 577-600.
- Oestreich, M. (1998). *Untersuchung von Schwingern mit nichtglatten Kennlinien*, Fortschr.-Ber. VDI Reihe 11, Nr. 258, VDI Verlag, Düsseldorf.

- Parker, T. S. and Chua, L. O. (1989). *Practical Numerical Algorithms for Chaotic Systems*. Springer-Verlag, New York.
- Pavone, D.R., Desplans, J.P. (1994). 'Application of High Sampling Rate Downhole Measurements for Analysis and Cure of Stick-Slip in Drilling'. *SPE* 28324. Paper presented at the SPE 69th Annual Technical Conference and Exhibition held in New Orleans, 25-28 September, 1994.
- Peterka, F. (1996). 'Bifurcations and Transition Phenomena in an Impact Oscillator', *Chaos, Solitons & Fractals*, **7**(10), pp. 1635-1647.
- Pfeiffer, F. (1991). 'Dynamical systems with time-varying or unsteady structure', *Zeitschrift für Angewandte Mathematik und Mechanik*, **71**(4), T6-T22.
- Pfeiffer, F. and Glocker, Ch. (1996). *Multibody dynamics with unilateral contacts*, Wiley, New York.
- Poincaré, H. (1899). *Les Méthodes Nouvelles de la Mécanique Céleste*. Gautier-Villars, Paris.
- Popp, K. (1992). 'Some model problems showing stick-slip motion and chaos', in *ASME WAM, Proc. Symp. on Friction Induced Vibration, Chatter, Squeal, and Chaos*, **49**, R. A. Ibrahim and A. Soom (eds.), ASME New York, pp. 1-12.
- Popp, K. and Stelzer, P. (1990). 'Nonlinear Oscillations of Structures Induced by Dry Friction', in *Nonlinear Dynamics in Engineering Systems IUTAM Symposium Stuttgart 1989*, W. Schiehlen (eds), Springer-Verlag, Berlin.
- Popp, K., Hinrichs, N. and Oestreich, M. (1995). 'Dynamical behaviour of a friction oscillator with simultaneous self and external excitation', in *Sādāna: Academy Proceedings in Engineering Sciences*, Indian Academy of Sciences, Bangalore, India, Part 2-4, **20**, pp. 627-654.
- Rasband, S. N. (1990). *Chaotic Dynamics of Nonlinear Systems*, Wiley-International, Chichester.
- Reithmeier, E. (1991). *Periodic Solutions of Nonlinear Dynamical Systems*, Springer-Verlag, Berlin.
- Roxin, E. (1965). 'Stability in General Control Systems', *Journal of Differential Equations*, **1**, pp. 115-150.
- Sastry, S. (1999). *Nonlinear Systems, Analysis, Stability, and Control*, Springer, New York.
- Sepehri, N., Sassani, F., Lawrence, P. D., and Ghasempoor, A. (1996). 'Simulation and experimental studies of gear backlash and stick-slip friction in hydraulic excavator swing motion', *ASME Journal of Dynamic Systems, Measurement and Control*, **118**, pp. 463-467.
- Seydel, R. (1994). *Practical Bifurcation and Stability Analysis; From Equilibrium to Chaos*, Interdisciplinary Applied Mathematics 5, Springer-Verlag, New York.

- Stelter, P. (1992). 'Nonlinear vibrations of structures induced by dry friction', *Nonlinear Dynamics*, **3**, pp. 329-345.
- Stelter, P. and Sestro, W. (1991). 'Bifurcations in Dynamical Systems with Dry Friction', *International Series of Numerical Mathematics*, **97**, pp. 343-347.
- Tikhomirov, V. M. (1989). 'Analysis II, Convex Analysis and Approximation Theory', in *Encyclopaedia of Mathematical Sciences*, Vol. 14, Gamkrelidze, R. V. (eds.), Springer, Berlin.
- Tondl, A. (1965). *Some problems of rotor dynamics*, Chapman and Hall Limited, London.
- Van den Steen, L. (1997). *Suppressing stick-slip-induced drillstring oscillations: a hyperstability approach*, Ph.D. Thesis, University of Twente, The Netherlands.
- Van der Heijden, G. H. M. (1994). *Nonlinear Drillstring Dynamics*, Ph.D. Thesis, University of Utrecht, The Netherlands.
- Van der Schaft, A. and Schumacher, H. (1997). 'Hybrid systems described by the complementarity formalism', in *Hybrid and Real-Time Systems, Proc. Intern. Workshop, HART'97, Grenoble*, Maler, O., Springer, Berlin.
- Van de Vorst, E. L. B. (1996). *Long Term Dynamics and Stabilization of Nonlinear Mechanical Systems*, Ph.D. Thesis, Eindhoven University of Technology, The Netherlands.
- Van de Vrande, B. L., Van Campen, D. H. and De Kraker, A. (1999). 'An Approximate Analysis of Dry-Friction-Induced Stick-slip Vibrations by a Smoothing Procedure', *Nonlinear Dynamics*, **19**(2), pp. 157-169.
- Wiercigroch, M. (1996). 'A note on the switch function for the stick-slip phenomenon', *Journal of Sound and Vibration*, **175**(5), pp. 700-704.
- Wiercigroch, M. (1996). 'On Modelling Discontinuities in Dynamic Systems', *Machine Vibration*, **5**, pp. 112-119.
- Wiercigroch, M. (1997). 'Chaotic Vibration of a Simple Model of the Machine Tool-Cutting Process System', *Journal of Vibration and Acoustics*, **119**(3), pp. 468-476.
- Yoshitake, Y. and Sueoka, A. (2000). 'Forced Self-excited Vibration Accompanied by Dry friction', in *Applied Nonlinear Dynamics and Chaos of Mechanical Systems with Discontinuities*, M. Wiercigroch and A. de Kraker (eds.), World Scientific, to appear.

Acknowledgments

I am very indebted to a number of people for their contributions to this thesis.

First of all, I would like to thank my promotor Dick van Campen for his tremendous support, faith and enthusiasm. He has been a great source of inspiration and encouragement through many stimulating in-depth discussions.

I also thank Henk Nijmeijer for his constructive criticism and valuable comments. The readability and consistency of this thesis have been greatly improved thanks to his effort.

Furthermore, I wish to acknowledge Bram de Kraker for his help and involvement as copromotor and Jaap Molenaar and Koos Rooda for their useful comments as members of the ‘kerncommissie’.

I wish to express my gratitude to the Dutch Technology Foundation (STW) for the financial support and the members of the STW users-committee for the fruitful discussions during our meetings.

I am grateful to Wout Keultjes, Pierre Kriesels and Albert Pols of Shell International Exploration & Production B.V., for granting the permission to publish the experimental data in Appendix A. Joram Manie dedicated his final engineering thesis project to the investigation of the experimental data and I thank him for all the work he has done and for the fine co-operation.

Many friends and colleagues have helped me over the years with practical problems. Among them are (in no particular order) Bram van de Vrande, Nathan van de Wouw, Pascal Etman, Rob Fey, Marko Vendelin, Jiazhong Zhang and so many others. Thanks for your friendship and help.

Leon van den Steen deserves a special mention, because he introduced me to drillstring dynamics.

Anne, Ruchi, Phil and Varvara, don't forget lunch time!

Especially, I would like to thank my parents and brothers who encouraged me during good and bad times with their unconditional love and support.

Last but not least I thank my girlfriend Ilse, to whom I have dedicated this thesis, for her love and making my life so enjoyable.

Remco Leine
Eindhoven, April 2000.

Curriculum Vitae

Remco I. Leine was born in 1973 in The Netherlands. He attended the Rijnlands Lyceum in Wassenaar between 1985 and 1991. Upon completion of his secondary school he started his academic education in Delft University of Technology in September 1991. He studied mechanical engineering and received his propaedeutic diploma with distinction in July 1992. He specialized in dynamics at the Department of Engineering Mechanics and conducted his final thesis project at Shell International Exploration & Production in Rijswijk, The Netherlands. In the summer of 1996 he received his Master's degree in mechanical engineering in the field of drillstring dynamics. After his graduation, he went to Eindhoven University of Technology to work with Prof. Dick van Campen, under whose supervision he completed his Ph.D study on bifurcations in discontinuous dynamical systems, which resulted in this thesis.

